Research Thesis: Declaration of Authorship

Print name:	Simon Watson

Title of thesis:	Using self-assembly techniques for green lubrication solutions in tribological contacts

I declare that this thesis and the work presented in it are my own and has been generated by me as the result of my own original research.

I confirm that:

1. This work was done wholly or mainly while in candidature for a research degree at this University;
2. Where any part of this thesis has previously been submitted for a degree or any other qualification at this University or any other institution, this has been clearly stated;
3. Where I have consulted the published work of others, this is always clearly attributed;
4. Where I have quoted from the work of others, the source is always given. With the exception of such quotations, this thesis is entirely my own work;
5. I have acknowledged all main sources of help;
6. Where the thesis is based on work done by myself jointly with others, I have made clear exactly what was done by others and what I have contributed myself;
7. Parts of this work have been published as:

S. Watson, M. Nie, L. Wang, and K. Stokes, "Challenges and developments of self-assembled monolayers and polymer brushes as a green lubrication solution for tribological applications," RSC Advances, vol. 5, pp. 89698-89730, 2015.

S. Watson, S. Dennington, L. Wang, M. Nie, S. Hinder, and K. Stokes, "Polymer brush lubrication of the silicon nitride-steel contact: a colloidal force microscopy study," RSC Advances, vol. 7, pp. 42667-42676, 2017.

Signature:		Date:	

Using self-assembly techniques for green lubrication solutions in tribological contacts

Doctoral thesis

Simon Watson

Primary supervisor: Prof Ling Wang

Second supervisor: Dr Mengyan Nie

Third supervisor: Prof Keith Stokes

Abstract

This thesis presents a novel lubrication solution for silicon nitride hybrid bearings developed through the use of polymer brush technology, specifically brushes created using surface initiated atom transfer radical polymerisation. This work also details a novel testing regime utilising custom colloidal probes to replicate, for the first time, this hybrid bearing under atomic force microscopy in both dry and lubricated conditions. Due to their promising tribological properties polymer brushes have the potential to be a lubrication solution for the hybrid bearing system where current lubrication solutions are not tailored to the surfaces and contain harmful components such as sulphur and phosphorus. Polymer brush systems have generated considerable interest in the academic community as a possible new greener lubrication solution.

To further understand the mechanism by which an effective polymer brush can be employed in a tribological contact this study was initiated. As the first known study to investigate the effect of the polymer brushes on the silicon nitride-steel contact, previous literature findings have been reapplied to a novel material for a novel application.

Grafting from the silicon nitride surface ensures that less additive competition will occur. Poly(methyl methacrylate) (PMMA) brushes were chosen for the reduction of steric hindrance within the polymer chain therefore allowing a higher density brush and better load carrying capacity in a tribological sense. These brushes act synergistically with a poly-alpha-olefin, a high quality base oil lubricant present in the type of engine where these hybrid bearing operate. The synergy here refers to the swelling effect in which the anchored macromolecule and base oil work as one to repel the asperity contacts, reducing friction whilst the brush system protects itself.

The formation of polymer brushes on a silicon nitride surface utilises atom transfer radical polymerisation (ATRP) and activators regenerated by electron transfer (ARGET) coupled with a surface initiation step. Initiating from the surface allows a strong covalent bond to the contact surface ensuring stability when the final brush is subjected to physical interactions, the main advantage being that by adding monomer molecules individually in situ the steric interaction of the chain-chain iterations in the growing brush is reduced so denser films can be formed, especially with small molecules such as MMA. By applying recent developments such as ARGET synthesis of the polymer brush is made much easier, as this technique allows reactions to occur with limited amounts of oxygen present as well as reducing the quantity of the copper complex needed for the reaction.

By investigating the chemical and mechanical properties of the polymer brush with techniques such as ellipsometry, atomic force microscopy (AFM), and x-ray photoelectron spectroscopy (XPS), it is possible to suggest explanations for the tribological properties of the polymer brush system. Detailed XPS analysis shows that bromine is still present at the surface, a key indicator that the

functional sites of the polymer process are still available to be bonded for increasing the chain length while also indicating that fewer termination reactions had occurred. With a lack of silicon visible in the XPS sample spectra it is clear that the polymer has achieved good surface coverage and should therefore exhibit better tribological characteristics. By using novel, custom made stainless steel colloidal probes, it has been possible for the first time to replicate the hybrid contact on the nanoscale, which allows high quality testing by accurately replicating the materials in contact and thus an effective evaluation of the lubrication solution. The importance of the polymer thickness, measured by ellipsometry, and the liquid in which they are solvated, is clearly elucidated by testing in multiple fluids, when highly synergetic fluids like the poly-alpha-olefin result in a significant reduction in friction whereas poor solvents like water can even be detrimental when compared to the bare surfaces in contact. In the worst case scenario under the highest load using the novel probes the lubricated polymer brush reduced the friction force successfully from 3.3 nN to 1.3 nN when compared to the bare nitride surface.

Preliminary work has been completed in respect to the transition from the nanoscale to the macroscale, and the polymerisation reaction has been scaled from 1 cm^2 silicon nitride wafers up to a 10 cm diameter silicon nitride discs. One of the reasons why the polymerisation can be scaled in such a way is due to the ARGET technique which allows polymerisations to occur in the presence of limited amounts of air. A tribological study of these PMMA modified disc surfaces using a pin-on-disc setup shows favourable results and on average a reduction of friction of 15% when comparing PMMA modified surfaces with unmodified ones in an oil lubricated environment.

Table of Contents

List of Figures

List of Appendix Figures

List of Schemes

List of Tables

Abbreviations

AFM	Atomic Force Microscopy
AIBN	Azobisisobutyronitrile
APTES	3-Aminopropyltriethoxysilane
APTMS	Aminopropyltrimethoxysilane
ARGET	Activators Regenerated By Electron Transfer
ATRP	Atom Transfer Radical Polymerisation
C12PA	Dodecylphosphonic
C18PA	Octadecylphosphonic
CFM	Chemical Force Microscopy
COF	Coefficient Of Friction
DCCD	N,N'-Dicyclohexylcarbodiimide
DCM	Dichloromethane
DLA	Diffusion Limited Aggregation
DLC	Diamond Like Carbon
DMF	Dimethylformamide
DSA	Drop Shape Analysis
DTS	Decyltrichlorosilane
EBIB	Ethyl 2-Bromoisobutyrate
EDX	Energy-Dispersive X-Ray Spectroscopy
FHOTS	Tridecafluoro-1,1,2,2-Tetrahydrooct-1-yl)Trichlorosilane
FOTS	Perfluorooctadecyltrichlorosilane
GO	Graphene Oxide
GPC	Gel Permeation Chromatography
HMTETA	1,1,4,7,10,10-Hexamethyltriethylene-Tetraamine
HTS	Hexyltrichlorosilane
IR	Infrared Spectroscopy
MAC	Multiply-Alkylated Cyclopentane
Me_6TREN	Tris(2-Dimethylaminoethyl)Amine
MEMS	Microelectromechanical system
MMA	Methyl Methacrylate
M_n	Number Average
MoDTC	Molybdenum Dithiocarbamates
MPTS	(3-Mercaptopropyl) Trimethoxysilane
M_w	Molecular Weight Average
NEMS	Nanoelectromechanical system

NMP	Nitroxide Mediated Polymerisations
NMR	Nuclear Magnetic Resonance
ODS	Octadecyldimethylchlorosilane
OTC	Octylthiocyanate
OTS	Octadecyltrichlorosilane
P12MA	Dodecyl Methacrylate
P18MA	Octadecyl Methacrylate
P6MA	Hexyl Methacrylate
PAO	Polyalphaolefins
PDI	Polydispersity Index
PEI	Polyethyleneimine
PEO	Poly(Ethylene Oxide)
PFDS	Perfluorodecyltriethoxysilane
PFPE	Perfluoropolyether
PI	Polyimide Film
PLL-g-PEG	Poly(L-Lysine)-Graft-Poly(Ethylene Glycol)
PMDETA	N,N,N',N'', Pentamethyldiethylenetriamine N''
PPO	Poly(Propylene Oxide)
RAFT	Reversible Addition Fragmentation Chain Transfer
RF	Radio Frequency
RGO	Reduced Graphene Oxide
ROMP	Ring Opening Metathesis Polymerisation
ROP	Ring Opening Polymerisations
RSC	Royal Society Of Chemistry
SAM	Self-Assembled Monolayers
SEM	Scanning Electron Microscope
SI-ATRP	Surface Initiated Atom Transfer Radical Polymerisation
STA	Stearic Acid
STM	Scanning Tunnel Microscopy
TEA	Triethylamine
TES	6-(3-Triethoxysilylpropylamino)-1,3,5-Triazine-2,4-Dithiol Monosodium
THF	Tetrahydrofuran
TPMA	Tris(2-Pyridylmethyl)Amine
UTS	Undecyltrichlorosilane
XPS	X-Ray Photoelectron Spectroscopy
ZDDP	Zinc Dialkyldithiophosphate

List of Publications

Journal publications

S. Watson, M. Nie, L. Wang, and K. Stokes, "Challenges and developments of self-assembled monolayers and polymer brushes as a green lubrication solution for tribological applications," RSC Advances, vol. 5, pp. 89698-89730, 2015.

S. Watson, S. Dennington, L. Wang, M. Nie, S. Hinder, and K. Stokes, "Polymer brush lubrication of the silicon nitride-steel contact: a colloidal force microscopy study," RSC Advances, vol. 7, pp. 42667-42676, 2017.

Conference Publications

S. Watson, L. Wang, M. Nie, K.R. Stokes, “Using self-assembly techniques for green lubrication solutions in tribological contacts” presented at the annual PGR conference, 2015.

S. Watson, L. Wang, M. Nie, K.R. Stokes, “Development of polymer brushes for the lubrication of silicon nitride–steel contacts” presented at the annual PGR conference, 2016.

S. Watson, L. Wang, M. Nie, and K. Stokes, "Development of polymer brushes for the lubrication of silicon nitride-steel contacts," presented at the 71st STLE Annual Meeting and Exhibition, 2016.

S. Watson, L. Wang, M. Nie, S. Hinder, and K. Stokes, "Polymer Brushes for Silicon Nitride-Steel Contacts: a Colloidal Force Microscopy Study," presented at the 72nd STLE Annual Meeting and Exhibition, 2017. **(Invited talk)**

Acknowledgements

I would like to thank all of my supervisors for their support thus far and in the future. I would also like to thank Dstl and EPSRC for their invaluable support. Particular thanks must go to Alistair Clark for help with EDX, SEM, and CA measurements and Dr Jurgita Zekonyte for spending a considerable amount of time helping with AFM. I am also grateful for the help from Dr Neil Wells for running the NMR samples. Thanks to Zondy Webber for assistance with both the deposition of the silicon nitride and ellipsometry. Thanks to Dr Terry Harvey for assistance with pin-on-disc. Many thanks to Dr Simon Dennington, if your guidance was not there this project would have struggled, I am very grateful for your input and I have learnt a great deal from you. The XPS completed here has been done in collaboration with the University of Surrey, so thanks to Dr Steve Hinder for help with the instrument and analysis. The GPC results have been done by the University of Durham so my thanks to Professor Lian Hutchings for his assistance. To Sue and Katherine, and by extension the entire admin team for their endless help. I am particularly grateful to everyone in 4061 for their proofreading skills as well as useful discussions. Thanks to my parents for everything they have done for me. Last but not least, special thanks to my wife, Chelsea, for pretending that you are genuinely interested in the lubrication of silicon nitride hybrid bearing systems.

1 Introduction to Project Background

Whenever two surfaces come into contact there will be energy wasted due to friction which will result in wear or degradation of the surfaces. In the privately owned passenger vehicle market as well as heavy goods vehicles and buses, a third of the energy from fuel is used to overcome friction [1, 2]. Significant areas of friction that need to be overcome are from such components as the drive train, engine and transmission, tyres and brakes. One way to reduce fuel expenditure on friction is to utilise correct and efficient lubrication solutions. Current liquid lubrication solutions are generally in two classes, organic friction modifiers and organomolybdenum compounds [3, 4]. Organic friction modifiers include carboxylic acids/free fatty acids, alcohols, esters and amines [4]. There are two accepted mechanisms that explain the mechanism of lubrication for organic friction modifiers. One mechanism is that the polar functional groups of the friction modifier adsorb onto the metallic surface, much like self-assembled monolayers (SAMs), and the carbon chains form a barrier to prevent substrate-substrate adhesion thus lowering friction [3, 5, 6]. The other mechanism is semi-ordered viscous multilayers forming on the surface preventing contact [3, 5, 7]. Free fatty acids are still used today to reduce friction, this is due to their ability to create closely packed monolayers on the metallic contact surfaces [5, 8]. Long chain amines are used in clutch systems, lubricated sliding contacts and MEMS devices [3, 9, 10]. Molybdenum dithiocarbamates (MoDTC) have been introduced into engine oils since the 1950s as antiwear additives, however, it was not until the 1970s where its application as a friction modifier was realised [3, 11]. However, MoDTC has been reported to form MoO_3 resulting in high wear rates as MoO_3 is abrasive [4, 12]. The decomposition of MoDTC produces MoS_2 sheets that bond onto surface asperities therefore reducing friction [4, 13-16]. The role of zinc dialkyldithiophosphate (ZDDP) and MoDTC has been reported as the additives are shown to synergize well [3, 4, 16]. However, in the current economic climate there is a greater need for more effective lubricants, this is complicated by new limits on the amount of sulphur and phosphorus that can be used in lubricating oils [17, 18]. The removal of sulphur and phosphorus in lubricating oils is required due to the effect they have on catalytic converters and increasingly rigorous emissions regulations [19]. The oxides of these elements are believed to come from the additives of lubrication and will block filters and reduce the effectiveness of catalysts in converters [19].

SAMs are thought to be a new lubrication solution and the relatively simple procedure for SAMs has definitely inspired researchers to develop new lubrication solutions in order to meet new regulations. Lubrication systems for tribological contacts such as engines have had SAMs applied with good effect. The ability of SAMs to form on a variety of surfaces has attracted tremendous effort to investigate applications of SAMs in surface engineering and tribological systems, such as

artificial joints, orthopaedic implants, corrosion protection and friction reduction [20, 21]. Lubrication solutions based on SAMs have been proven to be successful, especially for nanoelectromechanical systems and microelectromechanical systems (NEMS/MEMS), where normal lubrication methods are not suitable [22-24].

Since SAMs are typically only a few nanometres thick, their mechanical properties such as shear resistance may not be sufficient for friction reduction in tribological contacts [25, 26]. Polymer brushes have been considered to be a better lubrication solution than SAMs. Polymer brushes can reduce friction to very low levels with increased resistance to shearing in addition to higher resistance to compressive forces.

Controlled radical polymerisation techniques such as atom transfer radical polymerisations (ATRP), have been proven to produce high density, thick polymeric films capable of successfully reducing friction [27, 28]. Developments such as activators regenerated by electron transfer and surface attached initiators further strengthen the possibilities of polymer brushes. However, these processes may be too expensive to be easily adopted as an alternative to existing lubricants. The expense is likely to come from ensuring that the polymers are grown in a controlled way in the correct place. This is complicated when the fact that a chemical reaction has to take place in solution in a unique environment. The synergy with other compounds must also be considered in addition to addition of copper catalysts into the lubricating oil as well as applying them in situ.

Silicon nitride rolling element bearings have seen great success as hybrid bearing systems. Applications include automotive, aerospace, renewables and the railway industry. The main sought after property is the relative lightness of the ball bearing, with a 60% reduction in weight resulting in an 80% reduction in friction compared to classic steel bearings [17]. Compared to steel on steel contacts the coefficient of friction (COF) of hybrid systems is reduced to approximately 0.04-0.09 under oil lubricated conditions and between 0.1-1.0 for dry conditions [29]. However, most lubrication and protection solutions rely on lubricating the counter surface rather than silicon nitride.

1.1 Aims and Research Objectives

The main aim of the project is to develop a new lubrication solution for silicon nitride hybrid bearing systems. This must perform better than the current SAM technologies and conform to sulphur and phosphorus regulations. A number of objectives, as set out below, have been accepted as necessary steps to successfully provide a solution.

1. Complete a comprehensive literature review on both SAMs and polymer brushes to gain a key insight to the challenges present in the research field. This review will also look into what is missing in the state of the art research, therefore allowing a novel research route to be pursued.
2. Reproduce the work on SAMs formed on silicon nitride substrates previously completed at Southampton University and try to improve the SAM preparation methods. Critical to the

success of this step is the factors that are deemed to influence SAMs as discussed in the literature review.

3. Synthesize SAM based initiators and make use of the knowledge of SAM preparation on silicon wafers for silicon nitride substrates. This objective must also include any new information detailing the results of variables changed such as temperature, solvent and substrate.

4. Create polymer brushes via ATRP and evaluate the tribological performance of the resultant polymeric films.

5. Use novel characterisation methods to replicate the hybrid contact in nanoloaded conditions

6. Optimize polymer brushes tribological performance and scale up the formation of the synthesis so macro testing can be completed.

1.2 Structure of Report

This report contains six distinct sections, the first two sections contain an in depth literature review of both SAMs and polymer brushes. Provided in these sections are the state of the art solutions with regards to tribological contacts with silicon wafers and silicon nitride as focus materials. Also detailed are characterisation methods as well as ideal scenarios for synthesis of both SAMs and polymer brushes. The next section, titled “methodology” describes the way that the final aim of the project will be achieved, this includes the experimental plan. The main results are then discussed in the following section preceding a concluding section, in this section some of the preliminary work to enable future investigations is presented. The future work plan detailing further pin-on-disc testing is laid out in the last section. This concludes the main body of the report, additional information can be found in the appendix at the end of the report in addition to references.

2 Literature Review on SAMs

2.1 SAMs

SAMs are molecular assemblies formed spontaneously on surfaces by adsorption that are organised into ordered domains. SAMs were first reported by Zisman in 1946, where a monolayer was formed on a clean metal substrate to change the wettability of the surface [30]. Unfortunately little recognition of SAMs was gained till 1983, when Nuzzo and Allara discovered that SAMs can be prepared on gold (Au) by adsorption of di-n-alkyl disulfides from a diluted solution avoiding the use of moisture-sensitive chemicals and crystalline metal surfaces [31]. Over the past 30 years, a tremendous amount of research has been carried out to develop various SAMs and to investigate their functions and applications.

This section describes the formation mechanisms of SAMs on solid surfaces, the factors that are found to influence the quality of SAMs, the techniques that have been used to characterise SAMs and the challenges and the state-of-the-art development of SAMs as a lubrication solution.

2.2 SAM Formation Mechanisms

SAMs can be formed on surfaces either from a solution or through vapour deposition, while the former is more popularly used. Having selected a particular chemical for a SAM, it is usually dissolved in an appropriate solvent before a clean substrate is immersed or dipped into the solution for the monolayer to 'grow'. The growth rate and the structure of the SAM not only depend on the type of the molecule and the surface chemistry of the substrate, but also the concentration of the molecule and immersion time [17, 32-35]. Details of these factors will be discussed in the following sections.

A number of typical SAM structures are shown in Figure 2.1, illustrating some choices of the chemicals (e.g., a variety of head groups, chain/spacer types and functional/end groups) and the types of substrates being investigated [17, 32-36]. All SAMs are formed in a similar way, i.e., usually through various types of adsorption through head group-substrate interactions. The reactions between the molecule and the substrate can however be complicated, depending on the chemistry of the two. For example, the reactions of a trichlorosilane and trimethoxysilane with a hydroxyl group on a surface and their by-products are shown in Equation 2.1 and Equation 2.2 where "R" denotes the rest of the molecule. It can be seen that the trichlorosilane SAM has a hydrochloric acid by-product while the trimethoxysilane produces a methanol. This has to be carefully considered when choosing SAMs for engineering applications especially when corrosion is a problem. In another example for thiols on gold, a two-step reaction takes place, shown in

Equations 3 and 4 [21]. The thiol is firstly physisorbed onto the Au surface followed by S-H cleavage and chemisorption.

$$R - SiCl_3 + 3(-OH) \rightarrow R - Si - O_3 - \ + 3HCl \qquad \textit{Equation 2.1}$$

$$R - Si(OCH_3)_3 + 3(-OH) \rightarrow R - Si - O_3 - \ + 3CH_3OH \qquad \textit{Equation 2.2}$$

$$R - SH + Au \rightarrow R - SH_{Phys}Au \qquad \textit{Equation 2.3}$$

$$R - SH_{Phys}Au \rightarrow R - S - Au + \frac{1}{2}H_2 \qquad \textit{Equation 2.4}$$

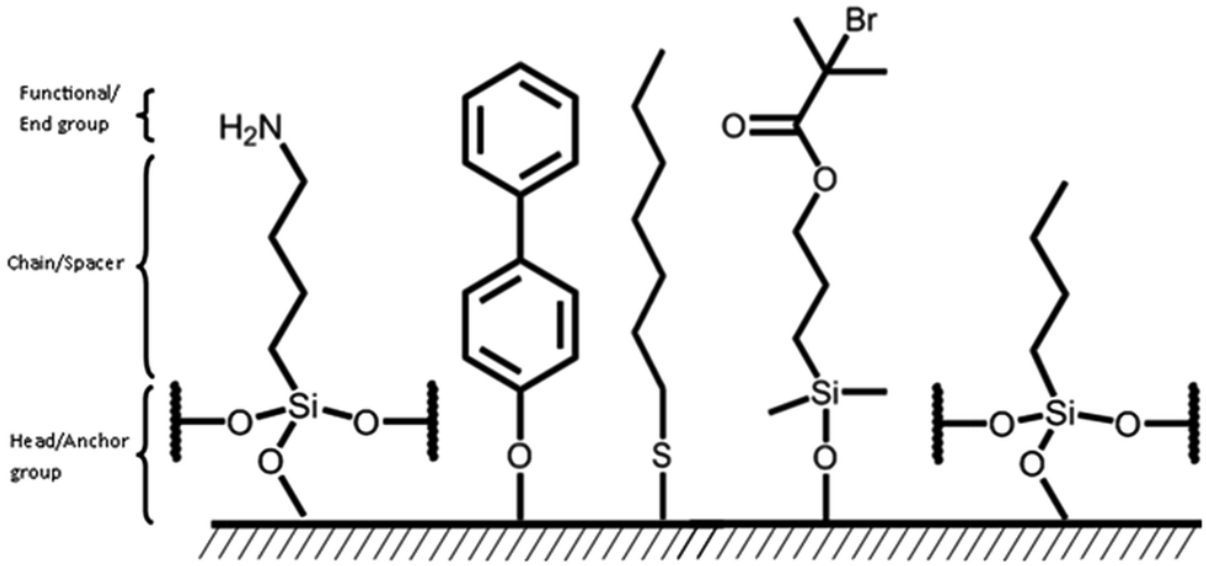

Substrates: Au, Si, SiO2, Fe, Ti

Head/Anchor groups: -SH, -SiCl3, -OH, -Si(CH3)2Cl, -Si(OCH3)3

Chain/Spacer: Alkyl, Aryl, Ethyleneglycol

Functional/End group: NH2, CH3, COOH, NO2, OH

Figure 2.1. A schematic illustration of SAMs formation.

2.2.1 SAM Formation Kinetics

Apart from surface preparation conditions, solvent and concentration of SAM solutions, the kinetics of SAM formation are also influenced by the types of SAM molecules and substrates [37].

- *Growth Rate*

As concluded by many researchers, the first minute of immersion has been found to be the most important time where SAMs grow at the highest rates. As Aswal *et al.* showed in their studies, an 85% coverage of an octadecyltrichlorosilane (OTS) monolayer on silicon (Si) was achieved within 50 s of immersion [38]. In a similar study of OTS on silicon, Balgar *et al.* also achieved approximately 80% coverage within 1 minute of immersion [39]. The reactivity of head groups has been found to affect their adsorption rate. For example, when OTS and octadecyltrimethoxysilane SAMs were formed on silicon nitride (SiN) under the same conditions, a complete monolayer of OTS was formed after 5 minutes of immersion while the octadecyltrimethoxysilane took 120 minutes due to the more reactive head group of OTS [17]. This is because the bond dissociation

energies required for OTS to replace the groups attached to the silicon atom with hydroxyl (OH) groups prior to adsorption are much lower than that for octadecyltrimethoxysilane [40].
The formation of SAMs for both thiols on gold and silanes on silicon is found to follow a same two-step process (illustrated in Figure 2.2, using information from [30, 41]).

1. Step 1 is a fast linear growth step following the Langmuir adsorption model. The Langmuir model explains the absorption of SAMs by treating them as an ideal gas in isothermal conditions. This also treats the active sites on flat plane of the surface as equal opportunities to adsorb onto. The growth in this step is limited by head-substrate interaction but can achieve up to 85% of the maximum coverage and near the maximum achievable contact angle. The duration of this step can range from a few seconds to a few minutes depending on the concentration of the precursor molecules.
2. Step 2 is a slow growing process and can take hours to complete. During this step, the SAM coverage plateaus and reaches to its maximum eventually. The maximum coverage is limited by adsorption from solution such as chain disorder interference.

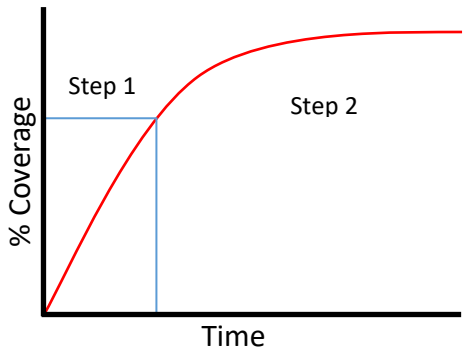

Figure 2.2. An illustration showing the two-step formation process of SAMs.

During the self-organizing process, step 2, the molecules in SAMs rely on weaker and less directional bonds, such as ionic bonds, hydrogen bonds, and van der Waals interactions, to organize atoms, ions or molecules into ordered structure, with the molecules or ions adjusting their own positions to minimize the thermodynamic energy. That is to say, the kinetics and equilibrium of SAM formation involve a delicate interplay between molecule-solvent interactions, substrate-adsorbate interactions, non-bonded interactions between adsorbates, and intra-molecular interactions such as bond stretches, angle bends, and torsion. Both chemisorption and intra- and inter-chain non-bonded interactions (e.g., van de Waals, steric, repulsive, and electrostatic forces) contribute to the packing and ordering of molecules in SAMs. The conformation of the individual chains within the assembly, and their packing and ordering with

respect to each other depend on the balance between inter-chain forces, the interactions with the surface, and the entropic effects as well.

- *Growth Characteristics*

Bierbaum *et al.* found that OTS monolayers appeared to grow from island like concentrations of SAM [37]. Similarly, Balgar *et al.* and Aswal *et al.* found that OTS as well as other long chain SAMs grew in an island-like model but not short chain SAMs [38, 39]. This is known as island nucleation growth.

In another experiment, Bierbaum *et al.* found that propyltrichlorosilane reacted with a clean silicon wafer extremely quickly and therefore it was not possible to determine whether island growth had occurred, possibly due to the shorter chain length not obscuring other sites for SAM adsorption [37]. They also found that propyltrichlorosilane did not achieve expected levels of contact angle for a CH_3 terminated SAM and suggested that the disordered monolayer was formed by short chain SAMs, which have small van der Waals forces that were not sufficient to force chains into order [42].

As shown in Figure 2.3, the OTS SAMs were grown initially from nucleation points on the silicon wafer where single molecules attached to the substrate, subsequent growth from these molecules is visible in 20 s [39]. The growth of a single island was indicative of diffusion limited aggregation (DLA). DLA is a process of aggregation formed by diffusion, where a mobile molecule will contact an already adsorbed molecule and form a cluster [43]. As the cluster grows an irregular shape can be formed. Branched structure can also be formed due to the low probability of a molecule contacting the middle of the cluster. The irregular shape is known as a fractal shape and is related to DLA [39, 44, 45]. However, adsorption in a solution can be considered to be a 3D adsorption model and the fractal shape may not be as pronounced. The cluster has been found to be the same height as the final monolayer, indicating that the molecules are “standing up” and held in ordered domains by van der Waals forces [39]. After reaching to a certain island size, new islands will be formed rather than adding to the existing ones. This continues until the monolayer is complete. Figure 2.3 shows the formation of an OTS monolayer from agglomerations to fractal shape to near full monolayer. Between 20 and 50 s it is clear that islands are growing, it is also notable that there are smaller islands appearing that are represented by small white dots. From 75 s the islands are seen to grow until they are indistinguishable from others. In excess of 90 s it would be expected that the monolayer would form in full.

Apart from OTS [32, 37-39, 46-48], the island nucleation growth has also been seen in the SAM formation of C12 alkylsilane [49], 3-aminopropyltrimethoxysilane [50], octadecylphosphonic acid [45, 51], octadecyltrimethylammonium bromide [45], (3-glycidoxypropyl)trimethoxysilane [52], octadecylamine [53], and 6-(3-triethoxysilylpropylamino)-1,3,5-triazine-2,4-dithiol monosodium [54].

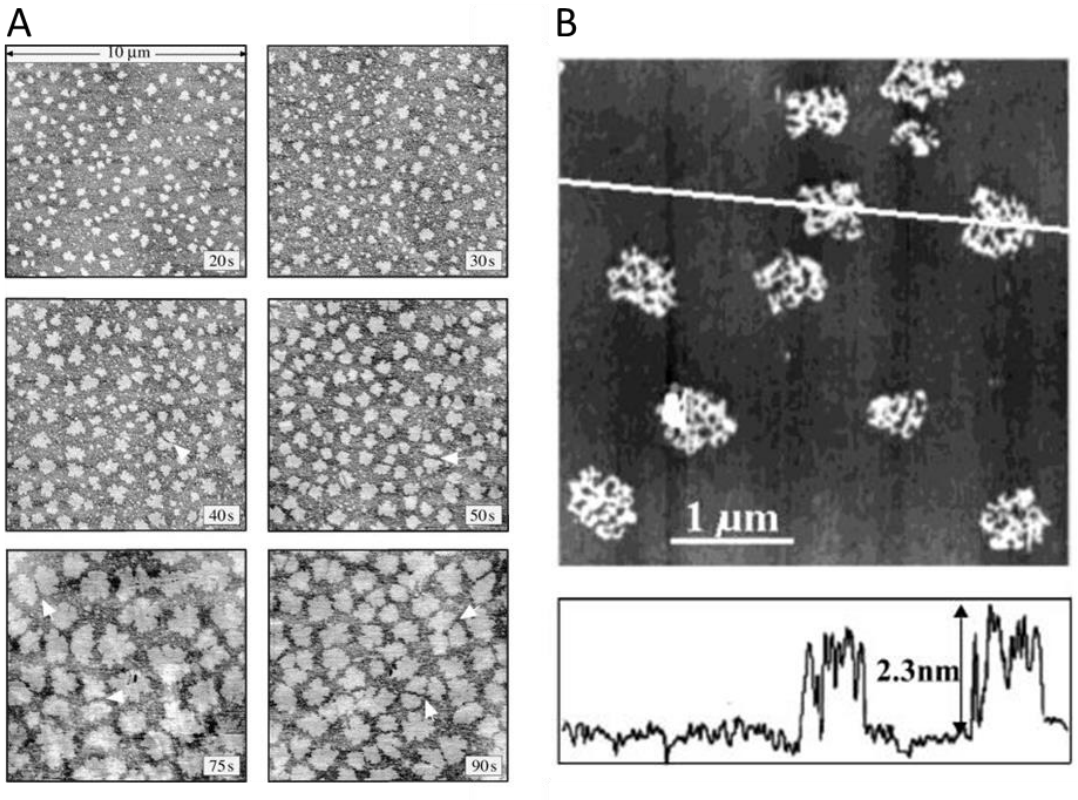

Figure 2.3. (A) OTS monolayer growth over time, from partial island growth to full monolayer. 10µm x 10µm sample on Si wafer. Reprinted with permission from [39]. (B) Is a line profile of the OTS monolayer clusters showing heights which coincide with the theoretical SAM height. Reprinted with permission from [55].

Although thiols follow the same adsorption steps as silanes described in Figure 2.2, they appeared to have different growth characteristics. Thiols are thought to go through a number of steps as illustrated in Figure 2.4 [21, 56]:

A. Thiol molecules are physically adsorbed onto the surface, see Equation 2.3;
B. Thiol molecules are covalently attached to the substrate and are in the “lying down” phase, see Equation 2.4;
C. As more molecules adsorb onto the surface, thiol molecules become denser and start the “standing up” phase;
D. The complete ordered monolayer is formed as more molecules from solution adsorb.

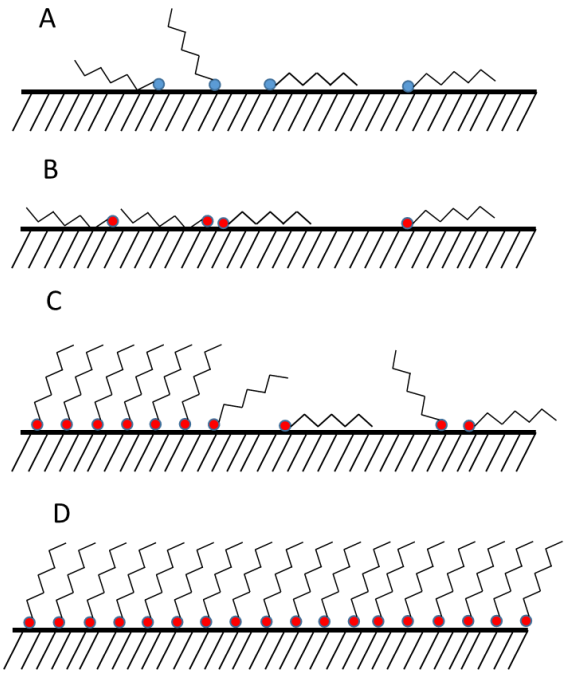

Figure 2.4. Illustration of thiol based SAM growth on gold from physisorption, covalent bonding, "standing up" to a complete ordered monolayer.

2.3 Factors Influencing SAM Formation

The growth rate and structure of SAMs are found to be affected by a large number of factors such as substrate surface preparation and cleaning process, concentration of the chemical, type of solvent, immersion time, humidity, and substrate orientation etc. [17, 32-35]. This section reviews the influence of key factors on SAM formation.

2.3.1 Surface Preparation

As mentioned above, the kinetics and equilibrium of SAM formation heavily rely on the surface chemistry and the type of molecule. Therefore, the surface chemistry and cleanness of the substrate would play a determinant role in the formation process and the quality of the formed SAMs. It has been found that dust and chemical residues on the substrate during surface cleaning can have a detrimental effect on the quality and coverage of SAM. A range of techniques have been adopted in surface preparation prior to creating SAMs.

A standard surface cleaning procedure involves ultrasonic cleaning in different solvents to remove surface containments and blow drying to get rid of solvents residues and dusts, but an additional step of hydroxylation is usually needed for silicon-based or metal oxides substrates. During the ultrasonic cleaning, the commonly used solvents are toluene, isopropanol, chloroform, acetone, deionised water, and ethanol. A normal procedure would involve cleaning the surface in a polar, then nonpolar, solvent to remove as many residues as possible. After the surface is cleaned, it is rinsed in deionised water then dried in air, argon or nitrogen [17, 57-64]. For systems that require a highly hydroxylated surface to form a high quality SAM a surface oxidation treatment is also employed using either piranha or plasma treatments.

Piranha hydroxylation treatment uses a solution of concentrated sulphuric acid (98%) and hydrogen peroxide (30%) at a ratio of 7:3, 4:1 or 3:1 vol:vol [32, 33, 46, 48, 54, 57, 59, 60, 64-78]. Silicon wafer samples are typically immersed in the solution at a temperature between 60 and 90°C for a duration of 30 to 60 minutes, although the majority of the studies chose to immerse their samples at 90°C for 30 minutes. The piranha treatment has been found to be an effective method to create a good OH-terminated surface where very low water contact angles of less than 10˚ can be achieved.

The plasma process is conducted through an oxygen plasma treatment, where suitable hydroxylation can be achieved within a few minutes. Plasma treatment will leave silicon-based substrates hydroxyl terminated in significantly less time than piranha [68, 79-81]. Wu *et al*. concluded that 10 minutes plasma treatment on silicon wafers resulted in a water contact angle of less than 5° indicating a very good OH-termination coverage [82]. Wiegand *et al*. also achieved similar contact angles on silica (100), SiO_2, surface using plasma treatment in less than 5 minutes [83]. In this work a PVA TePla 300 plasma asher was used for silicon wafer surface pre-treatment. Oxygen/nitrogen gas mix was used and wafer samples were loaded via placing in a petri dish, the petri dish containing wafers was then placed on a quartz boat and inserted into the chamber. Wafers are automatically processed with user pre-set conditions.

As an extra surface preparation, hydrofluoric acid (HF) is sometimes used as an etchant to remove native oxide layer for one of two reasons. For example, hydrofluoric acid can be used to etch SiO_2 leaving the substrate hydrogen terminated. Some authors used this treatment to enable the attachment of monolayers directly to the silicon atoms [22, 84, 85]. However, the monolayers formed are not strictly self-assembled as they require UV induced coupling or elevated temperatures [86-88]. Another reason surface etching using HF is to reform an oxide layer with a consistent depth by controlling the immersion time in piranha. Wang *et al.* achieved roughness of less than 0.5 Å that allowed them to grow ultra-smooth monolayers [48].

Although similar results are achievable from the piranha and plasma treatments, the former is more popular mainly due to the implementation of standard laboratory chemicals with a facile method. However, piranha is known to be a dangerous solution which requires careful handling and disposal. Any contact with organics can result in explosions and improper storage of waste in sealed containers have both resulted in injuries. Conversely, plasma treatment instruments add additional costs to processing substrates and for ultra-clean wafers it is known that clean room conditions are favourable. The influences of these techniques will be further discussed later in this review.

2.3.2 Solvent Selection

The solvent, in which SAM precursor molecules are dissolved, is also paramount to the successful adsorption of SAMs, as solvent properties, including polarity, solubility, molecular diameter and

viscosity, can affect solvent-substrate interactions and solvent-adsorbate interaction during SAM formation. Lee *et al*. observed with scanning tunnel microscopy (STM) that octylthiocyanate (OTC) SAMs formed on Au(111) in ethanol had a structure of mixed phases composed of ordered domains and disordered phases, but those formed in dimethylformamide (DMF) and toluene exhibited long-range ordered domains [89]. Manifar *et al.* explored the effect of solvent on the formation of OTS SAMs by comparing the contact angle of water on the OTS SAMs using hexane, toluene, ether, dichloromethane (DCM) and tetrahydrofuran (THF) as deposition solvents after immersion in 10 mM solutions for 6 h. Toluene outperformed the other solvents by producing a surface with a contact angle of more than 10° higher. By comparing dipole moments and partial charge distribution of OTS and the used five solvents, the authors postulated that solvent molecules with large dipole moments and being highly charged can help the formation of more uniform SAMs with the capability of hydrogen-bonding and highly localized partial charge which facilitate the attachment of OTS onto the surface [33]. Rozlosnik *et al.* compared toluene with heptane and dodecane and found that multilayers were formed using dodecane [55]. However, it is thought that the multilayers were physisorbed and could be easily removed by a glove dipped in hexane. Heptane also produced a full coverage of OTS SAM similar to other solvents, however toluene was still regarded as the best [55]. The reason for this is due to different solubility of water in these solvents, which can affect adsorption process of OTS on the hydrophilic silicon oxide surface.

In addition to solvent choice, water content is of a particular concern, especially for silanes, since the presence of water is required for initial hydrolysis of trichlorosilane group. However, too much water present in the solvent leads to polymerization of OTS in bulk solution, which competes with the surface reaction of single alkylsilane molecules for the monolayer formation [90]. McGovern et al. stated that the optimum water content in a solvent is 0.15 mg/100 mL [91]. The authors also found that less moisture can facilitate the formation of well-defined monolayer on the silicon substrate but slower adsorption kinetics, sometimes resulting in an incomplete monolayer. In anhydrous conditions, even in an argon-filled glove box, water is still present as a layer adsorbed on the silicon oxide surface, which can assist hydrolysis of chlorosilanes but confine the reaction to the oxide layer [41, 92].

2.3.3 SAM Precursor Concentration

From the points of view of kinetics and equilibrium of the SAM formation, the concentration of the precursors in the deposition solution would not only influence the SAM growth rate but also the structure of the SAMs. A compromise between the deposition time and the SAM quality is usually needed in order to achieve the desired surface properties in a reasonable time. For example, thiol based SAMs can be formed on gold in concentrations of 1 µM, however this can take up to a week to form a densely packed monolayer [93]. In practice, a considerably higher

concentration may be used to reduce the time required. It has been found that incomplete but notable monolayers can form under a minute at a concentration of 1 mM, see growth rate for more details [30]. Kulkarni *et al*. investigated the influence of SAM precursor solution concentration on the rate of OTS adsorption on silicon [32]. They tested a concentration range of OTS in toluene from 0.05 mM to 1 mM and found that the higher the concentration the faster the monolayer was formed. However, a full coverage was achieved by all concentrations after extended immersion durations. For example, a full SAM film was formed after 16 h of immersion in the 0.05 mM solution [32]. Wang *et al*. studied formation of OTS SAMs on silicon nitride and found that 2.5 mM was an optimum concentration for a good coverage over the range of 0.1-50 mM tested [17]. However, high SAM solution concentrations may lead to multilayer formation instead of the desired SAMs. Rozlosnik et al. found that high concentrations of OTS in poor solvent led to multilayers that were irregular or poorly distinguished [55]. It is generally considered that concentration and immersion time are inversely related but high concentrations and short immersion times promote monolayer growth [93].

2.3.4 Summary

There are a large number of factors that influence SAM formation. Apart from the ones discussed above, it is also important to understand the substrate because it dictates the selection of head groups. For example, -SH is suitable for Au/Ag/Pt etc. and silanes are more appropriate for oxide surfaces. It becomes more complicated if by-products from the reactions are also taken into account. For example choosing trimethoxysilanes over trichlorosilanes can avoid the production of corrosive hydrochloric acid. Silanes generally require extensively oxidized surfaces for stability hence plasma or piranha treatment can significantly improve the SAM quality. SAM growth is affected by both the solution concentration and immersion time. In general, a concentration between 1-5 mM is sufficient to form a good quality monolayer without wastage. Apart from the factors reviewed here, other factors such as humidity, age of SAM solution and substrate orientation, will also play a part in the fabrication of a perfect SAM.

2.4 Characterisation Techniques

As they form extremely thin layer of a few nanometers on surfaces, it is difficult to characterise and quantify SAMs. Over the years, a range of techniques have been used to confirm the formation of SAMs and characterise SAM properties, summarised in Table 2.1. Among them contact angle measurements, atomic force microscopy (AFM), X-ray photoelectron spectroscopy (XPS) and scanning tunnelling microscopy (STM) are most commonly used.

Table 2.1. A summary of the properties of SAM that can be collected through a selection of techniques

Properties of SAM		XPS	AFM/STM	XRD	Ellipsometry	IR	Raman	SFG	UPS	LEED	SIMS	SEM	RBS	ISS
Coverage	Overall coverage/ thickness	x	x	x	x	x								
	Pinholes	x	x							x	x	x	x	x
Elemental composition	Average	x											x	
	Surface	x												x
	Conc. profile	x											x	x
Functional groups	Bonding	x				x	x	x	x		x			
	Valence	x			x				x					
	Orientation	x	x		x	x	x	x	x					
	Conformation					x	x	x	x					
	Average composition	x				x	x	x	x		x			
	Depth profile	x			x			x	x		x		x	x
Ordering	Pinholes	x									x	x	x	x
	Long-range Dislocation		x			x			x			x		x
	Orientation		x		x	x			x			x		
	Interface ordering		x	x										
Substrate/SAM interface	Bonding	x			x	x	x	x	x		x			
	Pinhole		x							x		x		

Note: SFG, sum frequency generation spectroscopy; UPS, Ultraviolet photoelectron spectroscopy; LEED, low energy electron diffraction; SIMS, secondary ion mass spectroscopy; RBS, Rutherford backscattering spectroscopy; ISS, ion scattering spectroscopy.

2.4.1 Contact Angle Measurements

Contact angles are used to check the 'wettability' of surfaces, which is known to influence the friction and wear in tribological contacts of surfaces, and the effectiveness of SAMs in changing the surface's functionality [69, 94-98]. In addition, contact angle can give a representation of the coverage and quality of a SAM. Normally a deionised water droplet of a few microliters is pipetted onto the substrate of interest and the contact angle is measured based on the shape of the water droplet formed on the surface as illustrated in Figure 2.5, where angle Θ is defined as the contact angle. Hydrophilic surfaces typically are those with contact angles in the range of 0≤Θ≤90° whilst hydrophobic ones are Θ>90˚ [99]. When Θ is over 150˚, a surface is considered superhydrophobic [75, 99].

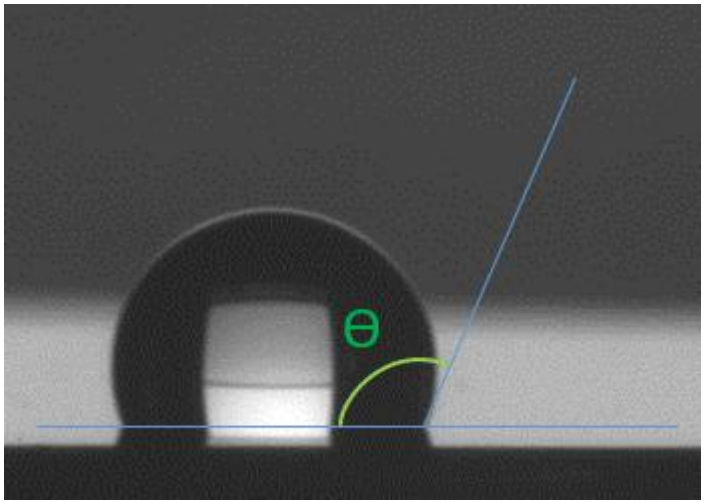

Figure 2.5. A sessile drop image detailing how contact angles are measured.

Contact angle measurements have been widely used in SAM characterisation due to the method's easy access, simplicity and low cost. Comparing the angles before and after surface modification provides an indication of whether and how well a modification has taken place. Some authors have made their own instruments due to the simplicity of the technique as well as carry out unique experimentation [100, 101]. Using a self-constructed instrument, Bormashenko *et al.* compressed the droplet with a precise moveable stage to study the Cassie-Wenzel transition. Contact angle calculations have also been utilised in surface energy calculations [95].

For ultra-hydrophilic surfaces (Θ <5°), water droplets may deform on the surface and it is difficult to obtain the contact angles [83, 102, 103]. Therefore, other liquids may be selected, such as diiodomethane, 1-bromonaphthalene, formamide, glycerol, or ethylene glycol [95, 104], to overcome this issue. However, different liquids will result in different contact angles; this is due to the difference in solid-liquid and liquid-liquid interfaces. Strong solid-liquid forces will result in the liquid spreading across a surface and therefore a low contact angle. Conversely, strong liquid-liquid interactions will cause liquids to stick together and therefore reduce contact angle. The surface tension at the solid-liquid interface is due to different intermolecular forces such as hydrogen bonding, polar interactions and acid/base interactions, for this reason changing probe

liquid can alter the shape of the sessile drop. Janssen *et al.* studied 21 different probe liquids on 11 different SAMs in addition to oxidised silicon wafers, where the different interactions and subsequent contact angles were observed [105]. For example, the contact angles for water and dichloromethane on a silicon wafer was found to be <10° and 14.4°, respectively. It is worth noting that the authors also could not consistently fit contact angles below 10° using the supplied software.

2.4.2 AFM

An AFM is an instrument that has been used to image SAMs on surfaces, providing topographic information such as surface profile and roughness. In addition, AFM has been used to study the growth of SAM by taking AFM scanning images at different stages, see Figure 2.3. 3D AFM images can provide details on the surface including nano-scale defects [106].

For nano-tribological studies of SAMs contact mode AFM is routinely used. Contact AFM investigates the friction between the AFM tip and the SAM surface. It measures single asperity contacts with an ultra-sharp cantilever without being influenced by the effect of surface roughness [23, 69, 107]. AFM is able to view both hard and soft surfaces in liquid as well as air, hence images of polymer brushes have been taken without collapsing [64, 108]. Figure 2.6A shows a 3D AFM image where dodecane residues are clearly seen within a fully covered OTS SAM on a silicon substrate. Although created intentionally Checco *et al.* show that many solvents can leave residues on surfaces as shown in Figure 2.6 [109]. Therefore, for high quality images to be taken these residues must be considered. Figure 2.6B is an example of an OTS SAM formed on a silicon wafer with a uniform film approximately the known height of OTS [32]. However, as this substrate was only immersed for 60 seconds it is unlikely that this is the smoothest SAM possible, see SAM Formation Kinetics, section 2.2.1. AFM has also been used to determine the thickness of SAM films by line profiles [32, 110, 111]. Figure 2.6C and D show an example of line profiling. Figure 2.6C is multiple-alkylated cyclopentane (MAC) deposited on top of a decyltrichlorosilane monolayer, the authors then concluded that the MAC layer was not uniform. MAC is thought to be a good lubricant due to a selection of desirable properties such as viscosity, volatility, pour point and thermal stability [112]. The droplets measured by AFM sectioning can be seen in D, and the ellipsometry height measurements were found to coincided with AFM vertical difference measurements [110].

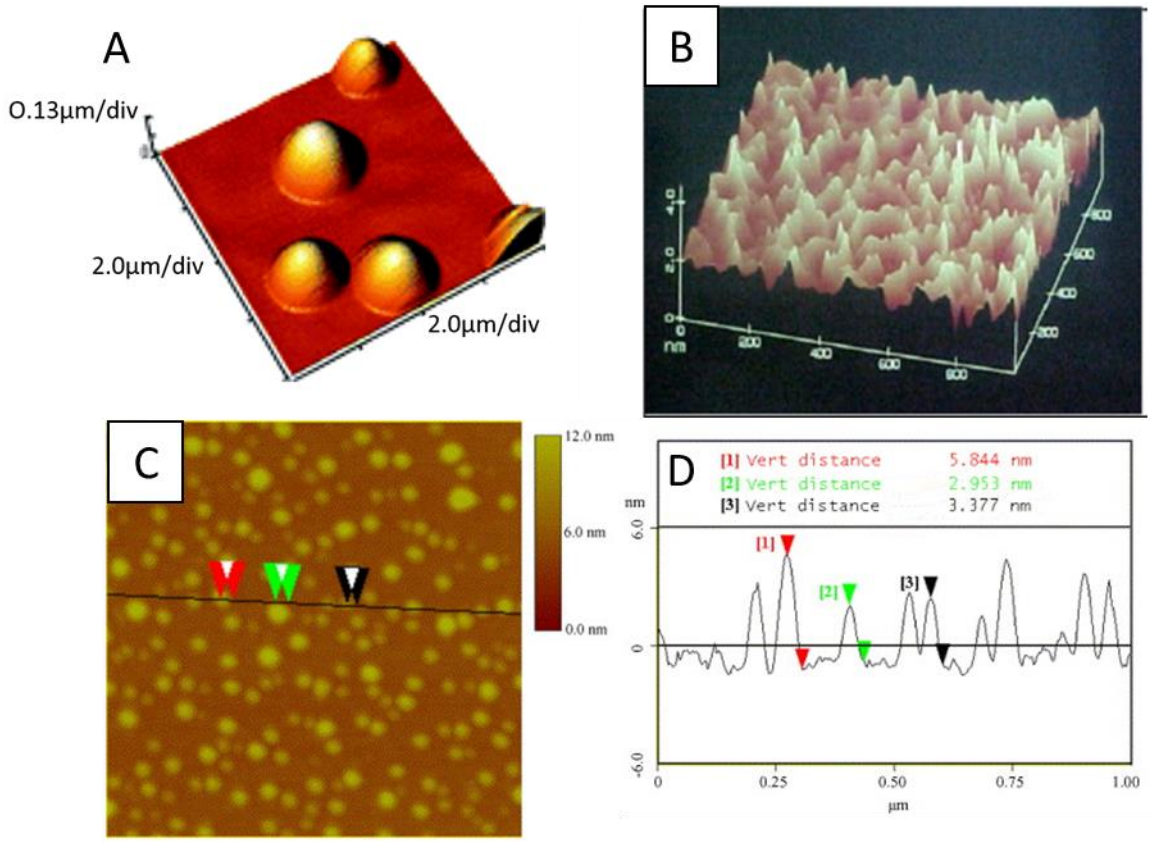

Figure 2.6. A is an AFM image showing dodecane residues on an OTS monolayer. Reprinted with permission from [109] Copyright 2006 American Chemical Society. B is a fully formed OTS monolayer on a silicon wafer. Reprinted with permission from [32]. C is a 2D image of multiply alkylated cyclopentane on top of a decyltrichlorosilane monolayer. Reprinted with permission from [110]. D is the corresponding section analysis with the line profile and markers indicated on C.

Figure 2.7 shows a simplistic version of the AFM in contact mode and particularly the twisting motion of the AFM cantilever. Therefore the cantilever spring constants are key parameters. Cantilever spring constants (*k*) were calculated for each individual cantilever by Thermal K methodologies [311]. *k* is the force required to bend the cantilever per unit of distance. This is usually measured in N/m. Nominal spring constants and ranges are supplied by manufacturers however slight changes will be present between cantilevers. Thermal K is a method where the cantilever is described as a simple harmonic oscillator and using the equipartition theorem the energy in the system at a momentum coordinate can be expressed as one half of the thermal energy of the system [312]. The equipartition theorem relates the temperature of a system with the average energies. Also key is the deflection sensitivity (α), this constant translates the cantilevers deflection from volts into nanometres. The deflection sensitivity is also calculated for each individual cantilever. This is completed through force distance curves. The force (F) between sample and tip can be calculated though Hooke's law as seen in $F=k.\alpha.V$. The deflection voltage (V) is measured directly through the quad photodiode detector as can also be seen in Figure 2.7.

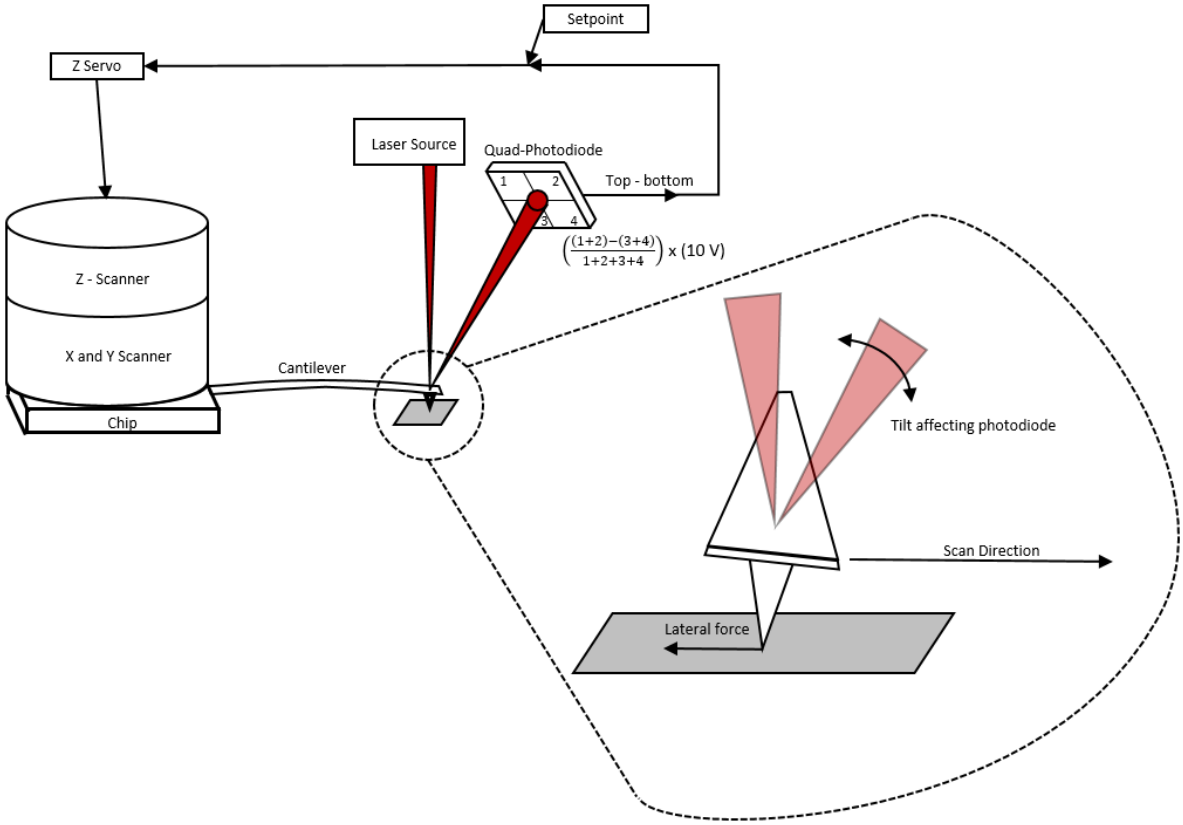

Figure 2.7. A simplified block diagram of an AFM in contact mode.

Swelling effects are key to unlocking the lubricating potential of polymer brushes. In a liquid environment the polymeric material is likely to swell as the liquid penetrates the polymer matrix. The polymer, driven by enthalpy and entropy, will undergo a number of transformations to find the lowest energy state, this of course is driven by the affinity of the polymer to the liquid. Even when an AFM tip of a small radius 8-10 nm makes contact with a polymeric film the molecular space is reduced and liquid is expelled. This reduction in molecular space results in a decrease in entropy and a resultant steric repulsion of the probe tip. When considering sliding tests of polymers there are two complicating factors:1) that bonds are likely to be created and broken at some level at the tip contacts which makes some stick slip phenomena likely, and 2) that the response of the polymer can be considered viscoelastic [313].

AFM cantilevers serve an important purpose and therefore the tip shape and “sharpness” are key. However, in reality the cantilevers are not points, the contact geometry is more like a hemispherical cap. As can be seen in Figure 2.8 the geometry of the tip can affect the ability to image small artefacts. Another more obvious limitation is the ability to observe narrow valleys and the other extreme, tall, narrow peaks. As simplified in Figure 2.8 these surface objects are not accurately reproduced. In standard cantilevers there is also the possibility that the slopes of the fabricated tip will contact the sides of an object before the “sharp” end and therefore distorting the actual shape of an object.

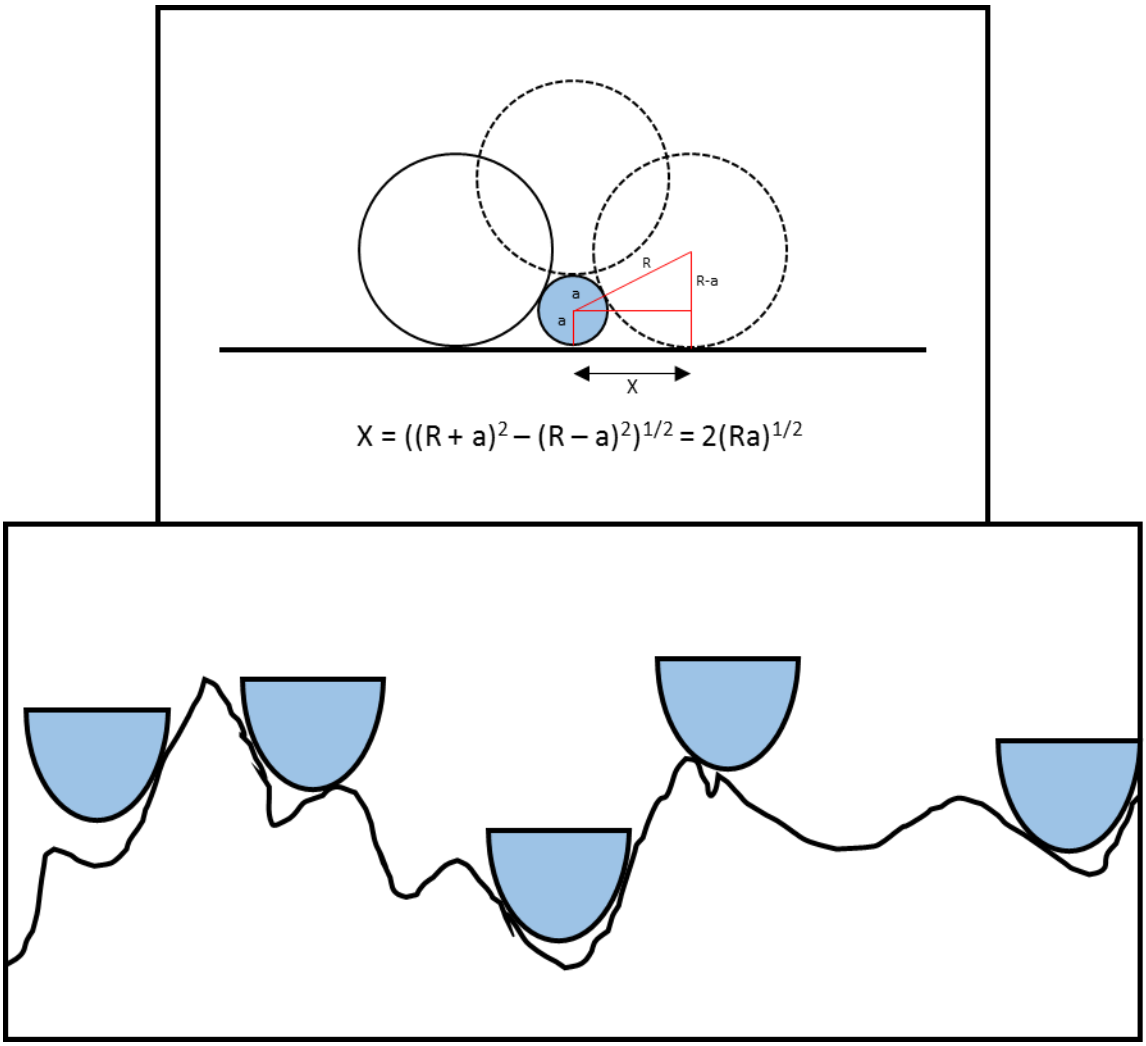

Figure 2.8 Top; a cross section of an object of interest on a flat substrate. The object has a radius of "a" although due to the tip geometry is imaged at a larger size, i.e. $2(Ra)^{1/2}$. Bottom; a 2D image of the cantilever making contact at various points across a nanoscale roughness surface.

The AFM that will be used is an Agilent Technologies AFM 5500, this AFM has two modes of interest in this work. Firstly non-contact AFM can be used to view the surface topography as well as calculate roughness, in addition this technique can produce 3D images and identify surface defects at the nanoscale. This mode can also be used to study the growth of SAM and the overall coverage. Nanotribological properties can also be studied using this AFM, where the single asperity contact between the cantilever tip and the sample surface can be measured. AFM is able to view both hard and soft surfaces in liquid as well as in air which will be useful so that polymer brushes can be viewed without collapsing. As shown in Figure 2.9 (R), an example of a cantilever used for AC tapping mode being tuned is provided. The oscillation frequency is purposely set below resonance to ensure good engagement of the tip, in all these experiments the off peak is -0.3 kHz. All AFM images here are presented after background correction. Notable steps taken

involve levelling and subtracting the 1st order polynomial as a line correction method. In addition, all images have been false colour corrected for ease of understanding.

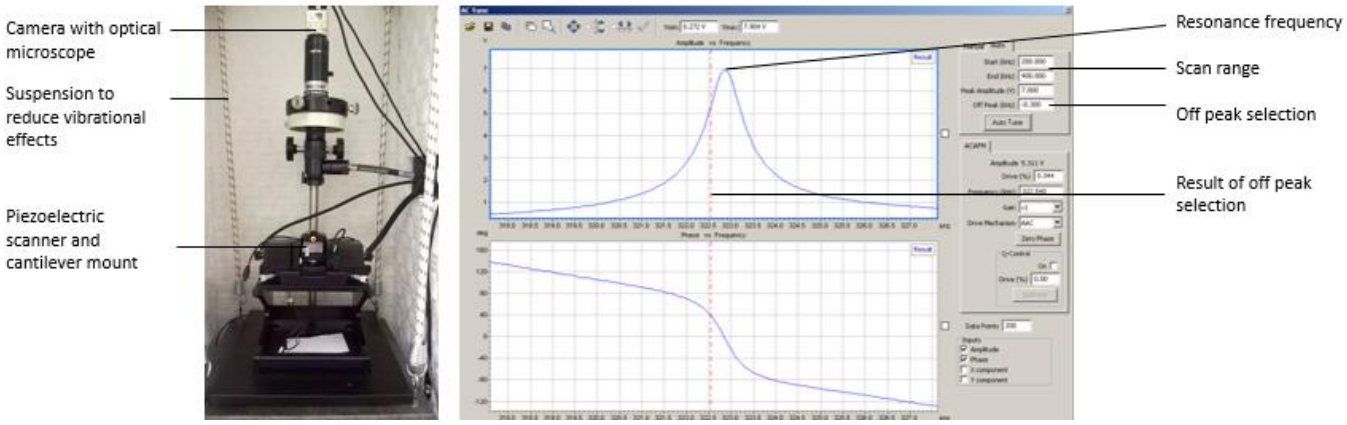

Figure 2.9. (L) An image of the Agilent Technologies AFM 5500 that is used in this research. (R) Tuning the resonant frequency of a silicon nitride cantilever.

2.4.3 STM

Scanning tunnelling microscopy (STM), similar to AFM, has been used to image surface topography down to the atomic scale [113]. STM images are created by bringing a small metal tip close to the surface of interest, applying a voltage bias and scanning across the surface [114, 115]. The small gap between sample and probe, typically in the order of angstroms, is maintained by the tunnelling effect across the vacuum [116]. The resultant image is essentially a map of topography. STM has been used to image thiols on gold showing the surface coverage of the SAM as shown in Figure 2.10 [30, 117, 118]. STM is however, limited to characterisation of molecules with relatively short carbon chains since substantial tunnelling currents are difficult to obtain for carbon chains longer than 12 C [34].

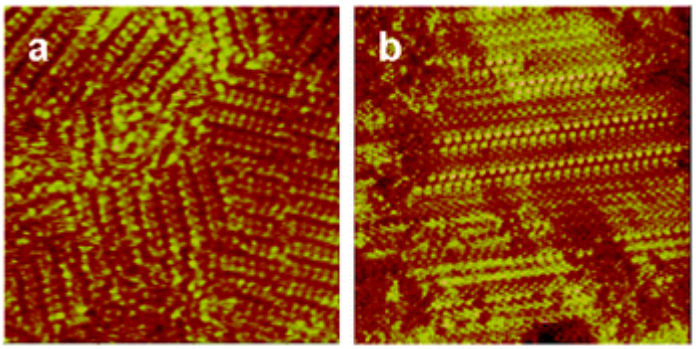

Figure 2.10. STM image of two different phases of hexanethiol on gold. A is a rectangular lattice structure and B is striped
Reprinted with permission from [21].

2.4.4 XPS

X-ray photoelectron spectroscopy (XPS) is primarily used to characterise the nature of the surface bonds [21, 119]. XPS is a frequently used technique owing to its ability to identify and quantify elemental composition as well as chemical states, see Table 2.1 [120]. By varying the take-off angle, i.e. the angle that the analyser is in relation to the sample surface, the chemistry of the top

most layers of a solid structure can be analysed [121, 122]. These properties make XPS a very useful instrument in the characterisation of SAMs. Figure 2.11 shows an example of an XPS spectrum of OTS SAM compared with that of a clean wafer. The lack of a Cl peak in the monolayer spectra showed the complete hydrolysis of OTS during adsorption [41]. The large O_{1s} peak in the wafer spectrum indicated a good level of oxidation on the surface and the significantly larger C_{1s} peak observed in OTS SAM confirmed the OTS SAM formation.

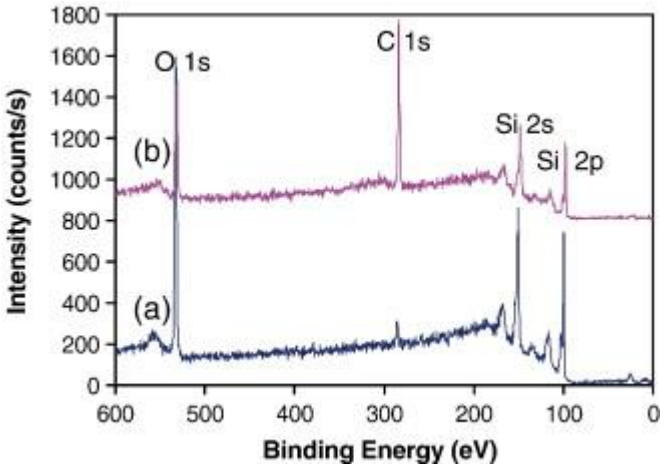

Figure 2.11. XPS survey spectra of (a) a clean silicon wafer and (b) OTS SAM. Reprinted with permission from [41].

In this work the XPS analyses were performed on a ThermoFisher Scientific (East Grinstead, UK) Theta Probe spectrometer. XPS spectra were acquired using a monochromated Al Kα X-ray source (hv = 1486.6 eV). An X-ray spot of ~400 µm radius was employed. Survey spectra have been acquired employing a pass energy of 300 eV. High resolution, core level spectra for C1s, O1s, N1s, Si2p and Na1s were acquired with a pass energy of 50 eV. High resolution core level spectra for Cu2p3 was acquired with a pass energy of 80 eV whilst a pass energy of 150 eV was used to acquire Br3d high resolution core level spectra. All spectra are charge referenced against the C1s peak at 285 eV to correct for charging effects during acquisition.

2.4.5 Ellipsometry

Ellipsometry has been used to identify the thickness of a thin film, for example in measuring the thickness of an oxide layer. It is an optical technique that relies on the difference between polarised light created by the reflection and refraction of a known light source. This technique has shown to be effective to characterize film thickness for single layer or complex multilayer stacks ranging from tenths of a nanometre to several micrometres. Hence, in addition to SAMs, it is also a useful technique in measuring polymer brushes, see details later [123] [46, 124]. Since ellipsometry needs a model to fit the raw data and normally does not take into account of surface roughness, small errors may be included in the thickness measurements. Ellipsometry is also used for investigating oxide thicknesses on silicon substrates [125, 126]. For the work presented here

an M-2000 Ellipsometer produced by Woollam was used. Modelling the data is performed with the commercial CompleteEASE package.

2.4.6 SEM

Environmental scanning electron microscopy (ESEM) will be used to study the wear on AFM cantilevers. A Phillips XL30 ESEM was used as it is able to image non-conducting samples via allowing a small amount of water vapour into the chamber as the cantilevers are predominantly silicon nitride. Figure 2.12 shows the effect of using cantilevers in tribological studies, the new cantilever with a sharp tip will be able to produce better images due to the sharpness. This will need to be monitored to be sure that cantilevers are in good condition to produce accurate images. Energy-dispersive X-ray spectroscopy (EDX) analysis was used as an attempt to characterise the surface of oxidised silicon wafers. SEM or optical microscopy may be used to study the wear of silicon nitride including wear scars and wear volumes. SEM was also used to check if successful modification of the tipless probes had been achieved, further details in section 4.2.8 Colloidal Probe Microscopy.

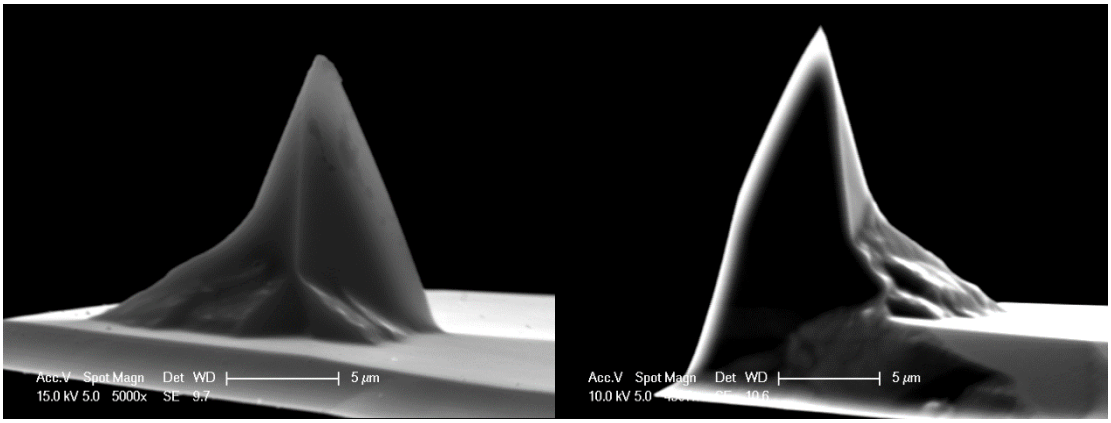

Figure 2.12 A SEM image comparing a worn AFM cantilever vs new.

2.4.7 Summary

A wide range of techniques are available for characterisation of SAMs. Each technique has its advantages and limitations, therefore it is important to consider using more than one technique in SAM characterisation. Contact angle has been the most widely used method due to the ease and low cost of the technique but it may become impractical for ultra-superhydrophilic surfaces (exceeding 150°). AFM images have mostly been used to understand the growth of monolayers; it is also routinely used for detailed analysis of surface structure and tribological testing. STM is rarely used due to the limitation in SAM chain length. Although XPS is an expensive technique, the wide range of data that can be collected reduces the need for multiple different techniques. Ellipsometry is more useful for polymers and can analyse partially formed films height which can reinforce data collected by AFM.

2.5 Achievements and Applications of SAMs

SAMs have shown growth in a number of applications especially in sensors such as pH sensors, organic and inorganic species detectors [127, 128] and biosensors [129-131]. As mentioned above, SAMs have also been used as a lubrication solution in MEMS/NEMS. Many SAM studies have been focused on their formation on silicon wafers, due to their well-defined surface morphology and extremely low surface roughness (R_a<0.001 µm), which maximises the functions of SAMs and helps SAM characterisation. This is a particular focus of this review due to the authors' interests in silicon nitride surfaces.

The type of SAM molecule limits the contact angle that is achievable. For example, with CH_3-terminated SAMs on silicon, the reported water contact angles do not exceed 110°-112° for hydrocarbon tails with more than 10 carbons. This is irrespective of the amount of chlorine atoms attached to the silicon head group [38, 132]. However, higher contact angles can be achieved by introducing fluorine groups and / or structuring surfaces. A facile method of increasing contact angles has been demonstrated by using (tridecafluoro-1,1,2,2-tetrahydrooctyl)-1-trichlorosilane and 1H,1H,2H,2H-perfluorooctyltriethoxysilane to form SAMs on silicon and nanofibrils with contact angles achieved at 120° and 130° respectively [133, 134]. This is because the CF_3 groups in SAMs can reduce surface free energy, thereby increasing surface hydrophobicity. Song *et al* demonstrated another approach to increase contact angles to the hydrophobic range by coupling SAMs with micro-roughened surfaces [135].

Apart from single molecule type SAMs, mixed SAMs have been developed to incorporate two types of molecules in one SAM where one type of species would preclude the other by steric hindrance [93]. Mixed monolayers have great potential in many different applications including microelectrodes [136], separation of biomolecules [137], environmental monitoring [138], biosensors [139] and tribology [65]. Feng *et al.* developed a mixed SAM containing both OTS and octyltriethoxysilane, see a schematic of the mixed SAM in Figure 2.13D [67]. Two methods were used to produce the mixed SAM: co-adsorption and stepwise as illustrated in Figure 2.13A-C. Co-adsorption is considered the easier of the two methods, where a clean substrate was simply immersed in a solution containing two precursor molecules, Figure 2.13A. Due to the different affinities of the molecule headgroups, typically the 'trial and error' approach is required to tailor the concentration and ratio between the two types of molecules to achieve the desired mixed SAM [67]. It was not possible to form a mixed SAM using OTS and octyltriethoxysilane but possible for OTS and dodecyltrichlorosilane [140]. This was due to the steric hindrance of the three ethoxy groups in addition to the quick binding of OTS to the substrate rendering octyltriethoxysilane unable to form structures [67].

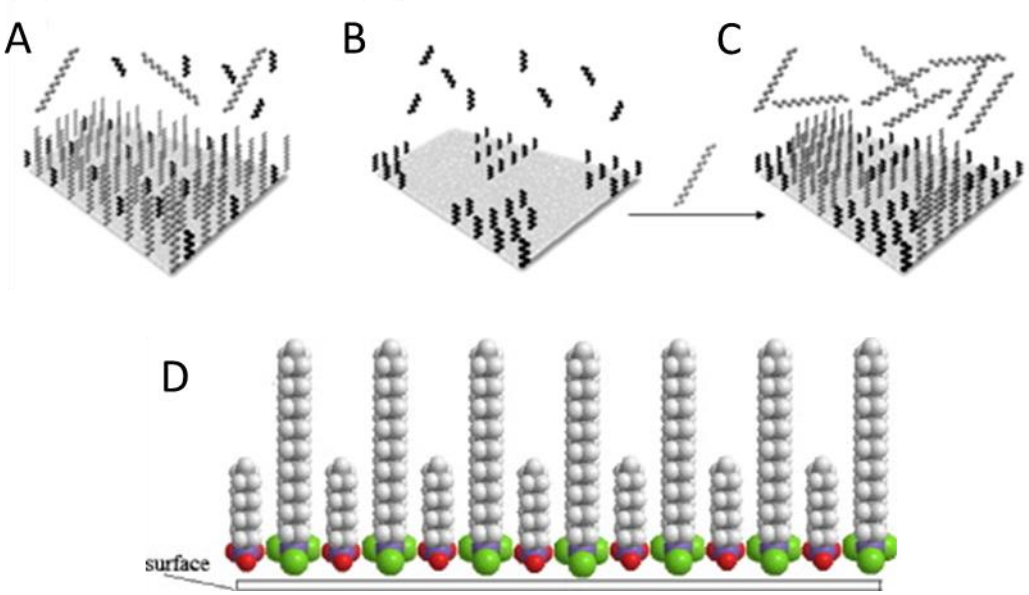

Figure 2.13. Showing the formation of an idealistic structure for the mixed SAM of OTS and octyltriethoxysilane in a stepwise method. Reprinted with permission from [67].

The stepwise method is illustrated in Figure 2.13B and C, this method was developed to overcome the problems of mixed co-adsorption. Firstly, a partial monolayer was produced by immersing a substrate in a solution of the first SAM forming molecules for a known length of time. Then the substrate was immersed in a secondary solution of a different molecule [50]. Gaps in the first monolayer were filled in by the second SAM-forming molecule [50, 67]. It was recommended that the SAM with a larger head group should be formed first as the smaller steric hindrance of the secondary SAM will allow it to fit in the gaps left by the larger SAM [67]. Gradient mixed SAM can be created by pumping toluene at a constant rate into a solution of OTS with a partially immersed substrate [65]. With the addition of more solvent the solution is more dilute meaning longer adsorption times for a full monolayer [32, 65]. This is facilitated by a partially immersed substrate where the addition of more solvent increases solvent level and therefore immerses more substrate. After removal of the partially formed monolayer from one solution, simple immersion in another solution containing (1-trichlorosilyl undecyl)trichloroacetate in toluene creates the full monolayer [65]. However, it has been found that in some cases phase separated islands of monolayer have been formed rather than well mixed monolayers. As previously discussed, the formation of mixed SAMs can be inhibited by molecules selected and therefore multistep adsorption may be required.

Bilayers and multi-layered SAMs are increasingly seen in research with self-assembling multilayers incorporating other layers such as gold nanoparticles [141]. Extensive research of bilayers has included self-assembling supported lipid layers, e.g. phospholipid bilayers are found to be useful in studying interactions with cell membranes [142, 143]. Supported bilayers of lipids are

commonly produced by spreading lipid vesicles on hydrophilic solid supports [144]. To create tethered bilayers authors have formed SAM of thiolipids on gold followed by the lipid bilayer below the critical micellar concentration, i.e. below the point at which micelles forms in solution [145]. Bilayers of thiols and silanes can be formed depending on end group, thiols such as 11-mercapto-1-undecanol will allow silane SAMs to form a bilayer on top although [146]. It is worth noting that –OH functional groups on the terminal end of SAMs are not as efficient as substrate groups at creating additional monolayers [146]. OTS has shown the ability to form multilayers in poor solvent on both steel and silicon, however, it is reported that the layers were found to be extremely rough indicating a consistent multilayer has not been formed [55, 147]. In addition, authors that have used MAC [72, 110, 112], apply the mobile lubricant through spin coating possibly limiting applications in some areas.

2.6 SAMs for Tribological Applications

2.6.1 Overview

SAMs have been implemented in NEMS and MEMs devices with research in OTS lubricated micromotors since the 1990s [148]. Although SAMs are only in the order of a few nanometres they have shown to act as boundary lubrication systems on both micro and nano scales [107]. SAMs have also been shown to significantly reduce stiction, the force that has to be overcome for movement of a stationary object, between two substrates which has led to applications in storage devices [70, 149]. As discussed above, a variety of SAM head groups are available for different substrates. For example OTS SAM can be formed on alumina surfaces of components in MEMS/NEMS for lubrication [150]. SAMs have also been considered for lubrication of aluminium and magnesium engine components via matching metal oxide to head group selection [96]. Fatty acids have been additives in lubricants for steel components for many years, where carboxylic acids are known to form monolayers on steel surfaces to reduce friction [6]. Silanes are an attractive alternative to some of the existing friction modifiers that contain sulphur and phosphorus, which is one of the reasons that research in SAMs has grown significantly over the years [17].

2.6.2 Tribotesters and Tribometers for SAM Evaluation

A variety of tribotesters can be used to measure the tribological qualities of two surfaces in contact, including wear and friction, such as pin-on-disc and ball-on-disc tribometers [29]. It is, however, very important that tribological testing replicates relevant service conditions [151]. Pin-on-disc has been used in SAM evaluation for replicating linear velocities in one direction for an unlimited amount of time also known as kinetic friction, see Figure 2.14B. Depending on the application, different contact geometries can be deployed such as balls or pins. However, some uncertainty during pin-on-disc testing for SAMs has been reported. Novak *et al*. found that misalignment of pin geometries increases error along with other pin-on-disc measurement

uncertainties, others including Burris *et al*. and Schmitz *et al*. have also studied uncertainty using reciprocating tribometers [152-154]. Figure 2.14A shows an example of friction traces for 4 different SAMs, where a sudden increase in the COF is seen when the lubricating properties of these SAMs cease to exist [58]. Linear reciprocating tribometers are used to replicate many engineering contacts such as piston ring on liner in automotive engines [155]. These tribometers generally have a pin of a known geometry sliding across a plate under load over a known distance, reciprocation allows friction to be recorded in both the forward and backward motions [156]. Measurements of static COF are also possible to be measured, see Figure 2.14B [157]. This can be measured where the contact is momentarily stationary. Microtribometers have also been used in SAM tribological testing especially for applications where small forces are used, such as MEMS devices [158, 159]. AFM nanotribological studies are frequently being used to investigate contacts at atomic level [69, 160-162]. AFM is useful for gaining understanding of asperity contacts in sliding contacts [160].

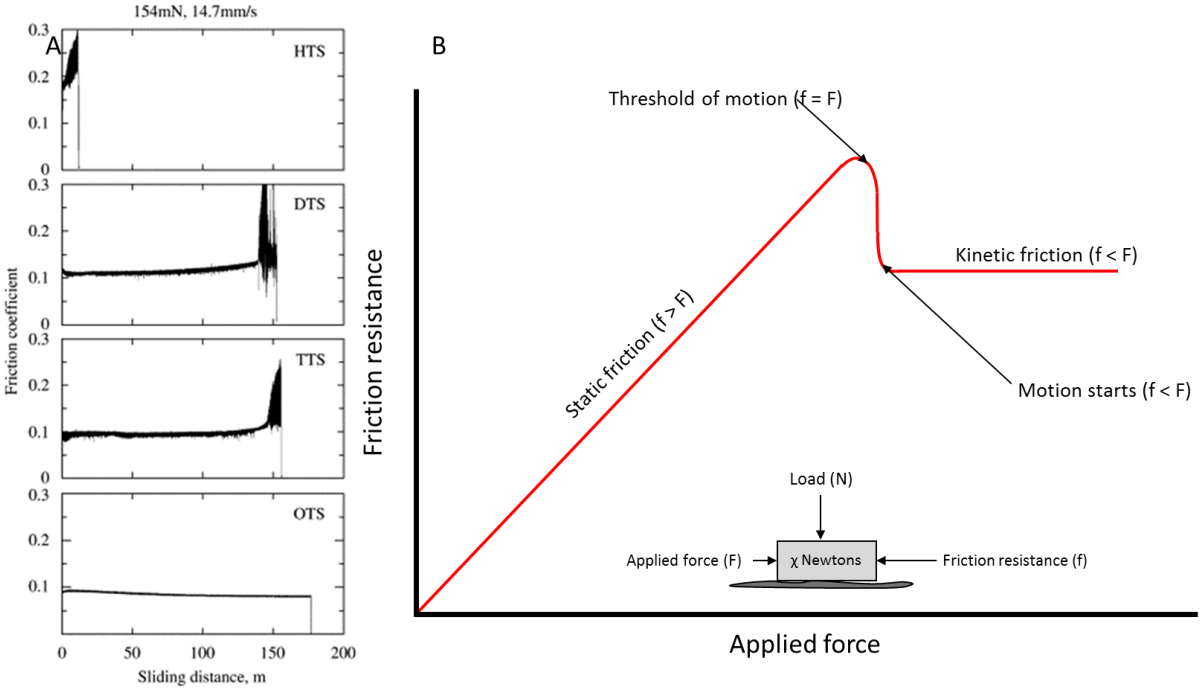

Figure 2.14. (A) An illustration of four friction traces detailing the COF of different SAMs obtained from pin-on-disc experimentation. (B) Is a simplified standard model of friction. A is reprinted with permission from [58].

2.7 SAMs on Silicon for COF Reduction

2.7.1 Single Component SAMs on Silicon

- *OTS SAM*

OTS SAMs have been extensively investigated for tribological performance improvement of silicon wafers in a wide range of load and speed [65, 73, 77, 163-165]. Using a steel ball and forming OTS SAMs on silicon wafer discs, Cha *et al.* recorded COF values in the range of 0.1 to 0.2 over a dry sliding distance of 75 m under a load of 50 mN for immersions in excess of one hour. No damage was found on the wafer discs for longer immersion compared with the wear tracks under 10 s and 1 h immersion. The authors found that immersion times of longer than 5 h had little effect on the

COF, however, relative humidity proved to influence COF. A higher humidity resulted in a higher COF. Booth *et al*. found that the tribological properties of single-component OTS monolayers were dependent upon the surface coverage and surface energy of the gradient monolayer [65]. They also demonstrated that the COF can be further reduced to under 0.1 on the OTS SAM fully covered silicon wafer under 98 mN loading, similar to the studies by DePalma *et al*. [164]. Satyanarayana *et al.* also demonstrated that with a stainless steel ball, COF of OTS SAM modified silicon disc can be reduced to 0.06 under 0.5 N compared to unmodified silicon (0.2-0.3) [77]. Ma *et al*. also performed similar tests under a load of 0.5 N, but found the COF stabilised at 0.13 on the OTS SAM modified silicon. However, the authors found the OTS SAMs instantly breakdown and failed under a higher load of 1 N. Garcia-Parajo *et al.* studied OTS SAMs on silicon with force distance curves and compressive forces, and proposed that rearrangement of OTS under compression and the subsequent reformation after load was removed contributes to the lubricity of OTS SAMs [166]. Flater *et al.* demonstrated that OTS SAMs can reduce adhesion of silicon wafers through pull off measurements using AFM, and also noticed that friction is reduced further when OTS SAMs are created on both the cantilever and substrate [165].

- *Influence of Chain Length and Head Group*

A number of studies have been conducted to investigate the influence of chain length and head group type on their tribological properties. Singh *et al*. studied trichlorosilanes with 6, 10 and 18 carbons chain lengths using a reciprocating ball-on-plate configuration with a silicon nitride ball on silicon wafer under a load of 4 mN [167]. At a 1 mm/s sliding speed over a 3 mm track OTS SAMs produced a COF of less than 0.1., whereas DTS and HTS produced COF values of approximately 0.15 and 0.25 respectively. The performance of the three SAMs was also compared using a contact AFM under 40 nN and 2 µm/s scan rate. Their performance in terms of friction was ranked as OTS>decyltrichlorosilane (DTS)>hexyltrichlorosilane (HTS), where OTS had the lowest COF. Masuko *et al*. performed similar investigations using 6, 10, 14 and 18 carbon chain lengths and found a COF of under 0.1 for OTS SAMs using ball-on-disc under 52.1 mN load at a sliding speed of 3.53 mm/s. Longer chain SAMs have been shown to have significant freedom of swing allowing rearrangement to the direction of shear stress, thus lowering COF [58, 72, 167]. By replacing one or two Cl atoms with CH_3 group, Masuko *et al.* also investigated effect of head groups on tribological performance of trichlorosilane SAMs on silicon [58]. When a Cl atom was replaced an increase of COF was observed. Further increase of COF was shown when two Cl atoms were replaced. The authors concluded that replacing Cl atom of trichlorosilane with CH_3 group increased steric hindrance, thereby making the formation of a dense monolayer difficult as well as the loss of cross linking between silicon atoms, which have an influential effect on stability and wear life of SAMs.

- *Other SAMs*

DePalma also studied undecyltrichlorosilane (UTS) and tridecafluoro-1,1,2,2-tetrahydrooct-1-yl)trichlorosilane (FHOTS) SAMs on silicon wafers, however, found that friction was higher than OTS SAMs in both cases, possibly due to the thicker films of 25 Å produced by OTS SAMs as opposed to 15 Å and 10 Å of UTS and FHOTS SAMs, respectively [164]. Satyanarayana *et al.* also studied 3-aminopropyltrimethoxysilane (APTMS), however, APTMS SAMs did not show any lubricating properties [77]. The increase in COF compared to a bare wafer is likely to be due to the hydrophilic terminal group producing a higher adhesive force which increases friction. However, Li *et al.* investigated tribological properties of 3-aminopropyltriethoxysilane (APTES) and phosphorylated APTES SAMs on silicon wafer using contact mode AFM under 20 nN load at 10 Hz scan rate, and observed that the COF was reduced from approximately 0.08 on bare Si wafer to around 0.03 on both APTES SAM and phosphorylated APTES SAM [70]. Kang *et al.* prepared a 6-(3-triethoxysilylpropylamino)-1,3,5-triazine-2,4-dithiol monosodium (TES) SAM on silicon, and investigated its tribological performance using ball-on-disc with a 4 mm steel ball under a 0.098 N load. The authors reported a lower COF value of 0.12 compared to bare silicon which kept stable for 130 s or approximately 300 cycles. The reduction of friction on TES SAMs was claimed to be the van der Waals forces between the terminal groups on the ring structures [54].

2.7.2 Multicomponent SAMs

Notable problems for monolayers in tribological systems involve high loads that remove the monolayer and therefore the lubricating qualities. Therefore, efforts have been made to improve the wear life of SAMs without losing their friction reducing capabilities. Two approaches have been implemented to achieve this, dual-component and multilayers. Dual-component SAMs use two different precursor molecules to form mixed monolayers where multilayers are produced through sequential steps to achieve the desired effect.

Booth *et al.* used OTS and (1-trichlorosilyl undecyl) trichloroacetate to create a dual-component gradient monolayer film on a silicon substrate [65]. Dry sliding tests with a ball-on-plate microtribometer demonstrated that these gradient SAM films exhibit excellent lubricating performance with significant reduction in friction in comparison to bare Si substrate. By creating dual-component monolayers with methyl and hydroxyl terminals, greater durability was achieved on the mixed SAM films with constant lubricating performance over 5 h at a sliding speed of 0.1 mm/s. The enhancement in tribological performance durability was proposed to stronger intermolecular interactions within dual-component mixed SAMs. Singh *et al.* observed contrary effect on mixed SAMs of OTS/DTS and OTS/HTS using microtribological tester with the deteriorated performance for both mixed SAMs compared to single component OTS SAM [167]. However, under nanotribological testing conditions using AFM, both mixed SAMs outperformed

the single component SAMs, which was postulated that the difference in carbon chain length provided less resistance as the AFM tip slides over the outer layer.

Satyanarayana *et al*. also investigated tribological properties of a composite film of OTS onto APTMS SAM. The authors demonstrated that the composite film exhibits lower COF and longer wear life than APTMS SAM, but nearly the same performance as OTS SAM. This film lasted slightly fewer cycles at equivalent COF to that of the OTS SAM before breaking down at 3000 cycles [77]. Ma *et al*. created dual-layer films OTS/multiply-alkylated cyclopentane (MAC) and tested them using a ball-on-plate tribometer with a steel ball at a sliding speed of 1.5 mm/s under 0.5 and 1 N loads. OTS/MAC dual-layer films maintained a similar COF to OTS SAM through the 0.5 N testing but improved wear resistance through higher loaded tests. The improvement was attributed to the MAC layer being able to reorganise and replenish the lubricant deprived area [72, 110]. Ren *et al.* prepared polyethyleneimine (PEI) SAM as well as a PEI-STA dual-layer film on silicon substrate by immersing the PEI modified substrate in a solution of stearic acid (STA) and N,N'-dicyclohexylcarbodiimide (DCCD) [74]. Using AFM and a unidirectional ball-on-plate tribometer, the authors demonstrated that the PEI SAM alone was not a good coating and only lasted a few cycles under low load. However, the PEI-STA dual-layer film shows much better tribological performance with a COF of 0.06 under the same load lasting for approximately 8600 cycles. The PEI SAM was not effective in reducing friction due to its minimal chain length and hydrophilic terminal group, while better performance of the PEI-STA film is possibly due to the long chain length of stearic acid which is able to rearrange the carbon chain in the shear direction and provides protection to wear. Yang *et al.* used (3-mercaptopropyl) trimethoxysilane (MPTS) to form a SAM on silicon followed by immersion in a silver nanoparticle solution resulting in a MPTS SAM doped with silver (Ag). The doped layer was immersed in an octanethiol solution to form a sandwich-like trilayer film. Nanotribological testing performed using AFM under a load of 20 nN demonstrated that compared with the bare Si wafer, MPTS SAM reduces the frictional force by 3.5 times, Ag-doped MPTS SAM further reduce by more than 40%, and tri-layer film further reduces additional 15%. The authors proposed that the long tails of the octanethiol are able to pivot and therefore rearrange with the sliding direction of the AFM tip reducing the frictional force. Using a reciprocal tribometer with a load of 0.5 N at a sliding rate of 2.5 mm/s, it is observed that under the selected macro-sliding conditions, the MPTS SAM is not suitable for surface protection of Si substrate with high COF as bare Si and a short film life of 200 s. However, improvement was evident after the SAM was doped with Ag nanoparticles and additional layer. The silver doped MPTS SAM exhibited an extended antiwear life of 13,000 s with a COF of 0.19, while the trilayer film showed over doubled lifetime of 29,500 s with a further reduction in COF of 0.16 [76].

To summarise, the most successful SAMs have proven to be longer chain SAMs and multilayers. However, multilayers have their own inherent problems with application to tribological contacts apart from NEMS and MEMS. This area appears to be where research is focussed with SAMs proving their worth, notably OTS. The majority of SAMs reviewed in this article, single, mixed or multiple, have been application driven with regards to NEMS/MEMS with exceptions for DePalma's earlier work which was purely interested in the tribological properties.

2.8 SAMs on Silicon Nitride

2.8.1 Silicon Nitride for Bearings

Silicon nitride rolling element bearings have seen great success as hybrid bearing systems. Applications include automotive, aerospace, renewables and the railway industry. Silicon nitride has successfully been utilised in engine components turbochargers and metal cutting since it was developed in the 1960s [168, 169]. Ball bearings up to approximately 8 mm in diameter can be formed by cold isostatic pressing, compacting powder granulates by dry pressing or rolling granulation of powder nuclei. The larger ball bearings (diameter>8 mm) are typically formed by cold isostatic pressing [170]. These silicon nitride bearing materials typically contain bindery additives such as Fe_2O_3, Y_2O_3 and Al_2O_3 depending on manufacturing procedure [17, 29, 170]. All ceramic rolling element bearings can operate at temperatures up to 1000°C with high chemical resistivity. The key property is the relative density of the ball bearing, with a 60% reduction in weight resulting in an 80% reduction in friction compared to classic steel bearings [17]. Compared to steel on steel contacts the COF of hybrid systems is reduced to approximately 0.04-0.09 under oil lubricated conditions and between 0.1-1.0 for dry conditions [29]. Research shows that centrifugal loading on the outer bearing raceway is reduced by a lighter ball bearing, it has also been identified that ceramic bearings perform better under lubricant starvation and hard particle contamination [17, 19, 171-173]. SiN is also more resistant to debris created by contact fatigue stresses which are suspended in the lubricant and create secondary wear mechanisms in which the suspended wear particles abrade, scratch and cut the surface creating further damage [29].

2.8.2 Silicon Nitride Tribology

With a 2 N loaded reciprocated tribometer, Dante *et al.* studied the effect of protective oxide layer of silicon nitride on tribological properties without any surface modification, and found that the hydroxylated oxidised silicon layers ($Si(OH)_4$) produced a lower COF than pure silicon oxide (SiO_2) [174, 175]. The authors also found that at a temperature above 400°C the silicon surface is dehydroxylated leading to a sustained high COF. Bal *et al.* also studied the tribological effect of silicon nitride and the protective oxidative layer and stated that the ability to re-oxidise after the oxidised layer has been removed can limit damage of the surface. The authors state that the two routes of degradation of silicon nitride are mechanical and tribochemical. The mechanical mode occurs under high loads and low speeds with frequent stop-start conditions. The tribochemical

wear is when silicon nitride reacts with water initially forming silicon dioxide and ammonia followed by the silicon dioxide reacting with more water to produce silanol groups [174-178].

2.8.3 SAMs for Silicon Nitride

Details of the crystal structure of silicon nitride are given in [179, 180]. A thin oxide layer (2 nm - 4 nm) is naturally found on the surface of silicon nitride and allows SAM attachment in the similar way as on silicon wafers [17, 174-176, 181-183]. The oxide layer on silicon is amorphous silicon oxide, conversely there is an interface layer of silicon oxynitride that is present on silicon nitride as shown in Figure 2.15 [180], which has been confirmed through TEM and XPS. Hydroxylation of silicon nitride can be achieved by both plasma and piranha solution treatment [183, 184].

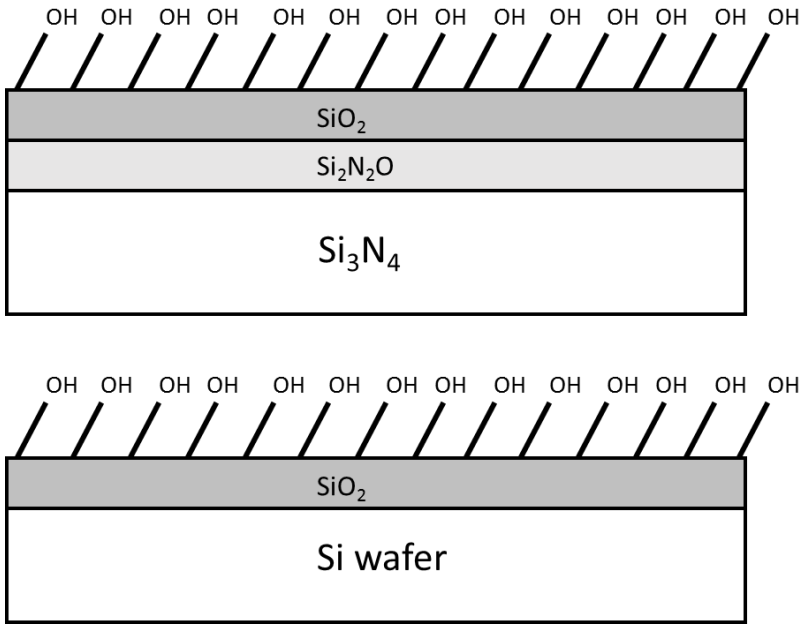

Figure 2.15. Detailing the oxide layer present on both Si wafers and silicon nitride.

Sung *et al.* showed that monolayers of octadecyldimethylchlorosilane (ODS) could be formed on silicon nitride [185]. After treating with HF, the monolayers were formed on silicon nitride from a solution of ODS in mixed solvents of hexadecane: chloroform (4:1) for one hour. Water contact angle of 110° are obtained on the ODS SAM modified silicon surfaces, which are similar to those reported for silicon oxide, showing a good monolayer was formed on silicon nitride surface [185, 186]. This study also demonstrated that the monolayers can attach directly to H-terminated silicon nitride as well as the naturally found silicon oxide. With piranha treated silicon nitride good quality SAMs can also be formed on the oxide layer, as Köbel *et al.* demonstrated the SAMs of chlorosilanes and ethoxysilanes formed on the piranha-treated silicon nitride exhibited equivalent contact angles to those SAMs formed on silicon wafers [187]. Stability testing by washing with solvent, storing in water, heating or storing in ambient conditions for months did not affect the contact angle [187]. Diao *et al.* successfully produced monolayers of APTES on silicon nitride with contact angles of ±5° comparable to that obtained on silicon wafers by Janssen *et al* [105, 188]. Wang *et al.* investigated SAM formation on silicon nitride using four silanes; OTS,

octyltrichlorosilane, chlorodimethyloctadecylsilane and octadecyltrimethoxysilane [17]. It was found that OTS and octadecyltrimethoxysilane achieved the highest contact angle of 108°. Like Kulkarni *et al.*, the authors found that the initial formation was very quick and 80-90% of the monolayer is formed within an order of a few minutes [32].

2.8.4 SAM Formation on Silicon Nitride and Tribological Applications

To further improve the performance of silicon nitride in tribological applications, the feasibility of forming SAMs on silicon nitride and their tribological performance has been investigated in recent years. The following section has been divided into macro and nanotribology of SAMs on silicon nitride surfaces, where the nanotribology focuses on the modification of silicon nitride cantilevers in AFM.

- *Nanotribology*

The majority of AFM tips are made of silicon nitride with pyramidal contact geometry. SAMs have been applied to AFM tips to create chemical force microscopy (CFM) [189], which is used to measure frictional response between the cantilever modification and substrate. The modified tip is useful for mapping different chemical functionalities across a substrate through the surface-tip interactions as some SAMs will result in different frictional responses. In some cases the cantilevers are first coated in gold then thiols are adsorbed, silanes have also been reported [190]. The gold layer can be detrimental to friction experiments as the gold is weakly attached to the silicon nitride so for nanotribology direct attachment to silicon nitride is preferable [190]. Adhesion testing is common with CFM, it can simply be explained as the force needed to retract the cantilever from the surface. Adhesion force measurements are related to the modified tip and surface interactions and can be used to measure stiction and combat adhesion related failures notable in NEMS/MEMS [191-193]. Direct comparison of adhesive forces can be misleading if different tip radii are present [190]. This is even more important if colloidal AFM cantilevers are used [194]. Ito *et al*. found that adhesion force of CFM probes is in agreement with the increase of contact angle of the same SAM on a planar silicon nitride substrate [195]. Headrick *et al.* shows an increase in pull off force when OTS SAM are applied to silicon nitride cantilever on a CH_3 terminated substrate [196]. OTS SAM cantilevers on COOH terminated surfaces show a slight increase in adhesion force in comparison to cleaved mica, this gives the unique ability to identify localised chemical groups on the surface through CFM through differences in pull off forces [196]. Tsukruk *et al.* modified both cantilever and substrate and found that larger force displacement curves are recorded with CH_3-CH_3 terminations rather than Si_3N_4-Si_3N_4 contacts [190]. Frisbie *et al.* modified gold coated silicon nitride cantilevers with both COOH and CH_3 terminating SAMs [197]. Figure 2.16A shows a representation of the lithographically defined SAMs. Figure 2.16B and C show the frictional response of a CH_3 terminated cantilever and a COOH cantilever, respectively. Brighter areas are areas of higher friction.

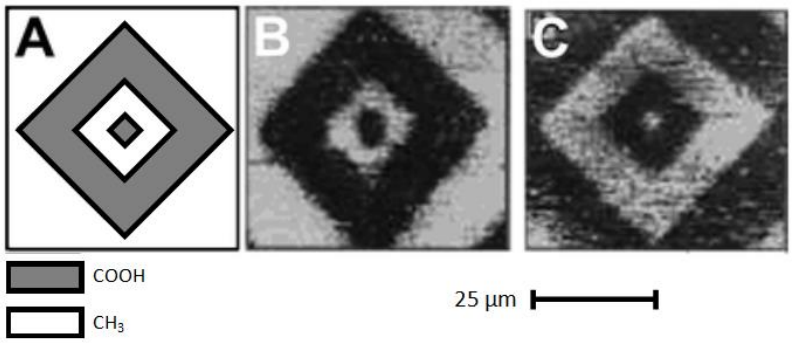

Figure 2.16. Representations of frictional force between a modified substrate shown in A. B is where a CH_3 terminated cantilever is used and C is with a COOH terminated tip. Brightness is related to areas of higher friction. Adapted from Frisbie et al. and Barattin et al. Reprinted with permission from [197].

- *Macrotribology*

An extensive literature search revealed little regarding silicon nitride modified with SAMs. The authors found one publication reporting the results on SAMs on silicon nitride at macro scale. Wang *et al.* investigated SAM the tribological properties of two SAMs, OTS and octadecyltrimethoxysilane on silicon nitride [17]. OTS is discussed here as it was a superior friction reducer. However, as the authors also pointed out, although octadecyltrimethoxysilane is not as good in reducing the COF as OTS, it may be more appropriate to use it instead of OTS as an additive for hybrid contacts, as there are fewer corrosive by-products than OTS (see Equations 2.1 and 2.2). Tribological testing was conducted using a ball-on-disc tribometer, where the COF of a SAM modified disc was compared to that of an unmodified disc under a 10 N load and at a constant speed of 0.198 m/s. Under dry conditions the OTS SAM produced a COF of 0.020 for 11.6 m before failure. When lubricated with a base oil the COF is reduced to 0.014. Interestingly the authors discovered that the best COF result comes from using OTS as an additive in a base oil, at concentrations of 2.5, 5 and 10mM were tested. After 1250 m sliding the COF has settled to a steady value of 0.008 for all three solutions.

2.9 SAMs on Metallic Substrates and Tribo-applications

Apart from silicon wafer and silicon nitride, SAMs have also been developed on many other substrates such as alumina, iron oxide, steel, zinc, copper, platinum, silver, Ti6Al4V alloy, as well as on gold, palladium, silver, copper and zinc. However, their applications in tribology are still limited [93]. This section reviews the development of SAMs on metallic surfaces based on the head groups of the SAMs

- *Silane Head Groups*

OTS is the most common head group that has been investigated on various metal surfaces. Zhu *et al*. developed a novel method of constructing OTS monolayers on stainless steel to reduce the corrosive effects of hydrochloric acid by-products which could also be related to silicon nitride. The extended storage of OTS in solvent increased levels of hydrolysis, this could then be neutralised to reduce the aforementioned corrosive effects (see Equations 2.1 and 2.2). This

method did not hinder the ability of the monolayer to form on the substrate and water contact angles of approximately 108° were regularly achieved, similar to that of silicon and silicon nitride. OTS monolayer formation was facilitated by a highly hydroxylated surface [147].

OTS has also been attached to amorphous alumina and the growth kinetics as well as resulting monolayer are shown to be very similar to that of a silicon oxide substrate. Facilitated by hydroxylated surfaces SAM growth occurs with reported contact angles of 100°. However, the authors did not achieve known contact angles with Qin *et al.* and Wang *et al*. achieving considerably higher angles ≈120° [198, 199].

Qin *et al.* investigated the performance of octadecyltriethoxysilane, 1H,1H,2H,2H-perfluorodecyltriethoxysilane (PFDS) and APTES monolayers on aluminium alloys (AA 2024) [119] using a reciprocating ball-on-plate test rig. A steel ball was used as the counter surface. APTES failed instantaneously possibly due to short chain length not preventing contact but also due to the head group. PFDS successfully reduced the COF under loads of 0.6, 1 and 2 N for sliding times of 600 s, but failure occurred at approximately 400 s under 3 N load. Octadecyltriethoxysilane reduced the COF the most and completed all of the tests as well as a 4 N test without failure, the authors concluded the same mechanism for lubricity exists on AA 2024 as it does on silicon. The long chain coupled with the ability to swing as well as inter-chain interactions all help to reduce COF [119]. Similar results were achieved by Devaprakasam *et al*. when 1H,1H,2H,2H-perfluorooctadecyltrichlorosilane (FOTS) and OTS were formed on polycrystalline aluminium and tested on both nano-and macrotribometers [96]

Panjwani *et al.* deposited 3-glycidoxypropyltrimethoxysilane on Ti6Al4V alloy, and then coated a perfluoropolyether (PFPE) layer on top of the preformed SAM. They tested the treated alloy against a silicon nitride ball on a ball-on-disc tribometer under 0.2 N, 41.9 mm/s and dry sliding conditions. It was found that the PFPE overcoat lasted over 900 times longer than without the coat due to its self-repairing characteristics [200]. Li *et al.* created an APTES SAM on titanium alloy (Ti–29Nb–13Ta–4.6Zr (TNTZ)) followed by a self-assembling graphene oxide (GO) layer as illustrated in Figure 2.17 [201, 202]. Reduced graphene oxide (RGO) sheets are prepared by heating GO sheets after assembly.

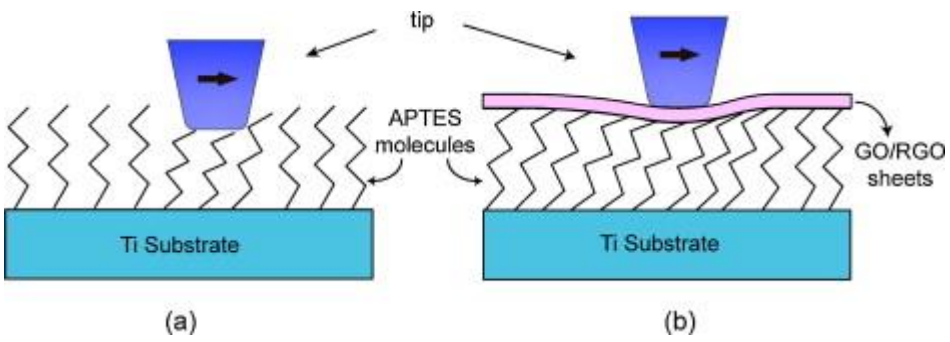

Figure 2.17. Showing the interaction between the pin and APTES film and the ideal interaction with the GO/RGO sheets. Reprinted with permission from [202].

The modified Ti surfaces were then tested using a reciprocating pin on plate tribometer under dry conditions against a silicon nitride ball under 100 mN load and 1Hz frequency. The APTES SAM showed a poor wear life and was destroyed within 500 s. The graphene oxide/APTES film however showed a COF of 0.19 and a life time of over 5000 s. This was further improved after heat treatment, where a COF of 0.16 and a life of 12000 s were achieved. It was suggested that it was due to less oxygen groups in the heat treated graphene layer resulting in a less environmentally sensitive layer with respect to relative humidity [202].

- *Other Head Groups*

Other head groups have been researched, notably carboxylic and phosphate. Carboxylic acids have been and still are used as friction modifiers and it is thought that they can form monolayers on surfaces [203, 204]. Carboxylic acids have been found to spontaneously adsorb on to numerous substrates, such as AgO, CuO and Al_2O_3. However, there is a difference in how the monolayers adsorb onto surfaces, Figure 2.18A and B shows the different methods. On AgO, for example, it has been found that the carboxylate binds symmetrically to the substrate unlike CuO which follows the arrangement shown in B. Figure 2.18C shows the bonding characteristics of alkylphosphonic acid on a substrate, this is dependent on the substrate properties [205]. Some examples are reviewed below [17, 18].

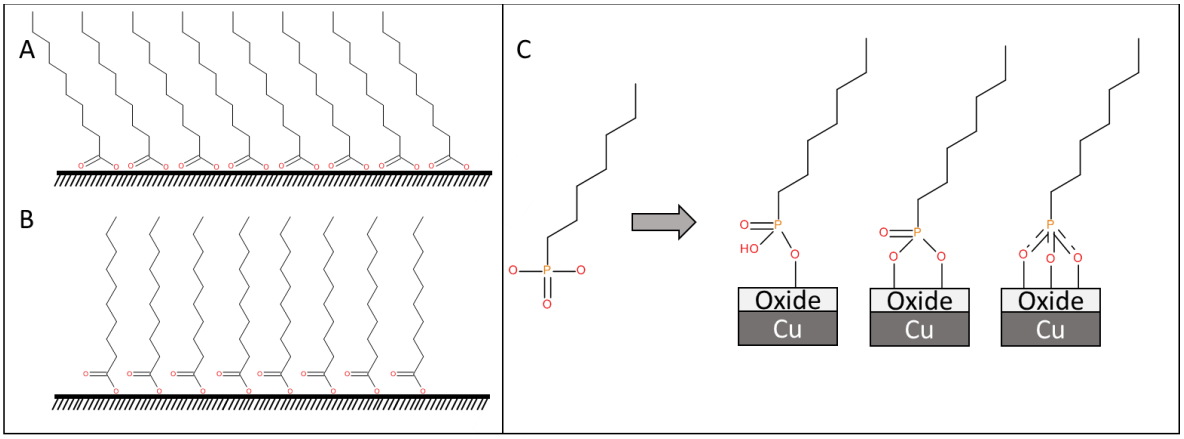

Figure 2.18. Illustrations of the formation of carboxylic acid monolayers (A and B) and the bonding characteristics of alkylphosphonic acid on copper oxide. Information from [203, 205].

Wan *et al.* created SAM of alkylphosphonic acids on copper surfaces, where dodecylphosphonic (C12PA) and octadecylphosphonic (C18PA) acids were chosen. Ball-on-plate reciprocating tests with 5 mm steel balls under a load of 0.5 N and sliding velocity of 10 mm/s were performed. The C12PA SAM remains stable for approximately 50 seconds before failure and the C18PA SAM lasts more than 500 s before slow failure. This follows the same rules as silanes with regards to length of chain providing increased lubricity and wear life. Etching the copper surface using NaOH before SAM formation greatly improved the wear life of the films, wear life of the C18PA SAM formed on the etched copper substrate exceeded 7200 s under a COF of 0.2. Etching also increases the contact angle of both C12PA and C18PA SAMs significantly which may play a part in friction

reducing [205]. The tribological application of both C12PA and C18PA on alumina was also investigated by using a reciprocating ball-on-flat microtribometer under dry conditions. In addition, it is shown that both acids can reduce the COF, however, the longer chain length reduced friction more which is consistent with the literature [150].

Zhang *et al*. investigated stearic acid (STA) SAM films on textured aluminium using a ball-on-disc tribometer with steel ball counterparts dry sliding at 10 mm/s under 0.1 N load. Surface texturing was completed using NaOH at 100°C for 1h, etching alone reduced the COF to below 0.6 from over 0.7 for non-etched Al surface. STA SAM on non-etched Al substrates reduced the COF to below 0.5, while the SAM on the etched substrates the COF was further reduced to under 0.15. The authors cited pivoting and rearrangement of the monolayer as an explanation for the reduction of COF [206]. As Wan *et al*. observed[205], Zhang *et al.* also concluded that SAM modification combined with chemical etching can significantly reduce friction with drastically increased durability, and low friction of the combined modification is due to the reduction in surface adhesion between steel ball and the films as well as the actual contact areas [206].

Carboxylic acids have been used to lubricate steel and diamond like carbon (DLC), in research completed by Simič *et al.* palmitic acid was the acid of choice. In the tribological tests palmitic acid was premixed into a poly alpha olefin base oil, testing was performed using a ball-on-flat reciprocating tribometer with steel on steel contacts or DLC on DLC at 25°C and 80°C with a load of 10 N at an average velocity of 0.01 m/s. Steel on steel testing at the lower temperature shows that the COF is reduced from approximately 0.15 to 0.10 for the premixed oils, at higher temperatures the reduction effect is increased attributed to the greater mobility of the additive palmitic acid. However, palmitic acid showed no effect on friction reduction for the DLC-DLC contacts at 25°C and a slightly negative effect at 80°C [207].

2.10 Challenges of SAM for Lubrication

The research literature shows that the uniformity and hydrophobicity of SAMs are critical to friction reduction of the SAM coated silicon substrates. This has been shown above by head group selection and limited adsorption before tribological testing. Another factor is chain length, many of the studies mentioned have compared the difference and it is regularly reported that longer, i.e. 18 carbons (OTS), performs best under a variety of tribological conditions. This appears to be valid over a range of substrates. This ability to reduce friction is commonly related to the ability to rearrange under shear stress with longer chains able to withstand compressive forces better. However, the durability of the SAMs is still a concern for practical applications as ultra-thin single SAMs easily break down under high loads or exhibit limited wear life. It has also been noted that high pressures and temperatures could remove monolayers [96]. Figure 2.19 shows that OTS can perform well under low loads in comparison to a bare silicon wafer (A and B), however under

higher loads the monolayer will fail. Nevertheless, there is still a reduction in wear indicating that the OTS SAM did not fail instantaneously (C and D).

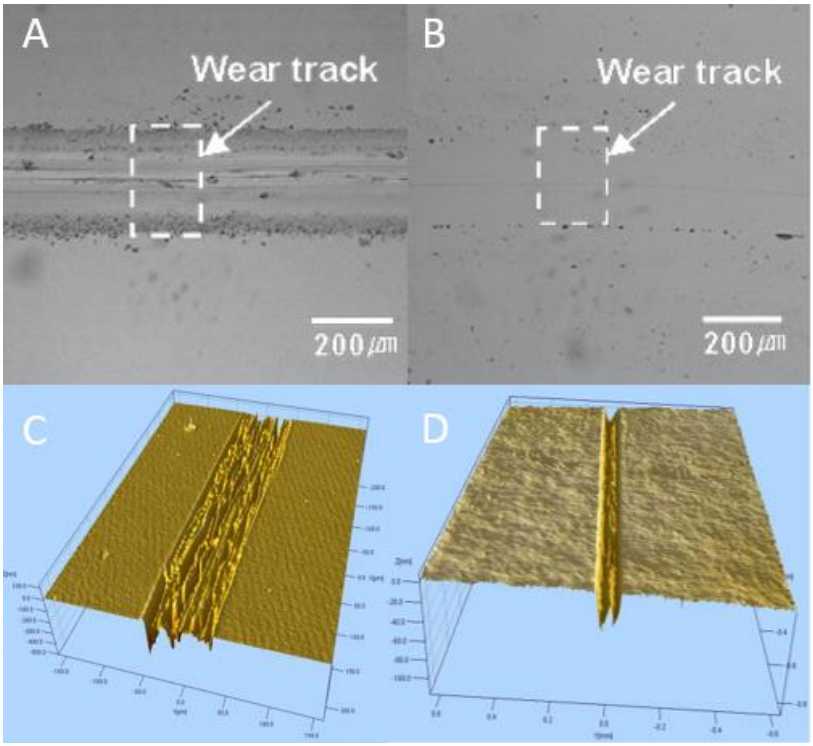

Figure 2.19. Comparison of the wear tracks of a silicon wafer (A) compared to an OTS SAM (B) that has not failed. D shows the wear track of an OTS SAM that has failed in comparison to a bare silicon wafer (C). C and D Reprinted with permission from [72]. A and B Reprinted with permission from [163].

Shear stress is a limiting factor of SAM lubrication, therefore research has focussed on forming composite SAM films or SAM multilayers. Multilayers, such as MAC, have shown promising results by improving the wear life of OTS SAM. These methods require different formation techniques such as extended spin coating or thermal annealing, for some applications such as in situ bearing lubrication this may not be feasible. This of course presents its own difficulties not just involving costs and maintenance but condition monitoring of lubricants. However, preformed SAM multilayers formed before use may prove feasible for applications. As there are no set testing standards the nature of investigations is inherently scattered. This means that it is difficult to comprehend all the findings of a wide variety different contact size, geometries, load, speed etc.

3 Polymer Brushes, Their Synthesis and Application in Tribological Systems

Whilst SAMs are advantageous because of their simple formation, e.g. thiols on gold and chlorosilanes on oxides, and the end groups are easily modifiable for specific functions. Their application as a lubricant in tribological contacts is limited as thin film SAMs are susceptible to shearing [25, 26]. In a similar way, polymer brushes are formed by adsorption of prefabricated polymers onto the substrate through their reactive function groups or by subsequent polymerization onto reactive-terminal group containing SAMs. Polymer brushes typically have longer carbon chain and better durability than SAMs, thus better capabilities of polymer brushes to withstand compressive force and shear stress are expected for a better lubrication solution [208, 209]. Polymer brushes have been used to change wettability, reduce friction and increase corrosion resistance by using a variety of polymers [210-216]. This section reviews the development of polymer brushes and their application in tribology systems.

Polymer brushes are formed onto surfaces through two methods, named 'grafting to' and 'grafting from' processes. The 'grafting to' method uses prefabricated polymers that can be attached to a surface using physisorption or chemisorption much like a SAM as seen in the left route of Figure 3.1. The film thicknesses of polymers produced through the 'grafting to' method are limited by the molecular weights of the preformed polymer in solution [215, 217]. Although this method is relatively easy to carry out as it works much like a SAM, there is steric hindrance that impedes the density of the final film that is formed [73, 218, 219]. In addition to this, the adsorption techniques are reversible so that the layers may be susceptible to high shear forces [215].

In the 'grafting from' techniques, also known as surface initiated polymerisations, the surface is first modified with a self-assembling initiator layer, which is then exposed to monomeric components with catalyst and, if needed, in an appropriate solvent [215, 220-222]. Generally this method is considered preferential due to the production of well-defined brushes [223]. This can be seen in the RHS route of Figure 3.1. It is imperative that the substrate to be modified has successfully had initiator molecules anchored to it, otherwise the solvent would become gelatinous due to polymerisation taking place. This in turn would affect the density of the polymer film by way of steric hindrance [215]. This method allows much more control over the final film and the grafting densities can approach 1 chain/nm^2 [213, 217, 223-226] compared to the 0.05-0.1 chain/nm^2 for 'grafting to' strategies [123, 227]. The improved density is due to the less steric hindrance from long chains to the substrate. In comparison to the limit of the films using 'grafted

to' methods (<100 nm thickness), the 'grafting from' method can produce much thicker films [215].

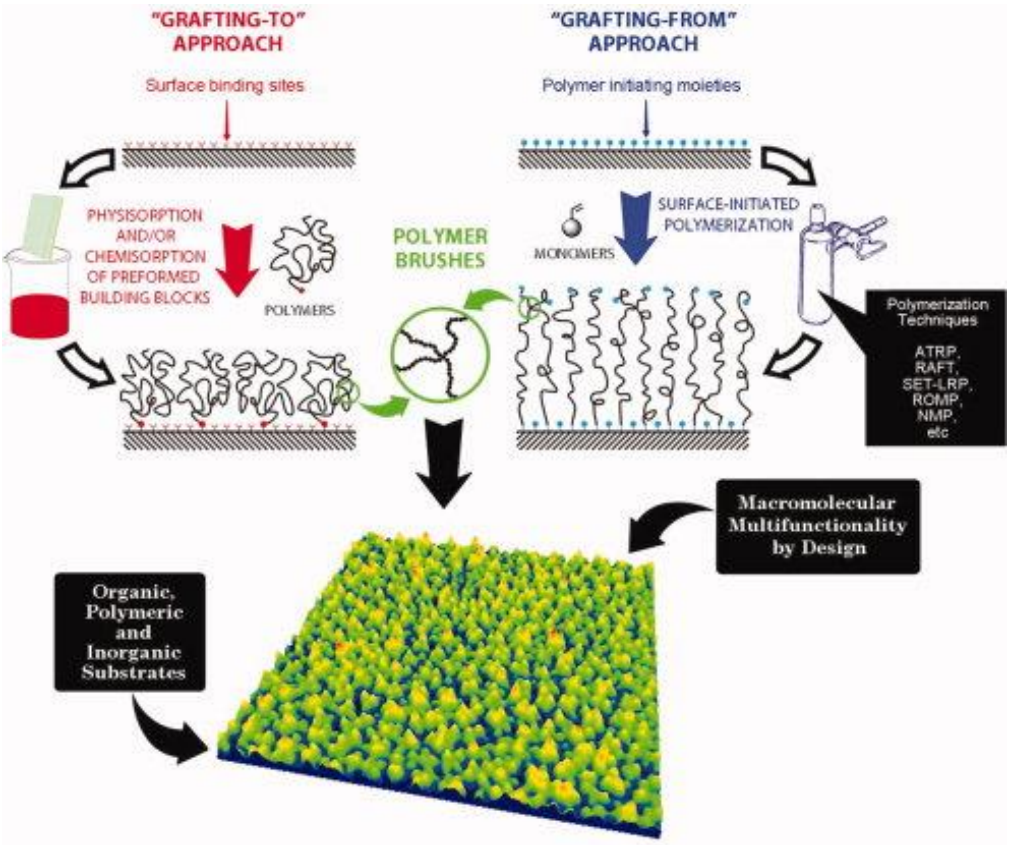

Figure 3.1. Schematics of the two different schemes of polymer brush formation and highlighting the density differences. The scheme also includes an AFM image showing (500 x 500 nm2) of poly(2-(methacryloyloxy)-ethyl-trimethyl-ammonium chloride) brushes grown from a Si wafer via surface initiated ATRP. Reprinted with permission from [210].

3.1 Radical Polymerisation

There are many different polymerisation reactions that can be used to initiate polymer brushes, such as ring opening metathesis polymerisations [184, 215, 217, 228], nitroxide mediated polymerisations [215, 217, 228, 229], reversible addition fragmentation chain transfer polymerisation [184, 215, 217, 228, 229], atom transfer radical polymerisation [3, 27, 184, 215, 217, 218, 220, 228-234], and living ring opening polymerisations [184, 215, 228]. The selected method is ATRP and the reasons why and the process are discussed in depth in section 3.2 Atom Transfer Radical Polymerisation.

- *Ring Opening Metathesis Polymerisation*

Ring opening metathesis polymerisation (ROMP) is a subsidiary of ring opening polymerisations (ROP) which is focussed on the breaking of carbon-carbon double bonds [235]. ROMP is a form of chain growth polymerisation where cyclic monomers produce straight or fewer ringed additions to the polymer chain [236]. Notable applications of ROP are the production of nylon 6 from caprolactam avoiding the patented route of polycondensation [237]. ROP of lactams has been investigated for over 40 years due to the ability to produce a variety of polymers in a controlled

manner [228]. Although surface initiated polymerisations are possible the focus has been on coating grafted polyesters [228]. ROMP are a variation of this procedure in which unsaturated monomeric components are polymerised but still contain unsaturated components [236]. The driving force of ROMP is ring strain enthalpy [235, 238]. Applications include rubber additives and super adsorbent materials [235].

- *Nitroxide Mediated Polymerisation*

Nitroxide mediated polymerisations (NMP) are based upon activation/deactivation of a chain end radical with a nitroxide leaving group [228, 229]. NMP provides a good route for polymer brush construction without the need for catalysts, but is still able to produce controlled polymers in a narrow molecular weight range [229]. Due to the simplicity of NMP and the ability to use alkoxyamines as initiating and mediating species applications have increased [239]. Polymerisation opportunities completed in solution have been increased due to the development of a universal alkoxyamines which has also resulted in the ease of use of NMP [240].

- *Reverse Addition Fragmentation*

Reversible addition fragmentation chain transfer polymerisation is a different type of controlled radical polymerisation by using chain transfer agents such as thiocarbonylthio compounds [228]. It is commonly initiated by azobisisobutyronitrile (AIBN) that decomposes to form radicals, which react with monomeric units to start polymerisation. To deactivate the chain, the polymer radical reacts with the chain transfer agent to create a reversible addition-fragmentation chain transfer (RAFT) radical adduct. The RAFT radical adduct can then fragment and lose either the radical polymer or the 'R' group which is a radical [241]. The success of RAFT polymerisation depends on the 'R' group. This allows the initiation of another monomer and the start of another active chain. RAFT polymerisations are capable of achieving very narrow molecular weight distribution (polydispersity), e.g. lower than 1.1, which is one of its advantages compared to other methods [242]. Approaching equilibrium between the propagating radicals, one from the original interaction with AIBN or similar and the other from the 'R' group radical and monomer, and the deactivated chain, means that all the chains have the same probability of growing, resulting in narrow polydispersity index (PDI) [243]. In addition, with environmental regulations to reduce the amount of sulphur in lubricants, RAFT polymerisations may not be a viable option as chain transfer agents for RAFT usually contain sulphur element [17, 244].

3.2 Atom Transfer Radical Polymerisation

Atom transfer radical polymerisation (ATRP) is the most popular type of polymerisation for brushes due to the relative robustness of the technique. For example, unlike the other techniques, rigorously dry working conditions are not needed and reactions are tolerant of a variety of monomers, ligands and catalysts. The commercial success of ATRP has been well

reported, in part due to this polymerisation's ability to be performed in commercially available equipment [215, 219, 228, 234, 245]. ATRP can form well-defined polymer brushes from easily synthesised initiators and is well known as a successful controllable polymerisation [36, 217, 246]. ATRP was independently developed by Matyjaszewski and Sawamoto, initially for controlled radical polymerisations [247, 248], and has been used to efficiently produce many different polymers [230, 231, 249-251] due to its effective control in the composition and architecture of polymers. Surface initiated ATRP (SI-ATRP) was first reported by Huang *et al.* who used benzyl chloride attached to a trichlorosilane head to form a monolayer on silicon surface then poly acrylamide brushes using copper(I) chloride and bipyridine with acrylamide to create new stationary phases for chromatography [229, 252]. Copper is usually the transition metal of choice for ATRP [27, 123, 229, 249-251, 253-255]. Through ATRP, Ejaz *et al.* synthesised methyl methacrylate brushes on silicon wafers using a Cu based catalyst after a trimethoxysilane initiator was immobilised on the surface using Langmuir-Blodgett techniques [229, 231, 253]. Since then the technique has been implemented onto gold, inorganic particles, organic latexes, formed dendrimers, highly functionalised linear brushes, and varied compositions and sizes [231].
The basic methodology for ATRP synthesis of polymer brushes is to have an initiator or monomer, and a catalyst made of a transition metal for successful grafting of chains. If the polymer brushes do not all grow at the same rate or time, the shorter chains can be inhibited from growing any further due to steric hindrance. This can be overcome by ensuring there are copious amounts of initiator sites on the substrate. There are two major steps in this polymerisation reaction, namely activation and deactivation. During the activation step, the metal complex breaks the alkyl halogen bond in the initiator, resulting in the formation of radicals. The radicals then propagate with the excess monomer and higher oxidation state metal complex. In the deactivation step, the radicals react with deactivators (e.g. polymer chain or activators) resulting in the formation of halide capped chains or reformed metal complex catalysts. For this to be successful, it is necessary to have a reversible reaction shifted to the dormant species, accompanied by fast initiation and deactivation. This is important as it can reduce the amount of terminations [230, 249]. Due to the importance of ATRP in polymer brush development, it is further reviewed in the next section.

3.2.1 Initiators and Synthesis

Initiators are key to ATRP, however, to increase densities tethering the initiator is required. ATRP uses simple initiators that usually contain one or more halides [217, 256]. The architecture of the polymers can be varied by the initiator, to produce linear chains of polymers in which only one halide is present. Using multiple halide systems can form other shapes, such as stars or combs [249, 257, 258]. Development of self-assembling initiators for surface initiated polymerisations bridges SAMs into polymer growth [228]. Much like SAM, for lubricating films, polymer brushes must be strongly attached to the contact surface, therefore, chlorosilane initiators are often

chosen to be anchored to substrates in ATRP in the same way that SAM forms as shown in Scheme 1 [259]. Ohno *et al*. also synthesized triethoxysilane initiators [260]. Initiators do not have to be anchored to a substrate. In some cases free initiator is used to control the ATRP reaction where gel permeation chromatography (GPC) can be used to calculate polymer conversions.

Liu and co-workers used the ATRP silane initiator 11'-trichlorosilylundecyl) 2-bromo-2-methylpropionate in their polymer brush formation [250]. The silane initiator was synthesised using the esterification route detailed by Matyjaszewski [261], followed by hydrosilylation using trichlorosilane and Karstedt's catalyst as shown in Scheme 2. The authors also refer to the work of Husseman *et al.* for this synthesis. Husseman however, used Speier's catalyst instead [262]. Karstedt's catalyst is more reactive requiring much lower amounts of Pt, Speier's catalyst is viewed as economically unattractive due to reactivity and that large amount of catalyst are rendered useless and unrecoverable [263]. Bielecki *et al.* followed a very similar route apart from using chlorosilane which produced a less reactive head group as shown in Scheme 3.

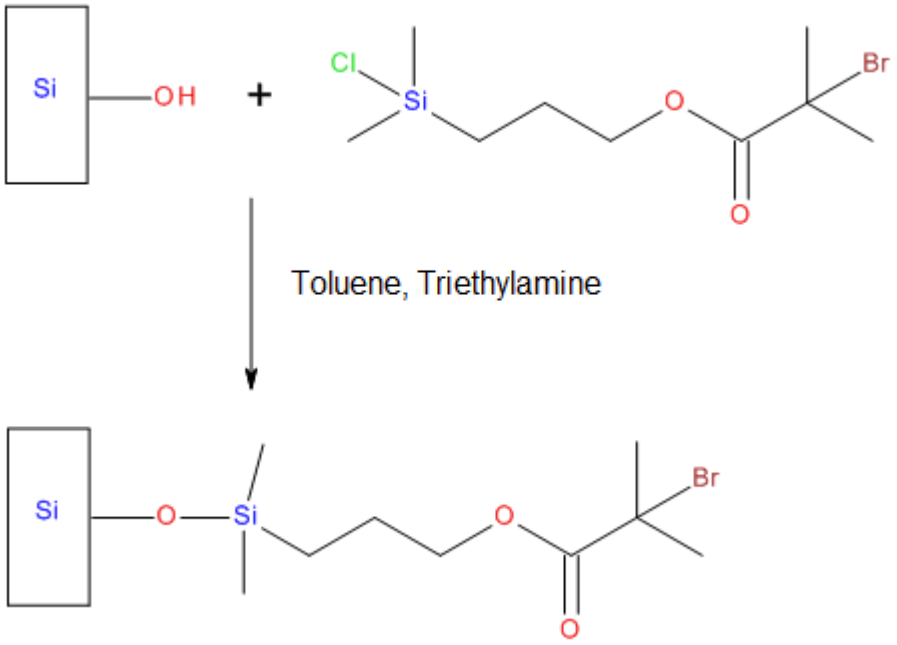

Scheme 1 shows SI-ATRP, the attachment of the ATRP initiator 3-(2-bromoisobutyryl)propyl)dimethylchlorosilane to a silicon wafer.

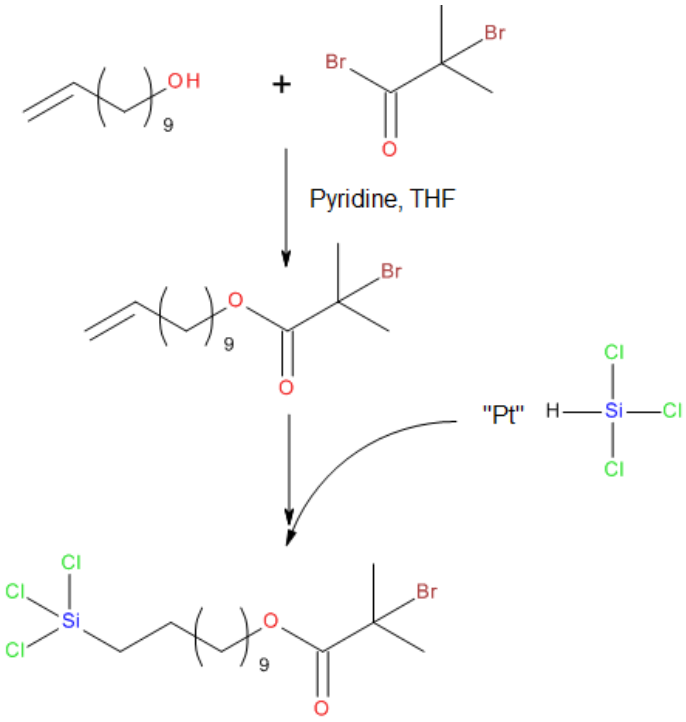

Scheme 2 shows the synthesis of the ATRP initiator (11'-trichlorosilylundecyl) 2-bromo-2-methylpropanoate via esterification and hydrosilylation.

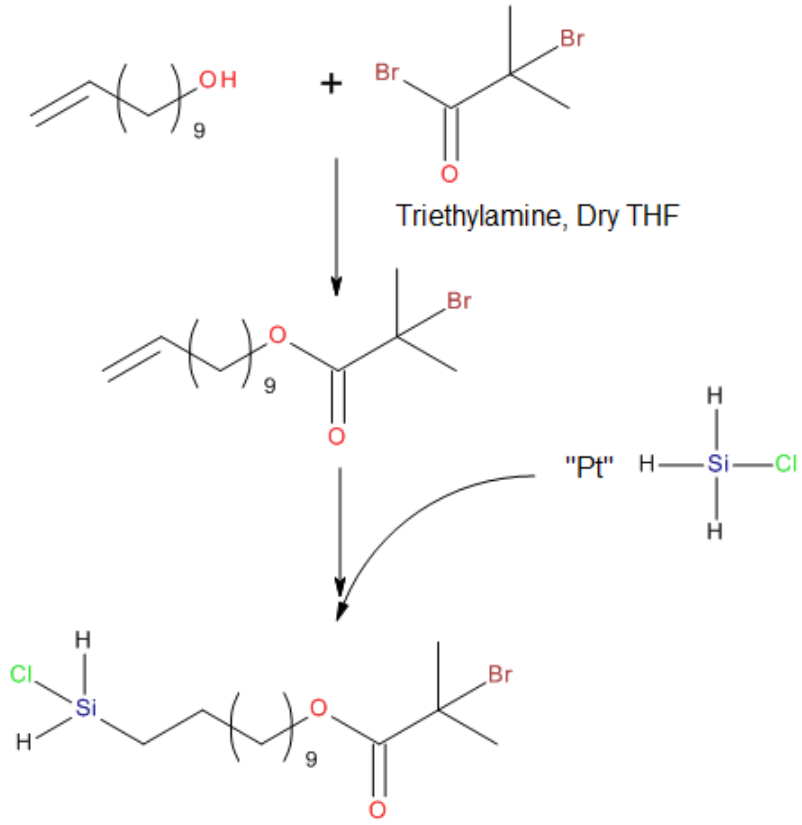

Scheme 3 detailing the ATRP initiator 11'-chlorosilylundecyl) 2-bromo-2-methylpropanoate via esterification and hydrosilylation.

Zhou *et al.* constructed an initiator monolayer on silica particles, then APTES self-assembled over the following 9 h to produce an amide functionalised end group. This was then reacted with 2-bromoisobutyryl bromide (BIBB) and pyridine for 12 h to form the anchored initiator [264]. Other

initiators include 2-bromopropionyl bromide which reacts with the oxide layer and triethylamine (TEA) at 0°C during gentle agitation.

3.2.2 Sacrificial Initiators

It is common that an additional free "sacrificial" initiator was added to form polymers in solution. Free initiators are added for two reasons, i.e. to help control polymerisations [215, 217, 229, 265, 266] and allow other characterisation techniques as discussed below in GPC [250, 267]. A sacrificial initiator has a similar structure to a surface attached initiator, for example, Figure 3.2A shows an ATRP initiator except it has no silane head group meaning that it will not form a monolayer and stay in solution [250, 264, 268]. Polymers formed in solution can be analysed by GPC, or size exclusion chromatography [126, 254, 264, 269, 270] to calculate the degree of polymerisation. The polymers formed via free initiators are shown to correlate well with surface attached initiators [271, 272]. Average molecular weights, molecular weight distribution and number average molecular weight can be determined from chromatograms, see examples in Figure 3.2B and C, where B shows a very narrow polydispersity indicating a well-controlled polymerisation and C a wider polydispersity. The time of elution is representative of molecular weight when compared to standards. Interestingly, due to the way that size exclusion chromatography works, larger polymers elute first which is unlike other types of chromatography, e.g. gas chromatography. As sacrificial initiators produce free polymer in solution, care must be taken to remove physisorbed free polymers for certain characterisation techniques of substrates, such as AFM.

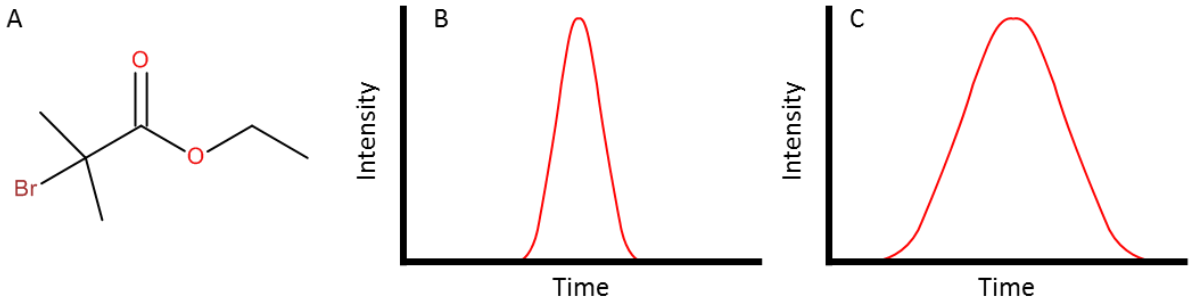

Figure 3.2. A Is the structure of a frequently used sacrificial initiator, ethyl α-bromoisobutyrate. B and C are examples of molecular weight distributions.

3.2.3 Catalyst Systems

The catalyst system is responsible for the creation of the radical by cleavage of the alkyl halide bond. As shown in Scheme 4, the equilibrium of the reaction is shifted to the left indicating that only a relatively small amount of chains have active species. This reduces the possibility of irreversible radical-radical termination [245, 273]. The persistent radical effect is thought to reduce P-P termination as well as increasing the controllability whilst accelerating polymerisation [28, 108, 255, 261]. In addition to this, the Matyjaszewski and the Sheiko groups showed that using additional quantities of the deactivator could improve the polymer brush by controlling the anticipated persistent radical effect [230, 255, 274]. The radicals can reversibly deactivate back to

dormant polymer chains, which also means that the metal is reduced to the lower oxidation state. Table 3.1 shows a selection of the catalyst systems used in rest of this review. A more in-depth review of copper complexes can be found in ref [275].

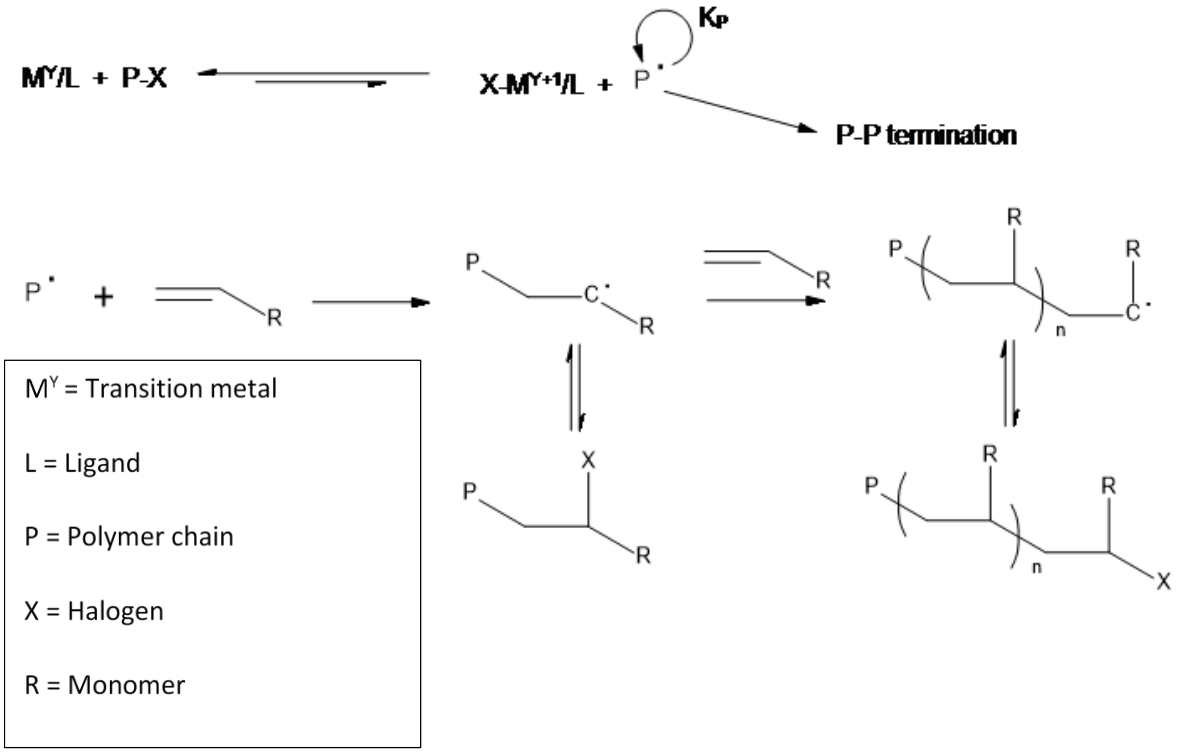

Scheme 4 showing the mechanism of ATRP with metal complex.

Table 3.1. A non-exhaustive selection of catalyst systems in this review.

Transition metal	Transition metal complex ligand	Added Ligand	Higher oxidation state transition metal (Y/N)	Temperature (°C)	Monomer	Reference
Cu	Br	PMDETA (N,N,N',N'', Pentamethyldiethylenetriamine N''-)	N	90	Lauryl acrylate	[270]
Cu	Cl	HMTETA (1,1,4,7,10,10-hexamethyltriethylene-tetraamine)	Y	125	Styrene Methyl methacrylate	[250]
Cu	Br	4,4'-Dinonyl-2,2'-dipyridyl	Y	110	Hexyl-, dodecyl- and octadecyl methacrylate	[27]
Cu	Br	2,2'-bipyridine	N	90	N-isopropylacrylamide	[126, 254]
Cu	Br	PMDETA	N	40	Oligo (ethylene glycol) methacrylate and 2-Propynyl methacrylate	[251]
Cu	Br	2,2'-dipyridyl	N	RT	Methyl methacrylate	[276]
Cu	Br	PMDETA	N	RT	Benzylmethacrylate	[268]
Cu	Br	PMDETA	N	90	2-(dimethylamino) ethyl methacrylate	[264]
Cu	Br	Tris[2-(dimethylamino)ethyl]amine	Y	30	4-vinyl pyridine	[277]
Cu	Br	PMDETA	N	50	N-isopropylacrylamide	[278]

3.2.4 ARGET and Polymer Brushes

Activators Re-Generated by Electron Transfer (ARGET) is a development of ATRP and can be used to reduce the concentration of metal catalysts up to 1000 times to ppm levels [249, 258, 266, 279-281]. In addition, polymerisations can be completed in the presence of limited amounts of air so reactions do not have to be deoxygenated [249, 267, 280]. In ordinary ATRP, the effect of oxygen is that Cu(I) is oxidised without being halogenated as illustrated in Scheme 5, showing the transition back to Cu(I) due to the reducing agent. In ATRP, a small amount of oxygen can result in a large drop in the rate of polymerisation. ARGET ATRP overcomes this problem by having a readily available source of a reducing agent. Therefore any Cu(II) generated is reduced back to the useful Cu(I). Zhu *et al.* used polydopamine as an ATRP initiator, methyl methacrylate as a monomer and (+)-sodium L-ascorbate as an ARGET [276]. After 24 h of polymerisation characterisation shows that 72 nm of methyl methacrylate brush was formed on top of the 58 nm initiator. In addition, over 72 h 239 nm of methyl methacrylate was formed.

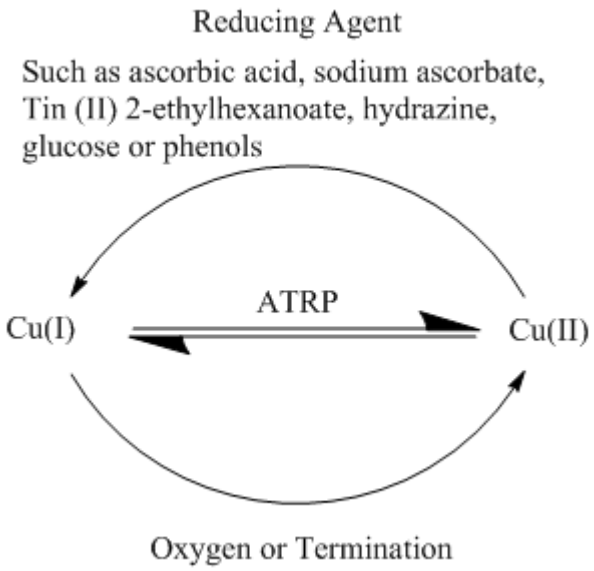

Scheme 5 Illustrating how the reducing agent can regenerate lost Cu(I) through oxidation or termination. Using information from [217, 249, 267, 276, 279, 282, 283].

3.2.5 Gel Permeation Chromatography (GPC)

Owing to the correlation in molecular weight between polymers formed in solution and those formed by SI-ATRP, GPC provides a facile way of determining average molecular weights as well as polydispersity. The polydispersity value will help to determine whether successful, controlled polymerisation has taken place. This technique will allow a comparison between variables such as substrate and solvent, silicon nitride/silicon wafer and anisole/PAO for example. In addition, the free initiator, as previously discussed, is known to help control polymerisations.

3.3 Polymer Brushes synthesis

One of the main advantages of polymer brushes formation by ATRP is the controllability of the polymerisations [246, 284]. Similar to SAMs, polymer brushes are influenced by a range of factors

such as temperature, solvent selection, presence of oxygen and free initiators. Unless otherwise mentioned, in this section polymer brushes are synthesised through self-assembling initiators and subsequent polymerisation from the active sites. An example is given in Scheme 6, showing a simplistic view of the polymerisation procedure from surface attached initiator monolayers to polymer growth. This was used by Munirasu *et al.* in forming polymer brushes of benzyl methacrylate with a copper catalyst, PMDETA ligand and free sacrificial initiator [268].

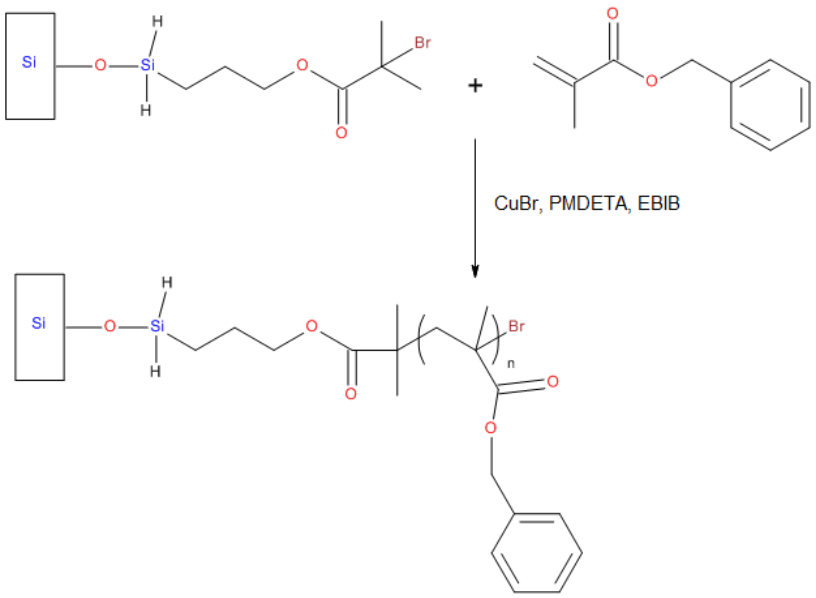

Scheme 6. A schematic of the simplified ATRP process.

3.3.1 Free Initiators

It has been reported that the addition of deactivators or free initiators are needed to control polymerisations to create uniform polymer films [285]. Öztürk *et al.* formed lauryl acrylate polymer brushes in the pursuit of an ultrahydrophobic surface [270]. With the addition of ethyl-α-bromoisobutirate (EBIB) as a free initiator the authors reported a linear trend between thickness and time. As characterized by AFM, it was found that the brushes collapsed in some places, which the authors dubbed footprints as seen in Figure 3.3. However, the relative roughness of the surface was found to be 0.8 nm - 1.6 nm. They successfully achieved a maximum contact angle of 163 ± 2.8°. They also found that the water contact angle increased linearly with the immersion

time and suggested that the thickness increased linearly with the time, hence concluding that the thickness was a tuneable parameter that could be accurately reproduced [270].

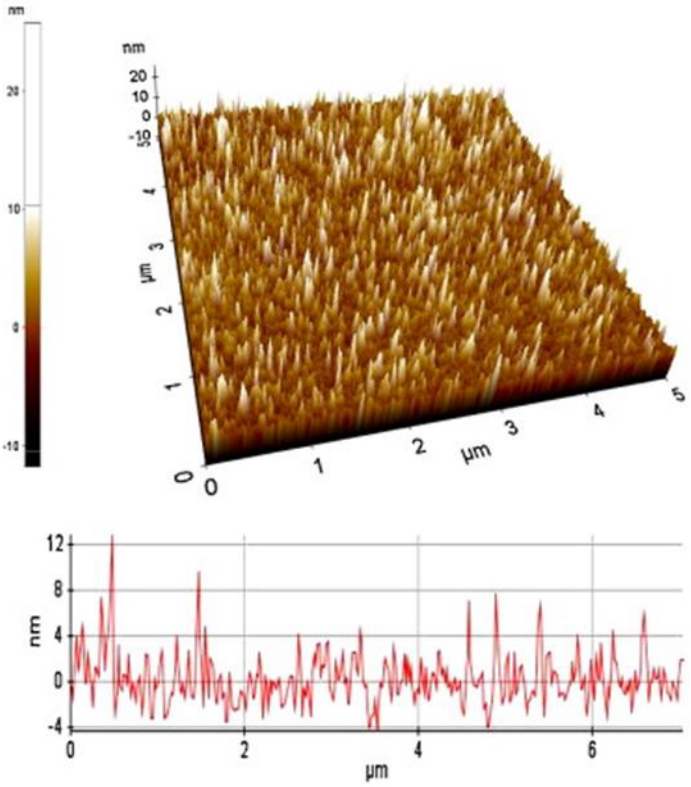

Figure 3.3. showing lauryl acrylate polymer brushes, some of which are partially collapsed and below a cross section. Reprinted with permission from [270].

Turan *et al.* studied the formation of poly(N-isopropylacrylamide) with the addition of a chain transfer agent, 2-mercaptoethanol [126]. Using varied amounts of 2-mercaptoethanol, polymer brushes were formed at 90°C over 18 h. The concentration of 2-mercaptoethanol was shown to control the chain length of the polymer brush with lower concentrations dictating longer chain lengths. However, higher concentrations resulted in lower roughness values although with reduced chain density. Turan *et al.* conducted another study on poly(N-isopropylacrylamide) polymer chains although without using an extra chemical additive to control polymerisation. Ellipsometry measurements showed a dry thickness of 66 nm. Munirasu *et al.* synthesised benzylmethacrylate polymer brushes as well as diblock copolymers with styrene on silicon wafer [268]. Benzylmethacrylate polymer brushes followed a linear trend with time showing that brush length can be controlled with precision due to the additional EBIB. Their GPC results from the free polymer showed very low polydispersity indicating that the surface attached polymer grew at a uniform rate. Styrene performed similarly in respect to the EBIB-thickness trends. Liu and co-workers studied methyl methacrylate (MMA) polymers, at 90°C they varied the amount of a free sacrificial initiator [250]. The thickest film produced had the lowest amount of EBIB added which is in agreement with Öztürk *et al.* Table 3.2 shows how the concentration of EBIB affects

thickness, which is inherently correlated to M_n (number average molecular weight). Also notable is the slight decrease in polydispersity with minimal effect on contact angle.

Table 3.2. Results of ATRP of methyl methacrylate (MMA) with EBIB as a free initiator.

Concentration of EBIB mmol L^{-1}	Conversion of MMA	M_n, g mol^{-1}	PDI	Thickness nm	Contact angle (°)
20	77%	46 800	1.4	30.5	72
40	99%	30 600	1.1	27.6	72
60	93%	28 300	1.3	26.4	72
80	99%	22 400	1.1	23.7	73
100	99%	17 400	1.1	17.1	73

Reprinted with permission from [250].

The same experiments were done with solely styrene except at an elevated temperature by Liu *et al*. [250]. The data shows an irregular trend with 50mM showing twice the thickness of the next highest thickness. The authors also created a random copolymer, using a ratio of methyl methacrylate to styrene of 2:1 and a range of EBIB concentrations the best compromise for conversion of monomers and thickness of film was found to be 50 nm however the thickest film was created by using 25 mmol/L. When the ratios of monomers was inverted, the thickness was less predictable much like what was shown when the styrene was the only monomer limiting the influence of EBIB as a controlling sacrificial initiator. Zhou et al. constructed poly(2-(dimethylamino)ethylmethacrylate) brushes on silica particles, where a native oxide layer was found similar to that on silicon wafers and other silicon based substrates. Free polymer that was produced through the addition of EBIB was precipitated, this allowed gel permeation chromatography to take place. GPC results allow the calculation of M_n and molecular weight average (M_w) in addition to increasing the control of the reaction [264, 286].

3.3.2 Polymerisation Time and Temperature

In addition to the effects of free initiators, polymerisation time and temperature can affect the final polymer that is formed. It is still worth considering that both temperature and time are inherently linked to a plethora of other variables. Temperature can have either positive or negative effects to polymerisations at elevated temperatures. For example, better control over the polymerisations may occur but this can lead to catalyst degradation or side reactions increasing [28]. In addition, the increase in temperature positively influences the activation rate constants especially for less reactive initiators [287]. When considering polymerisation time high levels of monomer conversion will result in the rate of propagation slowing dramatically and end group functionality may be lost [28]. Munirasu *et al*. synthesised benzylmethacrylate polymer brushes and achieved a thickness of above 300 nm after polymerisation for 37 h as seen in Figure

3.4 [268]. Figure 3.4 also clearly shows a linear trend with time. Diblock polymers were synthesised to show that the end groups are still intact therefore polymerisation was not complete and end group functionality still remained.

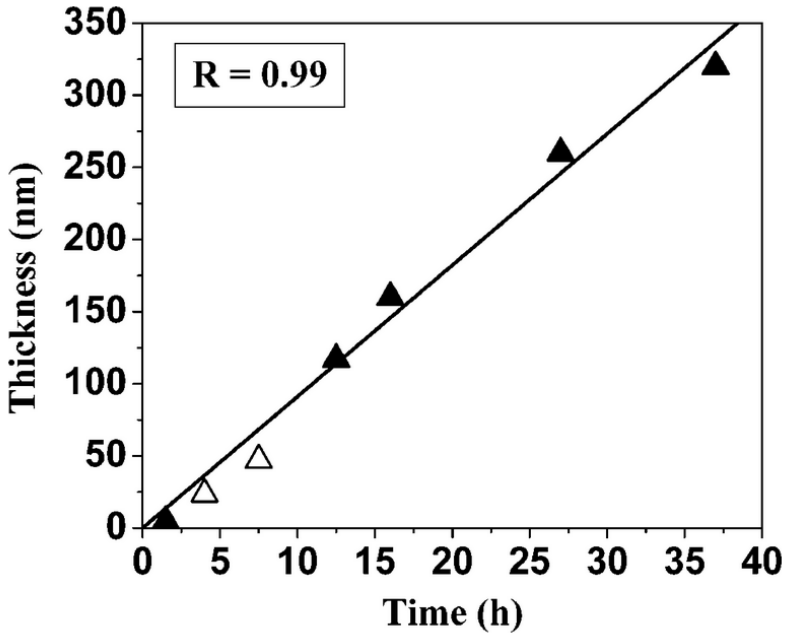

Figure 3.4. Showing the linear relationship between time and thickness of benzylmethacrylate polymer brushes. Open triangles are from a repeat of the same experiment. Reprinted with permission from [268].

Liu and co-workers synthesized polymer brushes from methyl methacrylate, styrene and a random copolymer consisting of both [250]. When the authors studied methyl methacrylate as a standalone monomer, the conversions reached 99% at 90°C with a small amount of EBIB. However, for styrene on its own, the conversion changed from 10% at 90°C to 95% at 125°C as can be seen in Figure 3.5 [250].

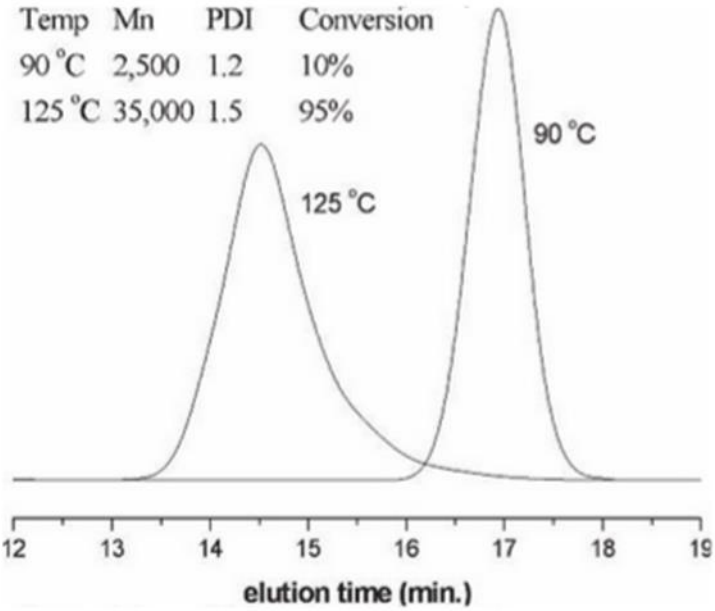

Figure 3.5. GPC results indicating low conversion of styrene at lower temperatures with increased polydispersity. Reprinted with permission from [250].

Song *et al.* produced a copolymer of oligo (ethylene glycol) methacrylate and 2-propynyl methacrylate[251]. This was introduced in a 60:40 ratio to form the polymer brush. After 12 h at 40°C the thickness of the brushes was found to be 26.8 nm. Interestingly, after formation of these films they were used for click chemistry, specifically click glycosylation [251]. Zhou *et al.* formed poly(2-(dimethylamino)ethylmethacrylate) brushes over 12 h at 90°C. Free polymer that was produced through the addition of free sacrificial initiator was precipitated, allowing gel permeation chromatography to take place and number average (M_n) was 6940 and molecular weight average (M_w) 11870. Although polymerisation time was 4 h less there is a considerable gap to the results produced by Liu *et al*. as can be seen in Table 3.2 [264].

3.3.3 Summary

As in the case of SAMs, there are numerous variables to consider before embarking on polymer brush synthesis. With respect to surface attached initiators, the principles of SAM formation also apply owing to the essential monolayer. Also highlighted here is the role of free sacrificial initiators and their role in controlling the polymerisation. This is something that should be considered as the free polymer can then be analysed giving a detailed representation of the polymerisation success as well as the state of the attached polymer. The temperatures covered range from 40°C - 90°C, although the lower temperature resulted in a much thinner film it is possible to conduct polymerisation at lower temperatures. As previously stated, excessive temperatures can result in catalyst quality reduction and an increase in side reactions. The catalyst complex design must take into account the kinetics of polymerisation, included in this is also the unique monomeric atom transfer equilibrium constant. If the constant is too small polymerisation will be very slow. Solvent selection has broadly the same considerations as in SAM. In addition, the solubility of the catalyst must be considered although this is linked to ligand

selection and temperature. Adequate control over polymer synthesis will produce the best films in terms of density and uniformity as well as reproducibility. Following this, there have been various developments of ATRP that facilitate the formation of the desired end polymers, such as the previously mentioned ARGET and sacrificial initiators.

3.4 Polymer Brushes on Silicon Wafers for Tribological Applications

The tribological properties of polymer brushes are dependent on the surface attachment, the swelling behaviour of brushes if a solvent is present, the type of stress encountered as well as contact pressures [123]. The pioneers of polymer brushes for tribology, Klein *et al*., also realised the importance of a good solvent to facilitate swelling and therefore better sliding performance [288]. The immersion of polymer brushes in good solvent allows brush swelling, known to help lubricate as illustrated in Figure 3.6 [223, 289-294]. Polymer brushes can also be based on zwitterionic monomers which are usually hydrated by water solutions, however these will not be covered in this review due to their poor characteristics in non-aqueous solvents such as motor oil. If the reader is interested in polyzwitterionic brushes they are referred to references [295-297]. The mechanism in which solvated polymer brushes lubricate is thought to be as follows [123, 298]:

A. The resistance to rearrangement of the grafted chains with the repulsive nature of the brushes as well as an osmotic pressure within the brush system;
B. Lubricant entrapment in the polymer brushes;
C. High concentrations of lubricant in the outer polymer brush creates a low shear area protecting the brush system.

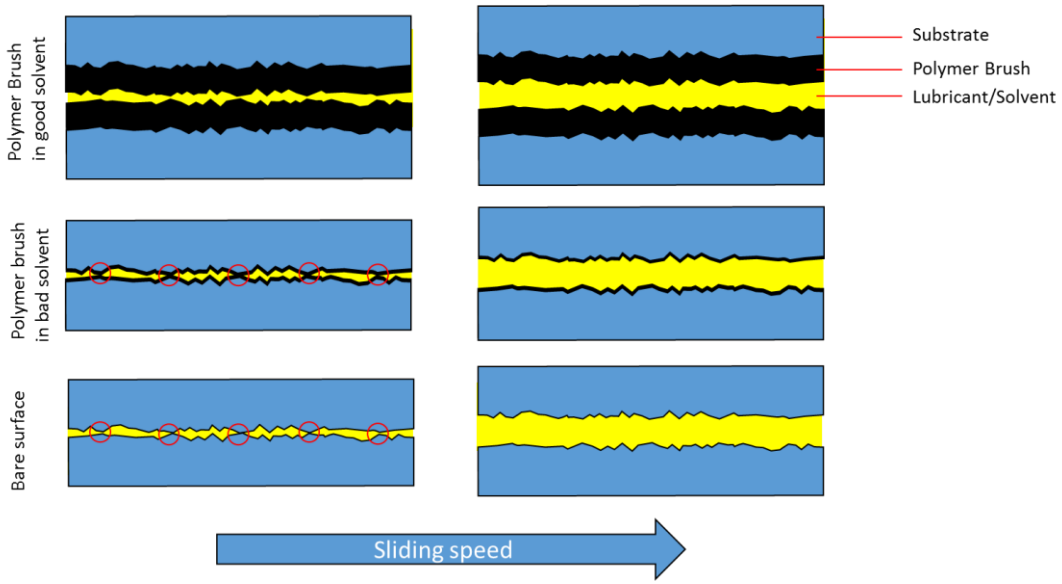

Figure 3.6. An illustration of swollen polymer brushes lubricating a contact in comparison to poor solvent and a bare surface. Note the possible asperity contacts in poor solvent.

3.4.1 Brush Thickness and COF

Thickness of polymer brushes is thought to have an effect on the lubrication system [299] Kang *et al*. and Bielecki *et al.* amongst others have been able to correlate polymer brush growth to

polymerisation time to confirm expected trends as can be seen in Figure 3.7 [123, 234]. Bielecki *et al.* synthesised methacrylates with different side chain lengths via SI-ATRP using hexyl- (P6MA), dodecyl- (P12MA) and octadecyl methacrylate (P18MA) monomers [27]. Ellipsometry measurements of the dry thickness of the P6MA, P12MA and P18MA polymer brushes showed thicknesses of 90, 250 and 230 nm, respectively.

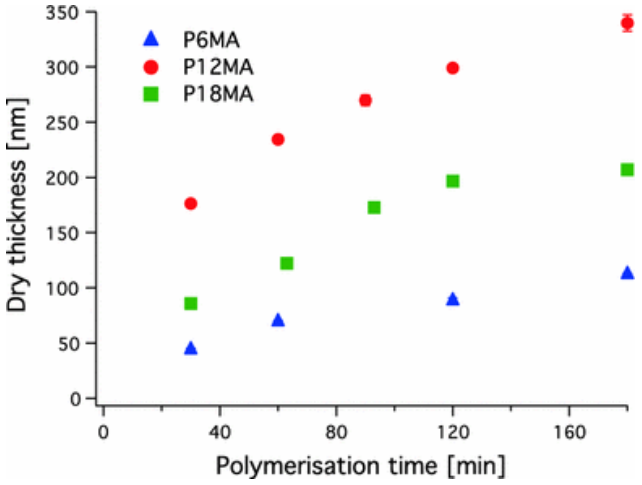

Figure 3.7. Hexyl-, dodecyl- and octadecyl methacrylate polymer brushes formed from ATRP. Dry thicknesses measured by ellipsometry. Reprinted with permission from [123].

Tribological studies were conducted using a ball-on-disc NTR2 tribometer in a reciprocating motion over 120° with the speed change being controlled sinusoidally. In a 20 cycle test with toluene all the brushes showed a low COF in the range of 0.01-0.02. It is worth noting that the much lower thickness in the P6MA polymer did not rule out a low COF in this case, although thicker brushes are usually related to lower COF values. The same experiment was completed using hexadecane, ethanol and PF350 oil as shown in Figure 3.8. The greater reduction in friction when lubricated with non-polar liquids may be due to brush swelling improving the lubricating qualities as mentioned above. In this experiment the two longer chain and thicker polymer films fared considerably better than P6MA which increased the COF of friction. In all cases the lubricating qualities of the 350 cSt petroleum fraction (PF350) were higher than that of hexadecane in the silicon borosilicate/silicon wafer contact. When the authors selected P12MA and created three different thicknesses of polymer, 70, 140 and 250 nm thick, the two lower coatings lost their friction reducing characteristics within a few meters. The 250 nm polymer film maintained a COF of 0.012 over more than 100 m.

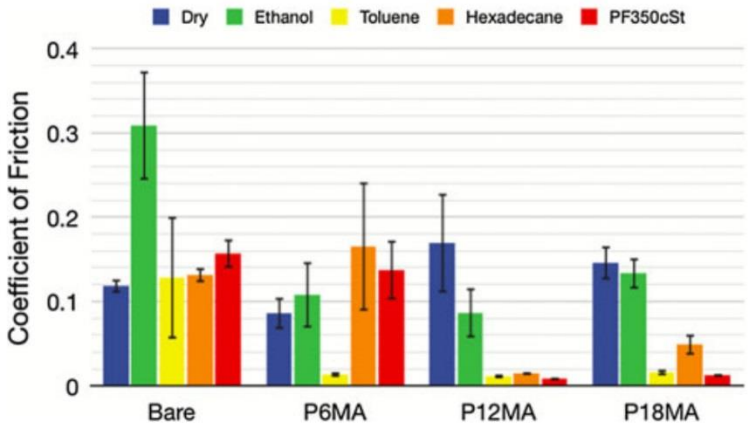

Figure 3.8. COF values for the polymer brushes in different lubricants or dry conditions. Reprinted with permission from [27].

The authors ascribed this to the fact that a thicker polymer film can be compressed more and reduce the likelihood of two hard counterparts coming into contact and the destructive high pressures destroying coatings. The application of a more viscous lubricant on the two thinner polymer coatings reduced the COF although the chemical instability may have been changed as there was a rapid failure of the 70 nm thick polymer in a more viscous ester fluid (EO500). The authors concluded that a greater initial brush thickness was more effective in separating the surfaces [27]. Bhairamadgi *et al*. compared the adhesion and frictional characteristics of a polymer brush that was synthesised using fluorinated monomers to one based on non-fluorinated monomers [300]. The fluorinated polymer brush showed a strong correlation between thickness and adhesive pull off force in the tested range of 5 N - 40 N. At every loading test brushes between 65-140 nm, thicker brushes resulted in a lower pull off force, however, between 9 nm and 29 nm there was some discrepancy but it was within the error bar limits. Non-fluorinated polymer brushes proved too high to measure due to the forces of attraction when the probe was bought near the surface. Lateral friction loading showed good correlation with other studies on polymer brush length vs COF. Fluorinated polymer brushes of between 10 nm - 140 nm were analysed and the COF was reduced in an almost linear fashion throughout to a lowest friction of 0.0057. In adhesion testing fluorinated polymers proved to be more successful at reducing friction than their non-fluorinated counterparts. The length of polymer brushes was also investigated by Sakata *et al*. who found that shorter chains of methyl methacrylate had a much larger margin of error [291]. The authors also concluded that a good quality solvent allows the extension of the brushes and in poor solvent they can be seen to be compressed. This was confirmed by tribological testing in good solvents, toluene and acetone, and bad solvents, hexane and cyclohexane. Similar behaviour has been observed with poly(2-methacryloyloxyethylphosphorylcholine) brushes and the swelling effects in poly(methylmethacrylate) and other methacrylate derivatives [301-303]. However, these brushes are hydrophilic so water can provide a suitable aqueous lubricant. Ramakrishna *et al.* also

concluded that a thicker brush, in this case poly(N-isopropylacrylamide) in water with a colloidal probe, performed better with regards to friction force [304]. Nomura *et al*. varied the composition of solvent to subsequently affect the swelling of a polystyrene brush and therefore the lubricating qualities of the modification [271]. Although not using ATRP, Limpoco *et al*. produced 117.6 nm polystyrene brushes [305]. The authors then varied solvent and Figure 3.9 shows the effect.

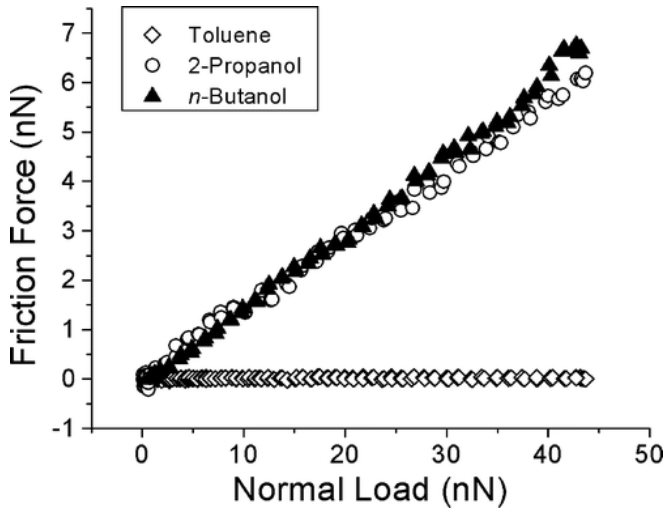

Figure 3.9. AFM friction force vs normal load in good and bad solvents. Reprinted with permission from [305].

As is the case with SAMs, friction is affected by the length of pre-formed adsorbed polymers. This is shown by Lin *et al.* who used the grafting-to approach [125]. Three different copolymer brushes, poly(propylene oxide)–poly(ethylene oxide)–poly(propylene oxide), (PPO–PEO–PPO), were used as lubricants. Namely a PPO–PEO–PPOs with a molecular weights of 2700 with 60% PPO, 2150 with 80% PPO, 3100 with 80% PPO, designated as 17R4, 17R2 and 25R2, respectively. Ellipsometry measurements showed that the thickest film produced was 25R2 polymer of around 6 nm, and the thinnest film was 17R4 of approximately 1 nm. This again highlights the differences in the film thickness produced between 'grafting to' and 'grafting from' procedures. Tribological testing was carried out using a pin-on-disc tribometer. The better tribological performances were attributed to the longer chains and thicker films that had been formed.

3.4.2 Sliding Speed and Load vs COF

Bielecki *et al.* constructed Stribeck curves for the ATRP synthesised polymer brush of P12MA monomers [27]. Under a constant load the brushes showed a good correlation with the shape of a Stribeck curve when lubricated with hexadecane and a range of oils with viscosities from 36-1300 cSt. In addition, the brushes all showed an improvement in friction over the bare substrate in a lubricated environment. Bhairamadgi *et al*. synthesized fluorinated polymer brushes; as expected, in both AFM adhesion and lateral friction testing the increase of load increased the pull off force and friction force [300]. In a range of loads from 10 nN - 90 nN the friction force increased in a linear manner across all thicknesses. Liu *et al.* studied poly(N-isopropylacrylamide) brushes

formed via ATRP [278]. After ATRP the samples were tested using a ball-on-disc tribometer using deionised water as a lubricant. Ellipsometry measurements gave the dry thickness of the brush to be approximately 76.2 nm. The polymer brush achieved the lowest friction which stabilised at 0.03 for 1062 s which was reduced to 0.01 under a load of 0.78 N and sliding speed of 41.66 mm/s. With an increased load of 0.98 N the polymer lubricant reduced the COF to 0.1, at a higher sliding speed of 55.54 mm/s the grafted polymer did not change significantly whilst the lubricant approached a COF of 0.125. With an increased load of 0.98 N the grafted reduced the COF less and at a higher sliding speed this was reduced once again to approximately 0.125. The polymer lubricant followed the same trend. The authors presented Figure 3.10 showing how the polymer brushes may interact with the deionised water as a lubricant with and without compressive forces. Heeb *et al*. also used water as a base for a buffer solution to lubricate hydrophilic brushes [290]. Tribological testing of poly(methacrylic acid) brushes was performed under similar conditions but slower slide speeds (PDMS ball/silicon wafer, on pin-on-disc, 1 N, sliding speeds of 0.25-10 mm/s) and achieved COF under 0.005 for each test.

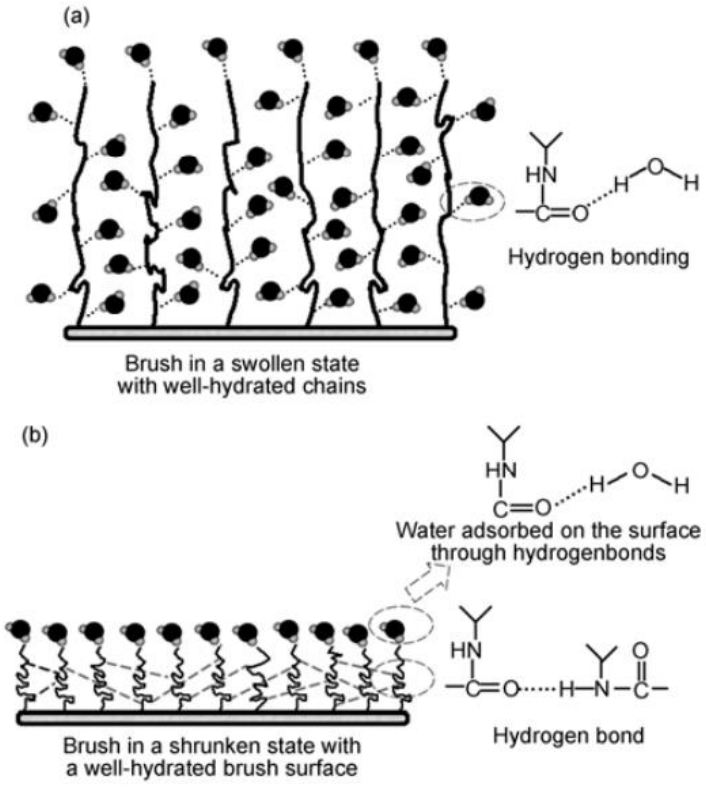

Figure 3.10. A representation of how polymer brushes can react with and without the presence of load. Reprinted with permission from [278].

The polymer brushes that Lin *et al.* previously introduced consistently reduce friction over the sliding speed range of 0.01 m/s - 0.1 m/s [125]. The effect of applied load was investigated by changing the load from 4 N - 8 N under a constant sliding speed of 0.01 m/s and constant concentration of polymer solutions. The notable changes in the COF are from a PPO–PEO–PPO copolymer with a M_w of 2700 which increased from 4 N to 5 N then levelled off, to a higher

molecular weight of 3100 which shows a slight increase in COF throughout the entire test but up to approximately 7.5 N surpassed the other polymers in friction reduction. A molecular weight of 2700 consistently showed COF values below 0.15 from 4 N - 7 N where it sharply reduced. The COF fell below that of the highest molecular weight test after 7.5 N. Sun *et al*. sought to improve the tribological resistance of a polyamic acid polyimide film (PI) [285]. They achieved this by synthesizing poly(glycidyl methacrylate) brushes that are epoxy terminated as an adhesive layer before application of the PI film. This increased the lifetime of the film from 6000 sliding cycles to in excess of 25000 under a 0.5 N load at 20 mm/s with a consistently low COF of 0.08.

3.4.3 Summary

As previously discussed there are numerous variables to be considered for polymer brush synthesis. However, polymer brushes have proven that low COF is possible. For NEMS and MEMS devices it should be noted that in the absence of liquid lubricant there will be no brush swelling, however, fluorinated polymer brushes have been shown to reduce both adhesion and pull off force, thus creating opportunities for lubrication solutions in this field. In liquid lubricated systems it has been shown repeatedly that swollen brushes have better tribological properties in a good solvent, for future applications this is a key finding. Thicker polymer brushes have been shown to resist the effects of load by coping with the compressive forces better than thinner polymer films. The thicker brushes have proven to reduce contact between surface asperities and therefore reduce friction as well as the shearing of the polymer. Polymer brushes could be used to reduce wear, however, as soon as the polymer brushes have been removed wear will occur. The strong attachment of the polymer brush to the silicon wafer is key to reduce wear.

3.5 Polymer Brushes on Silicon Nitride

Polymer brushes have been formed by ATRP on surfaces ranging from silicon nitride cantilevers to wafers. However, very few tests have been done regarding tribology. de Groot *et al.* used a silicon nitride nanoporous substrate to form poly(methacrylic acid) brushes using ATRP [306]. The ATRP initiator was deposited via vapour phase deposition over 16 h. Sodium methacrylate was polymerised and after 1 h ellipsometry measurements showed that the film thickness was around 60 nm thick. The swell and collapse of the polymer brushes were also investigated using AFM. Nguyen *et al.* constructed a zwitterionic polymer brush on silicon nitride using ATRP [233]. The silicon nitride was deposited on silicon wafers using low pressure chemical vapour deposition, then after etching with HF, 1,2-epoxy-9-decene was attached using UV light. After immersion in 1,2-ethlyamine the ATRP bromoisobutyryl bromide was attached using aforementioned techniques. The polymer brush of [3-(methacryloylamino)propyl]dimethyl(3-sulfopropyl)ammonium hydroxide inner salt monomers formed >20 nm of growth in the first hour and 70 nm in 8 h. A later paper by Nguyen and co-workers detailed the same procedure for attachment of initiator followed by polymerisation upon a silicon nitride surface [307]. However,

the purpose of both polymer brushes created by Nguyen was protein repulsion. Gabriel *et al.* have created brushes on silicon nitride AFM probes, using electro-initiated polymerisation techniques these authors successfully formed poly(N-succinimidylacrylate) brushes [308]. This was confirmed by approach and retraction curves using the cantilevers and a bare silicon substrate. The force curves could then be used as a form of sensing, in a similar way that monomers were used in chemical force microscopy (CFM). Although not created by ATRP, Hartung *et al.* used a preformed copolymer brush-like additive to lubricate Si_3N_4 contacts [183]. Poly(L-lysine)-graft-poly(ethylene glycol) (PLL-g-PEG) was dissolved in a buffer solution of 4-(2-hydroxyethyl)piperazine-1-ethanesulfonic acid in water (adjusted to pH 7), and the samples were immersed for 30 minutes before testing was carried out. The cationic backbone adsorbs onto a negatively charged surface, hence the need for a buffer. Ellipsometry showed that the dry film thickness was approximately 15.7 nm. Tribological testing was completed using a pin-on-disc tribometer with a silicon nitride pin. Under a load of 5 N and speed of 120 mm/s the COF was 0.02 after running in under the buffer solution, after the addition of the buffer and polymer solution the COF dropped to 0.003. The solution also effectively lubricated under a slower speed of 10 mm/s under a load of 2 N which resulted in a COF of 0.04. However, the polymer inhibits the tribochemical reactions leading to a roughened surface and micro fractures.

3.6 Challenges of Polymer Brushes for Lubrication

As is the case with SAMs there is no standardised testing regime, subsequently this results in difficulties in comparing all polymer brushes especially when considering the scale difference when comparing micro and macro tribology and the loads used as well as the contact areas. An additional consideration is that under microtribology conditions the surface properties play a much bigger part in comparison to macrotribology when it is the bulk material, which indicates that polymer thickness is a key factor [309]. Previous studies show the importance of controlling polymer brushes, thicknesses, swelling behaviour, initiator attachment and catalyst systems, all of which and more must be considered when attempting polymer brush synthesis. As documented above the technology and ability to produce high quality polymer brushes does exist. However, this will prove to be much more difficult when considering in-situ lubrication, such as an additive-like component in a lubricating fluid. This will be a main concern in macro systems, but micro systems may well have similar issues. Another problem with in situ lubrication is the time required to produce the thicker brushes that have been shown to be capable of producing low COF. The stability of the Cu complex catalyst and the oxidative effects have been thoroughly documented, yet even with the developments of ARGET this will appear as a point of interest for the application of polymer brushes in years to come. It has also been found that the unstable copper catalyst could be reduced by iron and therefore lose its reactivity [27, 310]. Although this could be reversed by ARGET it becomes another complication of the polymer brush system. Although it has

been shown that ATRP can be completed from silicon nitride, and that SAM attachment to silicon nitride has been proven, the lubrication of silicon nitride from SI-ATRP has not yet been performed.

3.7 Summary of Literature Review

This literature review has summarised the basics and the key developments in SAMs and polymer brushes with a focus on tribology. Several decades have passed since the original study of self-assembling thiols on gold surfaces was carried out, and SAMs have shown their feasibility for NEMS and MEMS lubrication. Although research has thrived in MEMS/NEMS, research has also been conducted to develop SAMs in macro applications especially on the controlling of interfaces and wettability that are key to the success of using SAMs. A multitude of SAMs have shown significant friction-reducing characteristics which opens up possibilities of additive applications in automotive engines, certainly regarding their ease of application in comparison to polymer brushes, however the shearing of such monolayers is still a concern. This growing area of research will continue to thrive due to the diverse disciplines that provide limitless potential applications. Following extensive research it is now possible to produce surface-initiated polymer brushes upon surfaces by using controlled polymerisation techniques. These living radical techniques such as ATRP have led to unrivalled control over chain length, architecture and composition. Polymer brushes are established in polymer science and their interesting structures will lead to commercial opportunities. Limited research has been completed on the application of polymer brushes to silicon nitride especially with respect to lubrication. However, the ability to create thin polymer films with specific functions means that meeting this challenge should be feasible. In addition, owing to the structure of silicon nitride, lessons learned from silicon wafers and the expanding nanoparticle field should provide a bridging step. That said, the air-sensitive nature of ATRP will be difficult to overcome in in-situ polymerisations although developments such as ARGET could combat these problems. It should be remembered that polymer brushes for tribological applications encompasses a wide range of disciplines and all of the skills from these areas will be required to create commercially viable solutions.

In summary, the author thinks that the synthesis of polymer brushes through ATRP will meet the requirements of many tribological contacts. The wide range of monomers that can be polymerised, the robustness of the technique, coupled with developments such as ARGET present attractive solutions.

4 Methodology

This section includes the techniques, materials and test programme to be used in meeting the objectives previously discussed in the section titled Aims and Research Objectives and also illustrated in Figure 4.1. The final aim of the project is to produce a surface-initiated polymer brush that successfully reduces the COF of silicon nitride whilst avoiding the presence of sulphur and phosphorus in the coating. Particular areas of interest are friction reduction, shear stress stability, load resistance, solvent synergy and thicknesses as these are key to lubrication. Significant milestones to be achieved are detailed in Figure 4.1. The notable milestones are replicating the literature values for the formation of OTS, the synthesis and attachment of an ATRP initiator, the synthesis of polymer brushes and the subsequent successful reduction in friction.

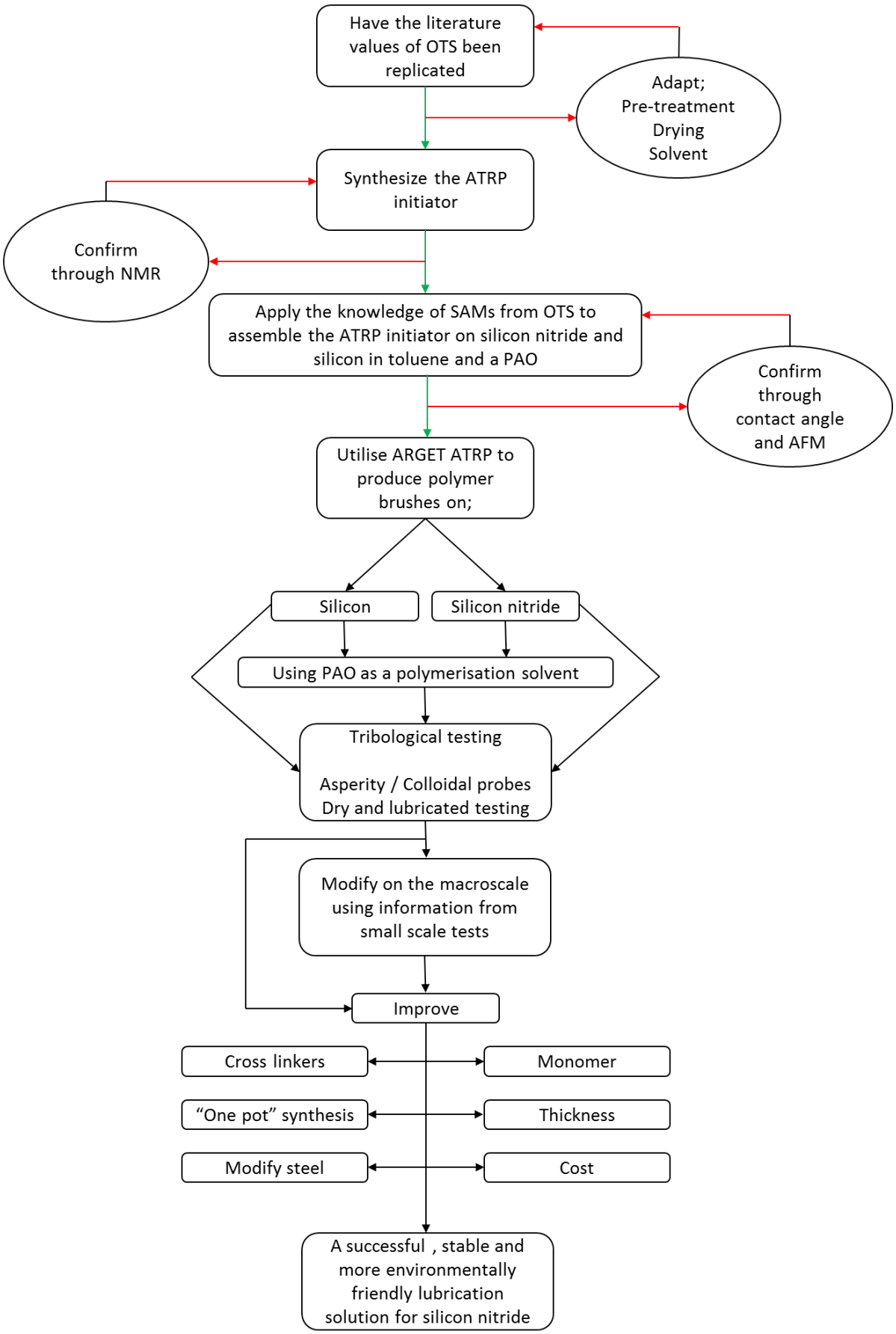

Figure 4.1. Flow chart of the proposed research route.

4.1 Materials

Table 4.1 shows the chemicals and suppliers that have been used in the project.

Table 4.1. Materials used in experiments

Item Description	Supplier	Application
(+)-Sodium L-ascorbate, crystalline, ≥98%	Sigma	ARGET
4x21.8mm Rounded End Loose Needle Rollers	Simply Bearings	POD pin
AFM cantilevers, NANOSENSORS™ PPP-NCHR	NanoWorld	Characterisation
Allyl 2-bromo-2-methylpropionate	Sigma	For ATRP initiator synthesis
Anisole, 99%	Sigma	Solvent
Chloroform-d ampules	Sigma	NMR solvent
Copper(II) bromide, 99%	Sigma	Polymerisation Catalyst
Decane, ≥99%	Sigma	Solvent
Ethanol, ≥99.5%	Sigma	Cleaning
Ethyl α-bromoisobutyrate, 98%	Sigma	Free Initiator
Hydrogen peroxide, 30 wt. % in H_2O	Sigma	Part of piranha
Methyl methacrylate contains ≤30 ppm MEHQ as inhibitor, 99%	Sigma	Monomer
N,N,N′,N″,N‴-Pentamethyldiethylenetriamine, 99%	Sigma	Ligand
NANOSENSORS™ PPP-CONT AFM probes	NanoWorld	Characterisation
Nitrogen, oxygen free	BOC	Drying gas
OTS, ≥90%	Sigma	SAM
Platinum on carbon	Sigma	For ATRP initiator synthesis
Polished Si Wafer, p-doped	Pi-KEM	Substrate
Prepacked column for removing MEHQ	Sigma	Inhibitor Removal
Silicon nitride discs,100 mm diameter 610 mm thick low pressure sintered	H.C. Starck	POD substrate
Sodium sulfate	Sigma	Drying agent
Stainless Steel Powder 420L Spherical	US nano research materials	Colloidal probe
Sulphuric acid, 95.0-98.0%	Sigma	Part of piranha
THF, reagent grade, ≥99.0%	Sigma	Solvent
Tin(II) 2-ethylhexanoate	Sigma	ARGET
Tipless AFM Cantilevers TL-CONT	NanoWorld	Characterisation
Toluene	Sigma	Solvent
Trichlorosilane	Sigma	For ATRP initiator synthesis
Two part epoxy	JB Weld	Colloidal probe

4.2 Experimental Programme

The development of the experimental progress is detailed in the next section, within this section the way in which a high quality SAM is formed is discussed. These techniques developed in SAMs are then carried over to the formation of the initiating species of polymer brushes synthesis. In addition the improvements made to the synthesis as well as the formation of the novel colloidal

probe are detailed in this section. The way in which the tribological tests were carried out are also detailed in this section.

4.2.1 Preliminary OTS SAMs

Preliminary experimentation involved a well-known SAM (OTS) formed on silicon wafers without surface pre-treatment to create a baseline quality which all other experiments can be compared to. From the open literature it can be seen that monolayers can be formed from 2.5 mM solutions, and a solution of OTS in decane was used in this work [17]. After cleaving the wafers into approximately 1 cm x 1 cm samples they were ultrasonically cleaned in ethanol then DI water for 30 minutes. The samples were then blown dry with compressed nitrogen. Following immersion in the 2.5 mM OTS solution for 2 h the wafers were washed with ethanol to remove the excess OTS and decane solvent from the surface. The samples were then ultrasonically cleaned in ethanol for 5 minutes immediately before characterisation

4.2.2 Plasma vs Piranha

To ensure successful SAM formation surface pre-treatment routes were investigated. The kinetics and equilibrium of SAM formation rely heavily on the nature of the surface chemistry and the type of molecule. Therefore, the surface chemistry and cleanliness of the substrate would play a determinant role in the formation process and the quality of the formed SAMs. Clearly dust and chemical residues on substrate during surface cleaning will have a detrimental effect on the quality and coverage of SAM. A range of techniques have been adopted in surface preparation prior to creating SAMs. A standard surface cleaning procedure involves ultrasonic cleaning in different solvents to remove surface containments followed by blow drying to get rid of solvent residues and dust, but an additional step of hydroxylation is usually needed for silicon-based or metal oxide substrates. For such systems that require a highly hydroxylated substrate to form high quality SAM an oxidation treatment is employed using either piranha solution or plasma exposure. Method 1 and method 2 as seen below were investigated. In all experiments detailed in this report, freshly cleaved wafers, approximately 1 cm^2 were used.

Table 4.2. Wafer pre-treatment methods

Method 1, “Piranha”	Method 2, Plasma
A solution of piranha was prepared by slowly adding hydrogen peroxide (30%) to sulphuric acid (98%) in the ratio 3:7 whilst stirring. The temperature was measured to ensure the resulting exothermic reaction was under control. Ultrasonically cleaned wafers exposed to piranha from 5 to 30 minutes at 50°C [59, 77]. The samples were then rinsed with copious amounts of water before drying and characterisation.	Ultrasonically cleaned wafers were then transferred to a PVA TePla 300 plasma asher and treated from 30-180 s. After 5 minutes ultrasonic cleaning in ethanol and water sequentially the wafers were dried in nitrogen then characterised.

4.2.3 OTS SAM

To verify that the quality of the SAMs produced by including the pre-treatment has increased OTS was formed on plasma treated wafers for comparative purposes. This will verify that the selected pre-treatment route is an acceptable route of surface preparation. Silicon wafers were ultrasonically cleaned, dried using an extended nitrogen drying cycle, plasma treated then immersed in 2.5 mM solution of OTS. After 2 h the modified wafer was removed from the OTS solution, rinsed in copious amounts of ethanol, ultrasonically cleaned in ethanol then DI water for 5 minutes each and blown dried in nitrogen. The monolayers were then characterised by contact angle and AFM.

4.2.4 ATRP Initiator Synthesis

The stability of polymer brushes is key, consequently they are required to be strongly bonded to the substrate. Using a surface-initiated reaction provides the strong covalent bond required. Initiators must be synthesized as they are not commercially available. High purity allyl 2-bromo-2-methylpropionate (Sigma) was used as starting material, which then undergoes hydrosilylation to produce the initiator (3-[chloro(dimethyl)silyl]propyl 2-bromo-2-methyl-propanoate) with a chlorosilane head group that can then self-assemble like SAM. This procedure is based on the following papers [261, 277, 314].

The ester (1.6 mL), dimethylchlorosilane (10 mL) and Pt on activated charcoal (10 mg) were refluxed for 24 h in an airtight microscale glass apparatus under nitrogen. The addition of the ester to the dry round bottom flask was carried out in a fume hood by volume to reduce exposure. The silane was syringed in through a septum. Due to the potential reactivity with water heating was by immersion in a sand bath on a hot plate.

The resultant solution was distilled to produce an oily liquid. This procedure removed the excess dimethylchlorosilane. The resultant oil was filtered through a 0.2 µm cellulose syringe filter to remove the majority of the catalyst and then passed over anhydrous sodium sulphate to remove the residual catalyst and to yield the initiator as shown below in Scheme 7, 3-[chloro(dimethyl)silyl]propyl 2-bromo-2-methyl-propanoate [277, 314-316]. Filtering over sodium sulphate was completed by creating a micro-column from a glass Pasteur pipette with cotton

wool plugs “sandwiching” a small amount of sodium sulphate. NMR was carried out to verify the structure of the product.

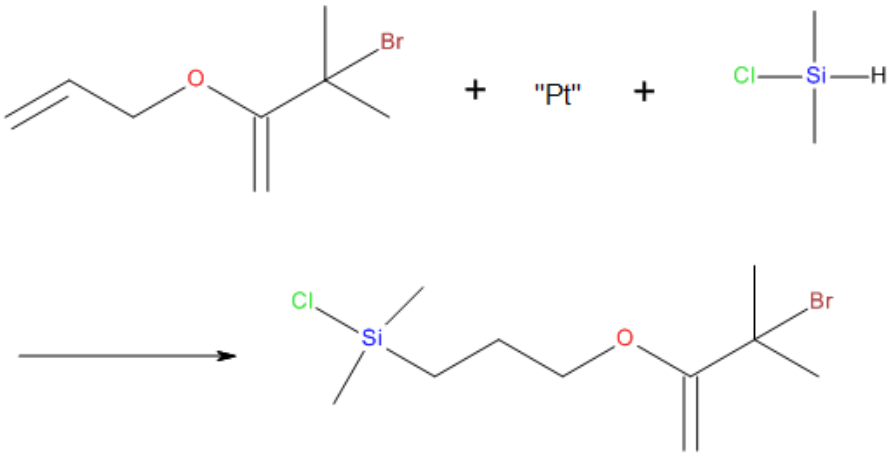

Scheme 7. Hydrosilylation under reflux of the ester and dimethylchlorosilane.

4.2.5 Adsorption of Initiator

Because of the chlorosilane head group, ATRP initiators assemble in the same way that SAMs do. However, from the literature, the time it takes to assemble is unclear as some authors leave the SAM to assemble over 18 h [261, 262, 268, 277, 314], which is unexpectedly long when considering trichlorosilanes adsorb over two hours, therefore this needs to be investigated. A range of contact angles have been reported for a good monolayer, for example Munirasu stated 70°±1° [268], de Groot achieved 77° [306] and Santonicola recorded a value of 85°±3° [317]. Table 4.3 shows a basic outline of the planned testing involving the use of silicon wafers with an ideal solvent, toluene, and the subsequent comparisons with silicon nitride and a polyalphaolefin (PAO) synthetic base oil.

Table 4.3. Test matrix for the adsorption of the ATRP initiator

initiator absorption for ATRP						
Silicon wafer				Silicon Nitride		
Solvent = Toluene	Time (h)			Solvent = Toluene	Time (h)	
Concentration (mM)	2	18		Concentration (mM)	2	18
1				1		
2.5				2.5		
5				5		
Solvent = Toluene	Time (h)			Solvent = Toluene	Time (h)	
Concentration (mM)	2	18		Concentration (mM)	2	18
1				1		
2.5				2.5		
5				5		

The reason why a PAO, specifically SpectraSyn 4 PAO Fluid (ExxonMobil), was selected is that the end goal of lubricating silicon nitride parts in military vehicles would rely on using an existing base stock. As can be seen in Table 4.4 the current military vehicles utilise mainly diesel engines. From the military defence standards there are a few lubricating oils that are used, namely OMD-55, OMD-90 and OX-90 [318]. OX-90 (NATO code O-1180) is specifically described as a synthetic base oil with additives therefore a PAO was selected to replicate the conditions.

Table 4.4. Military vehicles in service with the British Army and their respective engines.

Vehicle	Engine	Fuel	Ref
Bulldog	Rolls-Royce K60	Multi-fuel	[319]
Challenger Main Battle Tank	1200bhp Perkins-Condor CV12	Diesel	[320]
Coyote	5.9 litre Cummins ISBe Euro4	Diesel	[321]
Foxhound	Steyr M16-Monoblock engine. 6 cylinder, 4 stroke diesel w/turbo charger	Diesel	[322]
Husky	International VT 365. MaxxForce® 6.0D V8 .Turbo inter-cooled, direct electronic injection, four stroke	Diesel	[323]
Jackal	5.9 litre Cummins ISBe Euro3	Diesel	[321]
Mastiff	Caterpillar C-7 Diesel Mil Spec	Diesel	[324]
Panther	Iveco F1D Common Rail EURO. Diesel common rail engine with a power of 190 CV 3	Diesel	[325]
Scimitar	Cummins BTA 5.9, 190 hp diesel engine	Diesel	[326]
Snatch Landrover	3.5 litre V8	Petrol	[327]
Spartan	164 bhp Bedford 600 6-cylinder diesel	Diesel	[328]
Stormer	Perkins 6-litre, 6-cylinder diesel	Diesel	[329]
Vector	VW 5-cylinder Euro 3	Diesel	[330]
Viking	Cummins 5.9 litre, 6-cylinder Euro 3 diesel engine	Diesel	[331]
Warrior	Perkins V-8 Condor Diesel	Diesel	[332]
Warthog	Caterpillar 3126B. 7.2-litre engine, producing 350 bhp	Diesel	[333]
Wolfhound	Caterpillar C-7 Diesel Mil Spec	Diesel	[334]

The self-assembling initiator solutions were created by making up a solution of 100 mM initiator in the desired solvent followed by dilution to 25 mL of appropriate concentration using a micropipette and volumetric flask. The silicon nitride surfaces were produced by plasma enhanced chemical vapour deposition (PECVD) using an Oxford instruments PlasmaLabSystem 100 PECVD system. The gasses used are SiH_4 and NH_3 at flowrates of 12.6 sccm and 20.0 sccm (Standard Cubic Centimetres per Minute) respectively. The silicon nitride was deposited on a silicon wafer, which allows the same characterisation tests to be completed on both a silicon wafer and the silicon nitride coated wafer enabling direct comparison. These tests will show whether attachment of the ATRP initiator to silicon nitride in motor oil is possible and whether assembly is needed over 18 h. The characterisations of the SAM will be the same as performed on the OTS.

4.2.6 ARGET ATRP Polymer Brush Synthesis

To perform ARGET ATRP the monomer, sacrificial initiator, solvent, metal complex ligand and pre-functionalised wafers are all added to a reaction vessel/vial as shown in Figure 4.2. The solution can be degassed by bubbling nitrogen through and purging the headspace although when utilising ARGET this is not critical to the success of polymerisation. The reaction is started by the injection of a reducing agent thereby reducing the copper catalyst and making it active. The vial may then be heated to speed up polymerisations and agitated. If the reaction is subsequently exposed to air it will slow to a stop. However, the vial can then be resealed and more reducing reagent can be added to restart the polymerisation. In this work MMA will be used as MMA polymers are also known to synergize well with hydrocarbon-based lubricants due to their inherent hydrophobicity. The relative cost for a readily available monomer such as styrene or methyl methacrylate (MMA) is much lower than more complex structures to ensure this lubrication solution is not cost prohibitive. MMA has the ability to create much denser polymer brush films than other monomers due to its small molecular size [123, 354]. As previously stated, one of the modes of lubrication by a polymer brush is the ability to withstand lateral and compressive forces, by denser packing this is achieved. The monomer 2,2,2-trifluoroethyl methacrylate could be a promising solution, however, cost and the storage temperature of the fluorinated monomer (2°C - 8°C) may limit its practical applications. It is common that monomers are stored containing inhibitors, therefore removal of these may be necessary before use, either by passing through a basic alumina or other type of packed column. It is also common to used reduced pressure distillation to remove inhibitors in monomers to avoid high temperatures which could result in premature polymerisation. Utilising a sacrificial initiator to control the polymerisation and provide free polymer will be necessary, in this case ethyl α-bromoisobutyrate will be used. Initially the reactions took place in anisole as a solvent, however, later tests used PAO as a solvent. The catalyst system was based on CuBr, with either Tris(2-pyridylmethyl)amine (TPMA) or Tris(2-

dimethylaminoethyl)amine (Me_6TREN) or N,N,N',N'',N''-pentamethyldiethylenetriamine (PMDETA) as ligands. Currently PMDETA is a preferred ligand owing to its lower cost. However, the two other ligands have higher values for $K_{activation}$ compared to PMDETA which results in a higher polydispersity index. The use of a reducing agent such as tin(II) 2-ethylhexanoate or (þ)-sodium L-ascorbate will allow polymerisations to take place with ppm levels of catalyst.

In the current work the chemicals selected are as follows:, for surface initiated ARGET ATRP a 22 mL vial containing a previously modified silicon wafer with an initiator attached was charged with MMA (15 mL, 150 mmol), $CuBr_2$ (0.0056 g, 0.025 mmol) and PMDETA ((0.043 g, 0.25 mmol) in anisole (2 mL)) was added in addition to EBIB (0.048 g, 0.25 mmol). The vial was bubbled with nitrogen for 5 minutes then sealed. A solution of sodium L-ascorbate (0.0495 g, 0.25 mmol) in anisole (2 mL) was then syringed through the septum and the vial was placed in a thermostatic water bath at 70°C. The polymerisation was stopped by unscrewing the vial, thereby exposing the catalyst to air. The modified wafer is then removed and sonicated in tetrahydrofuran (THF) and dried in nitrogen before characterisation [335].

The samples were analysed using triple detection with RALLS (right angle laser light scattering detector). Conditions were Viscotek 302 with refractive index, viscosity and light scattering detectors, and 2 x 300mm PLgel 5µm mixed C columns, with THF as the eluent with a flow rate of 1.0 ml/min and at a constant temperature of 35 °C. The detectors were calibrated with a single narrow molecular weight distribution polystyrene standard using a value of dn/dc of 0.185 mL/g. The analysis was carried out using a dn/dc value of 0.085 mL/g – which is the value for PMMA.

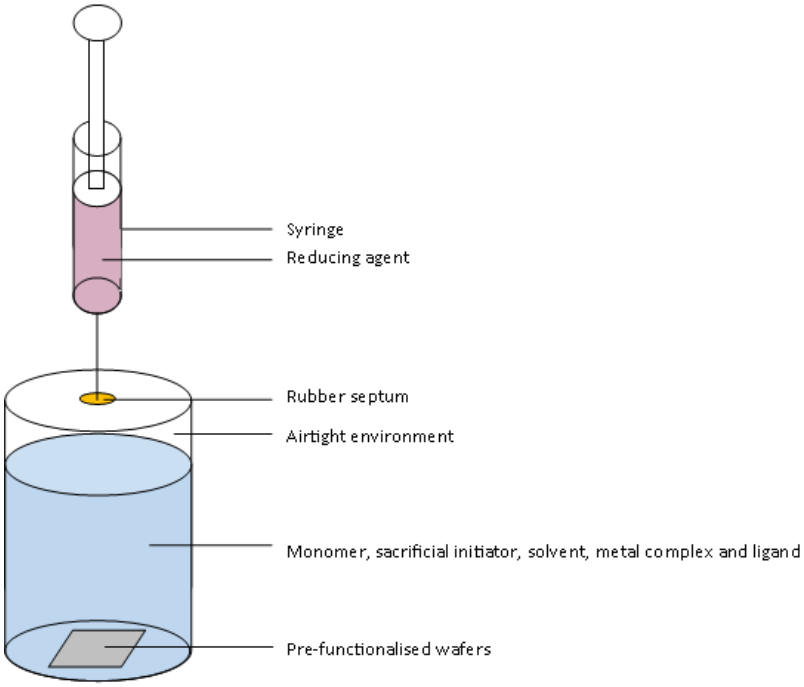

Figure 4.2. A simplified version of how an ARGET ATRP synthesis would take place.

4.2.7 Improved ARGET Polymer Brush Synthesis

After experimenting with using ascorbate as a reducing agent there were was room for improvement, the main issue with the ascorbate solution was its limited solubility in anisole causing varying amounts to be injected. As the ascorbate was in a solid form there were still some crystals in the syringe which resulted in poor injection volumes and blockages. Using tin(II) 2-ethylhexanoate was found to be a more acceptable way of injecting a suitable amount of reducing agent into the polymerisation vessel. Therefore the adapted method as followed was used.

To conduct the SIP a 15 mL vial containing a 1 cm^2 piece of the previously initiator-modified silicon nitride substrate was charged with MMA (7 mL, 0.065 mol), $CuBr_2$ (0.0028 g, 0.0125 mmol), PMDETA (26 µL, 0.125 mmol), EBIB (0.048 g, 0.25 mmol) and 6 mL of anisole as solvent. A solution of tin(II) 2-ethylhexanoate (130 µL, 0.125 mmol) in anisole (1 mL) was then added using a hypodermic syringe inserted through the septum and the vial was placed in a thermostatic water bath at 70°C. To stop the polymerisation, the vial was unscrewed, thereby exposing the catalyst to air. The modified substrate was then removed and briefly sonicated in tetrahydrofuran (THF) and dried in a stream of nitrogen gas.

4.2.8 Colloidal Probe Microscopy

Although polymer brushes repel interactions from sharp AFM probes, it is likely that the high local pressures will be in excess of what the brush can withstand and result in penetration of the brush system as seen in Figure 4.3 [216, 336, 337]. This may explain the results observed with dry polymer brushes on silicon, where a thinner polymer layer was found to be preferable under nanotribological testing. In order to understand the tribological performance of the polymer without losing the force sensitivity or penetrating the polymer, spherical colloidal probes are used

[194]. One of the benefits of this procedure is that the load is distributed across the sample surface whilst accurately recording the forces therefore making this a good technique for the characterisation of the mechanical response of polymer brushes. Colloidal probes can be fabricated in numerous sizes from 3 µm [300], 3.5 µm [338], 5 µm [271, 305], 12 µm [339] to 15 µm [123, 213, 340]. The ability to attach colloidal particles to tipless cantilevers results in a selection of materials being available for use, mostly SiO_2, PMMA and polystyrene, however, researchers in the Carpick research group have utilised steel colloids, as has Lee [340]. Use of a steel colloid allows a novel development to the project as it allows us to understand the interaction between silicon nitride and steel as well as polymer brushes on steel. Friction force measurements using colloidal probes can also take place in liquids and therefore the interaction between polymer and fluid can be investigated. The ability to understand the silicon nitride-steel contact on the nanoscale is a novel route to scale up to the macroscale. Colloidal probes are generally fabricated by using a micromanipulator with either an epoxy or a polymeric based glue that melts at 105°C, however, this necessitates the use of a hot plate under a microscope which may complicate the method. Using this method the spheres are carefully glued to tipless cantilevers.

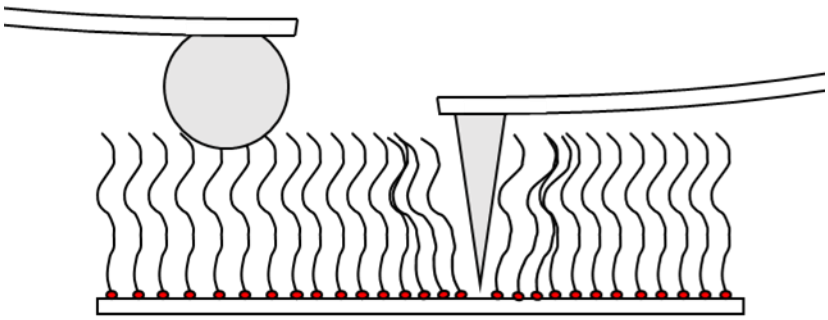

Figure 4.3. Comparing the interpenetration of the brush matrix by different shape tips.

To evaluate the friction behaviour of the polymer brushes on silicon nitride in a hybrid contact, the polymer-modified surfaces were tested using lateral force microscopy with steel colloidal probes. All lateral force microscopy testing was performed in ambient air, water or PAO at room temperature using an atomic force microscope (MAC Mode III, 5500 Scanning Probe Microscopy, Agilent Technologies, USA). PicoView 1.12 and PicoImage Basics 6.0 (Agilent Technologies, USA) software were used for data acquisition and image analysis, respectively. Colloidal probes were fabricated by attaching a steel ball (6.19-6.49 µm diameter) to a tipless cantilever by using two part epoxy adhesive [338, 340] using the method described below.

- *Fabrication of Colloidal Probes*

The fabrication of the probes involved the creation of a rig in which the cantilever can be carefully moved in the x, y and z axis to dip into epoxy and then to contact a single colloid particle. This rig is based around a micromanipulator and a plain steel bar that is attached to this to reach over the sample plate of the microscope as seen in Figure 4.4 A and B. The micromanipulator is raised to the correct height with a lab jack. Then a thin malleable length of wire is attached with Blu-Tak to the bottom of the cantilever so that the surface that will come into contact with the sample is facing down. The other end of this wire is then attached to the metal bar with Blu-Tak, shown in Figure 4.4 C. Two part epoxy is then mixed and smeared on a slide, and the cantilever is carefully brought into contact with the adhesive and lifted off. In image D the particles can be seen at 5 times magnification, after some searching a single colloid can be found, which, in the inset is shown at 100 times magnification. Then the cantilever is bought into contact with the colloid particle, lifted off and the epoxy left to cure.

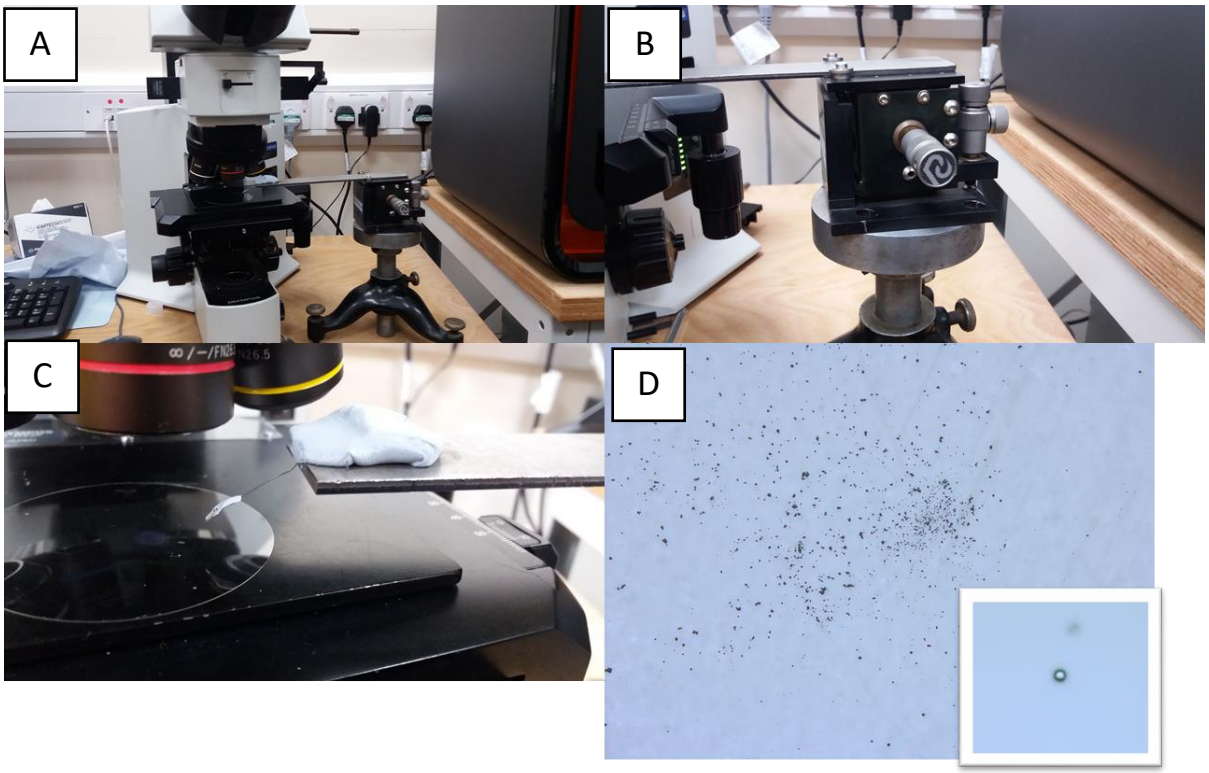

Figure 4.4. (A-C) Images of the rig used to bring the cantilever into contact with the epoxy or colloids. (D) Images from the microscope of the particles at 5X magnification. Inset is 100X magnification.

Before attachment to the cantilever the particles were viewed via SEM as seen in Figure 4.5. It can be seen that some of the purchased particles exhibited poor structures which would not allow good tip formation. Another issue is the replication of the probe size to ensure comparable results. As image B shows, a wide variety of sizes can mask smaller particles stuck on the larger colloid particle which will also result in poor tribological performance. Image D shows a successful

modification of a cantilever, all of the colloidal probes used were in the range of 6.19-6.49 µm diameter.

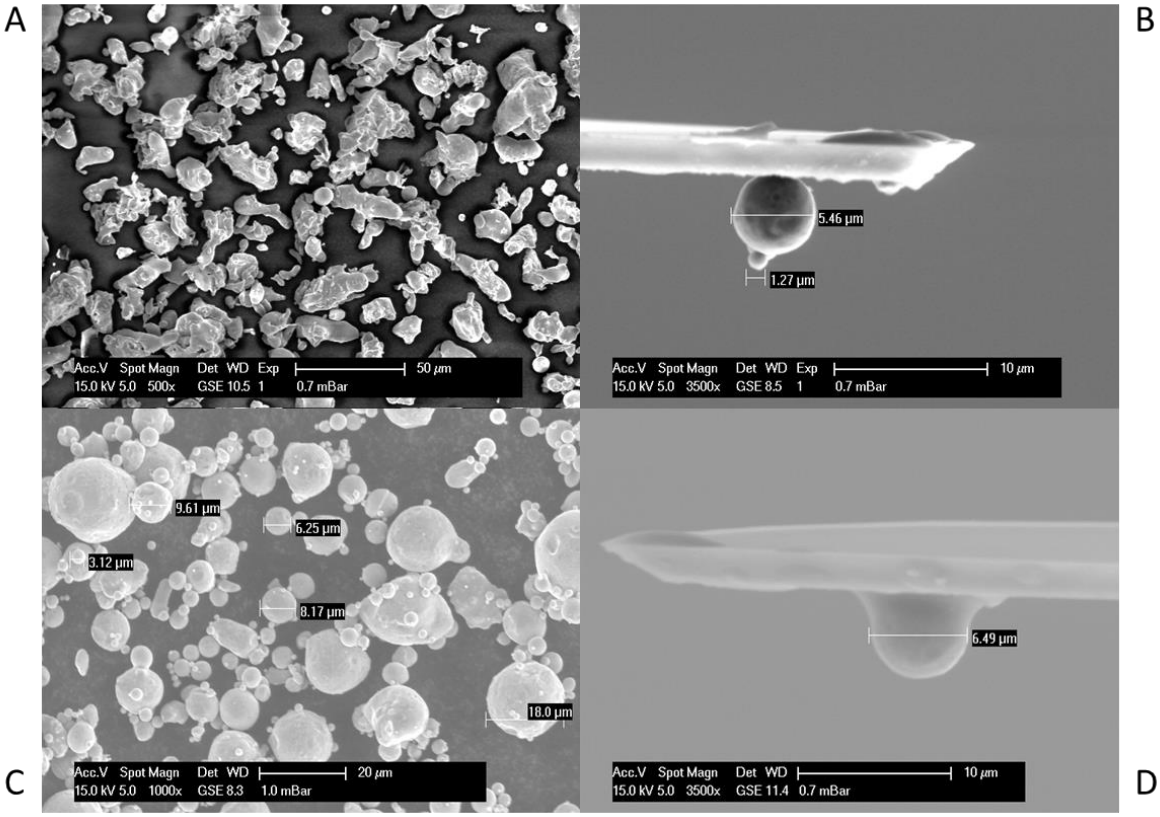

Figure 4.5. A is an image of particles that have been poorly formed. B shows the effect of a great size distribution. C shows a narrower range of particle size and better formation. D shows a successful modification of a tipless cantilever.

- *Calibration of Colloidal Probes*

The actual spring constant of the modified tip was calculated by internal built-in thermal noise methods [341]. Normal forces were calibrated by measuring the deflection sensitivity (nm/V) from the slope of the linear part of a force–displacement curve obtained on a flat silicon surface. The normal force, F_N, was set to zero at the point where the cantilever left the surface. The actual friction force is then calculated by averaging the forward and reverse scans.

- *Lateral Force Microscopy*

To determine the friction values of the polymers with respect to load area friction maps were completed. Areas of 4 µm × 4 µm consisting of 512 lines were scanned at a speed of 8 µm/s (1 line/s). The load was increased stepwise in steps of 20 nN every 400 nm to a maximum load of 180 nN depending on the probe, ensuring that at least 50 lines were attributed to each load. A minimum of three scans at different locations were carried out.

4.2.9 Macroscale Brush Formation

To form brushes on 10 cm diameter discs the previously described method was utilised. The disc was lapped using a Kemet lapping machine resulting in a roughness (Ra) of 0.0678 µm as measured by Talysurf 120L stylus profilometer. The disks were then washed sequentially with isopropyl alcohol and toluene before being dried under nitrogen. The discs then underwent the first stage of self-assembling the initiator monolayer in a 2.5 mM solution for 18 h as determined by small scale testing. After removal from the solution the disc was washed and placed in the reactor vessel (shown in Figure 4.6). To complete the polymerisation on a larger scale the procedure involving Sn(II) was scaled by a factor of 22 times, due to the volume that the new glassware could take, as well as the addition of more solvent to facilitate mixing, which allows the reaction to happen in a controlled manner. After the initial charging of the reactor it was sealed and placed in a thermostatic water bath. The Sn(II) solution was then injected through the septum and the reaction was initiated. As can be seen in Figure 4.6 agitation of the reactor contents was by a Teflon stirrer blade driven by a laboratory stirrer motor (IKA) passing through an airtight seal. After 6 hours the reactor was removed from the water bath and one of the stoppers was removed to stop the reaction. At this point a small sample of polymer solution was removed for GPC analysis. The modified disc was then removed and cleaned in THF before drying under nitrogen. Due to the size of the discs characterisation via AFM or XPS was not possible, however CA and GPC data could be obtained. GPC data was generated in the same way as before, CA data was gathered with water droplets measured in the same way as on the small scale to ensure data can be gathered from a representative sample.

Figure 4.6. Custom glassware to accommodate silicon nitride discs.

4.2.10 Macroscale Tribology

To complete the macroscale tribology testing regime a pin-on-disc tribometer was used, configured for pure sliding in lubricated conditions. This instrument was calibrated by attaching a pulley system to the strain gauge which was then loaded in 5 N steps up to 50 N and the corresponding voltage output measured. To reduce the variation of polymer thickness between tests the same disc was used but the distance from the centre of the disc varied as can be seen in Figure 4.7. By adjusting the distance from the centre and the rotations per minute of the disc a constant velocity of 0.5 m/s can be achieved for each sample. The tests were run in PAO to facilitate the good sliding properties of the polymer brush system within the hybrid contact. The hybrid contact was formed by using the silicon nitride discs with a 4 mm hardened chromium AISI 52100 steel pin. The pin was selected with a rounded end for two reasons, as with no angular edges like a traditional pin there is less chance of gouging or resulting in a converging wedge (thereby working like a thrust pad bearing due to poor contact geometry), and secondly, the curvature of the pin is considerably reduced allowing a larger contact area and therefore lower contact pressures. The pin was confirmed to have a good geometry when placed in contact with the disc whilst stationary. To run the tests PAO was recirculated and pumped back onto the middle of the disc which then spread the lubricant centrifugally ensuring the contact area was lubricated. The discs were spun up to the correct speed before the pins were gently lowered onto the discs with their load already in place. The tests were repeated once per load on the same disc to ensure that there was limited variation between thicknesses, which from smaller scale experiments has been shown to affect the results the most.

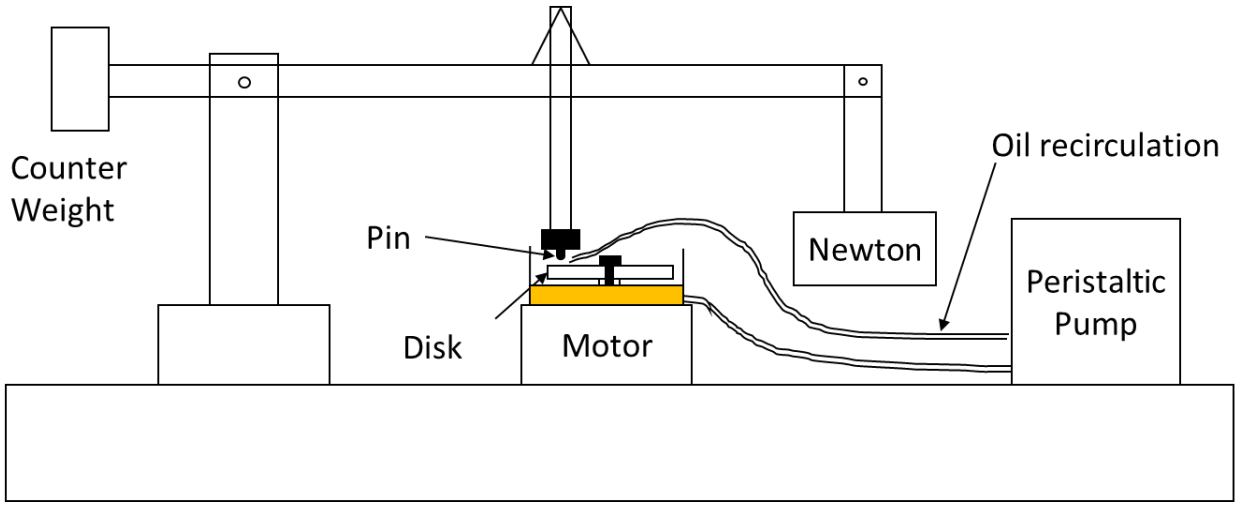

Figure 4.7. Basic schematic of the pin-on-disc tribometer

5 Results and Discussion

5.1 Preliminary OTS SAMs

Preliminary experiments had the aim of establishing a baseline standard monolayer that all other treatments can be compared to. These preliminary SAMs were also used for training purposes with AFM and contact angle techniques. Figure 5.1 shows bare silicon wafer surface viewed via AFM which is very flat. The ridges present are thought to be from the polishing process and small amounts of contamination are present on the surface.

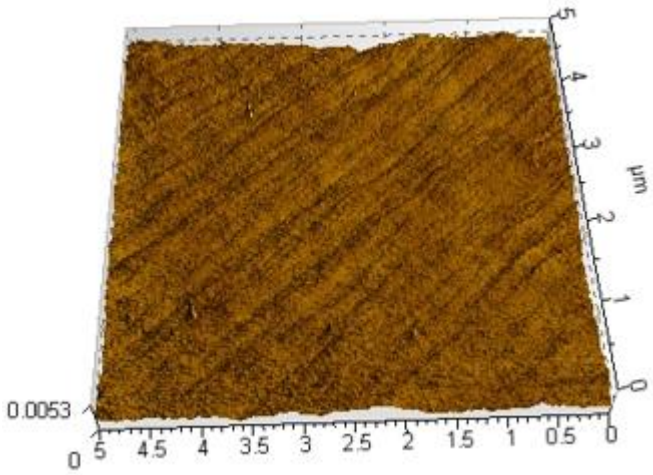

Figure 5.1. A bare silicon wafer with prominent ridges.

However, Figure 5.2A, also a bare silicon wafer, shows slight contamination, this could be due to a number of factors, but most probably because neither the laboratory where cleaning took place or the AFM suite are in a clean room. This allows contaminants such as dust to settle freely on wafer surfaces.

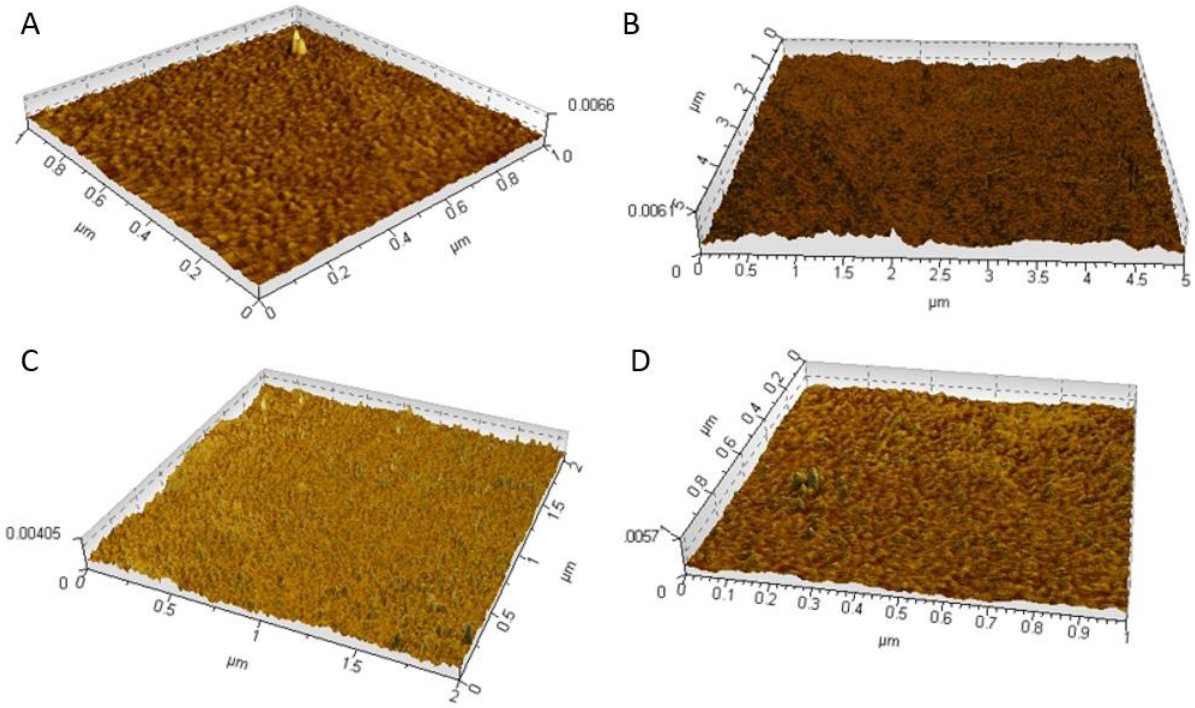

Figure 5.2. (A) AFM image of a bare silicon wafer 1µm x 1µm. (B) AFM image of OTS SAM on a silicon wafer 5µm x 5µm. (C) AFM image of OTS SAM on a silicon wafer 2µm x 2µm. (D) AFM image of OTS SAM on a silicon wafer 1µm x 1µm.

Figure 5.2B-D all show relatively good quality images of OTS SAMs formed on the wafers. However, visible on the latter two images are notable agglomerations of OTS. Further details are in Appendix A. Contact angle data confirmed a successful modification. Figure 5.3 shows that a significant contact angle change has occurred, namely an increase from 45±2° of base wafer to 102°±2° of OTS SAM, which shows that a SAM has been formed upon the wafer. However, this still leaves room for improvement as OTS SAMs can reach water contact angles of 112°. This usually indicates that the monolayer is not as densely packed as possible.

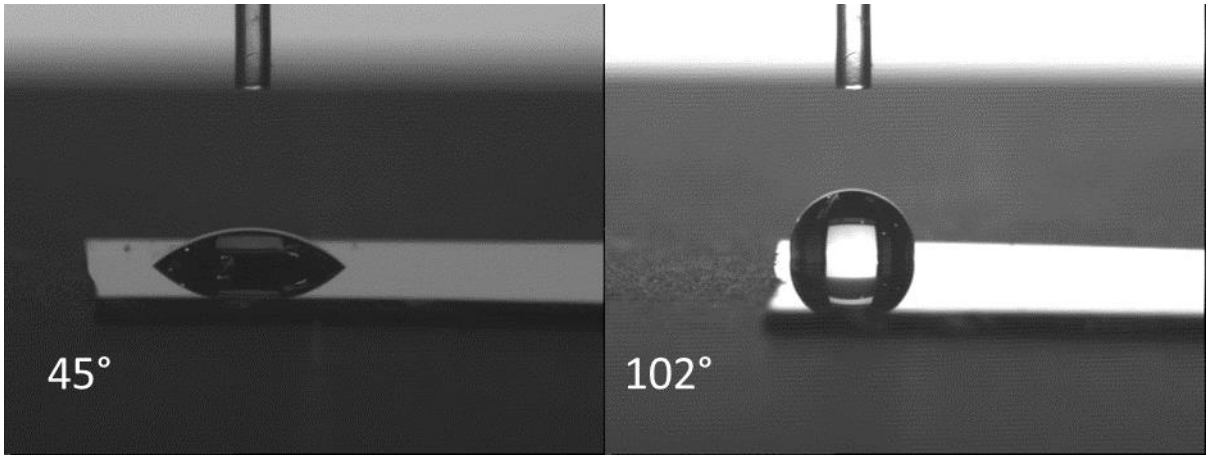

Figure 5.3. Contact angle of a bare silicon wafer and an OTS SAM modified wafer.

5.2 Plasma vs Piranha

Plasma and piranha surface treatments were selected as two ways of improving the quality of the SAM subsequently formed. Both methods were employed to enhance the surface qualities of the silicon wafer and attempt to encourage better quality SAM formation.

5.2.1 Piranha

The piranha treatment did not show a reliable reduction in contact angle of the bare silicon wafer at any time under the aforementioned conditions as seen in Figure 5.4. Although there was an initial decrease in contact angle from 74° to 44° the large error in every test means that the reliability of this pre-treatment method is unacceptable. In this experiment three wafers per time point were used and contact angle measurements were collected in triplicate. The AFM images, available in Appendix B, show some promising features, particularly the roughness qualities displayed. All of the AFM images produced after piranha treatment showed good roughness qualities, this indicates that an oxide layer is being grown in a controlled manner. The new layer also covers the ridges present in untreated wafers, further proof that some level of silicon oxide growth has taken place. However, the contact angle data rendered this method not to be viable as the amount of –OH bonds on the surface are more important than the thickness of the oxide layer. It was hypothesized that the limited reduction in contact angle could be due in part to the lower temperatures used during the oxidation reaction for safety reasons.

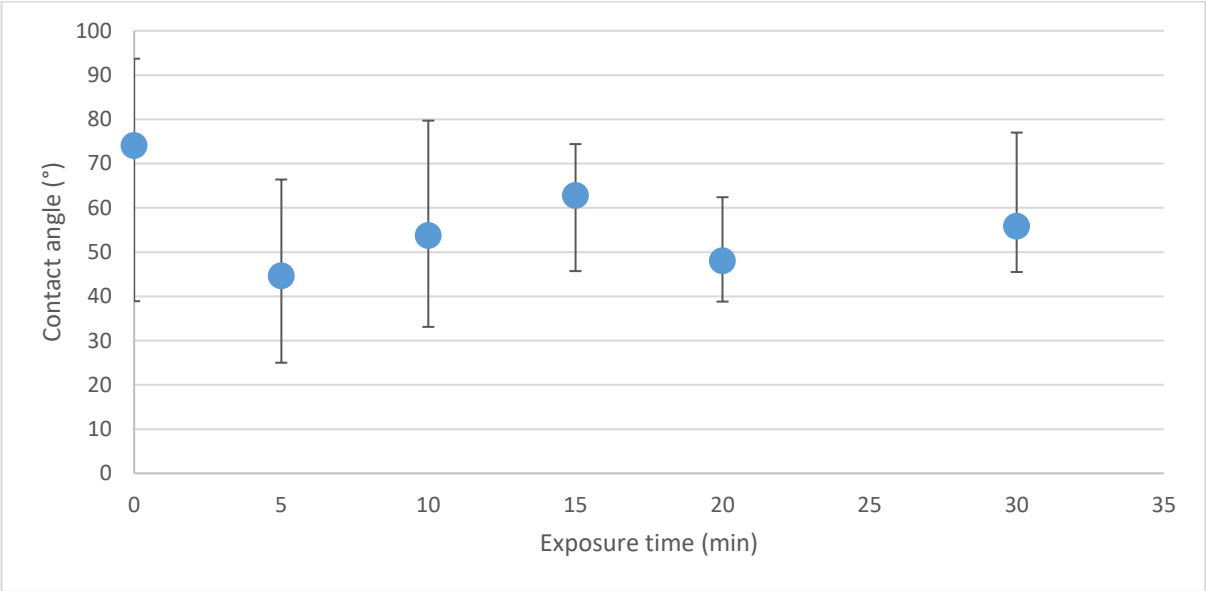

Figure 5.4. The relationship between piranha treatment and contact angle.

5.2.2 Plasma

Plasma treatment proved to be a suitable method of wafer oxidation as can be seen in Figure 5.5. It can be seen that after just 3 minutes plasma exposure the contact angle has reduced from 64° to 12°. In addition, the data shows a trend towards a smaller contact angle value with a reduction in error. Figure 5.5 illustrates the relationship between plasma exposure time and the resultant contact angle. In this experiment three wafers per time point were used and contact angle measurements were made in triplicate. However, although the treatment was successful and reduced the contact angle it also resulted in abnormal structures that were visible under AFM which are discussed in the next section.

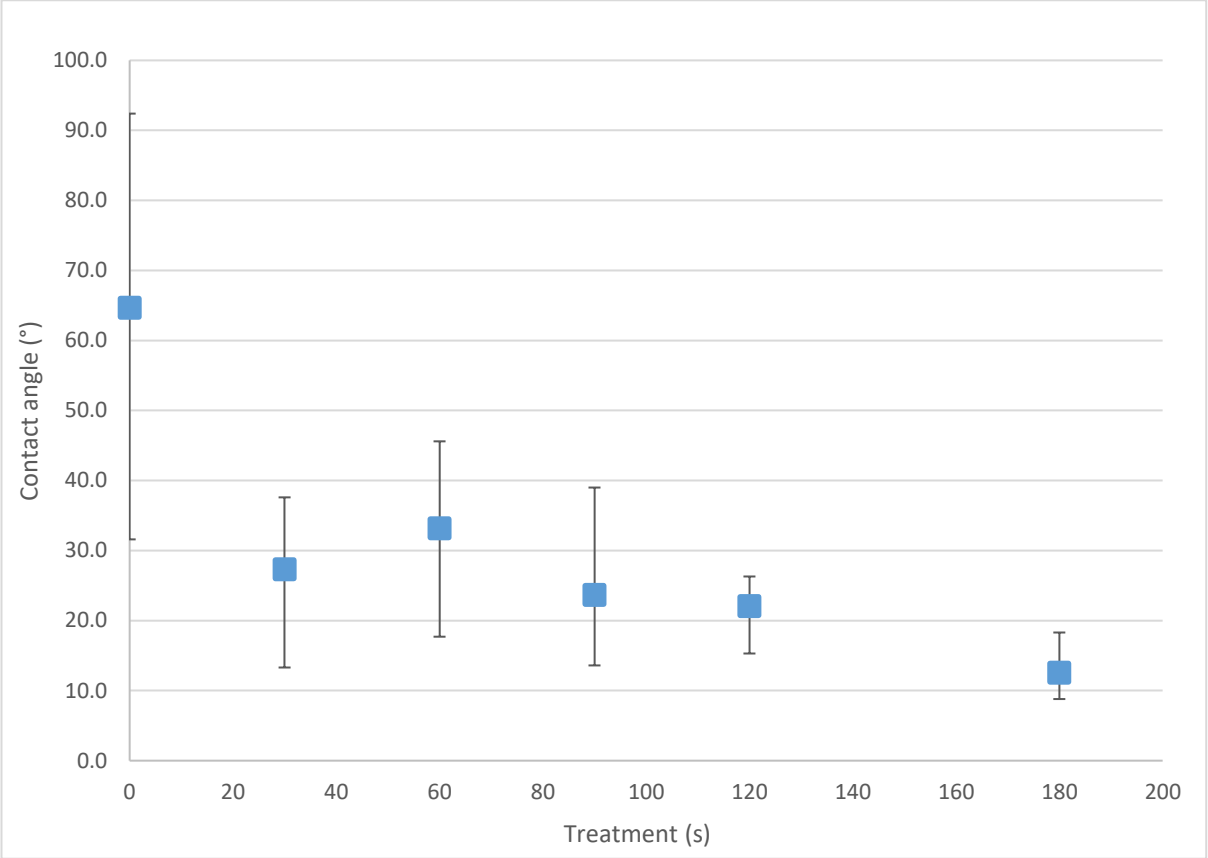

Figure 5.5. The relationship between plasma treatment and contact angle.

- *Solvent Residue*

During plasma experiments some of the wafers displayed abnormal shapes on the surface. The abnormal shapes are visible in Figure 5.6 A and B, these structures were suspected to be due to solvent residues, further images can be found in Appendix C. Image A is due to solvent residues or impurities that remain after the final drying procedure. Image B shows the resultant effect of residues that are present on the surface before plasma treatment. A shadowing effect is created and could be further investigated using line extraction as is shown in Figure 5.6. To improve the AFM images and reduce the shadowing effect present two methods of drying were used. A revised method involving an extended nitrogen drying regime and drying in an oven at 100°C overnight were used.

A B C

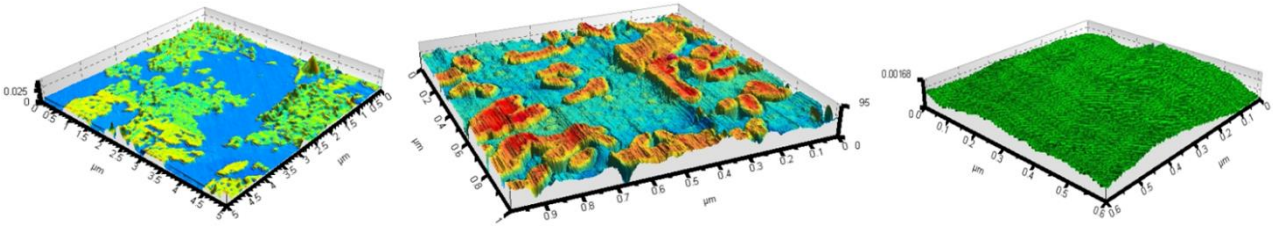

Figure 5.6. A selection of AFM images. (A) Shows solvent residue after ultrasonic cleaning. (B) Shows the effect of these residues on silicon wafers after plasma treatment. (C) Shows the results of an extended drying regime.

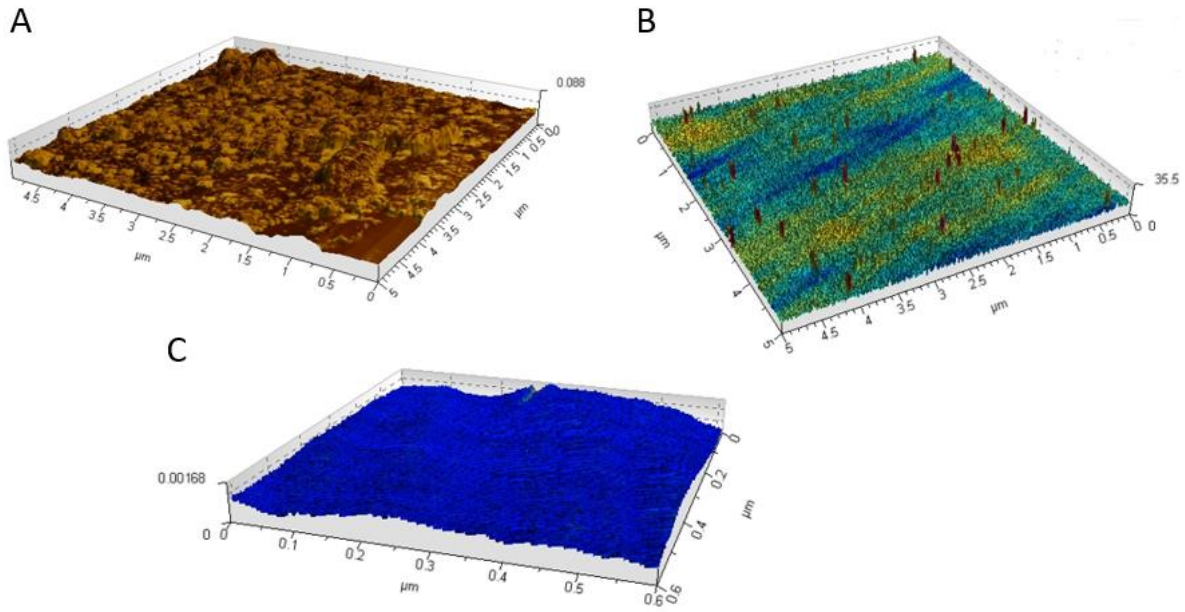

Figure 5.7. (A) AFM image showing the results of oven drying. (B) AFM image of plasma treated silicon wafers without pre-cleaning. (C) AFM image showing the results of extended nitrogen drying.

Figure 5.7A shows the results of overnight drying in an oven. This method produces an unacceptable appearance so was taken no further. To confirm that it was ethanol residues present a silicon wafer was exposed to plasma treatment without any ultrasonic cleaning steps, as seen in Figure 5.7B. This removes the possibility of ethanol contamination whilst still retaining the rest of the procedure and it is clear that the same structures are not visible. Figure 5.7C shows the much improved AFM image that is taken after extended nitrogen drying. This surface shows a very smooth surface ideal for SAM formation.

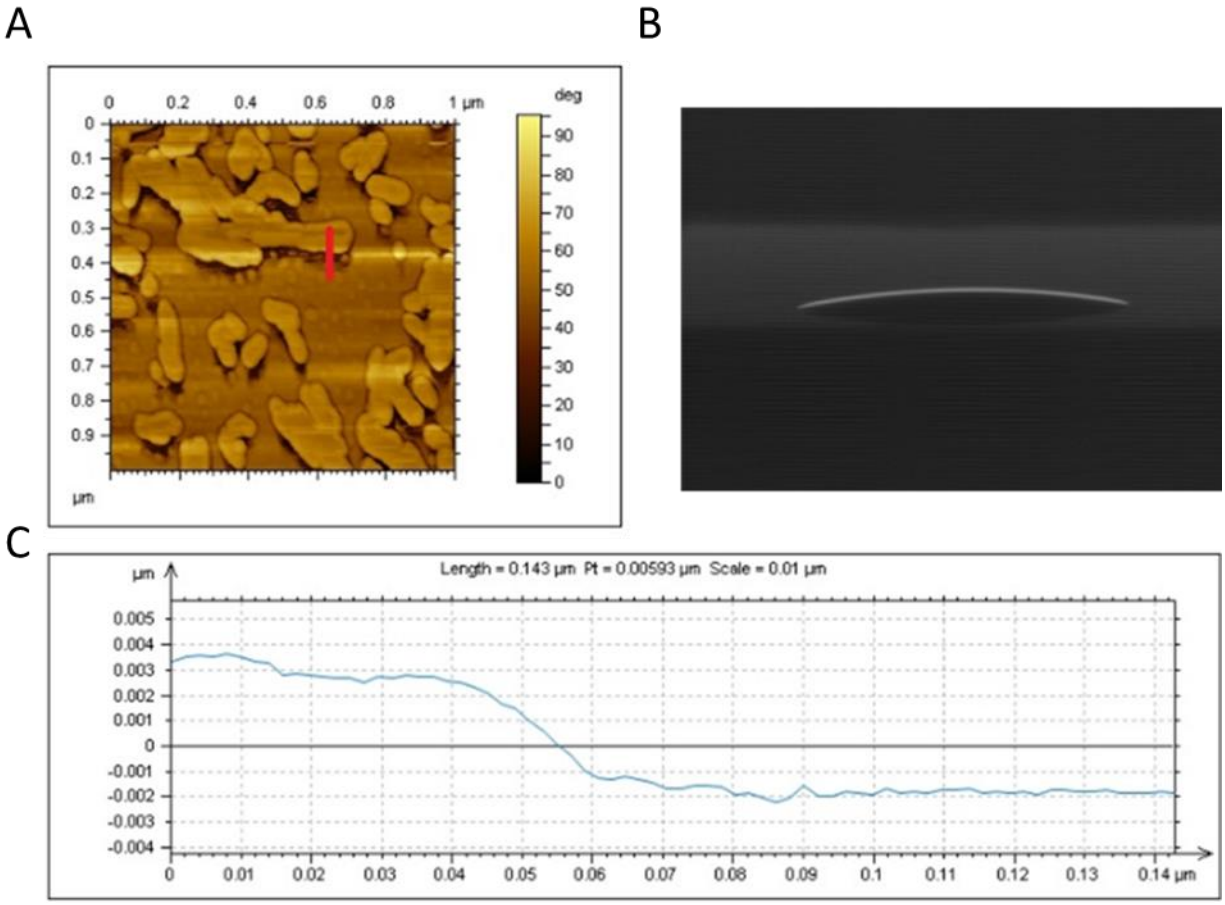

Figure 5.8. A and C detail the "shadow" as discussed above. B is a good example of an oxidised silicon wafer with a low contact angle.

Further testing with plasma resulted in lower contact angles than previously obtained when wafers were exposed for 0-3 minutes. Figure 5.9 shows the variation of contact angle across a wafer when exposed to plasma for less time than 3 minutes. The figure also shows the resultant contact angle after 4 minutes of plasma treatment and the additional drying steps. Due to the measurement limits of the equipment, as detailed in Section 2.4.1, Contact Angle Measurements, an accurate value is difficult to evaluate for the low contact angles using the software provided with the instrument. However, it can be said that highly successful surface oxidation has taken place.

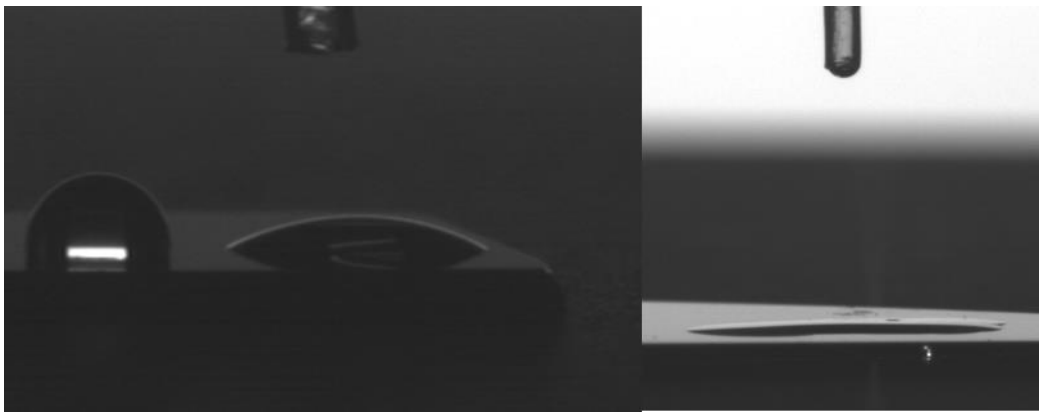

Figure 5.9. (L) Contact angle variations across a wafer treated with plasma. (R) Successful plasma treatment resulting in low contact angle.

Figure 5.10 shows the results of EDX on the surface of the oxidised wafers in comparison to untreated wafers. The Si+Si notation is due to two x-ray photons arriving at the detector at the same time, thus twice the keV is measured. This is a rare event and only happens with large peaks due to the increased probability.

Wet mode EDX, used to prevent charge build up on non-conducting samples, may mean that some of the x-rays are scattered, this could be a reason for the Al peaks on some of the samples as the mount is made of Al. Plasma S1(2) is an example of the middle of the wafer being analysed and therefore no Al peak. It is worth mentioning that there may well be Al contamination on the wafers even though it is small amounts. The same can be said about the carbon peak, which may derive from the sticky tab that attaches the sample to the SEM stub. Some of the carbon and oxygen may be from contaminants present on the wafers. It stands to reason that the carbon peak on samples may be higher due to organic contamination, this may be oxidised and therefore a smaller peak is present on the plasma treated sample. Plasma treatment does not increase the thickness of the oxide, however the reaction of oxygen radicals will remove carbon content. One of these contaminants is likely to be ethanol, which may be a reason for the reduction of an oxygen peak.

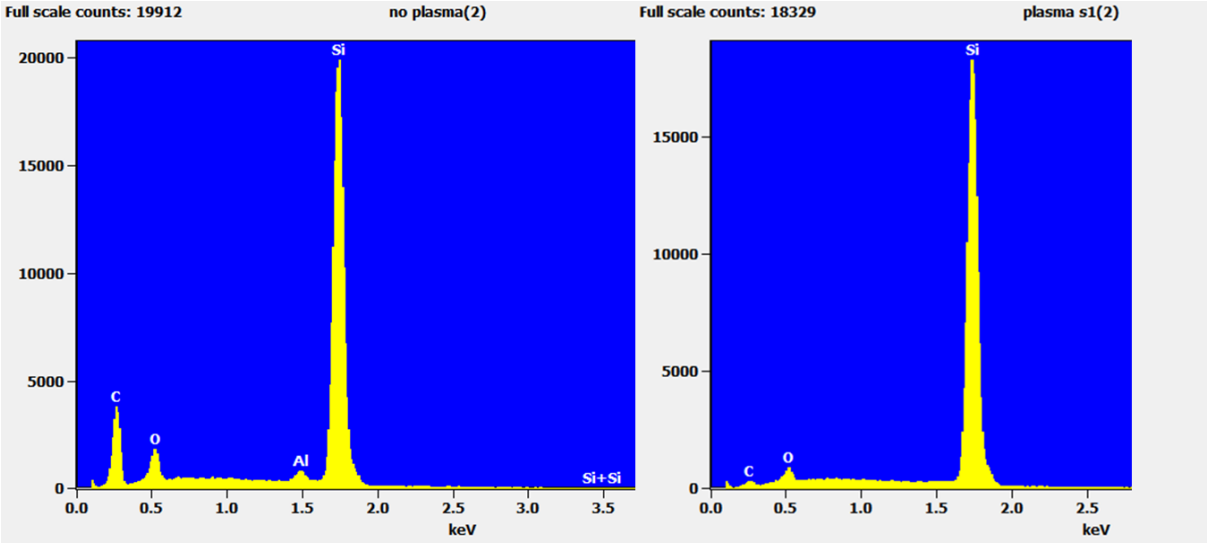

Figure 5.10. EDX results for silicon wafers before and after oxidation.

Surface cleaning is a key part of SAM formation and in this section it has been shown that the application and improvement of a cleaning strategy can successfully reduce contact angles down to acceptable literature values. The extended drying method allows good AFM images to be taken of the surface with no solvent contamination.

5.2.3 OTS SAM

OTS SAMs were then created on plasma oxidised surfaces. After oxidation the wafers were transferred to a freshly prepared OTS SAM solution for two hours at a concentration of 2.5 mM [17]. Figure 5.11 is of the monolayer viewed using an AFM, this shows full coverage and a dense monolayer. Figure 5.12 shows a line profile extraction and the resultant line does not fluctuate too much from the average and is more an indication of the substrate topography owing to the ultrathin SAM formed. However, the relative roughness may well be down to the individual molecules within the SAM. It is evident from Figure 5.13 that there has been a significant change in the contact angle of the plasma modified wafer with OTS compared to just OTS assembled with no pre-treatment. The contact angle that was recorded was > 110° in agreement with known literature values [164].

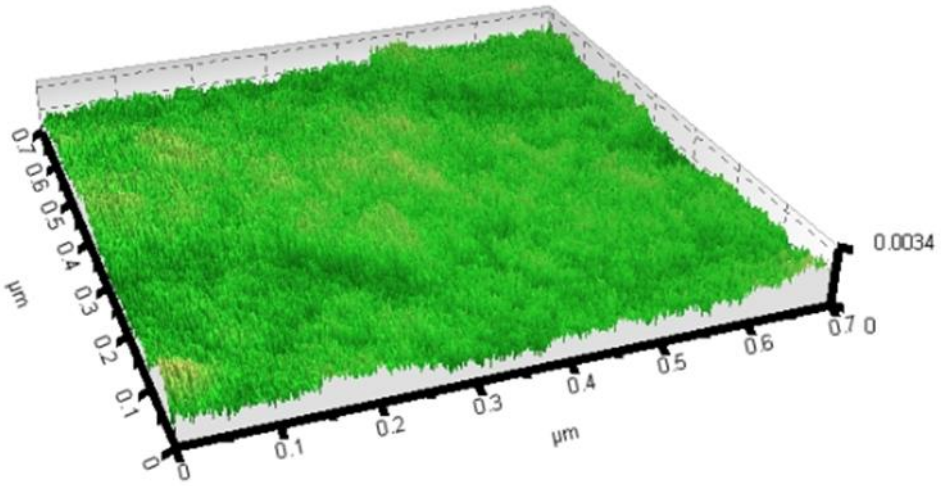

Figure 5.11. AFM image of OTS SAM formed on plasma-treated wafer.

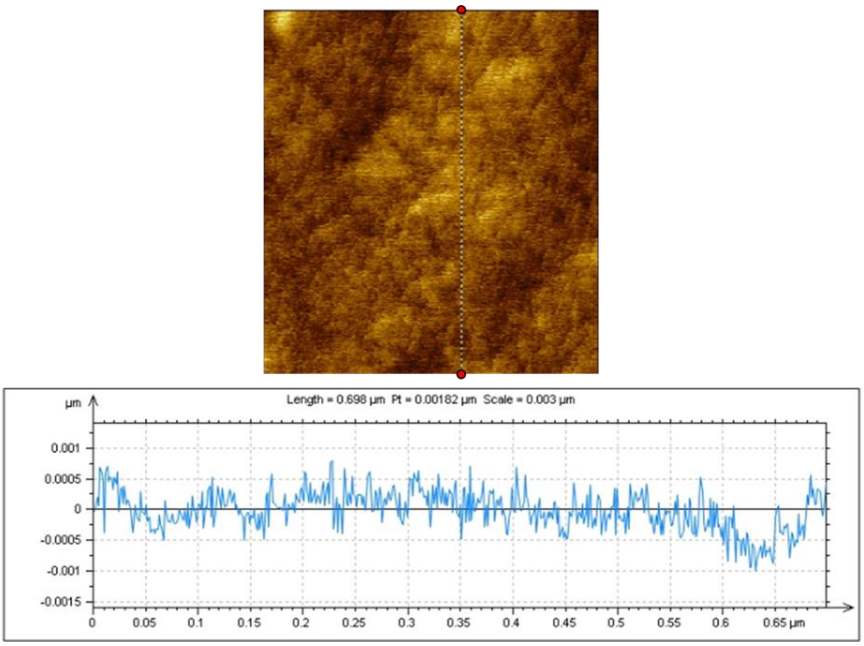

Figure 5.12. Line profile and resultant roughness of the OTS SAM.

By creating SAMs with the known literature value the surface pre-treatments can be justified. Further AFM images are in Appendix D. The images recorded pre- and post- modification show very different structures present on the surface of wafers. Also, the rings and domes observed during a previous unpublished study (B. Craig) were not present [342]. This may well be due to the additional drying procedure.

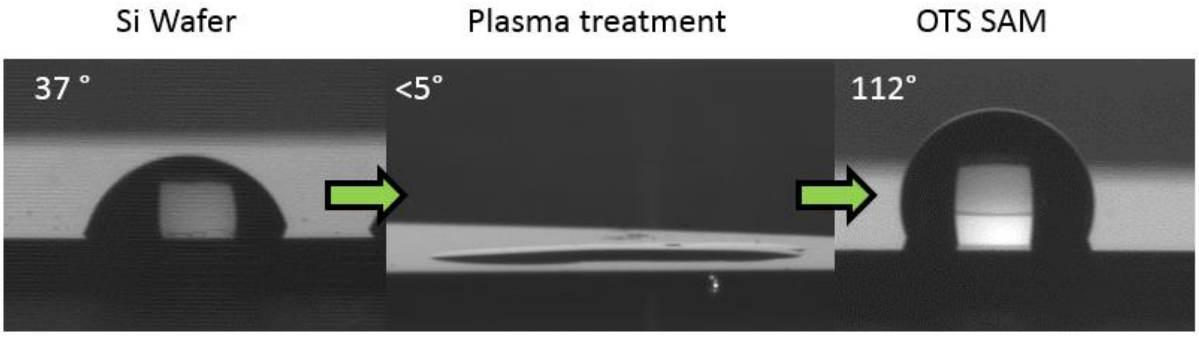

Figure 5.13. Contact angle images showing the development of contact angle through processing.

As can be seen in Figure 5.14 the XPS spectra of OTS assembled on both silicon nitride and silicon are presented. As expected the silicon nitride sample shows nitrogen and the wafer does not. A symmetrical carbon peak with no variation on binding energy implies that there is carbon in only one bonding phase, C-C. Chlorine, expected around 200 eV, is absent therefore it is likely that all three bonds to chlorine have undergone hydrolysis and bonded to silicon. Where silicon and nitrogen are present the horizontal or rising baseline after a peak often indicates that the elements in question are present towards the bottom of the XPS analysis depth (5-6 nm) and a large number of the electrons being photoemitted due to the incoming X-rays are inelastically scattered by the material overlayer. Such scattering leads to a loss of kinetic energy and an apparent increase in the electrons' binding energy (Eb = hv-Ek) hence the increase in the baseline on the higher binding energy side of the XPS peak.

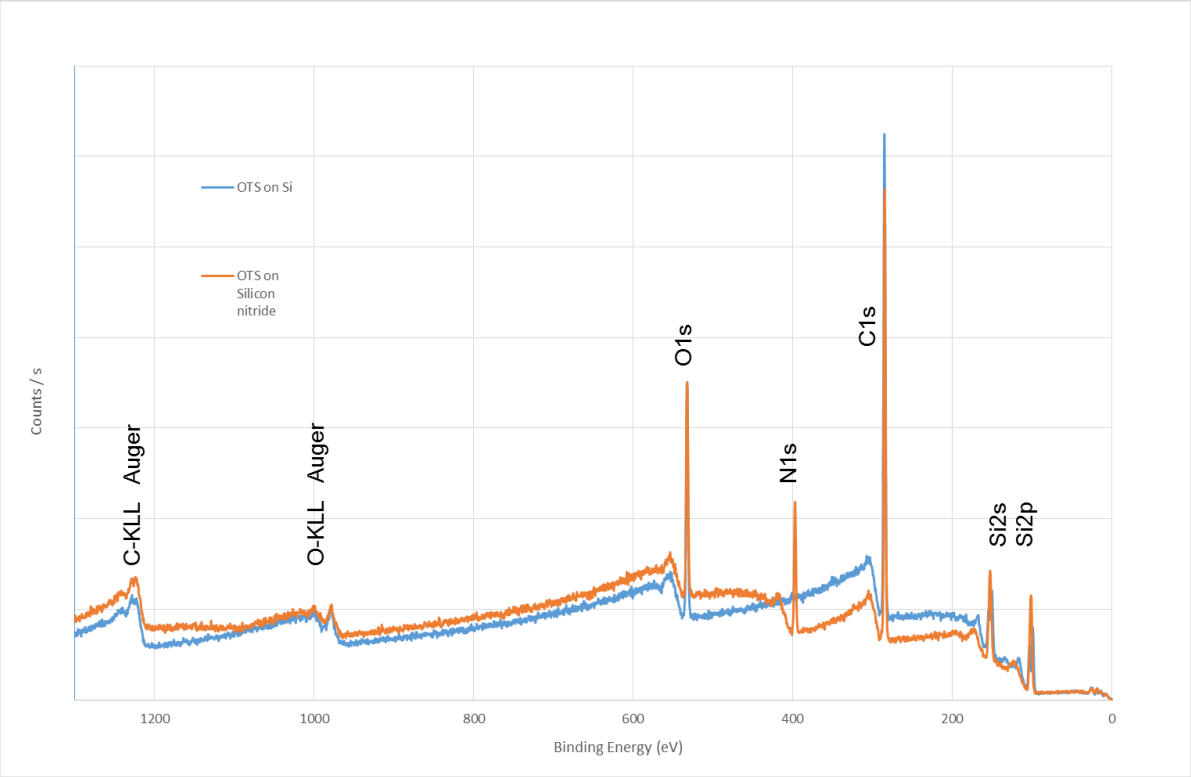

Figure 5.14. XPS survey spectra of OTS assembled on silicon and silicon nitride.

5.3 ATRP Initiator Synthesis

Prior to the hydrosilylation reaction the ester, allyl 2-bromo-2-methylpropionoate, was analysed by carbon and hydrogen NMR, as was the final product, an almost colourless oil, 3-(chlorodimethylsilyl)propyl bromoisobutyrate. NMR spectra were recorded on a Bruker AVIIIHD500 FT-NMR spectrometer in $CDCl_3$ at 298 K. Chemical shifts for proton and carbon spectra are reported on the delta scale in ppm and were referenced to residual solvent references or internal TMS reference. The full data set and NMR predictions are given in Appendix E. The predictions were carried out using the commercial software package ChemDraw Professional 15.

5.3.1 Ester NMR

The 6 different carbon environments within the ester show 6 different peaks and they correlate as shown below. A solvent peak of $CDCl_3$ is also present at approximately 77 ppm.

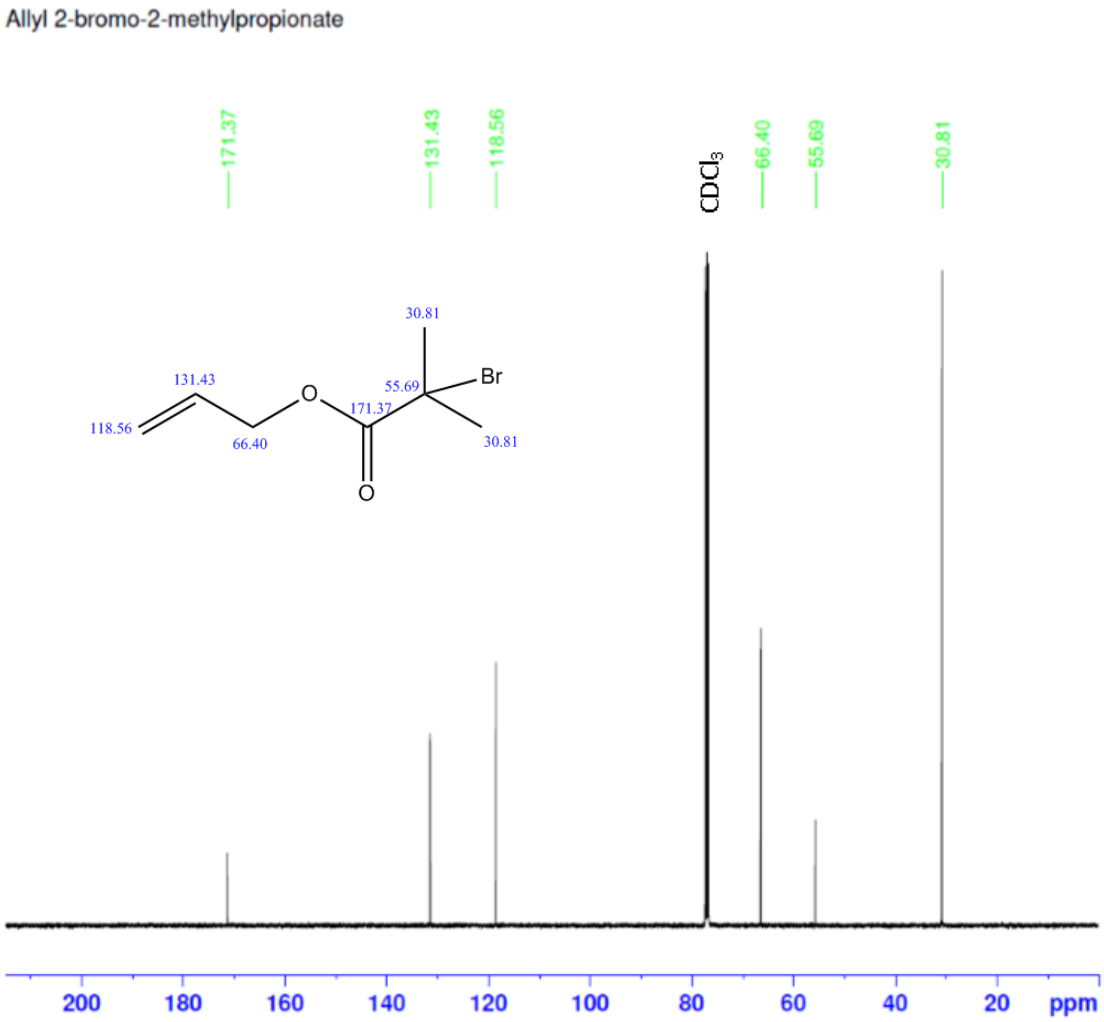

Figure 5.15 Carbon 13 NMR of the ester with peak assignment with inset with corresponding peaks overlaid.

The chemical shifts presented in Figure 5.15 can be summarised in the following notation. ^{13}C NMR ($CDCl_3$, 125 MHz): δ=171.37 (CO), 131.43 (=CH), 118.56 (=CH_2), 66.40 (CH_2O), 55.69 (Cter), 30.81 (CH_3).

Four different hydrogen environments produce the spectrum seen in Figure 5.16. Also shown is the integration data, this allows the ratio of hydrogens to be calculated. The splitting patterns are also shown and correlate as shown below. A solvent peak is also present at approximately 7.26 ppm in addition to a possible H_2O peak at 1.55 ppm [343, 344]. The relevant peaks are also transposed onto the chemical structure of interest in Figure 5.17. From the above NMR data as well as the modelled data present in Appendix E it is clear that the peaks match the structure of the ester.

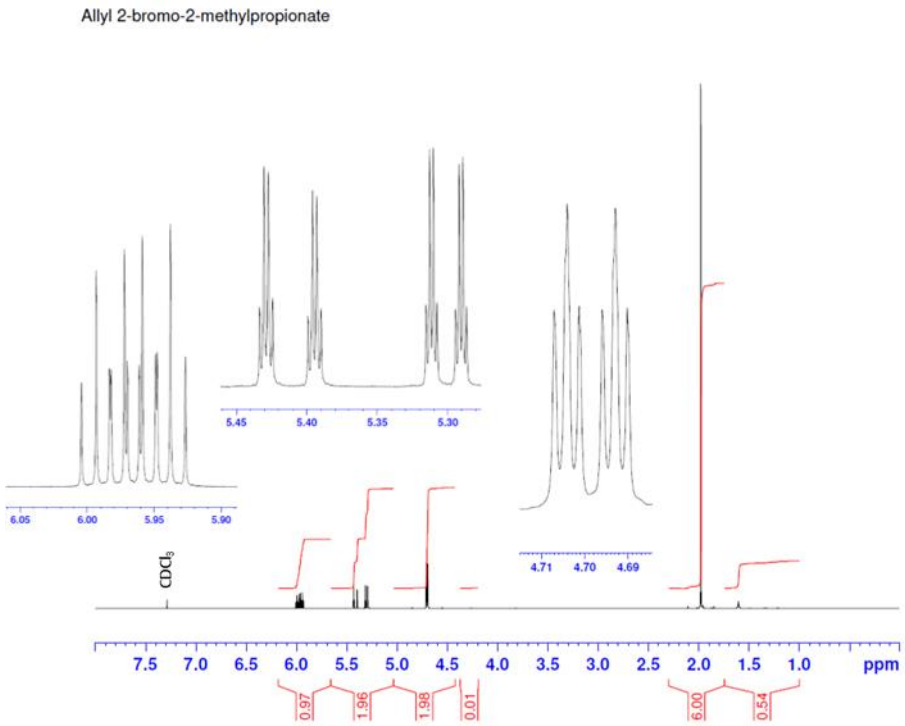

Figure 5.16. Hydrogen NMR of the ester with the addition of integration and embedded peak expansions.

Figure 5.16 can be summarised by 1H NMR ($CDCl_3$, 500 MHz): δ = 5.93-6.01 (m, 1H, =CH-), 5.28-5.44 (m, 2H, $=CH_2$-), 4.70 (d, 2H, $-CH_2O$-), 1.98 (s, 6H, CH_3).

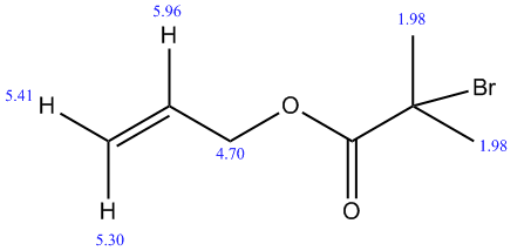

Figure 5.17. Peak assignment transposed onto the precursor ester.

5.3.2 ATRP Initiator NMR

The 7 different carbon environments show 7 different NMR peaks and they correlate as shown below. The chemical shift data has been transposed onto the initiator as can be seen in the inset of Figure 5.18. The peaks show good agreement with the predictions created by commercial software. Some of the spectrum is a little noisy, a probable cause is the degradation of the halogen bond and further impurities from the reaction mixture or vessel, particularly from the chlorosilane. A solvent peak is also present at approximately 77 ppm.

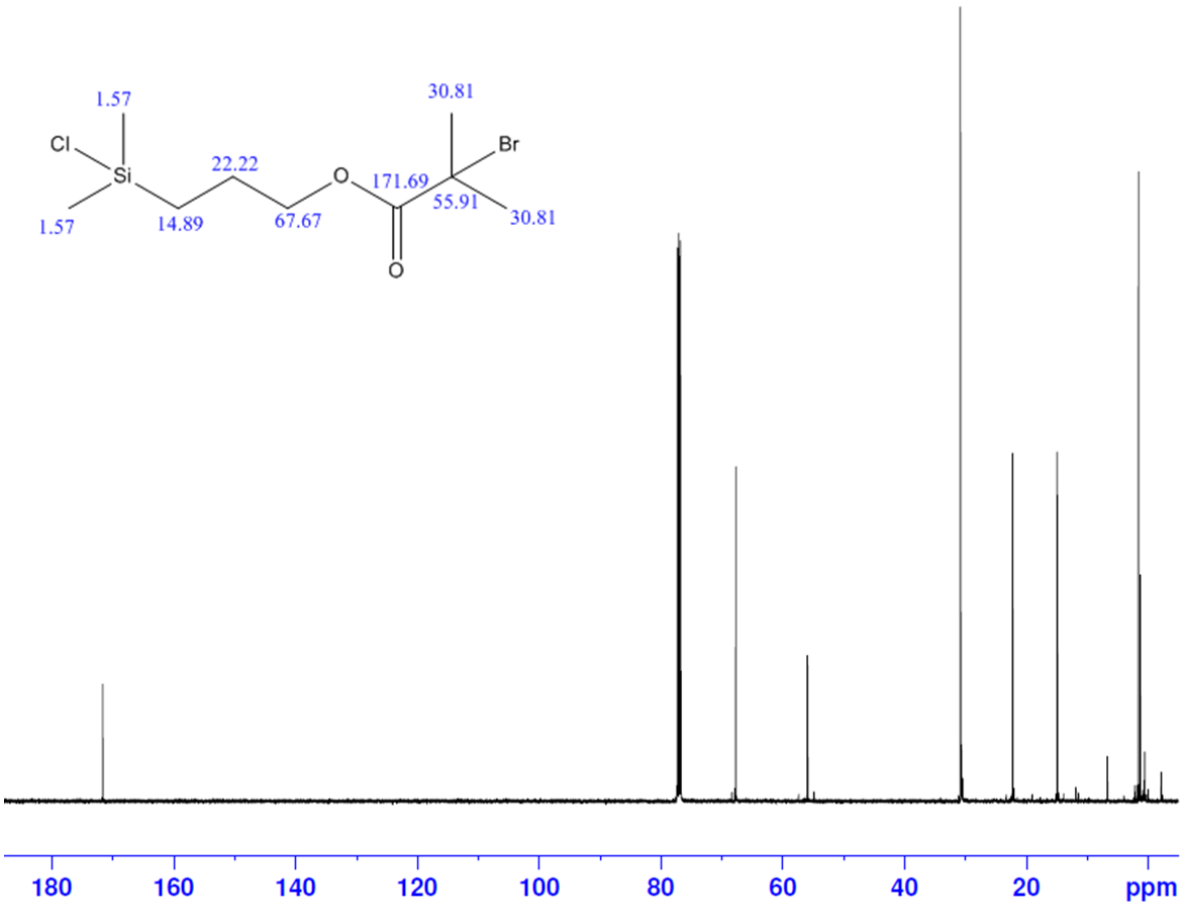

Figure 5.18. Carbon NMR of the ARTP initiator.

The above NMR readout can be given as the following notation.

^{13}C NMR ($CDCl_3$, 125 MHz): δ =171.7 (CO), 67.7 (CH_2O), 55.9 (Cter), 30.8 and 22.2 (CH_3 and CH_2), 14.9 ($SiCH_2$), 1.6 ($SiCH_3$).

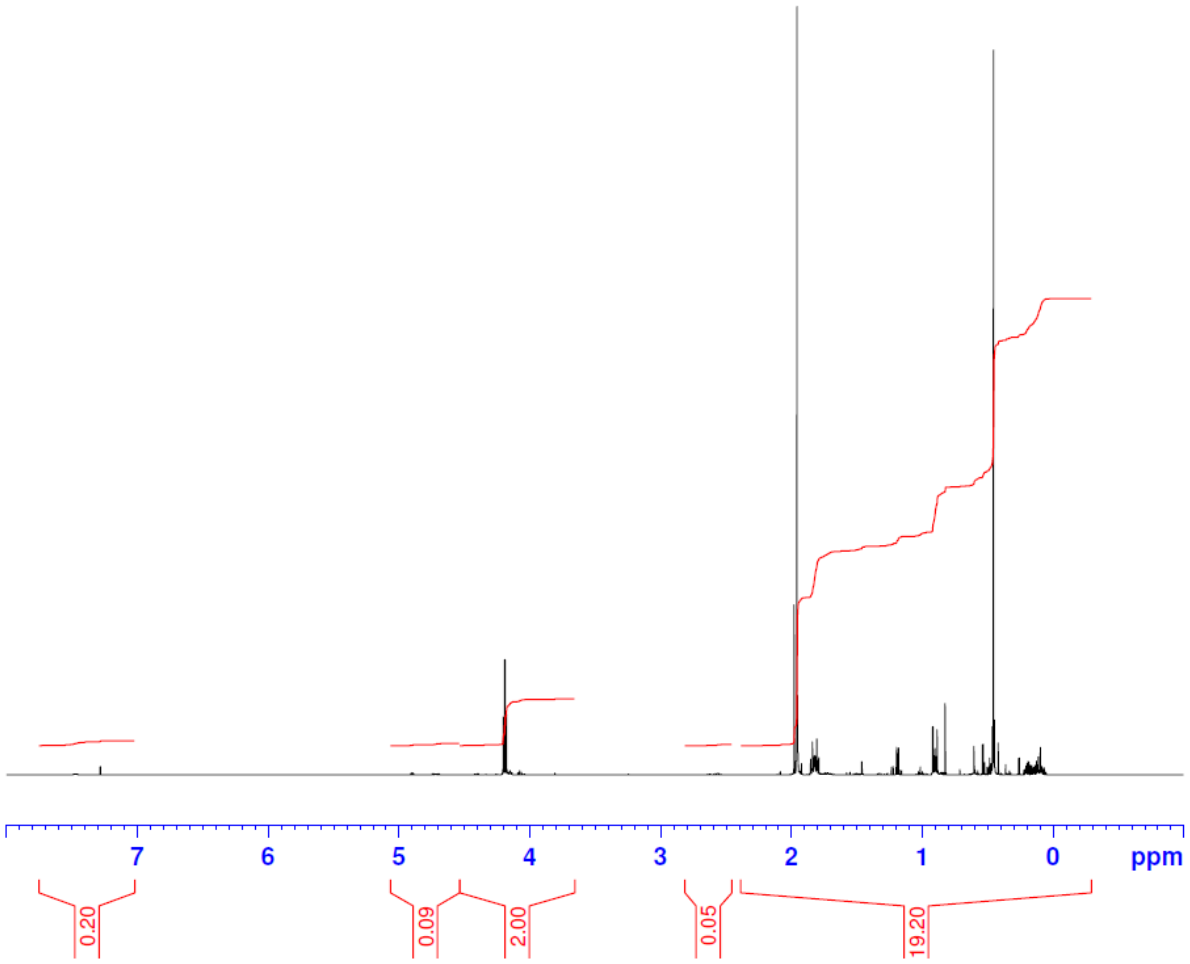

Figure 5.19. Hydrogen NMR of the ATRP initiator.

The following notation is derived; ^{1}H NMR ($CDCl_3$, 500 MHz): δ = 4.14-4.21 (m, 2H, -CH_2O-), 1.96 (s, 6H, -CH_3-), 1.78-1.88 (m, 2H, -CH_2-), 0.89 (m, 2H, -$SiCH_2$-), 0.45 (s, 6H, -$Si(CH_3)_2$-).

Five different hydrogen environments produce the spectrum shown in Figure 5.19. Although quite noisy between 0-2 ppm the peaks that have been assigned correlate well with literature values and the predicted data. This molecule is difficult to purify due to the high boiling point. Some of the small peaks may be due to degradation products such as the removal of the mildly unstable halogen groups however it is clear that the majority of product is the compound of interest.

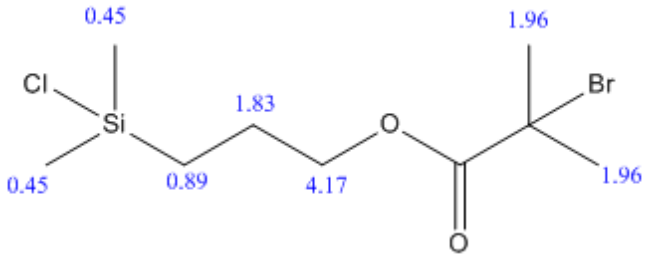

Figure 5.20. Hydrogen peak assignment transposed onto ATRP initiator.

5.4 Silicon Nitride Coating on Silicon Wafer and Evaluation

To investigate the ability of the ATRP initiator to attach to silicon nitride a suitable sample of this substrate needed to be prepared. Silicon wafers were coated with a layer of silicon nitride using PECVD. The thickness of the silicon nitride coating as well as oxide thicknesses was measured using ellipsometry. As ellipsometry measures the change in light polarisation, namely Delta (Δ, relative change in phase) and Psi (Ψ, relative change in amplitude) and does not directly measure thickness, this has to be modelled. The experimentally collected data was then modelled using the commercial CompleteEASE package, specifically the Woollam model for Si and native SiO_2 [345]. This model can be seen in Figure 5.21, which shows the fit for the thickness of the oxide layer. Figure 5.21 also shows the goodness-of-fit of the model with the collected data. The native oxide layer was measured to be 1.81 ± 0.057 nm thick, this is in agreement with the literature [346].

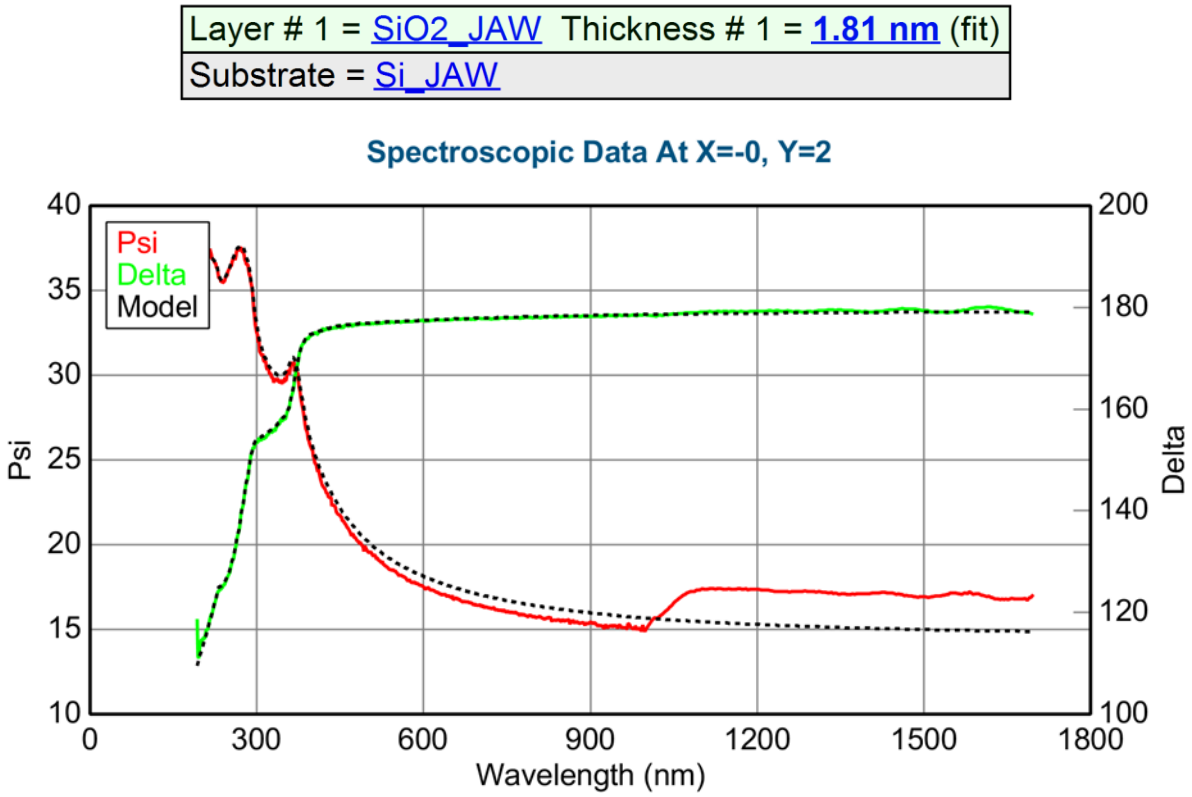

Figure 5.21. Experimentally collected data modelled to obtain the thickness of oxide.

Figure 5.22 displays the change in oxide thickness vs position on the wafer. The mean square error calculated by the model is also presented here. There does appear to be a large variation in one of the readings however when the silicon nitride has been deposited there is not a similar effect on thickness.

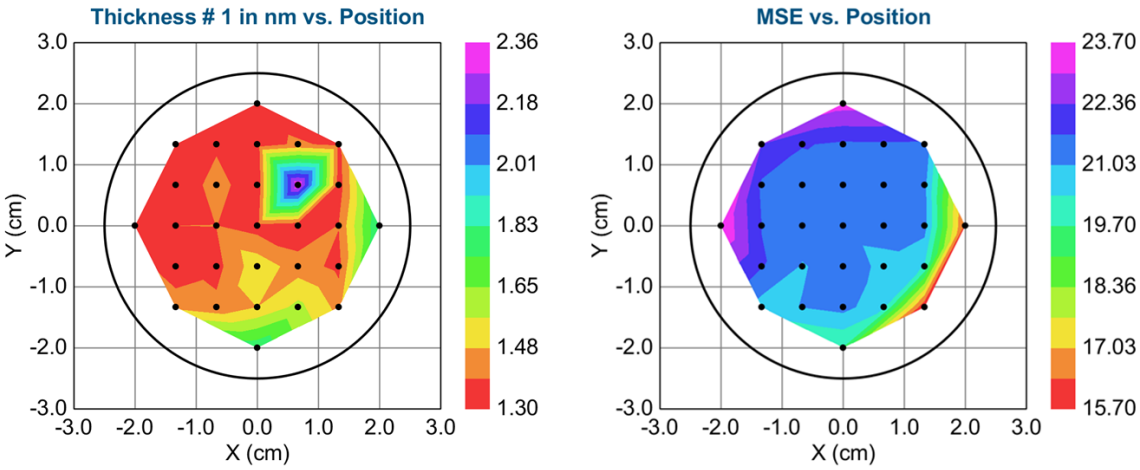

Figure 5.22. A map of the thickness and mean square error (MSE) across the silicon wafer

The wafers had silicon nitride deposited on them by an Oxfords Instruments PlasmaLabSystem 100 PECVD system. The gasses used are SiH_4 and NH_3 at flowrates of 12.6 sccm and 20.0 sccm respectively. A model was created for this based on the information collected previously in addition to the new layer. The new layer was based on the Tauc-Lorentz model which is a model that is commonly used to describe the dielectric constant of amorphous semiconductors from a few parameters that are easily collected by ellipsometry. The model is also capable of filtering out or recognising the back reflections from another layer such as the polished back of the wafer. The optical model is shown in Figure 5.23 and the model fitted to the data in Figure 5.24.

Layer Commands: **Add** **Delete** **Save**
Include Surface Roughness = OFF

Layer # 3 = SiO2_JAW Thickness # 3 = **1.30 nm** (fit)
- Layer # 2 = Si3N4 (TaucLorentz) Thickness # 2 = **596.55 nm** (fit) Amp. = **55.116** (fit) Brod. = **3.719** (fit) Eo = **8.138** (fit) Eg = **2.771** (fit) Einf = **1.476** (fit)
Layer # 1 = SiO2_JAW Thickness # 1 = **2.09 nm** (fit)
Substrate = Si_JAW Substrate Thickness = 0.5000 mm

Angle Offset = 0.00

- MODEL Options
Include Substrate Backside Correction = ON
Transmission SE Data = OFF Reverse Direction = OFF
Back Reflections = **0.756** (fit) % 1st Reflection = **100.00** (fit)
Model Calculation = Ideal

- FIT Options
+ Perform Thickness Pre-Fit = ON
Use Global Fit = OFF
Fit Weight = N,C,S
Limit Wvl. for Fit = OFF
Limit Angles for Fit = OFF
Max. Acceptable MSE = 100.000
Include Derived Parameters = OFF

+ OTHER Options
Configure Options
Turn Off All Fit Parameters

Figure 5.23. Detailed breakdown of the optical model for silicon nitride on a native oxide layer of a silicon wafer.

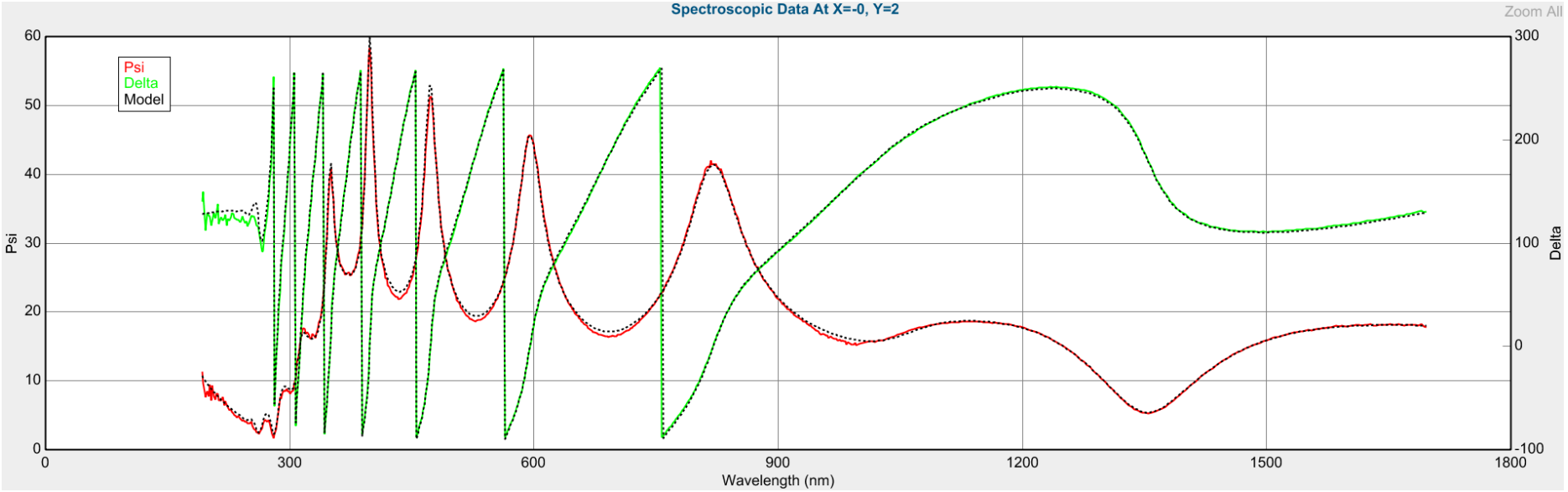

Figure 5.24. The experimental data with the model in black showing a good fit.

The thickness of the silicon nitride layer was calculated to be 596.55 ± 0.64 nm. Presented in Figure 5.25 are the maps of the variation in thickness compared to position as well as the MSE.

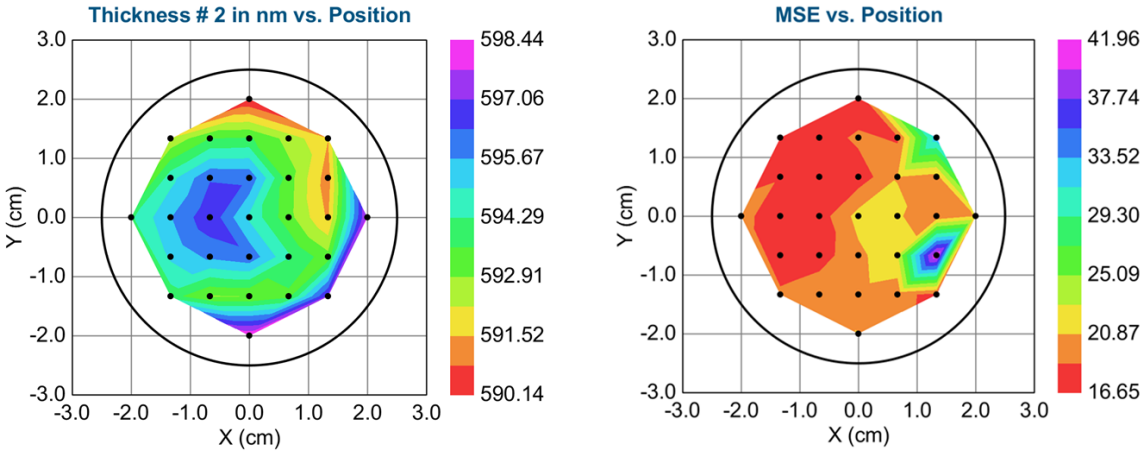

Figure 5.25. A map of the thickness and mean square error (MSE) across the silicon nitride layer.

The model also incorporates the natural oxide layer present on silicon nitride and is 1.30 ± 0.12 nm thick as can be seen in Figure 5.26

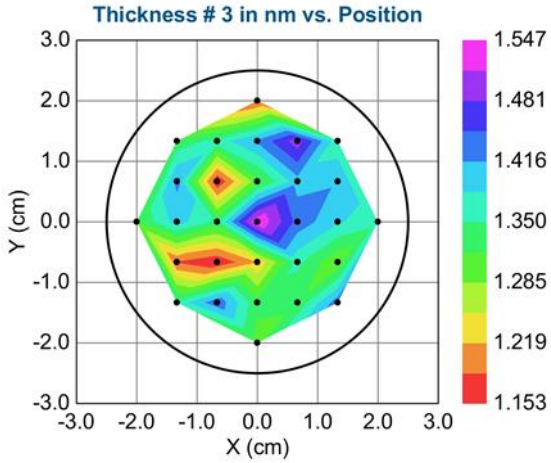

Figure 5.26. Thicknesses of the natural oxide layer present on the silicon nitride.

The surface was then investigated with AFM, SEM, EDX and contact angle. The contact angle of three samples was measured in triplicate giving an average of 27.2° which is in agreement with the literature [171, 190].

Table 5.1. Results of contact angle of water on a silicon nitride sample.

	Repeats			
Sample	1	2	3	
A	21.6°	30.0°	28.7°	Average = 27.2°
B	31.2°	32.1°	24.8°	
C	26.7°	24.4°	25.1°	

EDX was also completed and is presented in Figure 5.27. The EDX data presented in Figure 5.27 below is a comparison of a silicon wafer before (left) and after (right) silicon nitride deposition. Notably the nitrogen peak is present in the silicon nitride layer as further proof of a nitride layer being present.

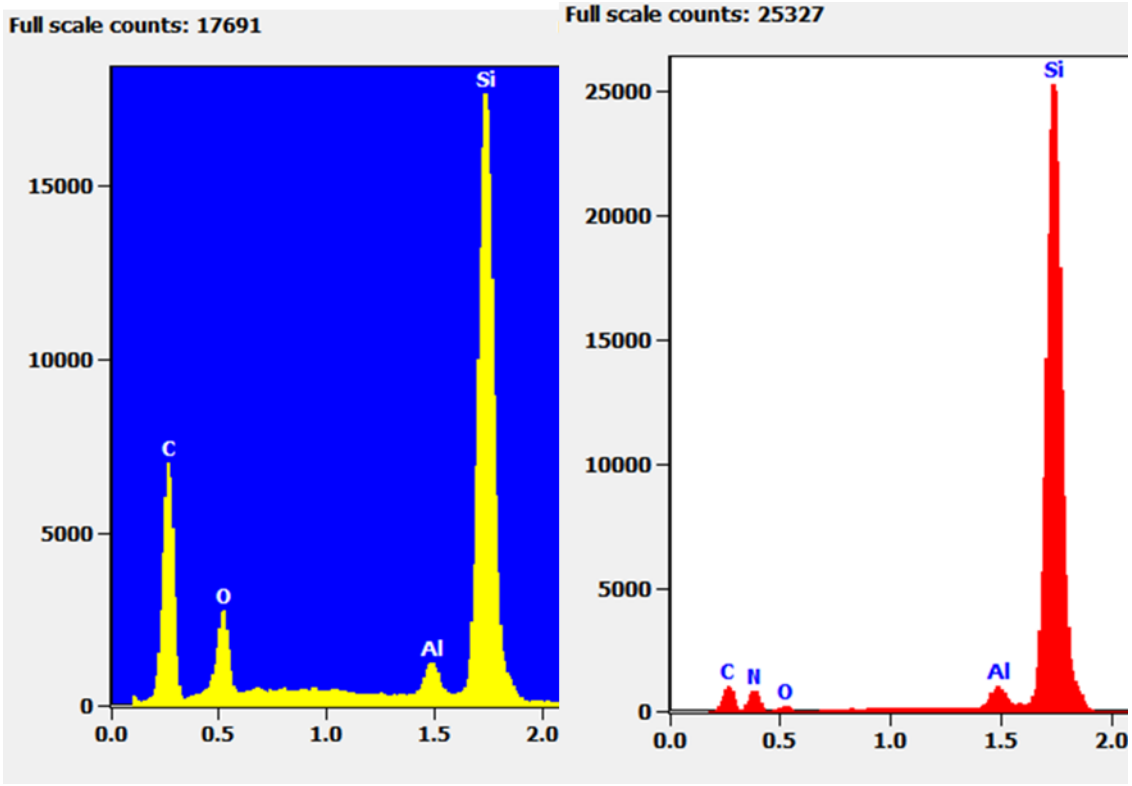

Figure 5.27. EDX of the silicon wafers before and after silicon nitride deposition.

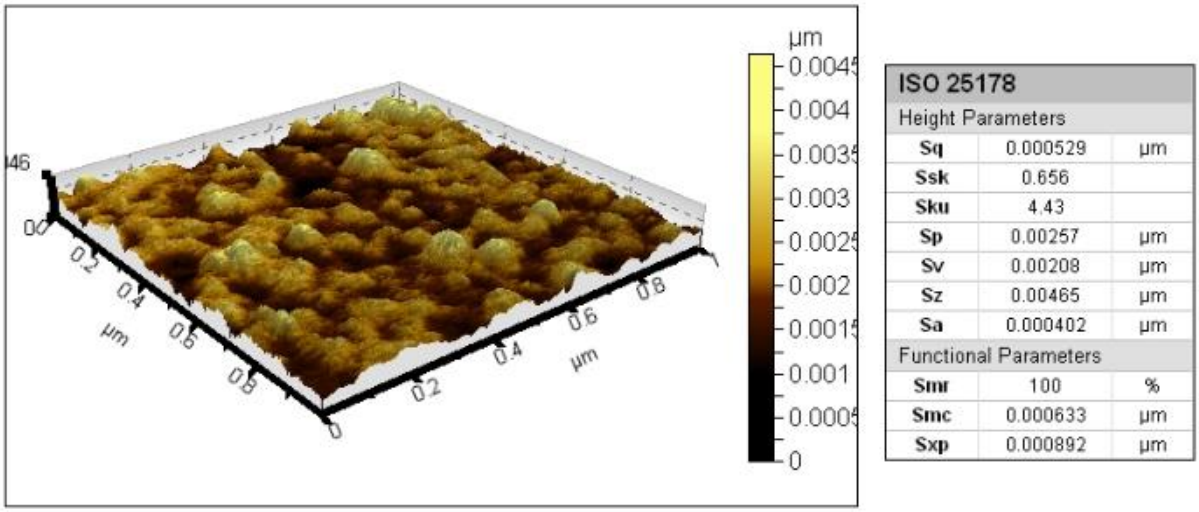

Figure 5.28. AFM topography of the silicon nitride surface.

The AFM image, Figure 5.28, shows the topography of the flat surface. This explains why when observing with SEM there is no change on the surface.

The XPS spectrum of the silicon nitride surface is shown in Figure 5.29. As expected oxygen nitrogen and silicon are all present, however carbon is also present, and it is nearly impossible to obtain a truly “clean” surface [347]. This adventitious carbon is found on surfaces exposed to the atmosphere and is generally thought to be some hydrocarbon species [348]. Some contamination is useful for analysis as carbon is used as a reference point. The silicon peak as shown in Figure 5.30 is slightly asymmetric due to the difference between the binding energies in silicon nitride and silicon oxide [349]. Auger peaks for both oxygen and carbon are clearly present too.

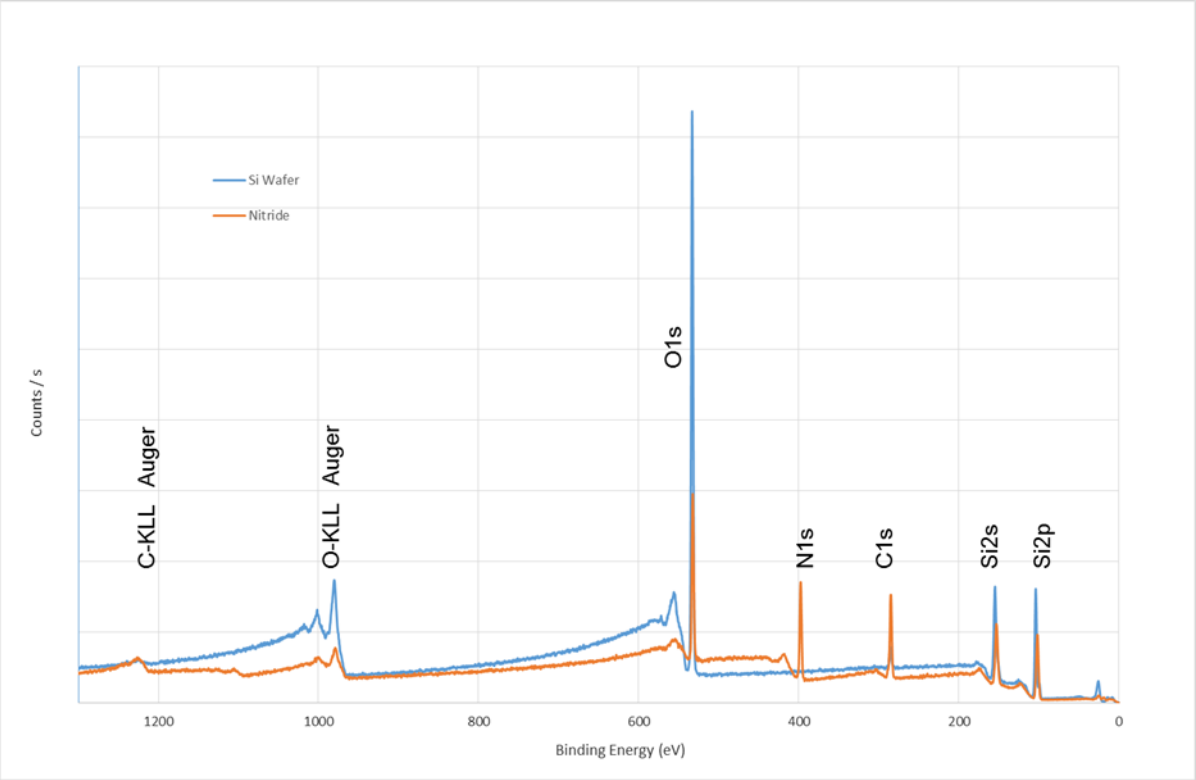

Figure 5.29. XPS survey spectra of silicon nitride.

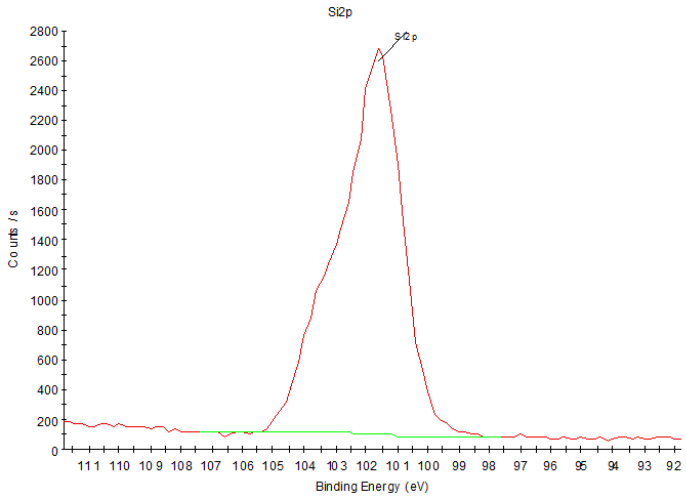

Figure 5.30. High resolution core spectra of silicon from the silicon nitride sample.

5.5 Adsorption of Initiator

5.5.1 Initiator on Silicon Wafer in Toluene

Self-assembled deposition of the initiating monolayer was expected to take a longer amount of time than that of OTS due to the steric interference of the larger head group. This can be clearly seen in Figure 5.31 where the maximum contact angle was achieved over a longer time. From Figure 5.31 it appears that the maximum contact angle of 84° in toluene can be achieved in a 2.5 mM solution in 18 h. Therefore, to reduce wastage and cost of using more initiator this finding was carried forward.

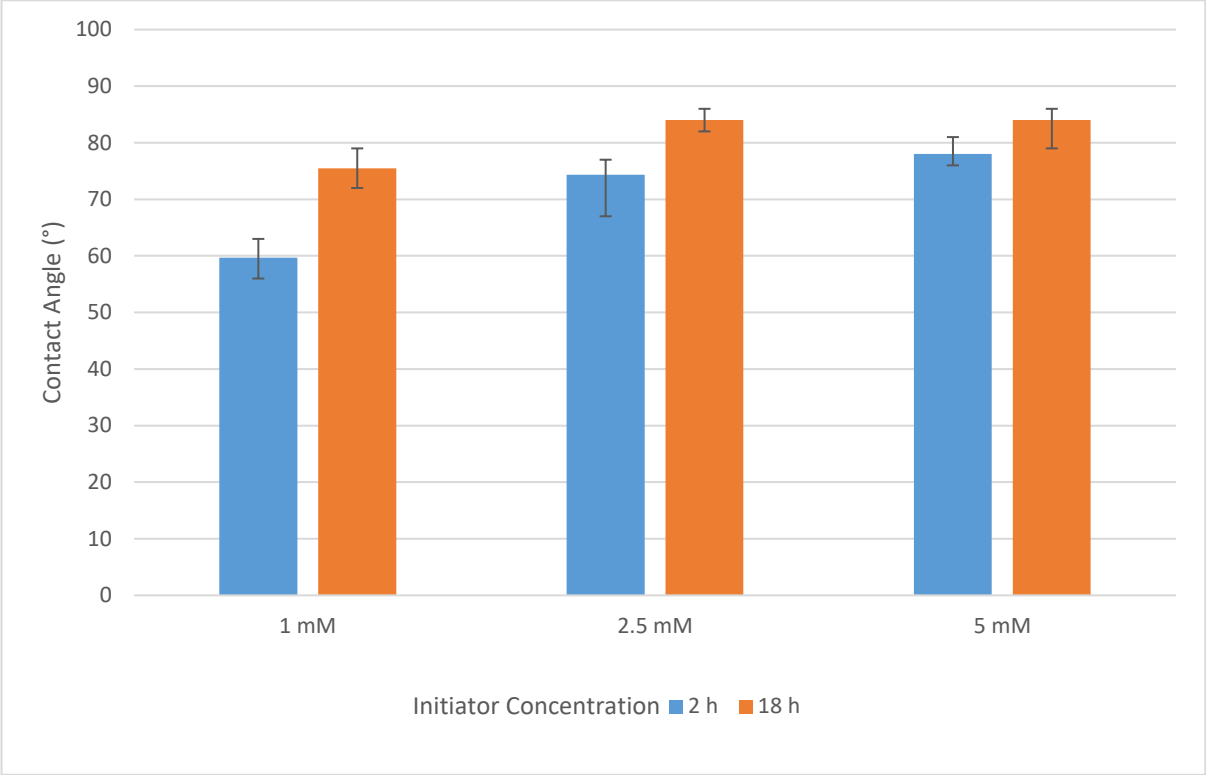

Figure 5.31. The relationship between time and concentration of initiator compared to the resultant contact angle in toluene.

AFM images show the presence of SAMs on all samples as expected from contact angles. As the initiator is an extremely small molecule the SAM will follow the topography of a silicon wafer, which explains the extreme flatness of the samples. In Figure 5.32, the 1 mM 2 h sample differs the most from the rest of the images, this correlates to the lower contact angle achieved and indicates a partial monolayer creation. Monolayers created in the 2.5 mM solution show uniformity even though there is more variation in the height. Also present in the 18 h sample are a few agglomerations, a trend that is more notable in all of the 18 h samples. The samples that performed the best, 2.5 mM 18 h and 5 mM 18 h, do look slightly different, the 5 mM sample appears to be more uniform however both samples, without agglomerations, achieve similar heights. When comparing the 2 h samples of both 2.5 and 5 mM there are many similarities in the shape and frequency of the SAMs on the surface, this can also extend to 1 mM 18 h sample and is not surprising as they seem to be in the same stage of growth, as indicated by the contact angle.

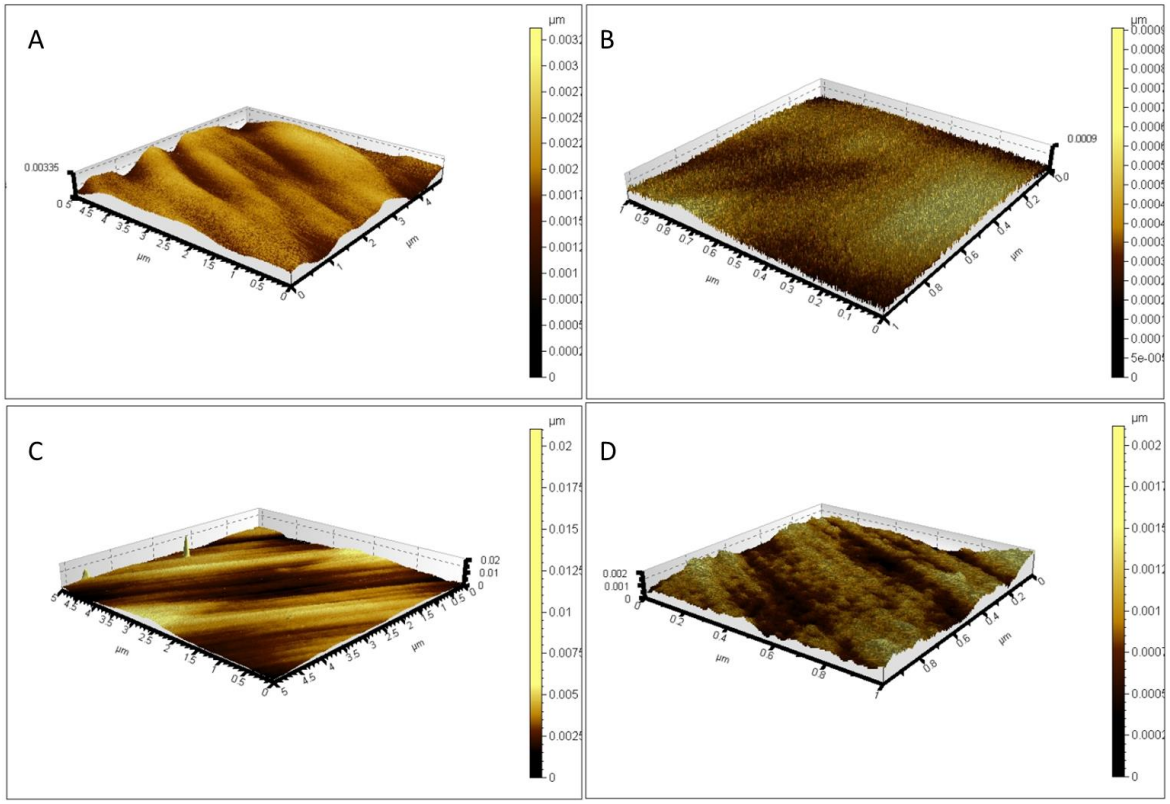

Figure 5.32. AFM images of the 1mM SAM. A- 5x5 µm 2h, B- 1x1 µm 2h, C- 5x5 µm 18h, D- 1x1 µm 18h

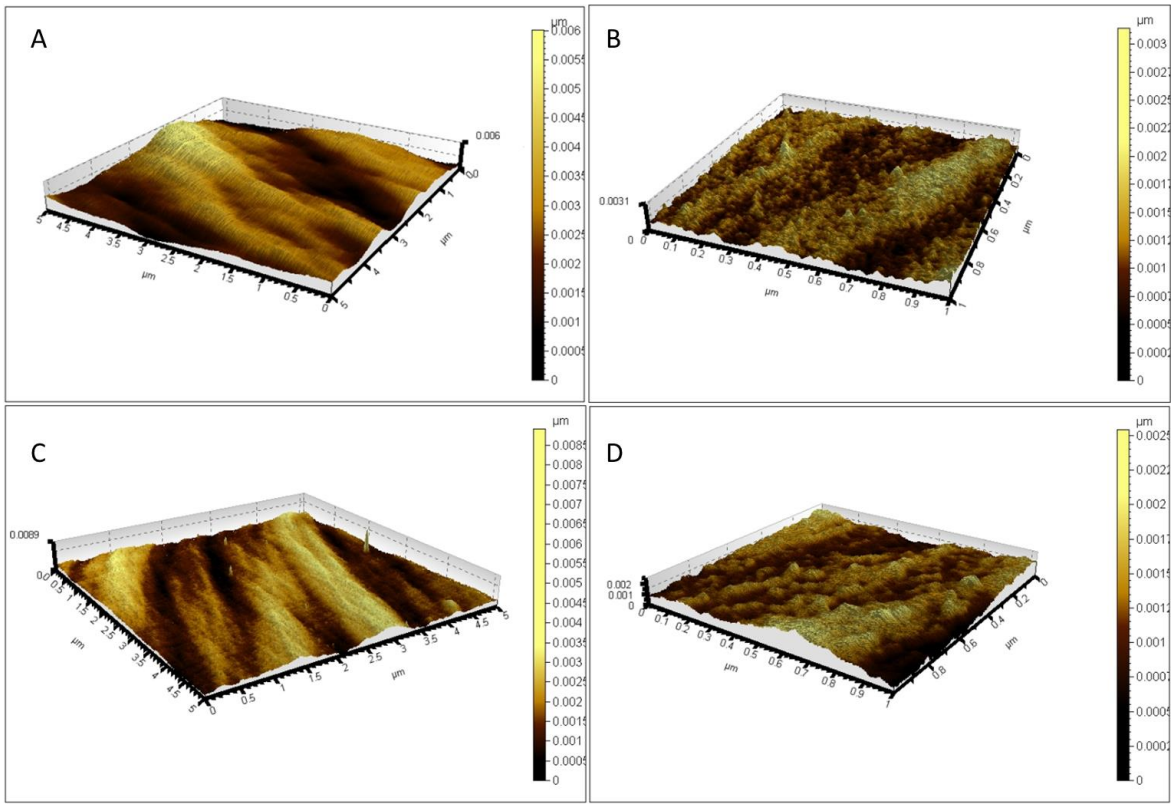

Figure 5.33. AFM images of the 2.5mM SAM. A- 5x5 µm 2h, B- 1x1 µm 2h, C- 5x5 µm 18h, D- 1x1 µm

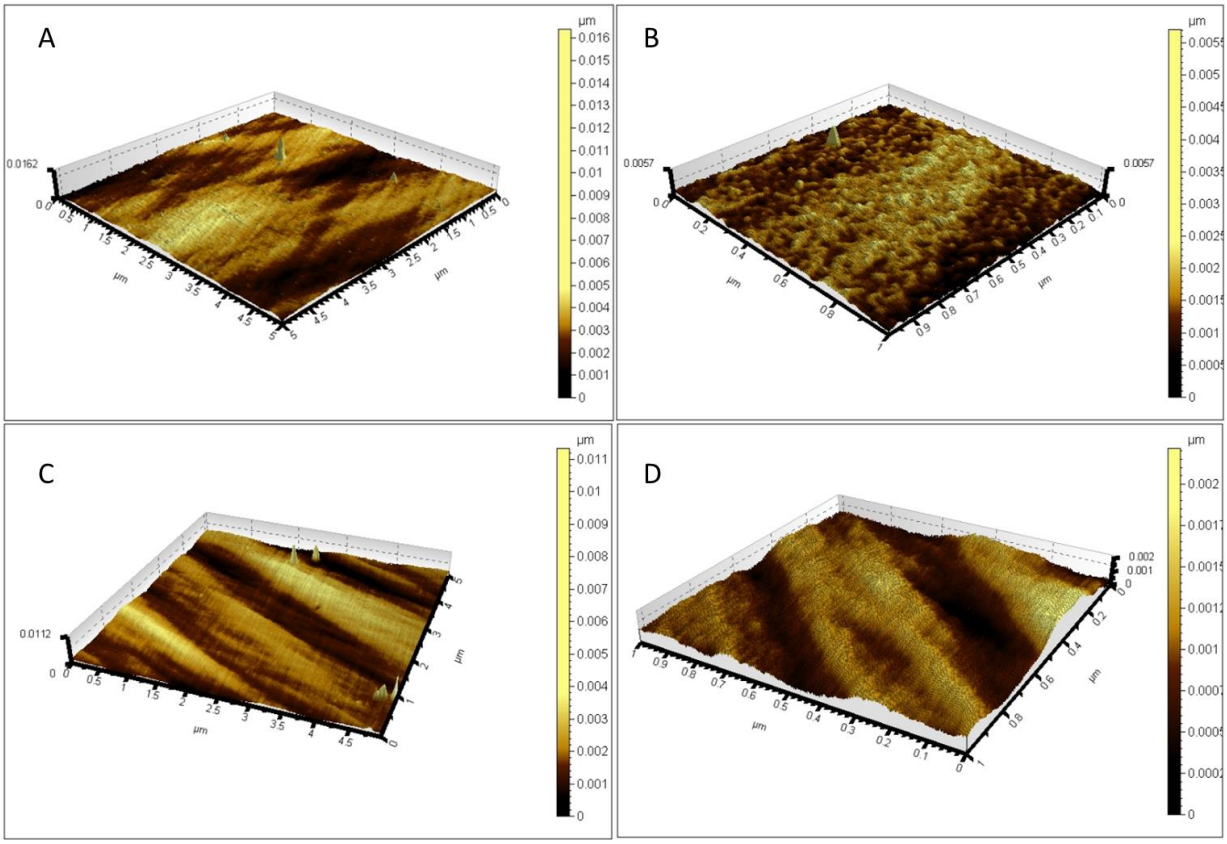

Figure 5.34. AFM images of the 5mM SAM. A- 5x5 µm 2h, B- 1x1 µm 2h, C- 5x5 µm 18h, D- 1x1 µm.

5.5.2 Initiator on Silicon Nitride in Toluene

As seen in Figure 5.35 immersion in the 1 mM solution failed to achieve the desired contact angle in either 2 h or 18 h. The most successful were 2.5 mM and 5 mM which both achieved an average contact angle of 83°. The suspected reason for the longer assembly times is steric hindrance. Therefore the initiator concentration has been shown to influence the maximum contact angle achieved and in the case of self-assembly on silicon nitride there is no difference.

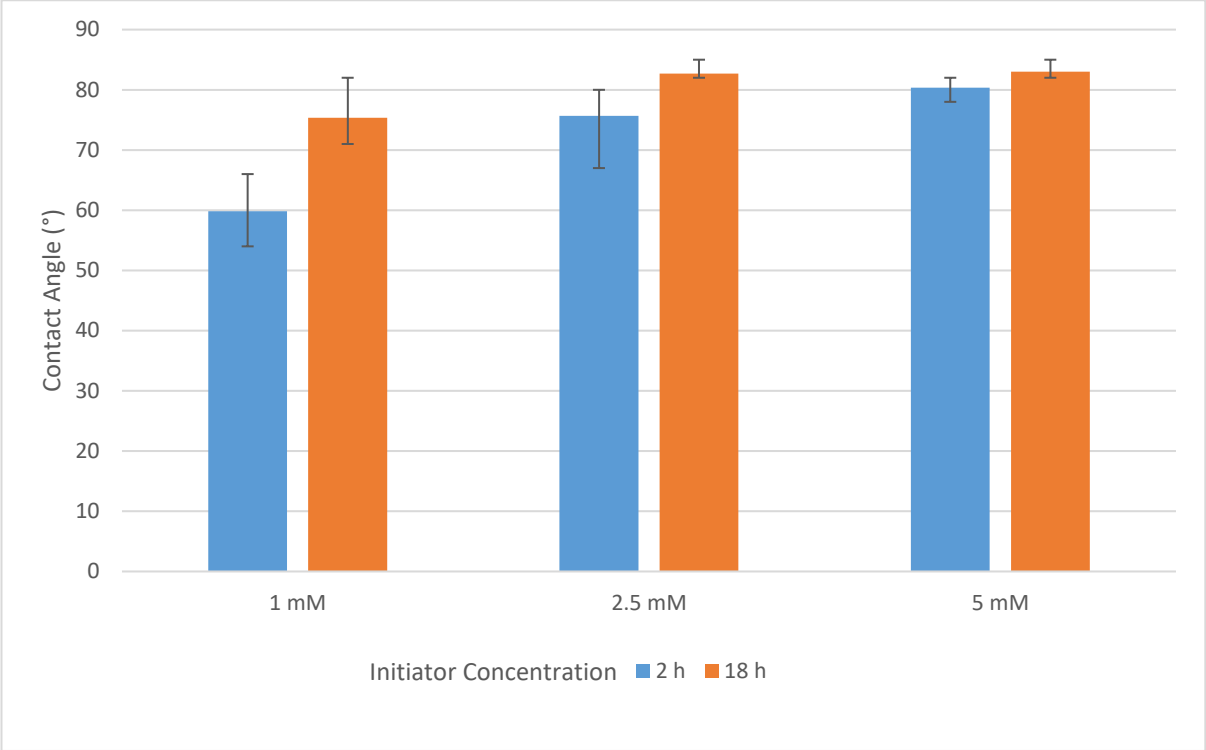

Figure 5.35. The relationship between time and concentration of initiator compared to the resultant contact angle on silicon nitride in toluene.

Due to the surface chemistry of silicon nitride, seen in Figure 2.15, and the similarities to that of a silicon wafer a similar contact angle should be possible. The comparison of contact angles is present in Figure 5.36. A few trends are clear, most notably that when restricted to 2 h of self-assembly the increase in concentration facilitates a notable increase in contact angle. In addition, irrespective of time, the two higher concentrations achieved higher contact angles as expected.

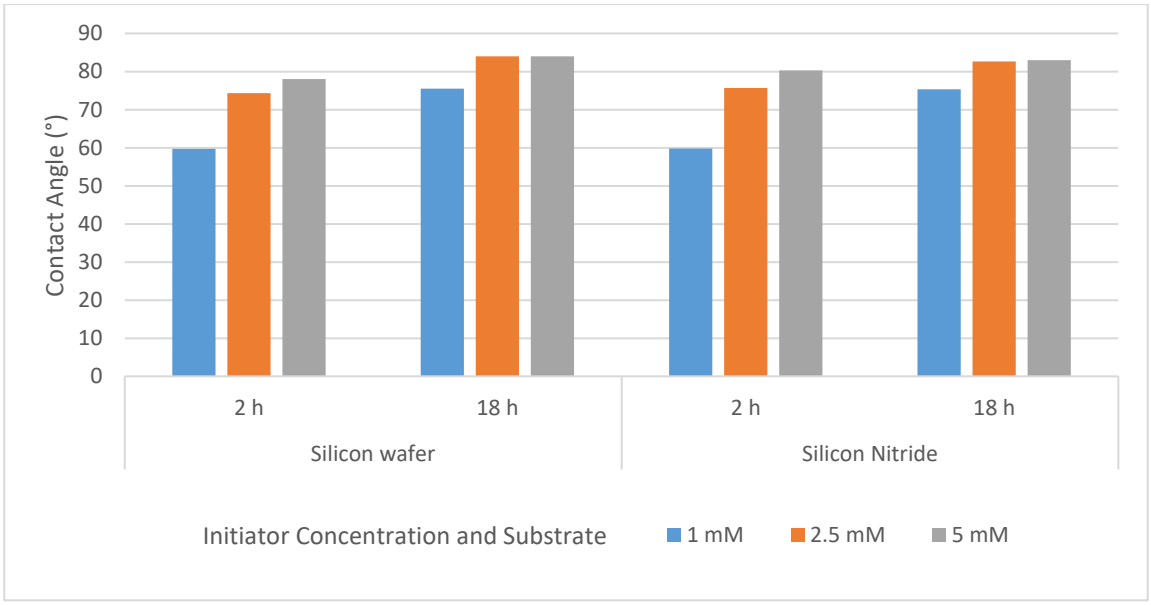

Figure 5.36. A comparison of the contact angle when the substrate is changed.

Figure 5.37 shows AFM images of the topography of the ATRP initiator which has self-assembled onto the silicon nitride. As can be seen below, the 1 mM solution of the ATRP initiator has had

limited success in creating a full monolayer both at 2 h and 18 h. It can be seen that the film was only partially formed. Comparing 1 mM and 2.5 mM at 18 h immersion shows the difference between a full monolayer which is present on the 2.5 mM solution. Whereas, the 1 mM SAM shows clear gaps in the film which is detrimental to the contact angle as can be seen above in Figure 5.36. The 2.5 mM and 5 mM produce full coverage at 18 h with relatively smooth topography. There are a few notable gaps in the 5 mM 2 h SAM, however, in comparison to 1 mM they are both smaller and have had less effect on the overall monolayer.

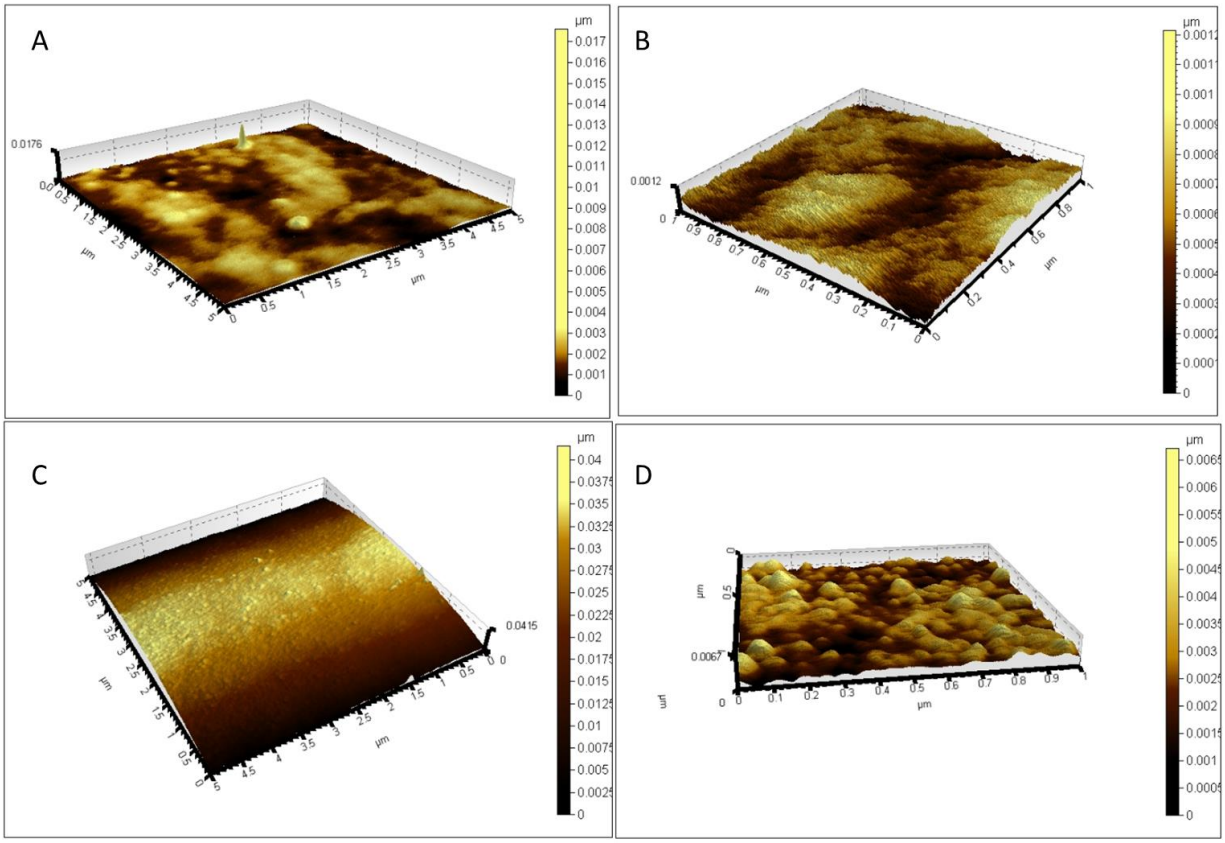

Figure 5.37. AFM images of the 1 mM SAM. A- 5x5 µm 2h, B- 1x1 µm 2h, C- 5x5 µm 18h, D- 1x1 µm.

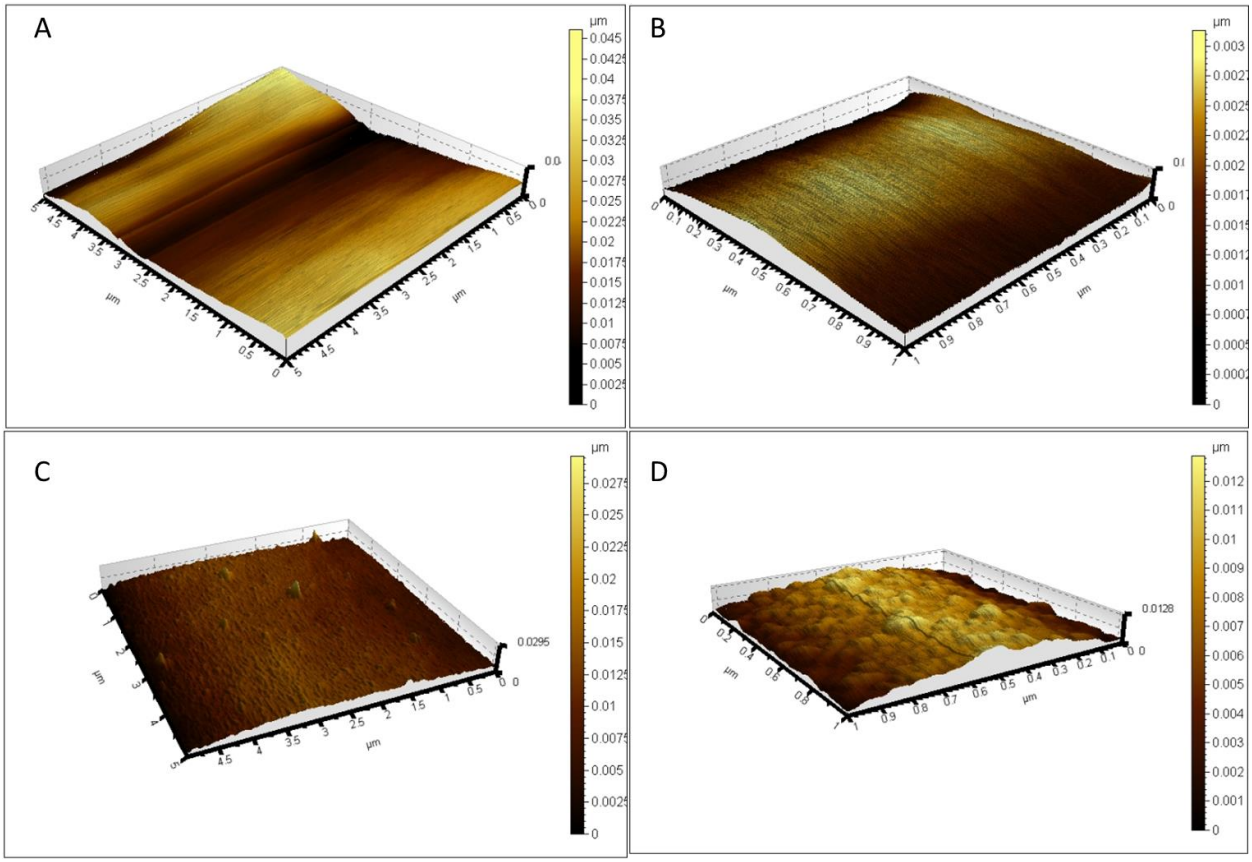

Figure 5.38. AFM images of the 2.5 mM SAM. A- 5x5 µm 2h, B- 1x1 µm 2h, C- 5x5 µm 18h, D- 1x1 µm.

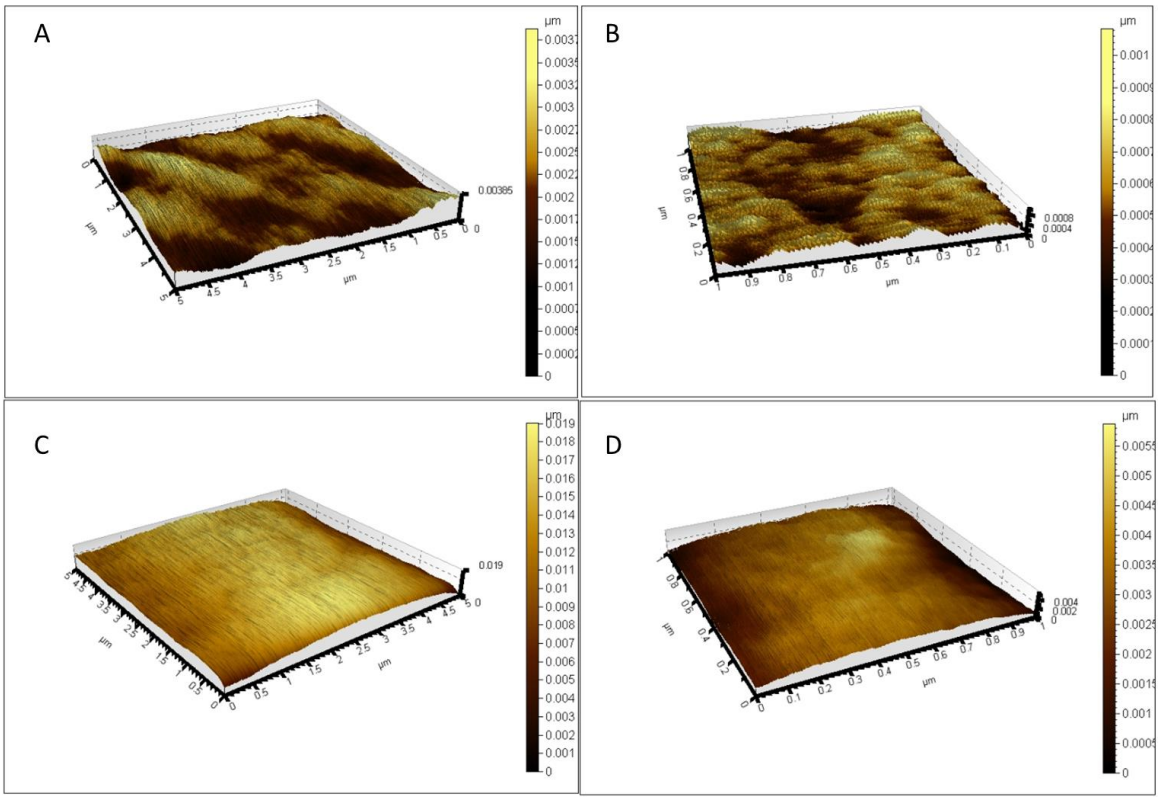

Figure 5.39. AFM images of the 5 mM SAM. A- 5x5 µm 2h, B- 1x1 µm 2h, C- 5x5 µm 18h, D- 1x1 µm.

5.5.3 Initiator on Silicon Wafer in PAO

From results of the previous experiments it was decided that the 1 mM solution was unable to produce a maximum contact angle in either of the allotted timeframes under ideal conditions of solvent and time. Therefore further investigation of this concentration was needed. Firstly, it must be noted that a maximum contact angle was unlikely to match that of toluene due to the use of an imperfect solvent as discussed in section 2.3.2, Solvent Selection. Another factor that should be considered is the water content with the PAO capable of containing five times more than toluene [350]. The contact angle data shows that in all cases a monolayer has been formed to some degree. As can be seen in Figure 5.40 and as expected from toluene experiments the 18 h test resulted in a better contact angle with a maximum of 82.5°. In comparison to the tests in toluene the difference between 2.5 mM and 5 mM is relatively small, and somewhat surprising is the slightly higher contact angle achieved in 2 h. However, the difference in final contact angle is overshadowed by the maximum contact angle achieved by toluene which was unobtainable by the test conditions with the PAO. The AFM images presented below have a few common features, it can be noted that there are relatively more agglomerations present on the surface of both silicon and silicon nitride possibly due to the water content of the PAO. When analysing the initiator on silicon wafers it can be seen that even though the monolayer appears to follow the general topography of a silicon wafer there is some variation, possibly where the SAM has not entirely formed such as in the instance of 2.5 mM.

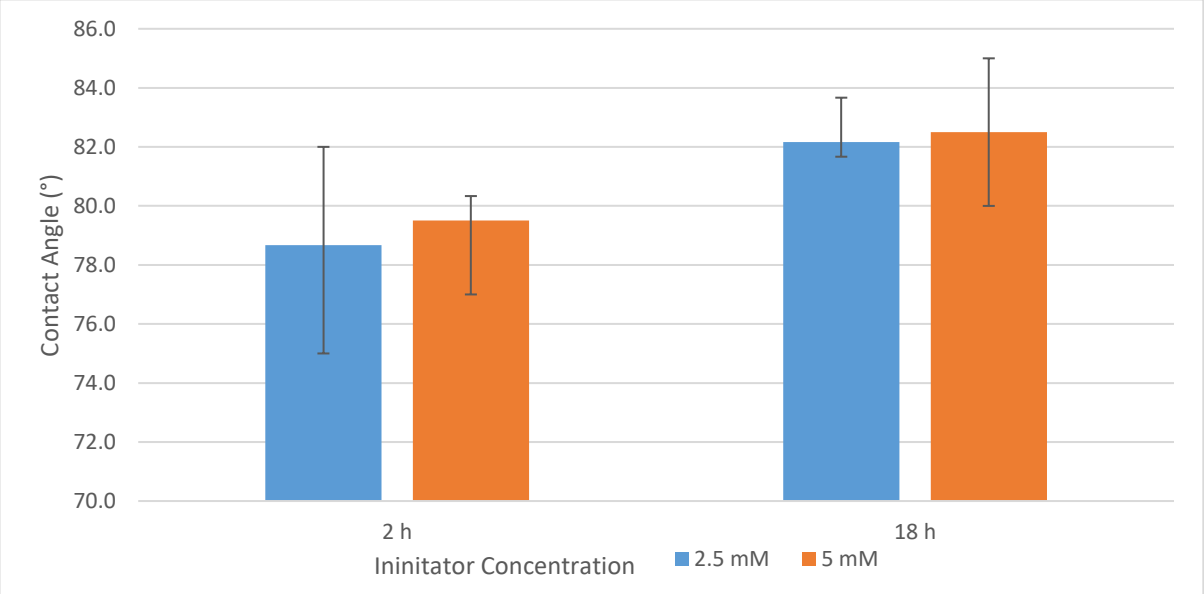

Figure 5.40. The relationship between time and concentration of initiator in PAO on silicon compared to the resultant contact angle.

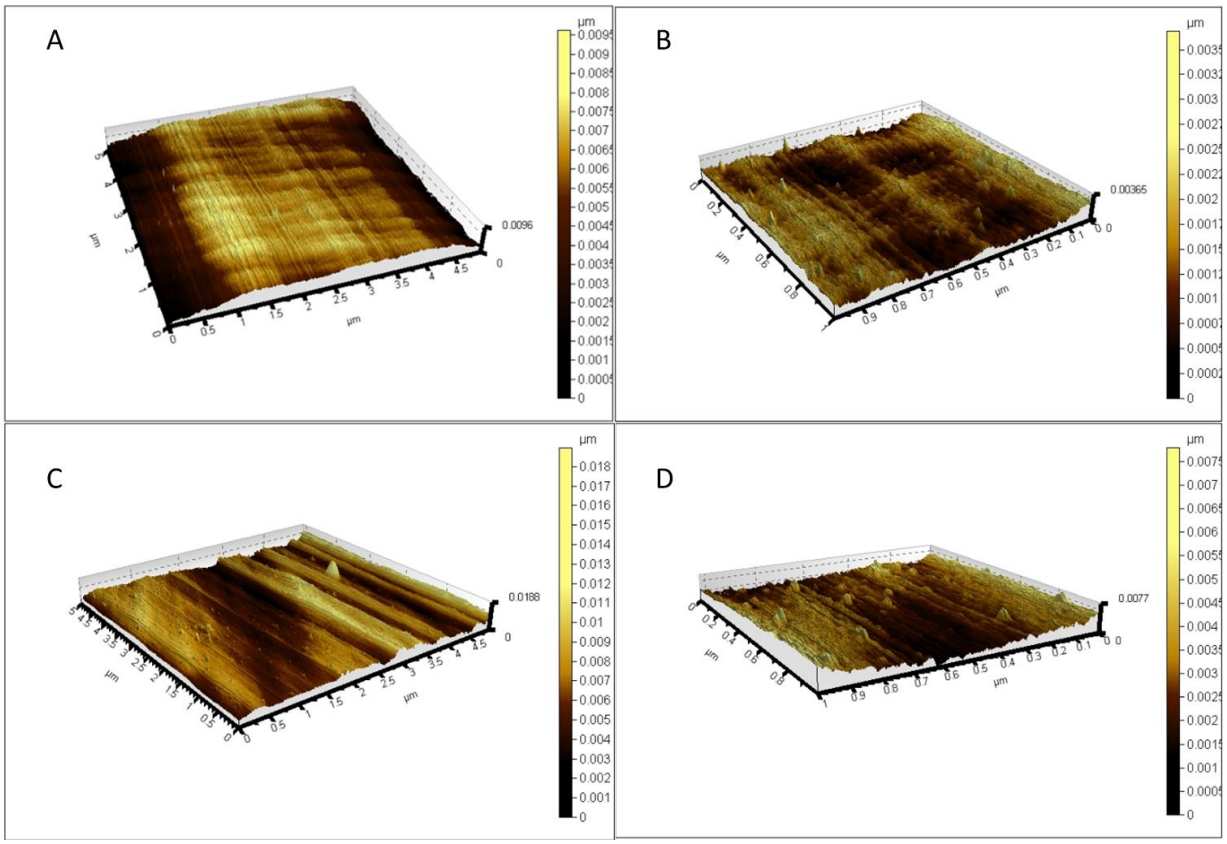

Figure 5.41. AFM images of the 2.5 mM SAM. A- 5x5 µm 2h, B- 1x1 µm 2h, C- 5x5 µm 18h, D- 1x1 µm.

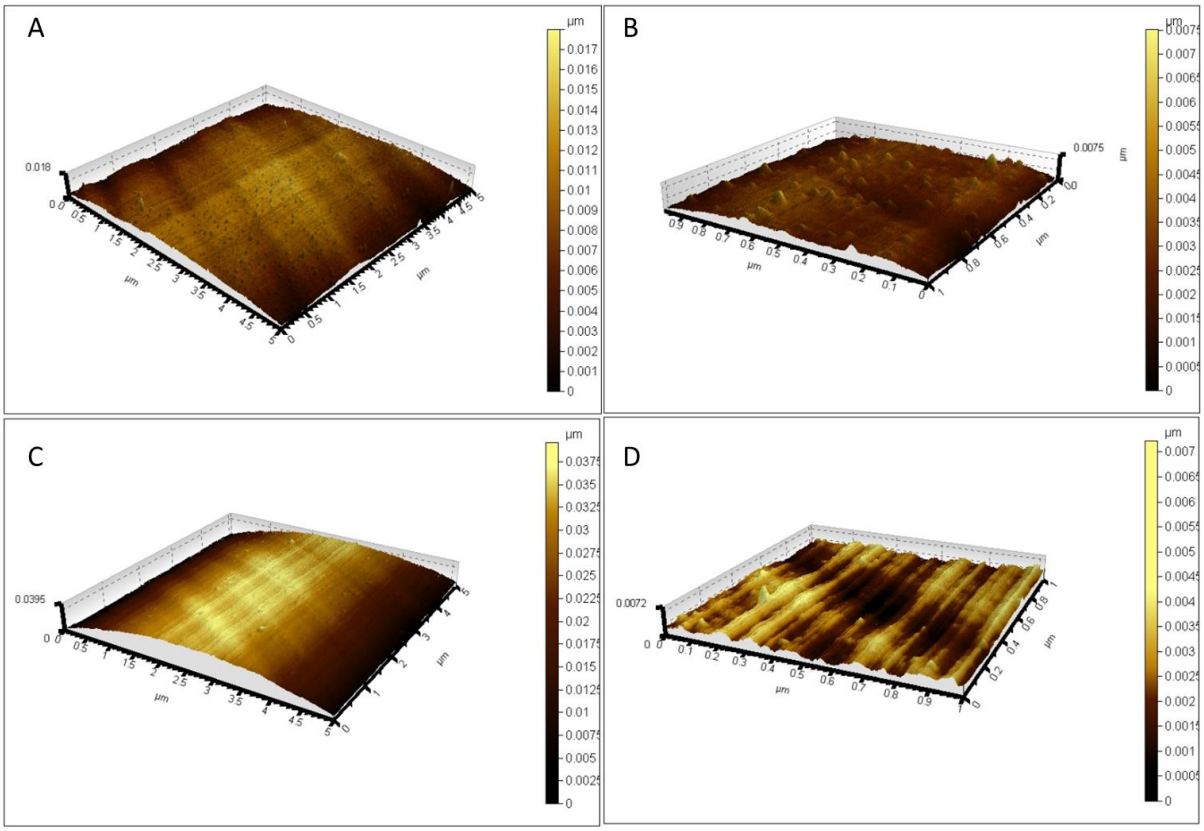

Figure 5.42. AFM images of the 5 mM SAM. A- 5x5 µm 2h, B- 1x1 µm 2h, C- 5x5 µm 18h, D- 1x1 µm.

5.5.4 Initiator on Silicon Nitride in PAO

In Figure 5.43 the final contact angle from 2.5 mM, 18 h is significantly less than can be achieved, however, that obtained in 5 mM solution rivals the maximum contact angle achievable. In this case the maximum contact angle of 82.5° was achieved in 5 mM over 18 h. AFM images, from Figure 5.44, show the silicon nitride displaying partial monolayer growth at all but 5 mM 18 h, however there appear to be very small gaps in the monolayer, possibly due to variation in the silicon nitride deposited layer. The 5 μm^2 images show the variation in coverage much more clearly, with the higher concentration for a longer time resulting in a more uniform monolayer being created. The relative roughness and topography of the other samples indicate that a complete monolayer has not formed. The PAO seems to have had more of an effect on the final contact angle than could be achieved by the initiator on silicon nitride. At 2 h the contact angle of the two concentrations are almost identical and lie between those achieved in toluene.

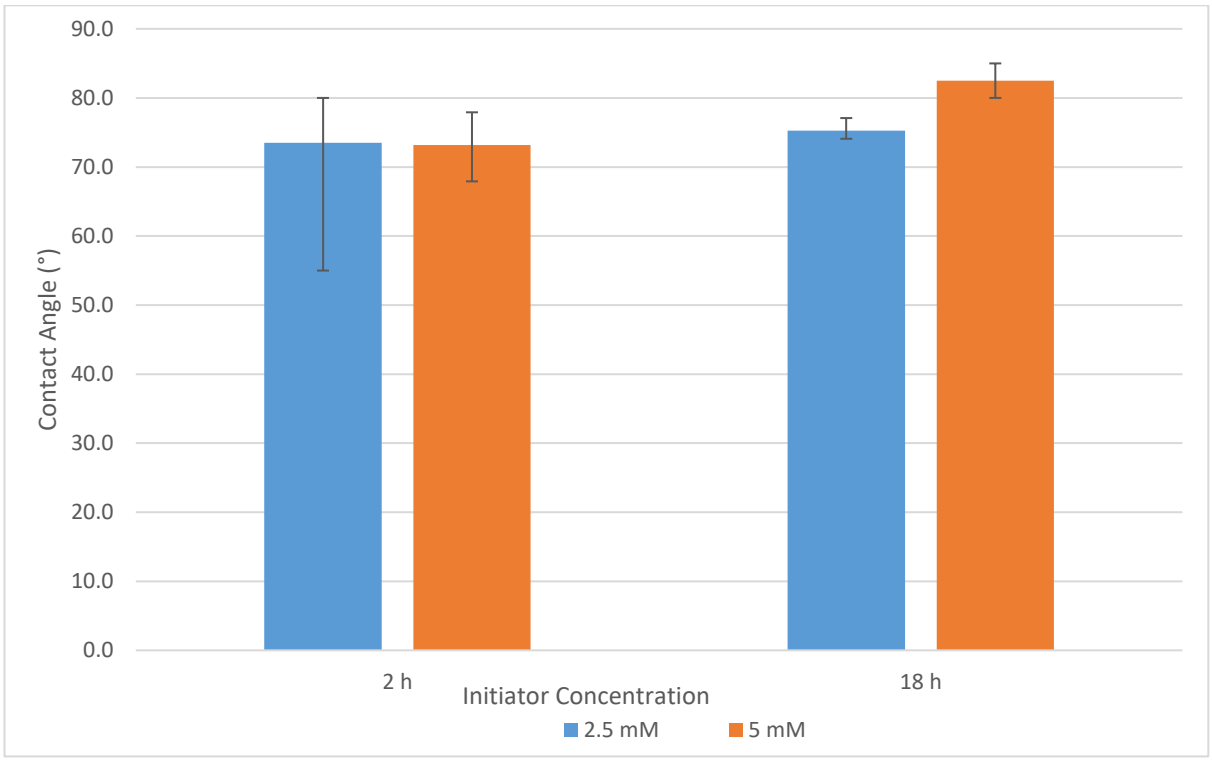

Figure 5.43. The relationship between time and concentration of initiator in PAO on silicon nitride compared to the resultant contact angle.

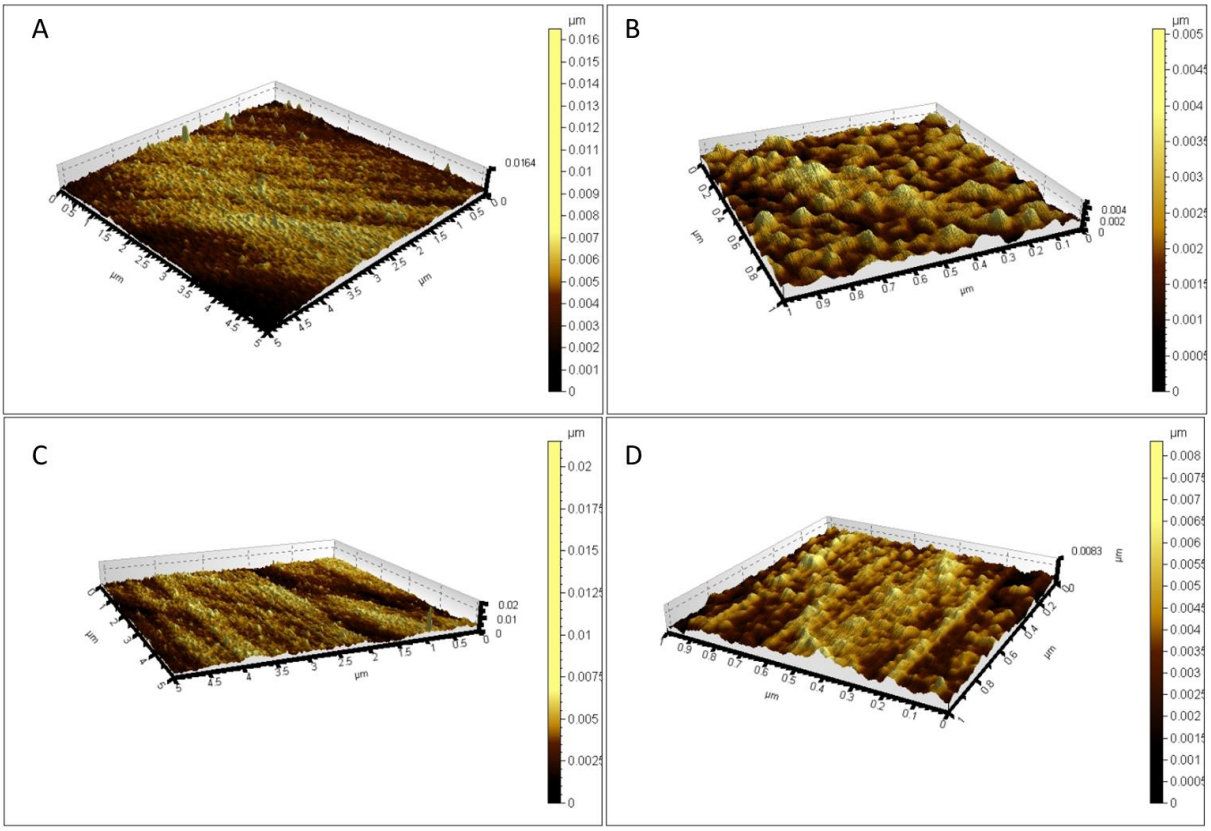

Figure 5.44. AFM images of the 2.55 mM SAM. A- 5x5 µm 2h, B- 1x1 µm 2h, C- 5x5 µm 18h, D- 1x1 µm.

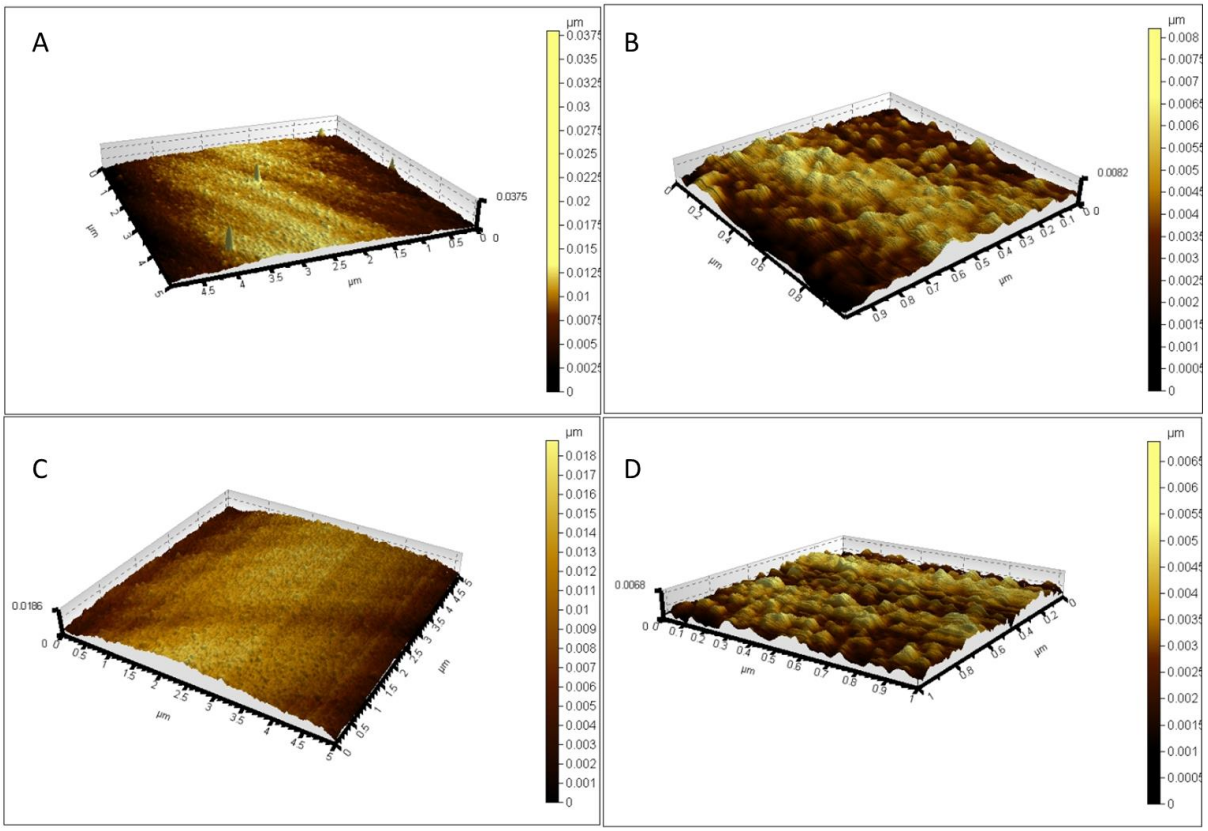

Figure 5.45. AFM images of the 5 mM SAM. A- 5x5 µm 2h, B- 1x1 µm 2h, C- 5x5 µm 18h, D- 1x1 µm.

5.5.5 XPS Analysis

As presented below the ATRP initiator has been assembled onto silicon nitride using both toluene and PAO as solvents. The key indicator of success here is the presence of a bromine peak demonstrating that end group functionality is intact. This is key for the subsequent steps of polymerisation that are dependent on the alkyl halide bond cleavage. Much like OTS there is no chlorine present indicating there has been full bonding to the substrate. As expected the signals from toluene are slightly stronger than that from the PAO which is not surprising due to the preferable solvent selection. Line scans were performed on Br-containing samples so that the X-ray spot did not reside on any area of the sample for more than 2-3 minutes as it was felt the C-Br bond might be fragile. The multi-level linescan data for each element was collapsed and averaged during processing of the XPS data.

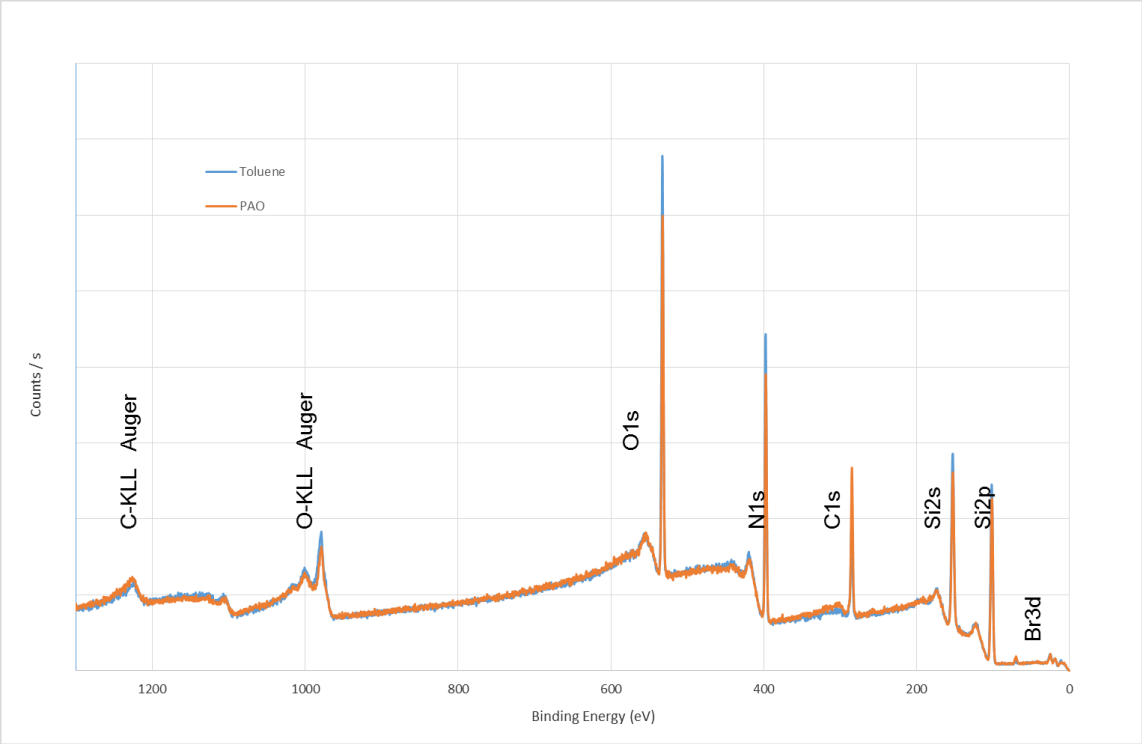

Figure 5.46. Survey spectra of ATRP initiator assembled on silicon nitride in toluene and PAO.

5.5.6 Discussion

The entirety of the contact angle data is presented in Figure 5.47. The trend that is most clear is the effect of solvent on the facilitation of contact angle. This is highlighted in the correlation of concentration of initiator and contact angle. This trend is not visible when the initiator is assembled on silicon nitride. It is also apparent that due to the low reactivity of the initiator the longer self-assembling times are necessary to produce a high quality monolayer. Steric hindrance may also play a part in assembly in addition to the lower reactivity of the single chlorine on the

chlorosilane head group. This leads to the conclusion that 2.5 mM for 18 h is the lowest concentration needed to create a good monolayer in toluene and 5 mM is needed for the PAO.

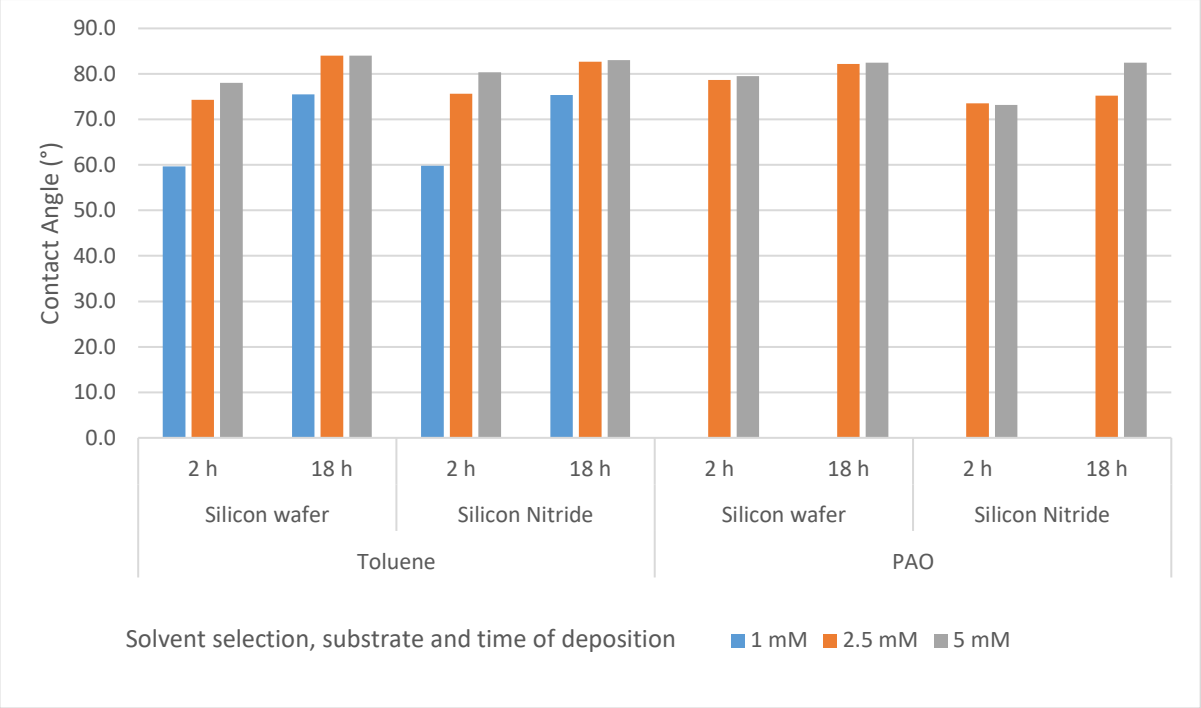

Figure 5.47. Comparison of all contact angle data for the ATRP initiator assemblies.

5.6 Polymerisations

5.6.1 XPS Analysis

The XPS of two thicknesses of polymer grown from silicon nitride is shown in Figure 5.48. As expected silicon, nitrogen, carbon and oxygen are present. Having bromine also present is a good sign as it denotes that the end group of the PMMA polymer is intact as seen in Figure 5.49. This allows further polymer to be grown if desired. Also present are copper and sodium, understandably so as they are used in the polymerisation procedure. A high resolution bromine scan is visible in Figure 5.49.

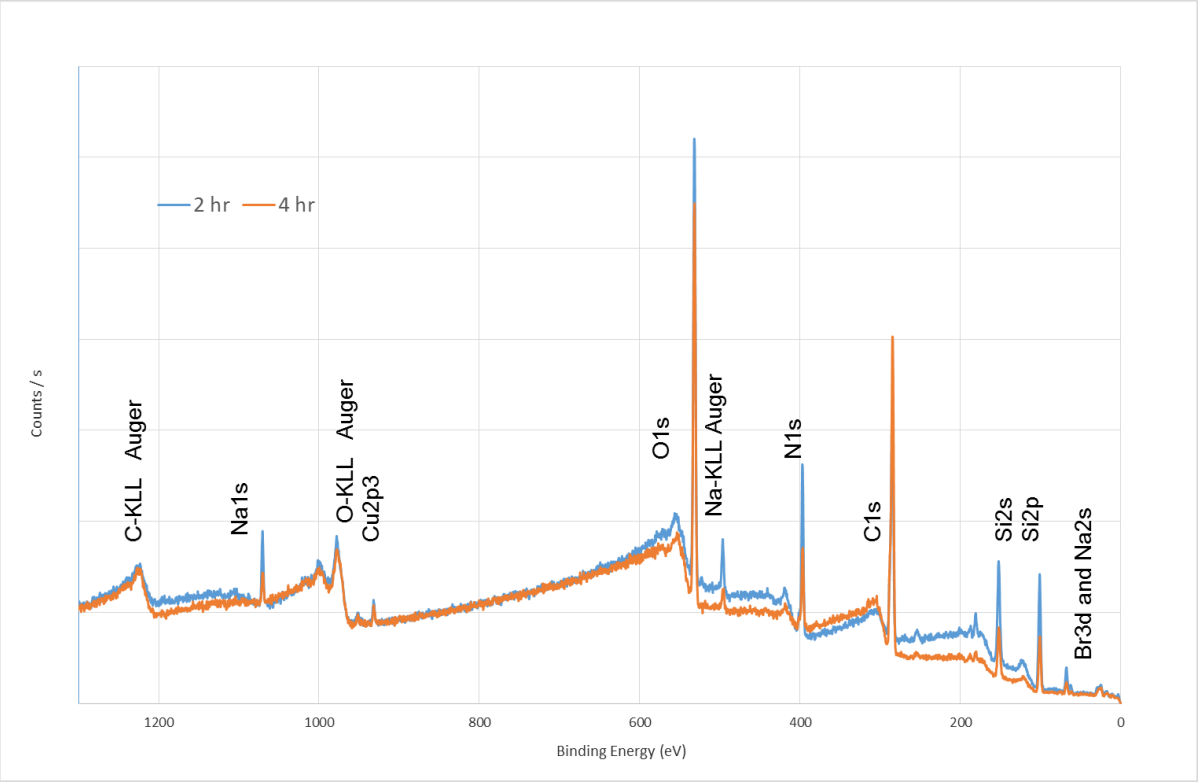

Figure 5.48. Survey spectra of PMMA polymers.

The shape of the C1s peak is used to define the carbon species present. Typically the main peak at 285 eV is due to hydrocarbons, a shoulder (or asymmetry or a distinct peak) at 286.5 eV is from C-O as in alcohols or ethers but is also present for esters such as PMMA. Peaks at 287-288 eV are typically from C=O as in ketones whilst 288-289 eV are carboxylic acids or esters where the carbon has 3 bonds to oxygen as in PMMA.

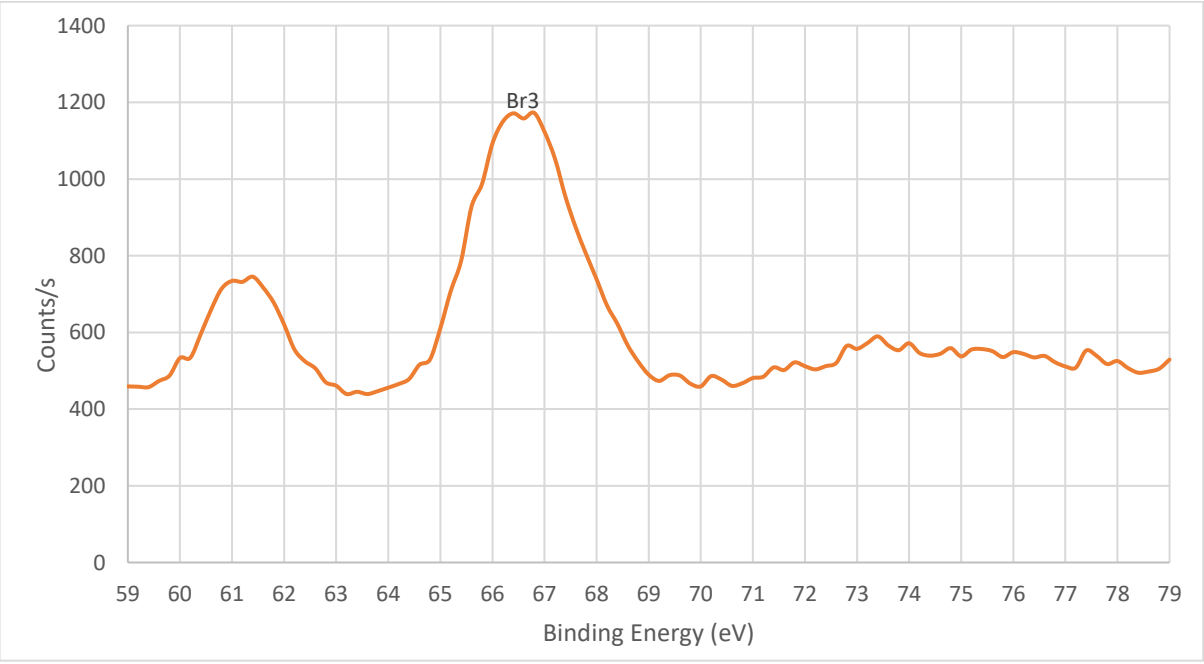

Figure 5.49. High resolution core spectra of bromine from PMMA.

5.6.2 Thickness vs. Time

The PMMA brushes were successfully formed on the silicon wafer by the ARGET ATRP method as proved by the XPS data, and the thickness of all the polymer brushes was measured by a Woolham M-2000 spectroscopic ellipsometer. The data was modelled using a three component model consisting of Si/SiO_2/Cauchy under the assumption that the polymer layer is isotropic and homogenous [123, 351, 352]. Figure 5.50 shows that the thickness of polymer film grows with time as expected, the line of best fit is only present to guide the reader as more data points would be required to prove that it grows in a linear manner. Each data point on this figure was compiled by averaging three points from random areas of the sample.

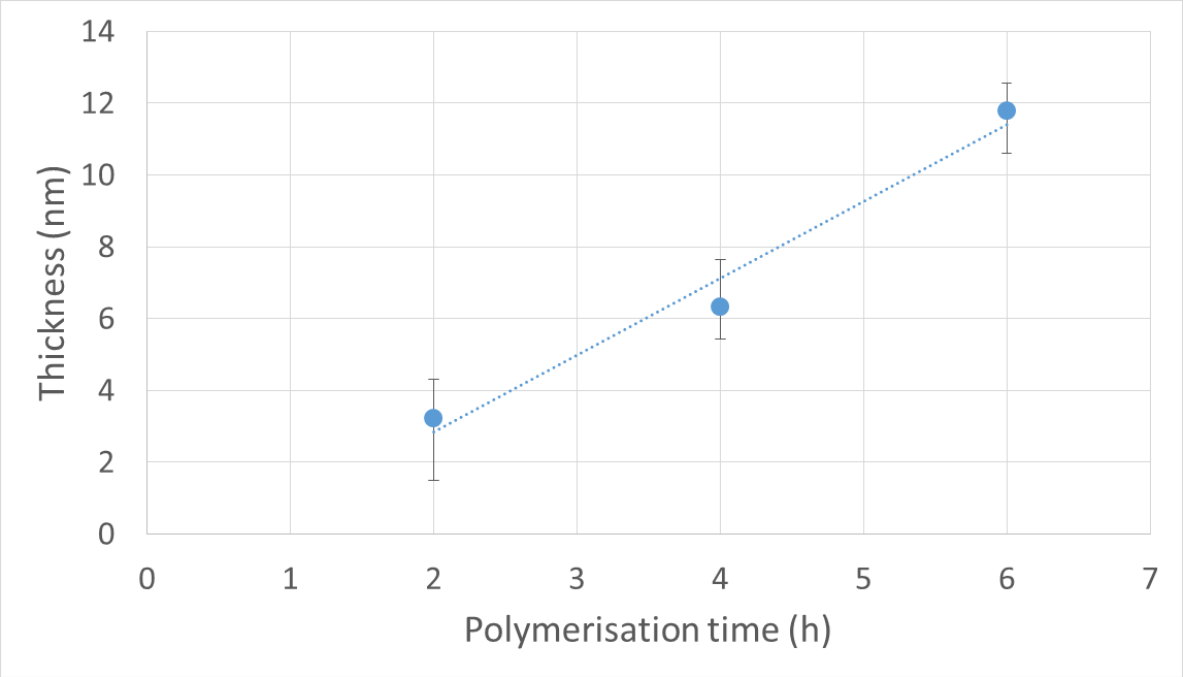

Figure 5.50. SI-ATRP ARGET PMMA film thickness with respect to time.

5.6.3 Nanotribological Performance of Polymer Brush on Silicon Wafer

Nanotribology experiments were conducted on the polymer brush modified silicon wafers using an atomic force microscope (MAC Mode III, 5500 Scanning Probe Microscopy Agilent Technologies, USA). Nanotribological tests were performed under ambient conditions in air. Standard force modulation silicon probes with nominal spring constant of 2 N/m and tip radii of 8 nm − 10 nm were used. Actual spring constant values for every cantilever were obtained using built-in thermal noise method [353]. The determined constants varied between 1.11 N/m and 1.13 N/m. Normal forces were calibrated by measuring the deflection sensitivity (nm/V) from the slope of the linear part of the force−displacement curve obtained. Measurements were taken by increasing the load in known increments across the slow scan axis in which at least 12 lines were attributed to each load step. This was repeated in three separate locations per sample. As can be seen in Figure 5.51 the steps are clear and the relative variation across the surface is shown in an example polymer sample.

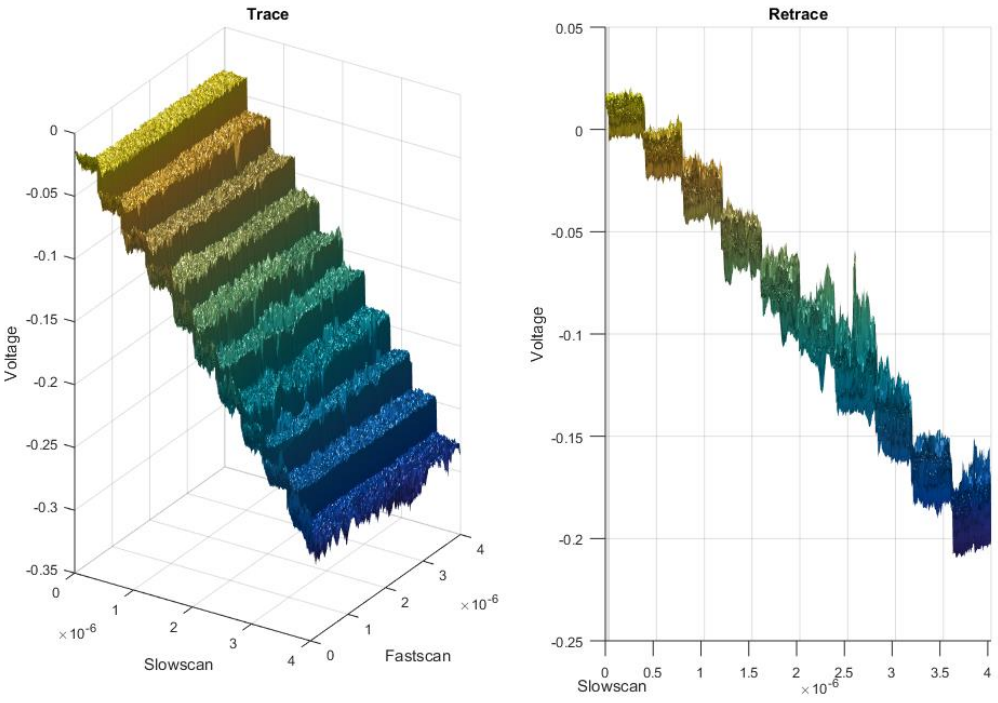

Figure 5.51. Matlab processing of raw LFM data

As seen in Figure 5.52, significant reduction in friction was achieved for all the polymer brush films under a wide range of loads. However, the influence of the polymer thickness is not obvious or unidirectional, i.e. the thicker polymer may not provide a lower friction force. It is surprising that the tribological performance of the thicker polymer brush films at 4 h and 6 h polymerization is not as good as at 2 h polymerization at the nanoscale under higher loads than 20 nN.

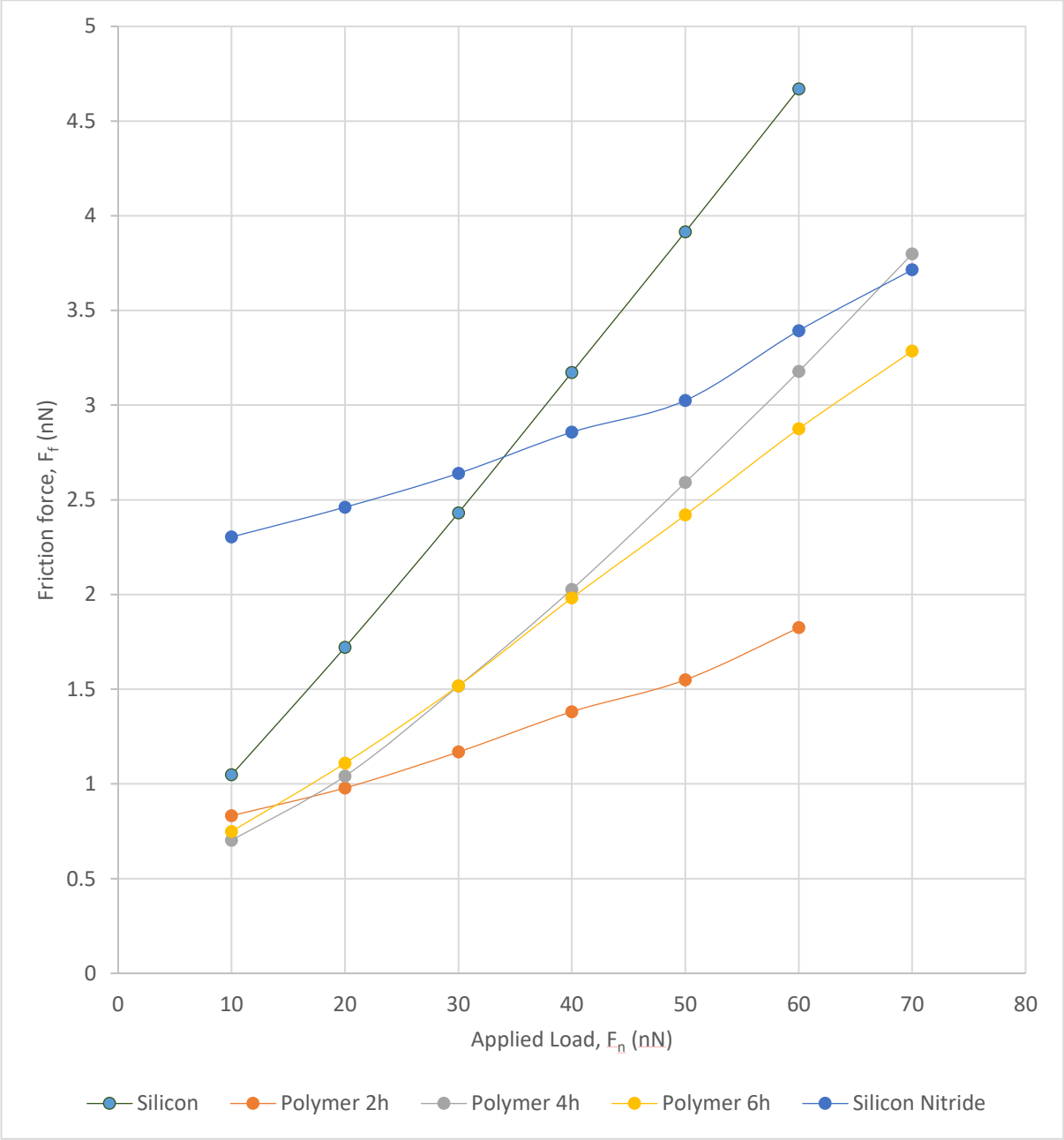

Figure 5.52. Average results of friction force as a function of load for various thicknesses of polymer with respect to silicon.

5.7 Colloidal Probe

5.7.1 Polymerisation of MMA

The initiator functionalised silicon nitride surface was analysed using sessile drop contact angle (CA) measurements to check the coverage and quality of the attached initiator monolayers. The water contact angle results show that the modified surface has an increased contact angle of 83.0 ° ± 3.0 ° compared to 27.2 ° of the bare silicon nitride, which confirms that the surface modification has occurred [354].

The polymerisation was also quantified through the thickness analysis of the polymer films formed at different polymerisation durations using ellipsometry. The thickness of the polymer formed on silicon nitride was measured at three random locations on each sample, and the

average value was plotted against polymerisation time (Figure 5.53). The results show that as the polymerisation time increases, the polymer on the surface is growing thicker.

The molecular weight of the polymers formed at different durations are also plotted on Figure 5.53. It can be seen that the thickness of the dry polymer film on the surface correlates well with the molecular weight of the polymer formed in solution at the same polymerisation time. A 37 nm thick polymer film has been formed in 150 min polymerisation time. The polymer brushes were not analysed with respect to surface morphologies as when they are immersed in a good solvent the measurements would not be relevant as discussed in more detail in 5.7.4. Under these conditions within the lubrication system roughness and morphology are unlikely to play a large role in determining friction [123].

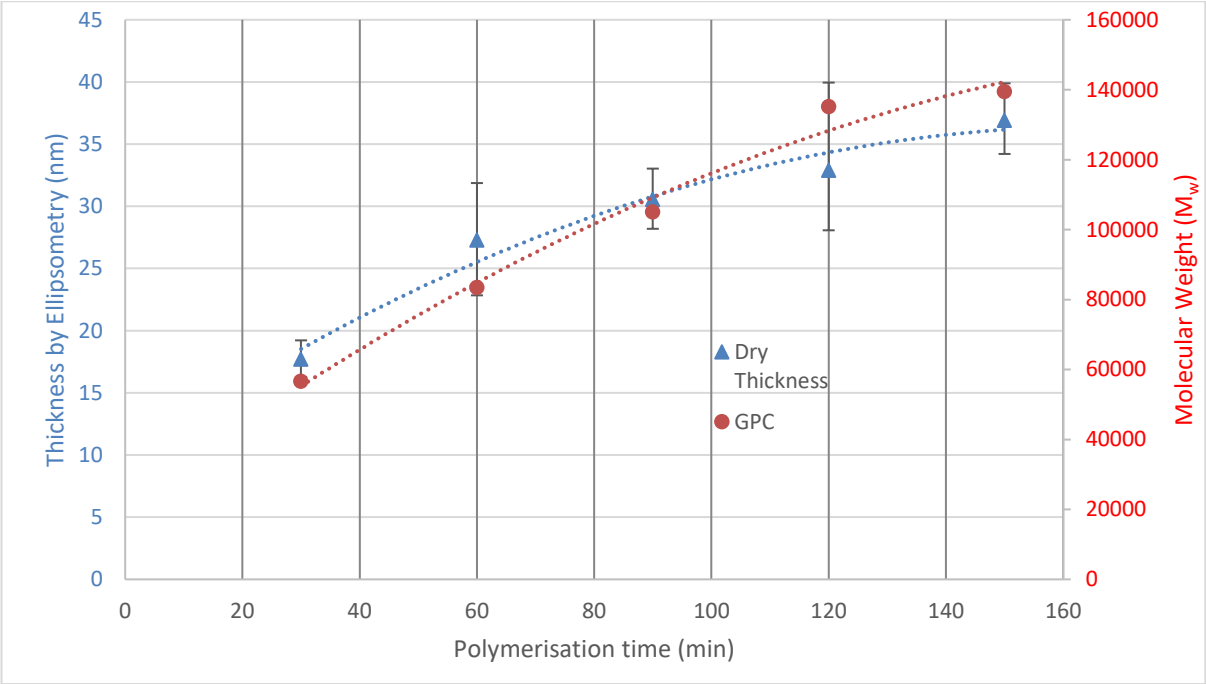

Figure 5.53. Polymer brush thickness, and molecular weight as a function of time.

5.7.2 XPS Spectra

To confirm the initiator bonding and polymer formed on the silicon nitride surface, XPS analysis was conducted on the silicon nitride and silicon nitride surfaces modified with initiator and polymer (see Figure 5.54). Line scans were performed on both initiator and polymer modified surfaces so that the X-ray spot did not reside on any area of the sample for more than 2-3 minutes. The multi-level linescan data for each element was collected and averaged during processing of the XPS data.

Compared to the bare silicon nitride surface, an additional weak peak for Br3d at ca. 68 eV was observed in the spectrum of the initiator modified silica nitride surface, which confirmed the Br-containing initiator was successfully attached onto the silicon nitride surface. In addition, a carbon peak at 285 eV was observed on both bare and initiator modified silicon nitride surfaces due to

adventitious carbon present on all XPS samples. The presence of a bromine peak indicates that the end group functionality of the initiator layer is intact, which is the key for the subsequent steps of polymerisation that are dependent on the alkyl halide bond cleavage (as illustrated in Figure 2.2). The absence of Cl peak is clearly shown in XPS spectrum for the initiator-modified surface, indicating that no chlorine residuals exist in the initiator-modified surface layer and the initiators fully bonded to the substrate through complete hydrolysis of the Si-Cl bond. The survey spectra of a PMMA brush formed on the silicon nitride surface is also shown in Figure 5.54. With respect to the polymer the lack of a Si or N signal indicates the silicon nitride surface was fully covered by a thick polymer film.

High resolution core spectra from PMMA formed on the silicon nitride substrate, as seen in Figure 5.55 and Figure 5.56, show the development of the oxygen and carbon peaks. The shape of the C1s peak is used to define the carbon species present in the surface layer. The carbon spectrum is made up of three distinct peaks, due to the three different bonding environments of the carbon present in the polymer. Typically the main peak of C1s at ca. 285.0 eV is assigned to C-C and C-H bonds in hydrocarbon backbone of PMMA, a shoulder (or asymmetry or a distinct peak) at 286.5 eV is from C-O functional groups as in alcohols, ethers or esters such as in PMMA. The peak at 289.0 eV is assigned to C=O bond in the ester groups of PMMA. The two peaks for O1s in Figure 3.4 indicate two different bonding environments exit for oxygen species, namely C=O and C-O bonds in the ester groups formed within the polymer PMMA on the surface. The ratio of oxygen and carbon in their respective states is expected due to the stoichiometry of PMMA. Both high resolution core spectra of C1s and O1s confirm that the ester groups exist in the polymer structures, and the polymer PMMA was successfully formed onto the surface as shown in Figure 2.2. Core spectra as shown inset in Figure 5.54 show the presence of Br meaning that end group functionality is retained.

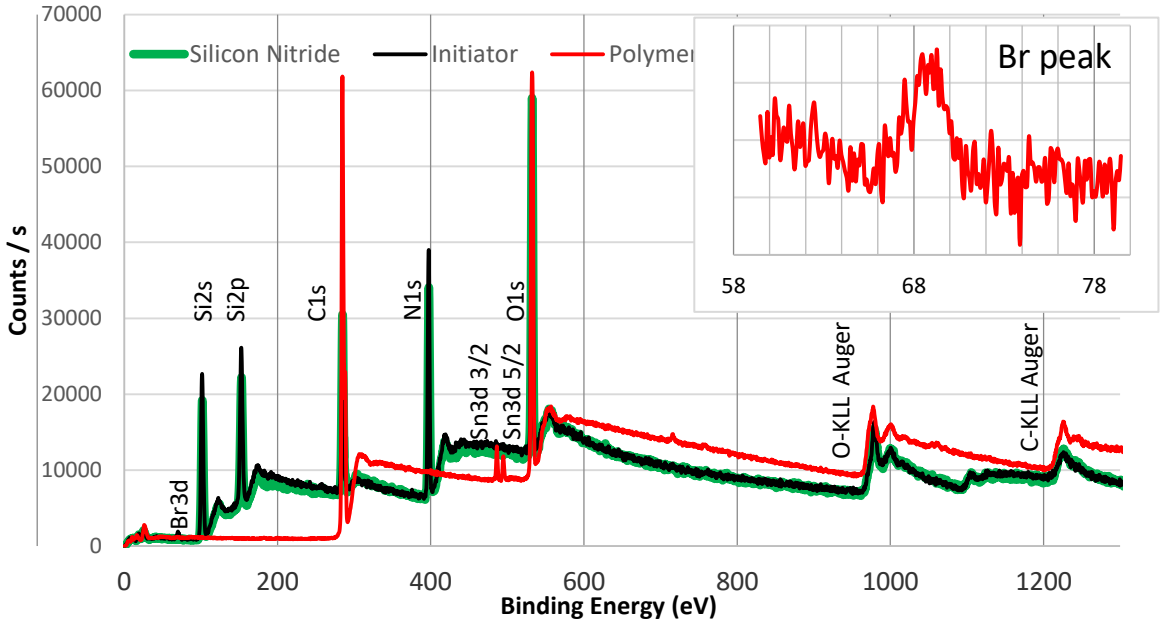

Figure 5.54. Survey scan of PMMA with peaks assigned. The inset shows a zoomed in spectrum of the Br peak present in the polymer.

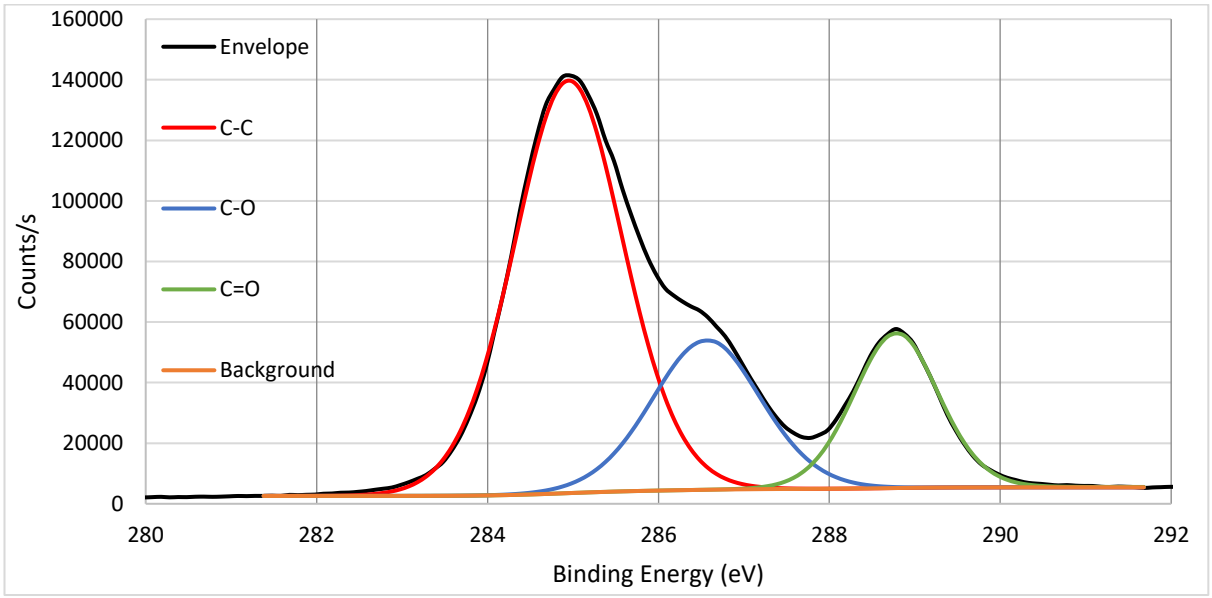

Figure 5.55. High resolution core spectrum of carbon within PMMA with fitted peaks.

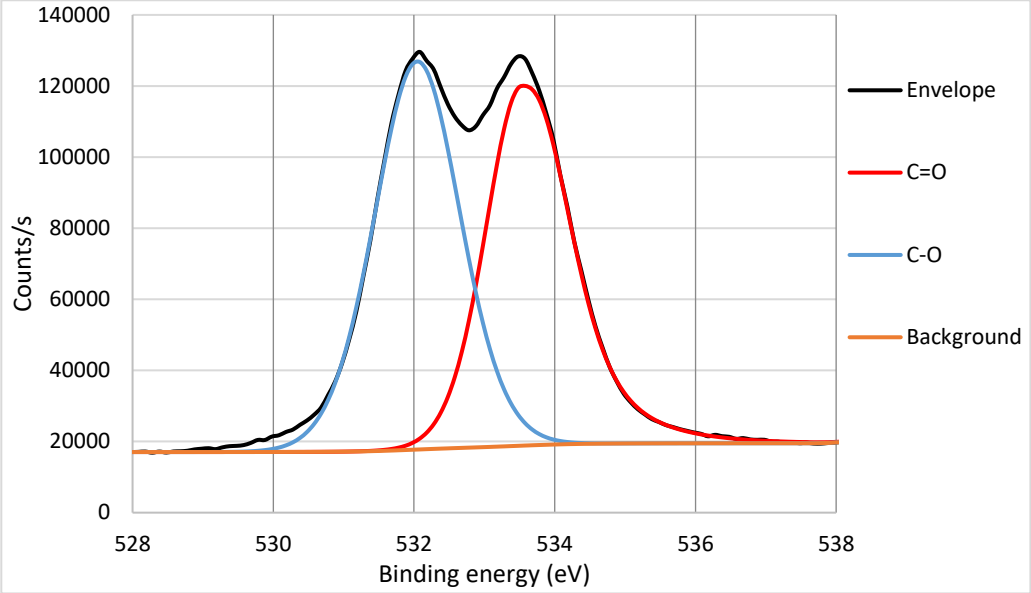

Figure 5.56. High resolution core spectrum of oxygen within PMMA with fitted peaks.

5.7.3 Friction Behaviour of the Polymer Brushes

To explore the lubricating properties of the polymer coatings, the silicon nitride coated silicon wafer as well as polymer brush modified surfaces were tested against a steel colloidal probe using lateral force microscopy under a range of nano-newton loads. The surface was tested under standard laboratory conditions (dry), water and PAO oil lubricated conditions to evaluate its friction behaviour. For each test the stepped friction maps were completed in three different areas then averaged for load.

- *Dry sliding*

Figure 5.57 shows the results of friction force vs. the applied load for the silicon nitride as well as polymer brushes (formed at different polymerization durations) against a steel colloidal probe (6.5 µm diameter) under dry conditions. It is seen that the thinnest polymer (17 nm), formed in 30 minutes, shows much higher friction forces over the whole load range compared with the bare silicon nitride surface, hence does not provide any lubricating effects. The large variations observed for the 17 nm thick polymer brush tests indicate that an unstable film was probably formed on the surface. However the thicker polymer brushes clearly show a significant reduction in friction forces for the applied load up to 150 nN.

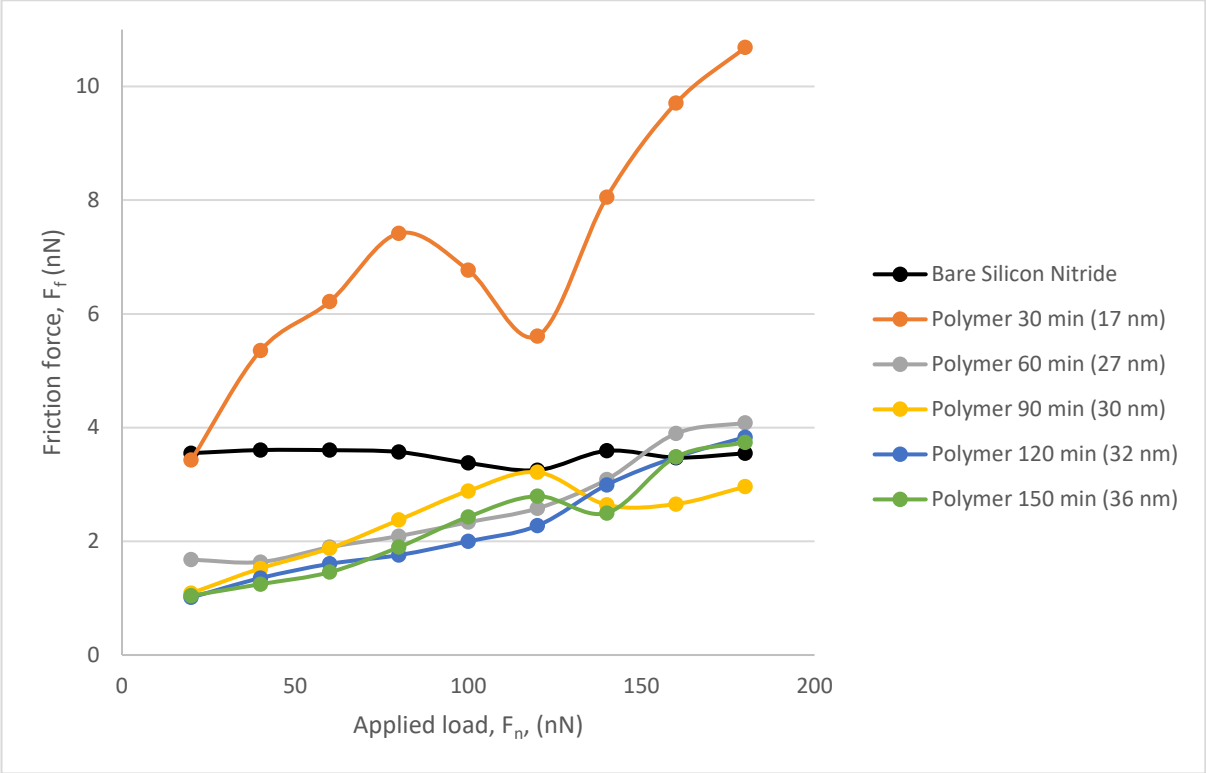

Figure 5.57. Unlubricated polymer friction force, F_F, as a function of load, F_N, measured with CFM.

- *Lubricated sliding*

As aforementioned, one of the key mechanisms by which polymer brushes are thought to lubricate is through swelling effects. To further characterise the polymer-solvent interface, the polymer brushes were tested under both water and PAO lubricated conditions.

The water lubricated test results with a 6.2 µm probe resulted in friction forces are shown in Figure 5.58. It can be seen that all polymer brush modified surfaces show higher friction force compared that of the bare silicon nitride surface in the water-lubricated sliding test. No obvious trend is seen between polymer brush thickness and the resultant friction force.

For bare silicon nitride surfaces, the friction force is much lower under water-lubricated conditions than when dry, which is not true for the polymer brushes. All the polymer-modified surfaces follow a similar trend with a slight increase in friction force occurring at a load of around 100 nN under water lubrication. This is also true for the bare silicon nitride surface, where there is a slight increase in friction force. Silicon nitride also performs much better for lower load than the polymer with no noticeable gradient until a load of 80 nN is reached. Therefore water is not a good solvent for the polymer brushes in the hybrid contact.

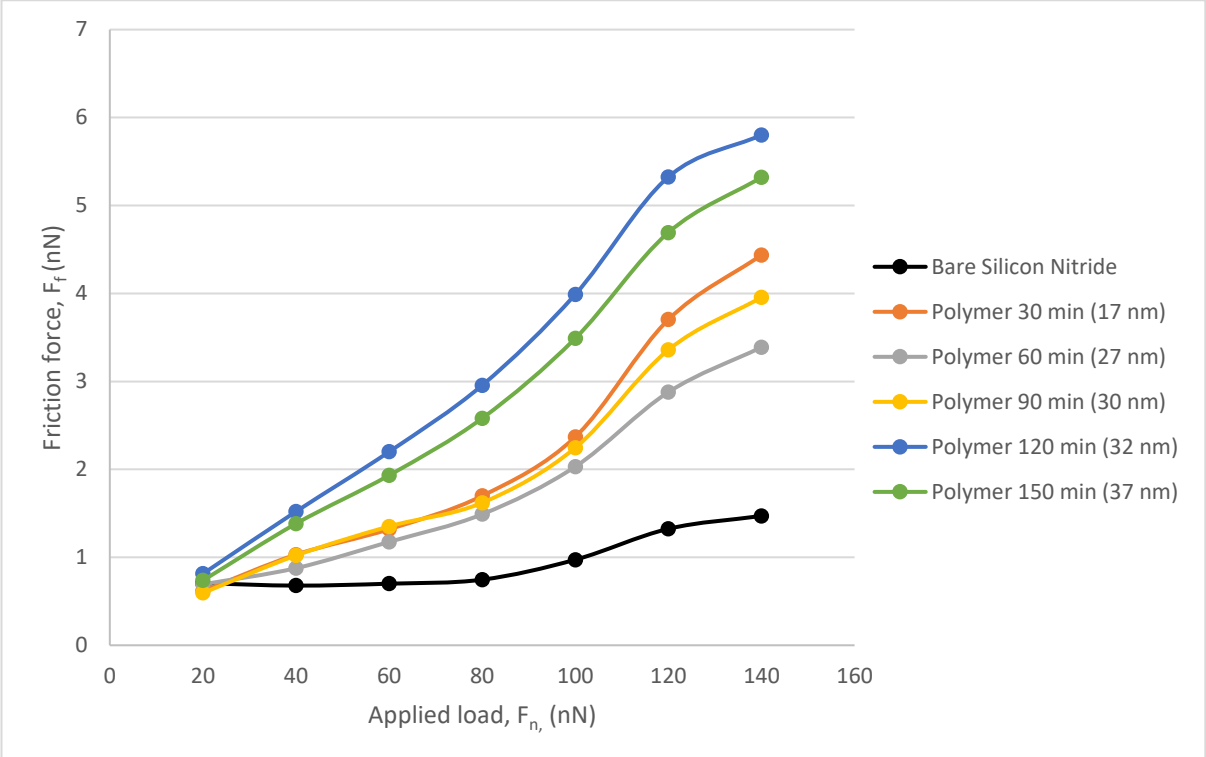

Figure 5.58. Friction force, F_F, as a function of load, F_N, for the polymer lubricated with water, measured with CFM.

Figure 5.59 presents the frictional response of the steel colloid in PAO on bare silicon nitride and on the polymer coated samples. All polymer samples successfully provided a lubricating effect at all loads which resulted in a lower friction force than on bare silicon nitride. The thinnest polymer, although outperforming bare silicon nitride, degraded under load. Although it was subject to degradation, this thickness of polymer still reduced the friction within the hybrid contact. A somewhat similar trend is present when observing the behaviour of the 27 nm polymer. Above a load of 120 nN the lubricating properties of the polymer degrade almost linearly up to the maximum load of 180 nN. At this load the frictional force is indistinguishable from the force experienced with the 17 nm polymer. The resultant three polymers follow a similar trend with a low mean average error (0.188 nN).

Figure 5.60 gives coefficient of friction data. The COF data from the 17 nm polymer shows degradation under load as expected from the frictional force graph. A similar trend can be seen from 27 nm polymer in which the additional load means that at 120 nN the COF rises to just below that of bare silicon nitride. The remaining polymers perform well with COF decreasing with increasing load. The thicker polymers tend to show a much more stable COF result with the lowest COF being recorded at 0.00665.

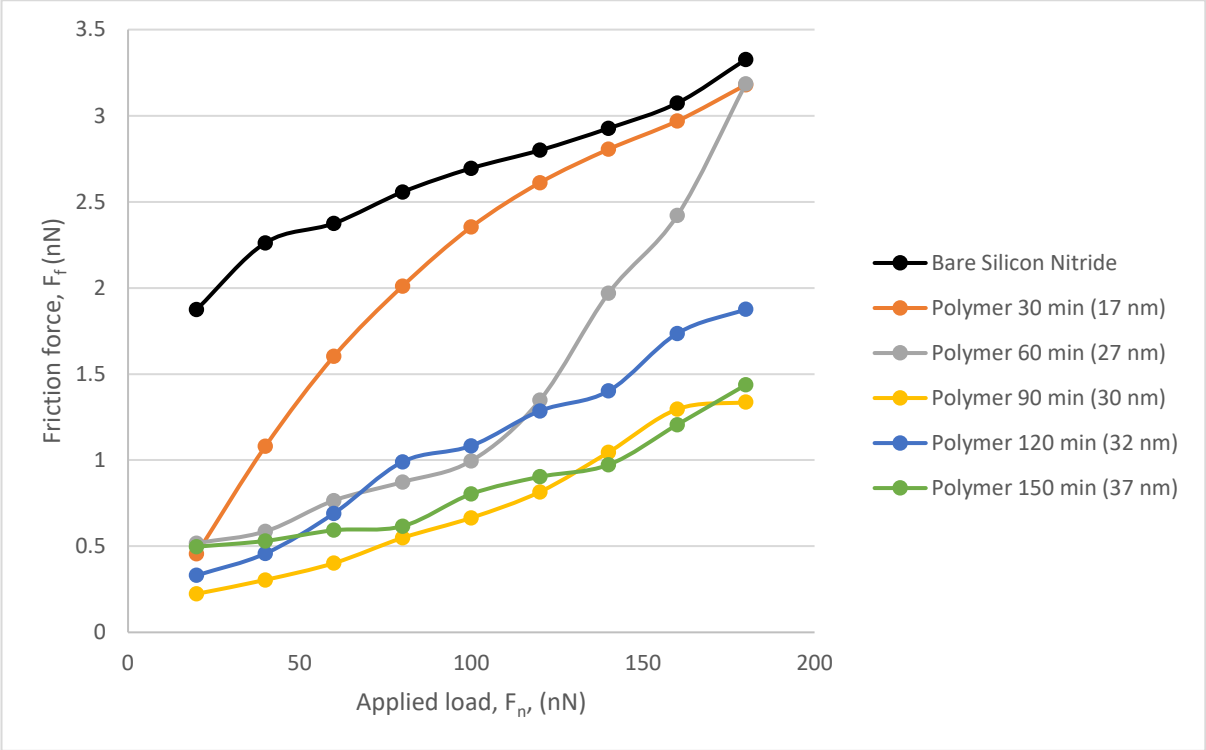

Figure 5.59. Friction force, F_F, as a function of load, F_N, for the polymer lubricated with PAO, measured with CFM.

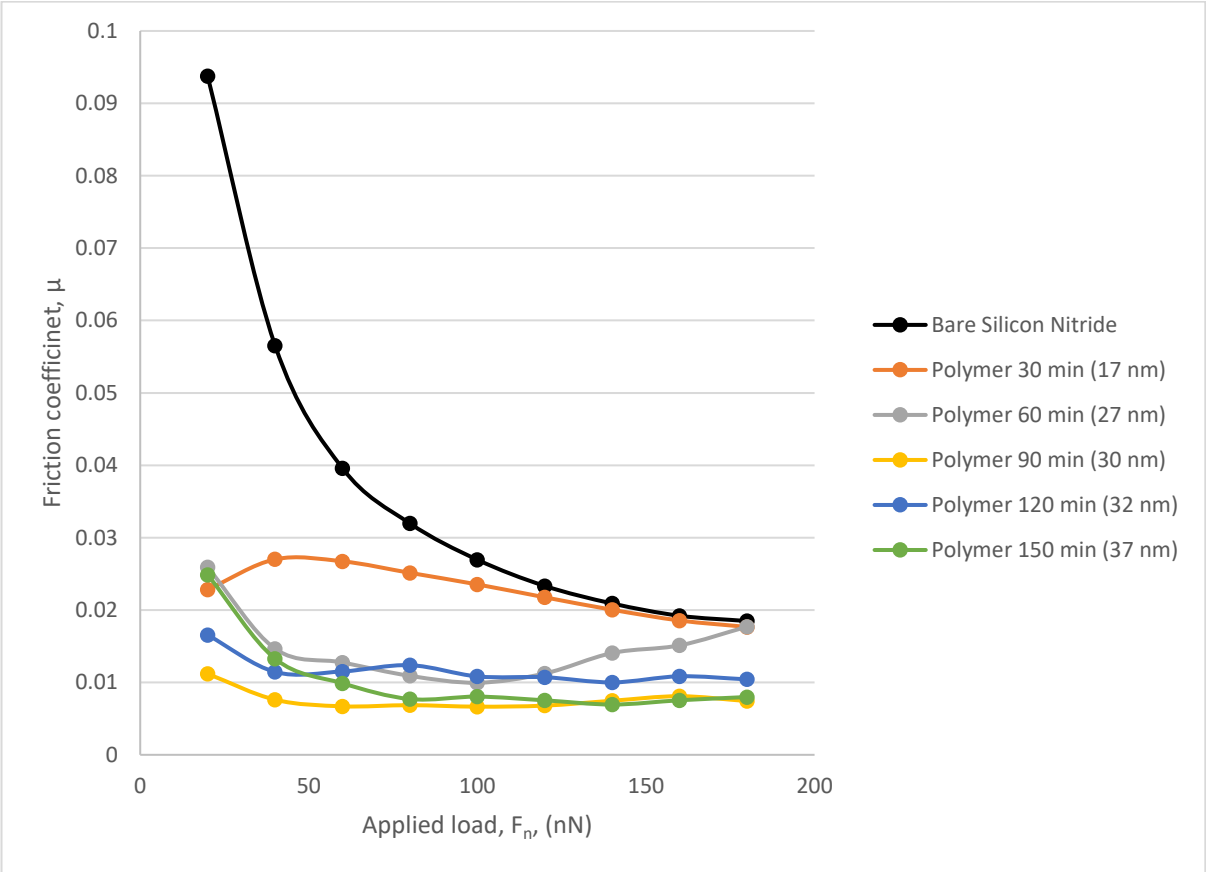

Figure 5.60. Friction coefficient as a function of load, for oil lubricated polymer coatings measured with CFM.

5.7.4 Discussion

- *Surface Preparation and Polymerisation*

The synthesis of methyl methacrylate polymers both in solution and surface initiated has been widely reported in the literature mainly through the use of free radical polymerisation techniques [257]. In this study PMMA has uniquely been grafted from a silicon nitride surface using a process that is commonly performed on silicon wafer substrates. A primary objective of SI-ATRP is for complete initiator coverage onto the silicon nitride surface to facilitate polymerisation. As expected, the initiator monolayer formation took 18 h, which is much longer than other well-known SAMs such as octadecyltrichlorosilane that typically take less than 2 h to form [17]. This is a result of steric hindrance due to the two methyl groups and a larger terminal group on the silane [354]. A maximum contact angle of 83° has been achieved using a 2.5 mM solution of the initiator in toluene over 18 h.

Although high grafting densities are possible for initiators it cannot be assumed that all of these initiator sites will be utilised for SI-ATRP [355]. Based on Equation 5, the molecular weight (M_w) can be estimated from the grafting density (σ), thickness (d, nm), density (p, g/cm^3) and Avogadro's number. It is reported in the literature that grafting densities can approach 1 chain per nm^2 for "grafting from" strategies, PMMA is thought to have a grafting density and density of 0.7 chains/nm^2 and 1.188 g/cm^3 respectively [123, 354].

$$M_w = \frac{dpN_a}{\sigma} \qquad \text{Equation 5}$$

The equation above is often used to estimate molecular weight, however the results should be treated with caution. The theoretical M_w values calculated based on the equation above are shown in Table 5.2. These estimates can then be compared to the GPC measurements. By rearranging equation 4.1 above, theoretical thickness can also be calculated from the molecular weight obtained by GPC.

Table 5.2. Comparing the theoretical values from Equation 5 to recorded data.

THEORETICAL M_W FROM MEASURED THICKNESS		**THEORETICAL THICKNESS FROM MEASURED M_W**	
THICKNESS (NM)	Theoretical M_w	M_w	Theoretical thickness (nm)
17	17374	56608	55.38
27	27594	83439	81.64
30	30660	105034	102.77
32	32704	135140	132.22
37	36792	139477	136.47

The significant discrepancies in either thickness or molecular weights estimated from ellipsometry and GPC approaches may possibly result from the swelling effects of the polymer brushes grafted to the silicon nitride surface. Ellipsometry measures the thickness of the polymer film on a dry surface, in which the polymer is not hydrated and will be in a collapsed state. This is clearly not comparable to GPC for two reasons: on one hand, the polymer is dissolved in the solvent for GPC measurement, thus in hydrated/swollen state; on the other hand, the GPC data is based on free polymer produced in solution where there will be less steric hindrance for the polymer growth. In addition, the actual grafting density may also be different to that reported in the literature. Bielecki et al. also pointed out that under a good solvent poly(dodecyl methacrylate) achieved nine-fold step height changes, well within the limits calculated here [123].

- *Tribological Performance*

The tribological performance of the polymer brushes formed on silicon nitride has been evaluated using a spherical steel colloidal probe under applied loads up to 180 nN during sliding testing. The bare silicon nitride and modified surfaces were tested under dry, water and PAO lubricated conditions.

In the case of dry tests, a small reduction in friction was achieved when the thickness of the polymer brushes was sufficiently high (>17 nm) and under relatively low loads (< 150 nN). Hence the polymer brush has provided a certain level of lubrication to the dry hybrid contact. When the polymer brush layer is very thin, it may be susceptible to the probe gouging through the polymer thus resulting in higher friction. In the case of the dry polymer brush the collapsed polymer brush will be very resistant to the leading edge of the probe resulting in high shear forces as the probe travels through the brushes. When comparing this to the well know low friction hybrid contact the collapsed polymer brush is likely to hinder the friction force recorded. Due to atmospheric humidity, higher adhesion may occur due to the formation of a water meniscus between the contacting surfaces since PMMA is known to be susceptible to moisture [300].

Under the PAO oil lubricated conditions, the polymer brushes formed on silicon nitride significantly reduced the friction of the hybrid contact, and generally the thicker the polymer brush, the lower the friction force observed. A maximum reduction of <2 nN in F_f was obtained with the polymer brushes 30 nm thick. The swelling of PMMA brushes in PAO is key to the lubricious qualities of the polymer film. The ability of this synergistic solvent allows the polymer brush to fulfil the aforementioned criteria of polymer brush lubrication. The variation of thickness and the resultant friction force shows a trend that is somewhat similar to that previously reported, in which the strong resistance of compression at higher loads is dealt with more successfully with longer brush length [272]. The higher loads applied during lateral force microscopy on thicker, longer chain polymers result in a lower friction characteristic, considered

to be an effect of grafting density and reduced interaction with the probe through repulsive forces, in agreement with Casoli et al [356]. The long chain polymer brush is thought to act more like a solid which requires a higher external pressure to impart movement in the brush system. This is due to the repulsion of brush-brush interaction within the system which gives rise to entropic stabilisation. Also key to the low friction force is the grafting density of the polymer brush, as has been shown by multiple researchers comparing spin-coated or adsorbed PMMA samples and the corresponding tribological results [272, 291]. Yamamoto et al. also concludes that a higher density of PMMA results in a higher repulsive ability in addition to more resistance to compression [227].

However, the friction of the polymer brush modified hybrid contact was increased when lubricated by water for all the polymer brush thicknesses even under the lowest load of 20 nN. As discussed above, the performance of polymer brushes relies on the swelling effects when a solvent is involved. Since PMMA is insoluble in water, the polymer brushes will be collapsed when the contact is lubricated by water thus not providing any repulsion of the probe or lubrication effect. This may give some understanding to the frictional response, it is likely that the stretched out brush conformation is not present resulting in a poor frictional response. The relative success of the bare silicon nitride contact may be due to the hydrated silicon layer offering a lubricating effect [357]. Sakata et al. also suggested that in a poor solvent, PMMA brushes may preferentially interact with stainless steel probes resulting in a relatively high friction force [291]. No clear relationship between the thickness and F_f was found in water lubricated PMMA brushes.

5.8 Macroscale Polymer Brush Synthesis

5.8.1 Polymerisation of MMA

One silicon nitride disc with polymer grafted was produced, and confirmation that a modification had taken place was first given by CA analysis in which a value of 76.5 ° ± 3.0 ° was recorded in comparison to the bare surface at 69.2 ° ± 3.0 °. This increase is marginal but was generated by numerous data points across the disc to ensure a representative sample had been taken. This is considerably lower than the value of PMMA on the small scale tests. This confirms that a degree of surface modification has been achieved, a lower CA is likely due to a lower quality PMMA film. An aliquot of the polymerisation solution was taken for GPC analysis and resulted in an M_w of 65980, when using the polynomial generated by the trend line of the LFM samples an estimate of thickness can be found. The value of 21.05 nm is based on Figure 5.53. For reasons discussed earlier the roughness of the polymerised substrate was not measured as under swelling effects the data would not be relevant.

5.8.2 Tribological performance

To explore the lubricating properties of the polymer coatings, the bare silicon nitride disc as well as polymer brush modified surfaces were tested against a steel pin under a range of newton loads. The contact was tested under PAO oil lubricated conditions to evaluate its friction behaviour. Each load step was performed in a new area. For the bare silicon nitride the test was stopped when a stable friction value was obtained. This was the same for the modified disc, except in the clear case of 100 N where the test was stopped after a jump in friction that did not settle to the same values as before. A basic schematic of the tribometer is available in 4.2.10.

- *Unmodified Sliding*

Figure 5.61 shows the resultant friction force at various loads over time within the lubricated hybrid contact. As expected it is clear that with larger normal load the resulting friction force increases, it can also be seen that there is a friction spike during first contact. The disk started without the pin being in contact with it, then was gently lowered into place, therefore this is most likely due to the first contact from the arm that the pin is attached to with the sensor before settling. The trace for 100 N shows a change in resultant friction force before levelling off whilst all other loads stabilise quickly with no further change. Table 5.3 shows the average of the flat part of the friction trace. Also in this table is the contact pressure calculated from the Young's modulus (steel: 200, silicon nitride: 231) and Poisson's ratio (steel: 0.275, silicon nitride: 0.255) [358, 359]. These measurements are provided as a guide only, as they are based on a perfect hemispherical cap and the rollers in this case are rounded which offers no constant geometry. The roughness of the bare disc will affect the friction traces from POD. For this reason the bare disc roughness was measured by a Talysurf profilometer resulting in an average Ra of 0.0678.

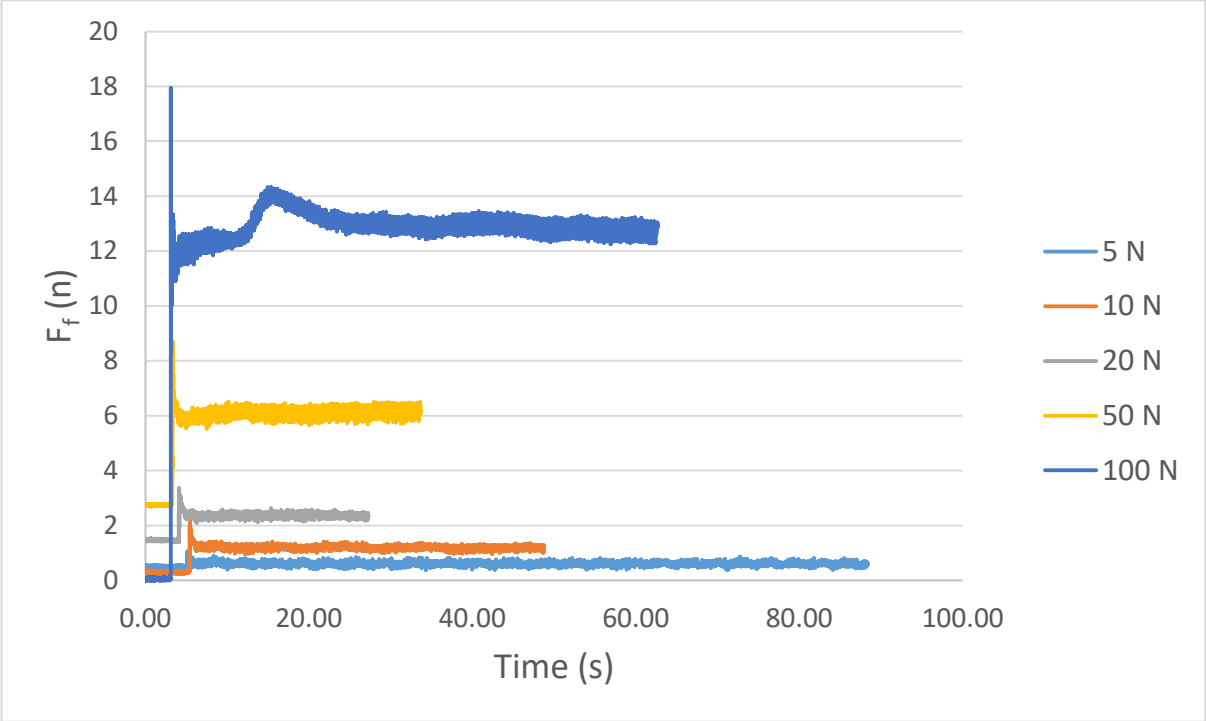

Figure 5.61. Friction traces from bare silicon nitride pin-on-disc experiments over time where F_f is the resultant friction force.

Table 5.3. Averages of the flat portion of the friction trace relative to load.

Load (N)	Average friction force (N)	Contact pressure (GPa)
5	0.604	1.48
10	1.190	1.86
20	2.372	2.34
50	6.090	3.18
100	12.855	4.01

- *Lubricated Sliding*

Figure 5.62 shows the relationship between friction force and load over time with respect to PMMA modified silicon nitride discs running in a lubricated environment. It is thought that the spikes in friction occur for the same reason as before and it can be seen that immediately after contact with the sensor the trace flattens out. When comparing the shape of the traces it is clear that the PMMA modified disc has much more noise within the trace resulting in a larger range of values even though the resultant friction values are lower as can be seen in Table 5.4 and graphically in Figure 5.63. From the 100 N trace there is a rise which then levels off to a comparable value to that of the bare silicon nitride. The calculated COF of the lubricated PMMA hybrid contact is 0.104.

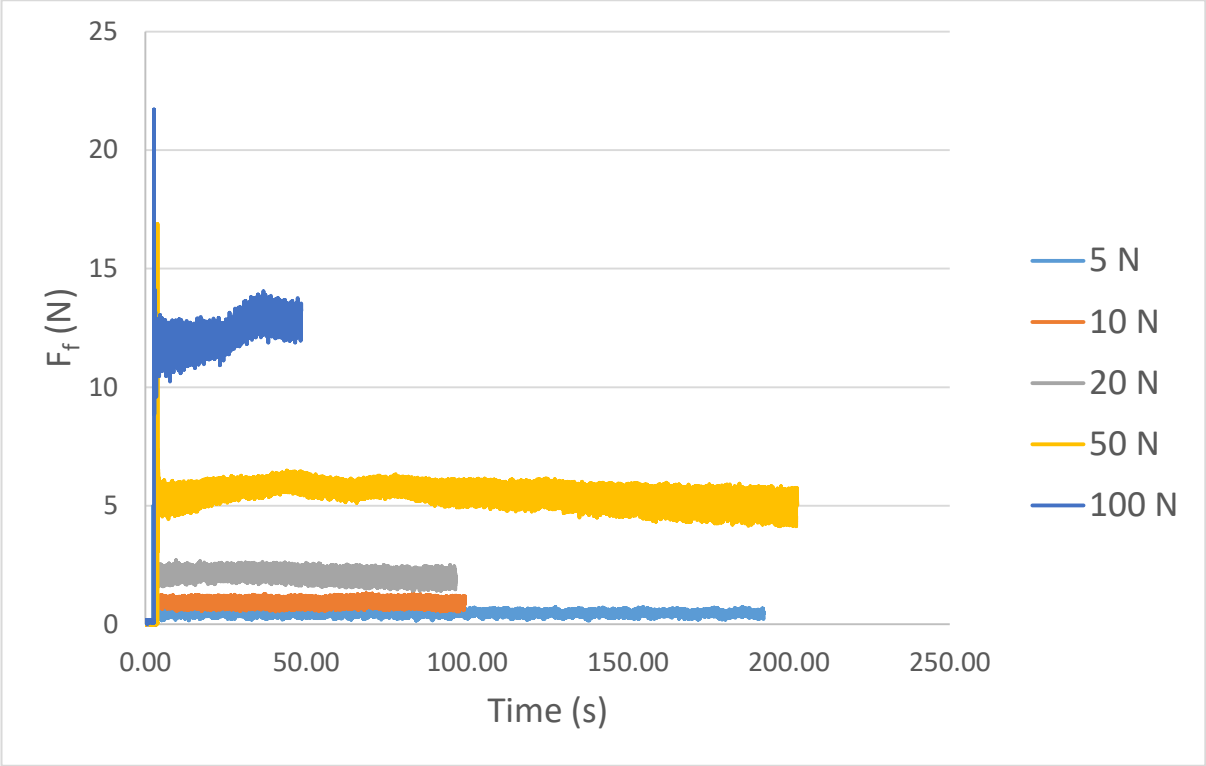

Figure 5.62. Friction traces from a PMMA modified silicon nitride pin-on-disc experiments over time where F_f is the resultant friction force.

*Table 5.4 Averages of the flat portion of the friction trace relative to load with bare silicon nitride as a reference. *Indicates that this average is taken before the failure of the brush.*

	Average friction force (N)	
Load (N)	Bare silicon nitride	PMMA modification
5	0.604	0.476
10	1.190	0.923
20	2.372	2.025
50	6.090	4.986
100	12.855	11.929*

The graph in Figure 5.63 was created by averaging the flat part of all the graphs in order to compare the data. In the case of the modified disc the data presented here is based on data before the failure of the brush system. There is a trend that the PMMA modified silicon nitride discs have reduced the friction force at all loads. As can be seen from the table below the COF has been calculated and shows a little over 15% reduction in friction.

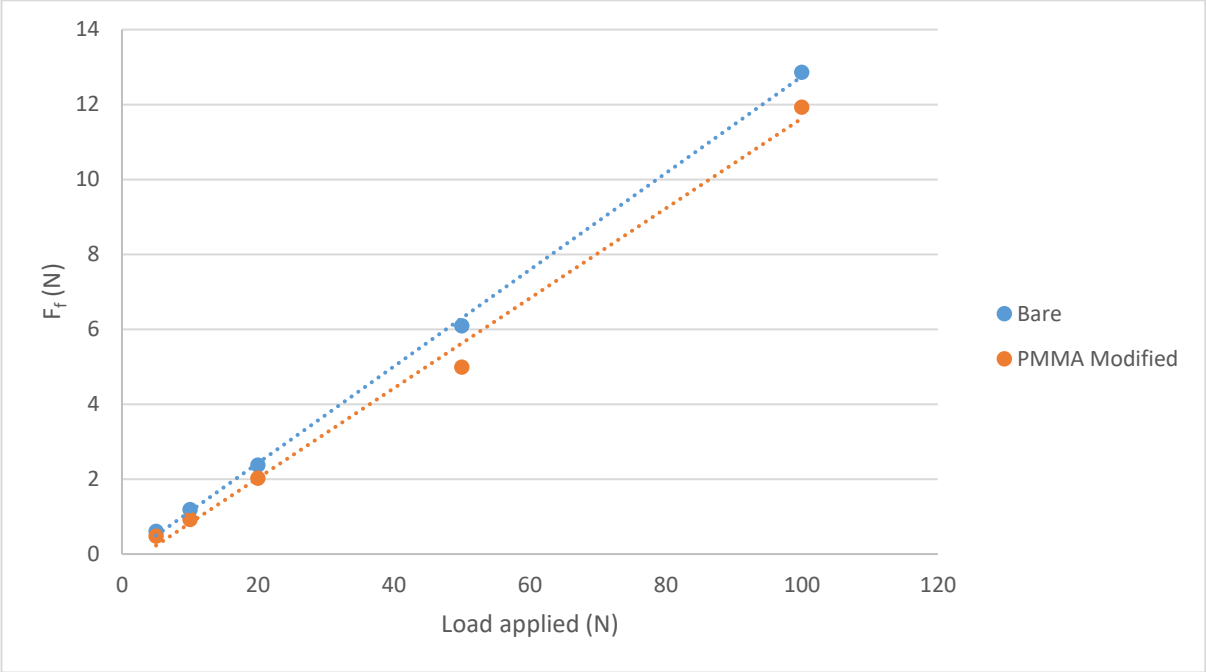

Figure 5.63. F_f of modified and bare silicon nitride discs with respect to load

.

5.8.3 Discussion

The formation of the initiator was expected to follow a similar trend with regards to time as on the smaller scale and was therefore left to assemble for 18 h owing to the aforementioned steric hindrance issues. When confirming the polymerisation by contact angle a value of 76.5 ° was measured, this is considerably lower than the maximum of 83 ° recorded in the best case scenario. There are numerous reasons why this may be the case, the fact that the disc was only cleaned ultrasonically and was not exposed to plasma will be a major contribution to a lower angle as has been shown previously in this work. In addition the ultra-flat surface provided by the silicon nitride wafers will certainly help the grafting density which is known to affect the final brush system formed. The GPC data shows a M_w of 65980 and from previous work this can be estimated to be around 21 nm thickness. From the rearrangement of Equation 5 the thickness can be calculated as well. This calculation gives a thickness of 64.56 nm but the previous discussions that can be found in section 5.7.4 indicate that this data must be treated with caution.

Bare silicon nitride and PMMA modified silicon nitride have been evaluated using a pin-on-disc tribometer under lubricated conditions with loads up to 100 N. With the tests that have been done the polymer layer performed very well with regards to friction force. Where it is clear that there was a failure within the system is at 100 N where the polymer failed after a relatively short amount of time and this is clear in the friction trace where there is a rise. The friction force that the trace rose to matches that of the bare silicon nitride. The contact angle data indicates that the best possible polymer brush system has not been formed and therefore this may lead to some localised patches providing more lubrication effects than that of others resulting in the larger

range of values. However the polymer brush system has significantly reduced the friction force observed in the hybrid contact, over 22% in the case of 10 N load. When comparing the resultant drop in COF there is a 15% reduction by modifying the silicon nitride with PMMA. Of course, as proved previously, the swelling effects of testing in lubricated conditions are key to the polymer brush creating and sustaining a friction reducing environment. There is a possibility that due to poor quality of the polymer brush the film failed during the 100 N test. It is possible that if the grafting density of the brushes was higher that this would have a positive knock-on effect with regards to the entropic stabilisation of the system and would therefore require a higher external pressure to impart the movement within the brush system [272].

Conclusions

This study focussed on the tribological properties of PMMA polymer brushes within the silicon nitride-steel hybrid contact and the potential for large scale applications whilst also removing potentially harmful elements such as sulphur and phosphorus. Polymer brushes have previously been utilised in numerous applications, including some in the field of tribology, but never before has the hybrid contact been investigated.

To address this, polymer brushes, synthesized through a robust method of ARGET ATRP, have been grown in a controlled manner on silicon nitride. The physical, chemical and tribological properties of the PMMA brush were investigated using a wide range of analytical techniques, notably novel interactions with a steel colloidal AFM cantilever but also by ellipsometry, XPS, CA, pin-on-disc and GPC. From the literature as well as in this study the influence of several factors such as AFM cantilever tip shape, SAM performance, polymerisation time, ARGET compound, thickness and synergetic lubricant were found to be key factors affecting the tribological performance of this brush technology.

This is the first study to investigate the ability of polymer brushes to lubricate the silicon nitride-steel hybrid contact on both the nanoscale using state of the art custom cantilevers as well as on the macroscale proving the ability of ATRP to be utilised to functionalise large scale surfaces in a facile and cost effective manner.

Key cleaning regime/ SAM initiation

The polymer brushes investigated in this study depend on the self-assembled monolayers which chemically attach them to the contact surface, allowing better stability for the polymer as well as denser packed brush formation. These initiating SAMs have the benefit of short chain length and occupy a low spatial area allowing dense monolayers to be formed. The key behaviour of the SAM is the ability to react with the substrate of interest and generate an initiating layer. This is all dependant on the binding surface and the quality of this is therefore highly important. This work confirms the literature findings where solvent cleaning, plasma cleaning and careful drying steps are shown to be key for producing good quality initiation sites. Although initiators have been formed in ideal solvents such as toluene, using PAO oils has not been attempted before and this study demonstrates that low concentration solutions can successfully create films. However, higher concentration is preferential as are longer assembly times as they give better results. CA data as well as AFM indicates that an incomplete monolayer is produced if the reaction time is too short. XPS analysis found no evidence of chlorine remaining on the surface indicating that full

hydrolysis of the initiator has occurred at all concentrations whilst AFM shows there were no agglomerations visible.

Probe selection

Lateral force microscopy with sharp tip probes showed that PMMA exhibited interesting characteristics where thinner polymer layers resulted in lower friction force readings. This study theorised that probe penetration within the individual polymer chains resulted in additional friction forces. This is likely to be due to the gouging effect that the sharp tip will have on the polymer, also resulting in excessive wear to the polymer. By the application of a thin layer of polymer the separation of the contact by a small lubricious layer was successful. To avoid this gouging effect and to successfully characterise the mechanical properties of the PMMA brush without penetration of the brush a novel colloidal steel probe was produced. This allowed a distribution of load across the contact surface giving a much clearer understanding of the properties. By customising the colloidal probe to be made of steel a replicate of the hybrid contact can be scaled to the nanoscale. This allows direct comparison of the bare contact and the PMMA layer interacting with the steel.

Lubricant selection

By carefully matching the polymer to the lubricant, such as the combination PAO and PMMA, the lubricious properties of both are synergistically enhanced. The use of a good solvent results in solvated polymer brushes that are able to withstand high pressures because this interaction lowers entropy between adjacent polymer chains within the brush system so that they resist compression and ultimately reduce friction force.

Thickness of the brushes

The mechanical properties of the polymer brush layer were investigated through AFM and POD revealing the relationship between the thickness of brush and good lubricious qualities. Thicker polymer brush results in lower friction as clearly presented in this work, the main characteristic being their ability to compress to a higher degree. Longer brushes are able to undergo more transitions, driven by entropy and enthalpy, to resist movement and shear forces from the counter surface. Synergy between thickness and brush-lubricant allows a higher concentration of lubricant to be kept in the contact.

- Nanotribology

Experiments using colloidal force microscopy show that PMMA brushes can successfully reduce friction within the silicon nitride-steel hybrid contact. Through controlled polymerisations using ARGET ATRP the brushes were grown on the silicon nitride in an even manner, as shown by AFM, which contributed to the overall decrease in friction force. During the nanotribological testing it was shown that in lubricated conditions with a PAO oil a maximum reduction of over 2 nN Ff (approx. 25%) can be obtained. Using a poor lubricant such as water was detrimental to the friction force results even when compared to the bare silicon nitride/steel hybrid contact.

- Macrotribology

Scaling experiments explored PMMA growth on a larger area. This was performed successfully and allowed pin-on-disc testing to occur. Successful application of polymer brushes to macroscale objects and the use of an appropriate lubricant in the hybrid contact was able to reduce the COF over 16%. These results show that the application of surface initiated PMMA polymer brushes could be a successful solution to the challenging problem of lubricating hybrid contacts in oil lubricated conditions.

In conclusion, the polymer brush system that has been synthesised on silicon nitride has proven to be able to reduce the friction force under lubricated nanotribological interactions with a steel AFM probe as well as in testing on the macroscale. The process that has been described here allows the formation of high quality polymer brush systems capable of reducing COF, however, this technique is not just reliant on the polymerisation procedure. The self-assembly of monolayers is also a key step in the functionalisation of friction reducing polymers.

Future Work

Further Pin-on-disc Testing

Improving the grafting density would be one of the first steps that would be taken, this may allow the load carrying capacity to exceed the limitations of 100 N in the current work. In addition there is a clear need to experiment with different thicknesses of polymer to elute the most effective thickness. This can be facilitated by extended polymerisation times or by using the terminal bromine group and restarting the polymerisation procedure by injecting new ARGET chemicals after thickness testing.

Although it has been proven that the polymerisation can occur in anisole which is known to be a preferential solvent for this reaction, in-situ polymerisations should be conducted in unideal solvents such as PAO.

If successful steps will be taken to improve the lubrication solution by changing elements of the synthesis, possibly utilising the following techniques:

- The addition of cross linkers, such as (3-ethyl-3-oxetanyl)methyl methacrylate or ethylene glycol dimethacrylate, thus creating gels or hydrogel like structures to improve load carrying capacity [292, 360, 361].
- Experimentation with a range of ligands to find an acceptable balance between cost and effectiveness to improve the likelihood of in-situ formation being cost effective.
- The formation of copolymers to improve the structural integrity of the final polymer brush or the final lubrication effect that can be tested.
- Modification of the steel surface in addition to the silicon nitride to investigate if polymers on both surfaces results in entanglement within the contact or if the lubrication effect is enhanced.

6 Appendix

6.1 Appendix A. Preliminary AFM images

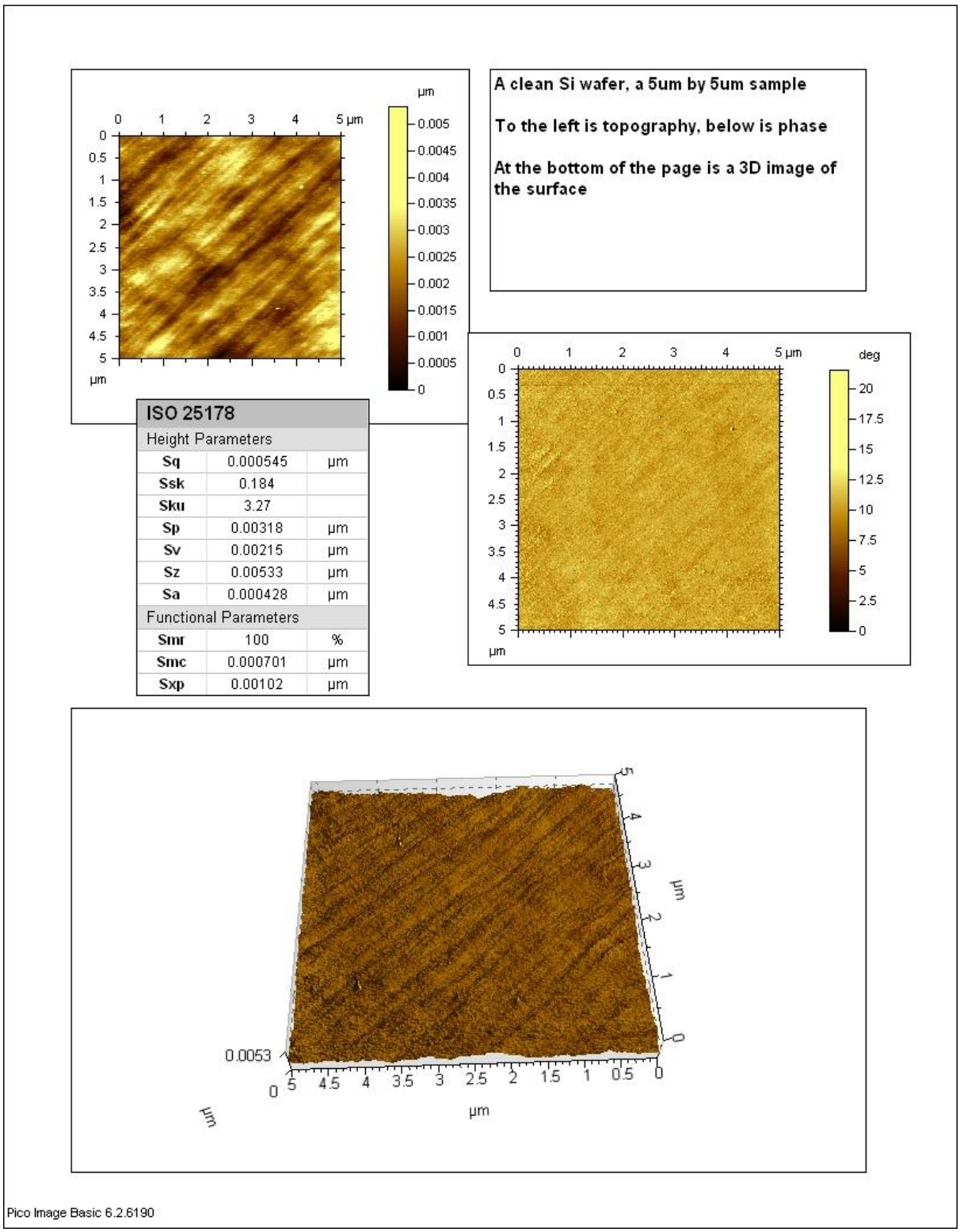

Figure A1. AFM image of a bare silicon wafer 5µm x 5µm.

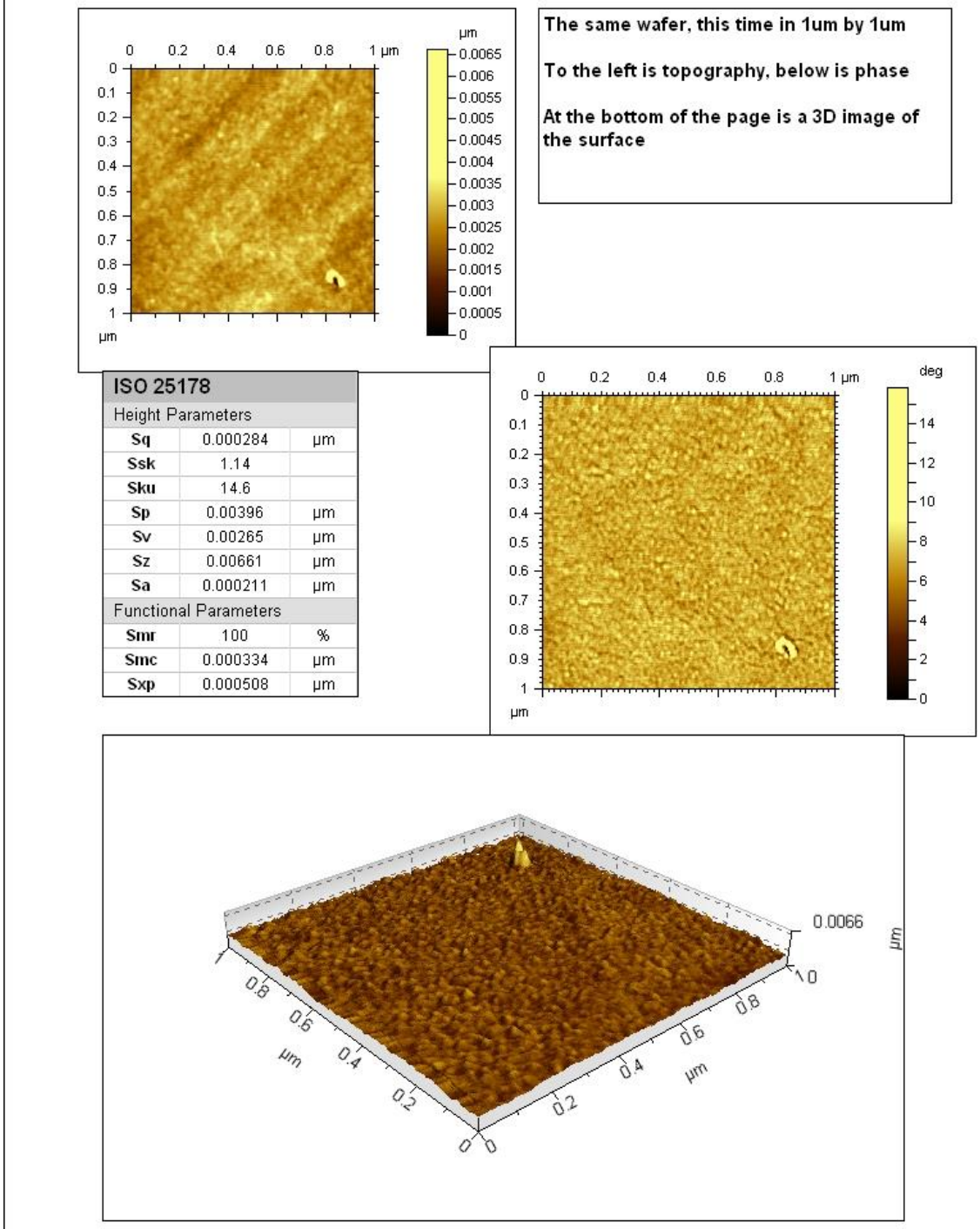

Figure A2. AFM image of a bare silicon wafer 1µm x 1µm.

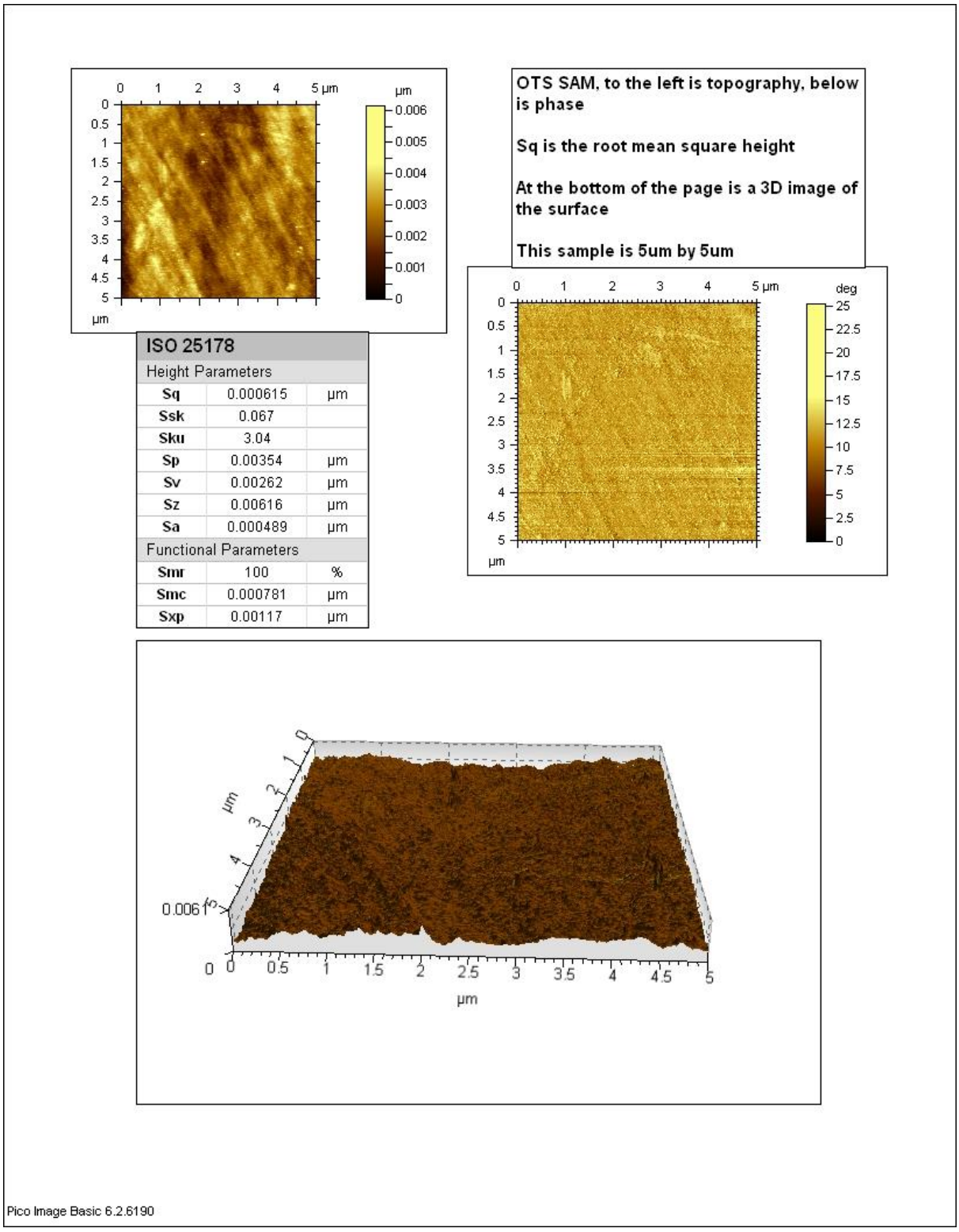

Figure A3. AFM image of OTS SAM on a silicon wafer 5µm x 5µm.

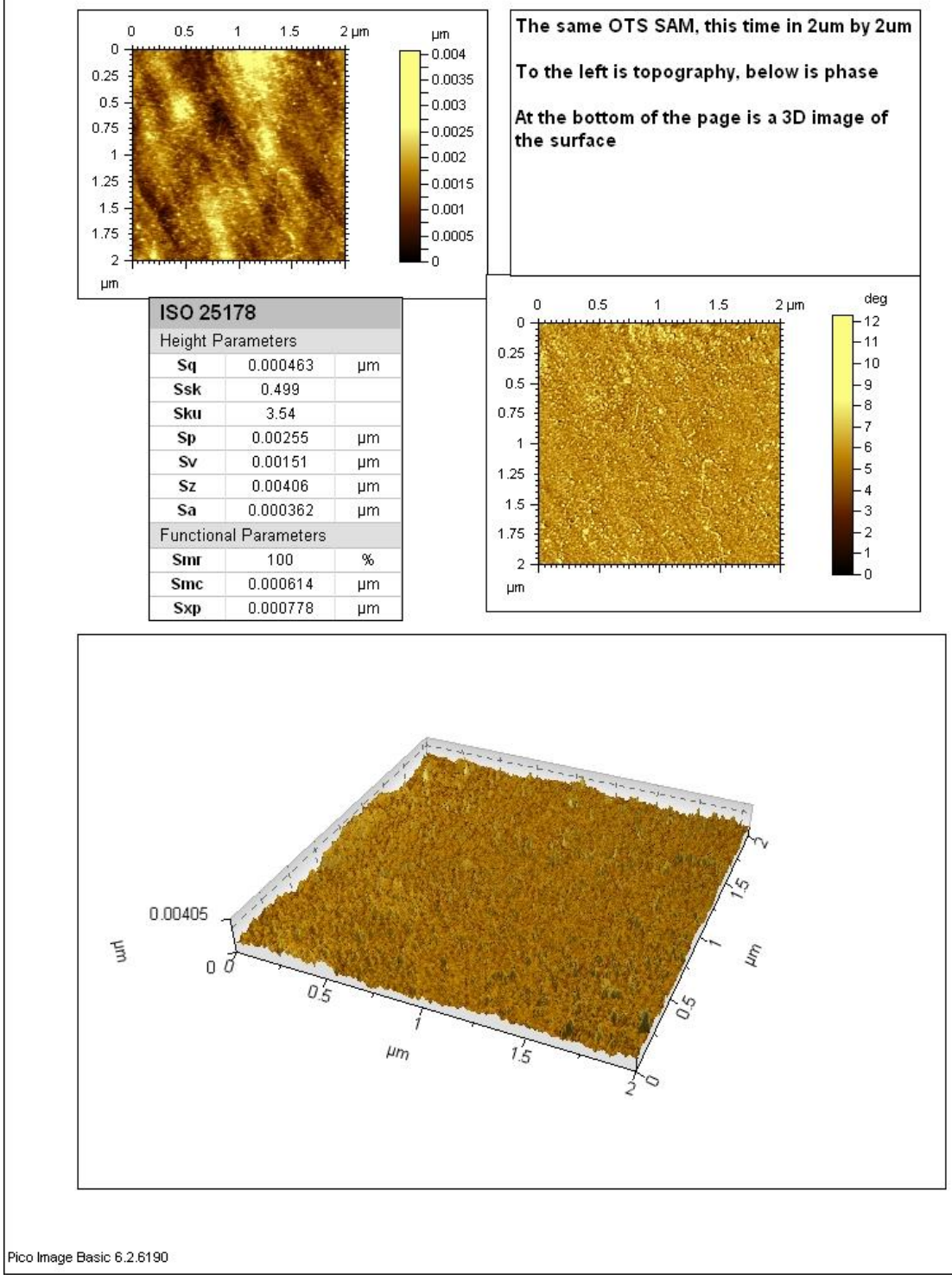

Figure A4. AFM image of OTS SAM on a silicon wafer 2µm x 2µm.

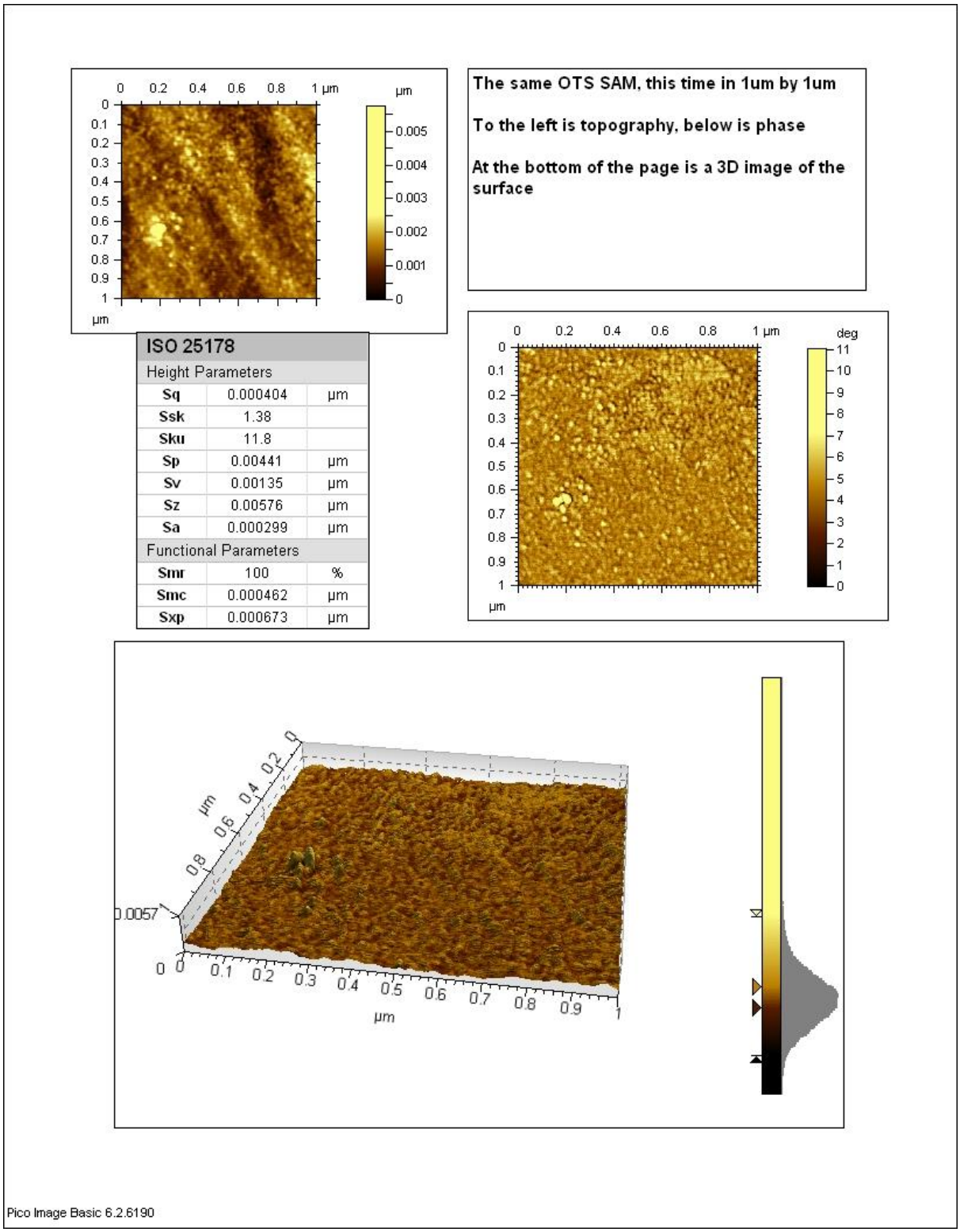

Figure A5. AFM image of OTS SAM on a silicon wafer 1µm x 1µm.

6.2 Appendix B. Piranha AFM images

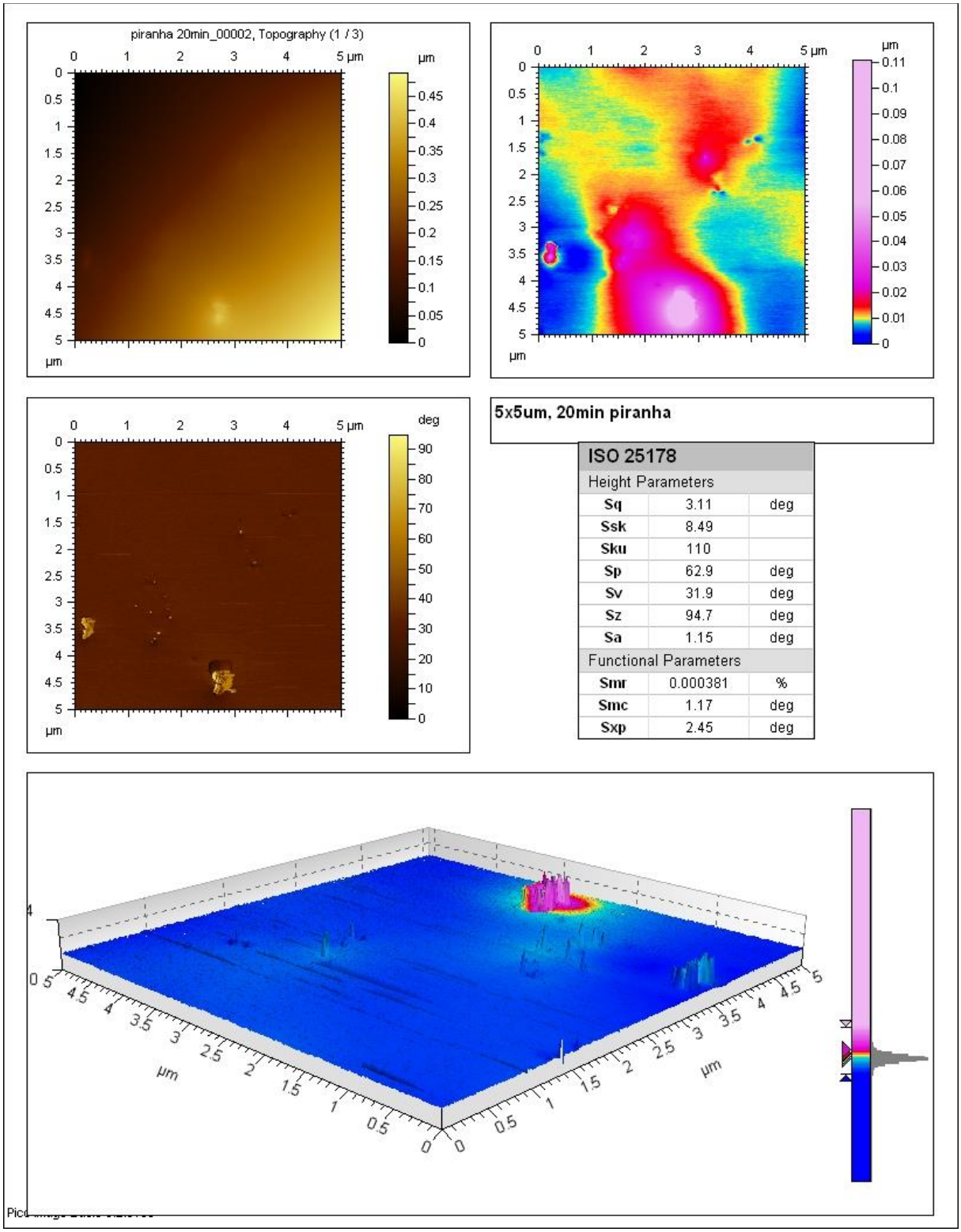

Figure B1. AFM image of a silicon wafer treated with piranha for 20 minutes.

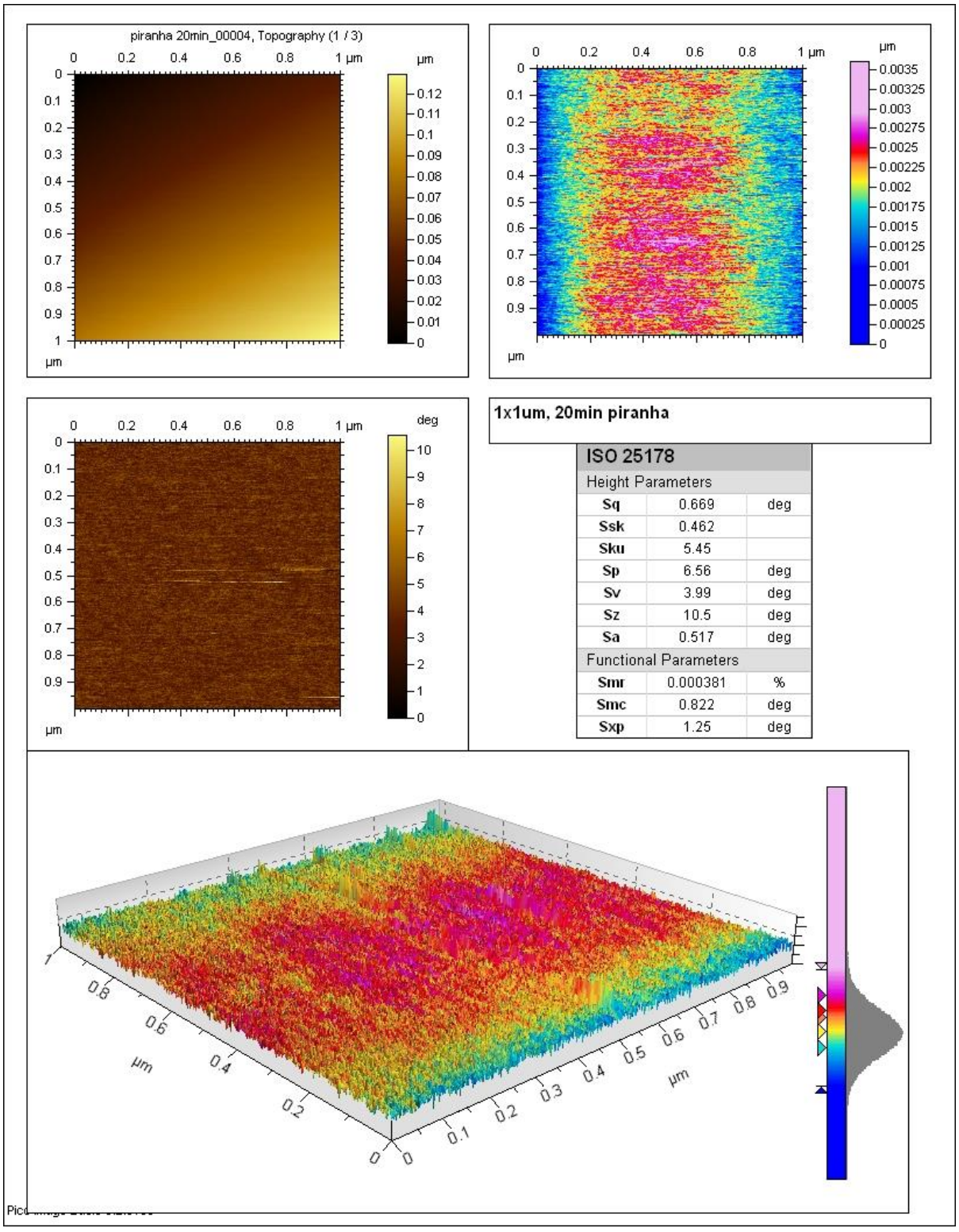

Figure B2. AFM image of a silicon wafer treated with piranha for 20 minutes.

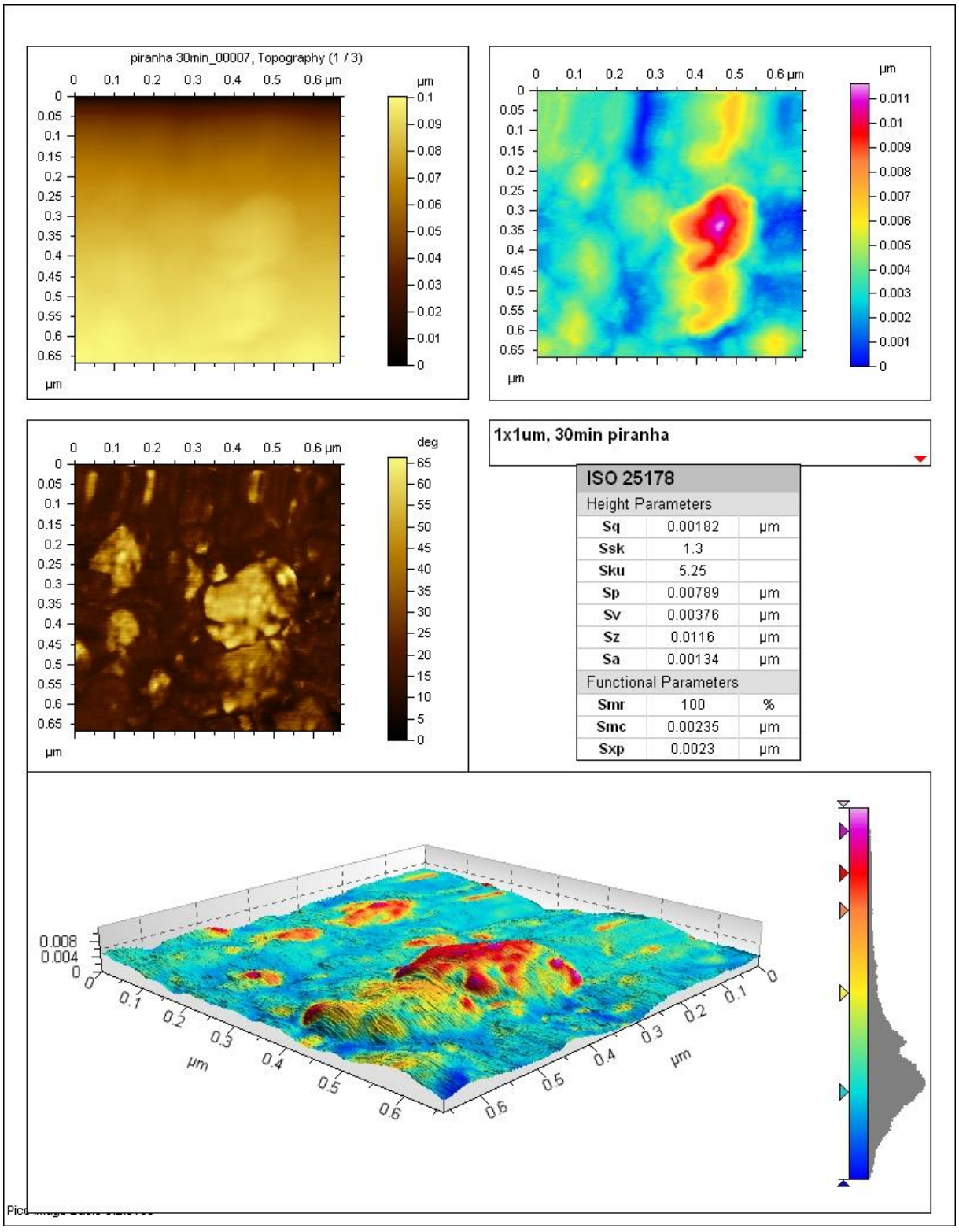

Figure B3. AFM image of a silicon wafer treated with piranha for 30 minutes.

6.3 Appendix C. Plasma AFM images

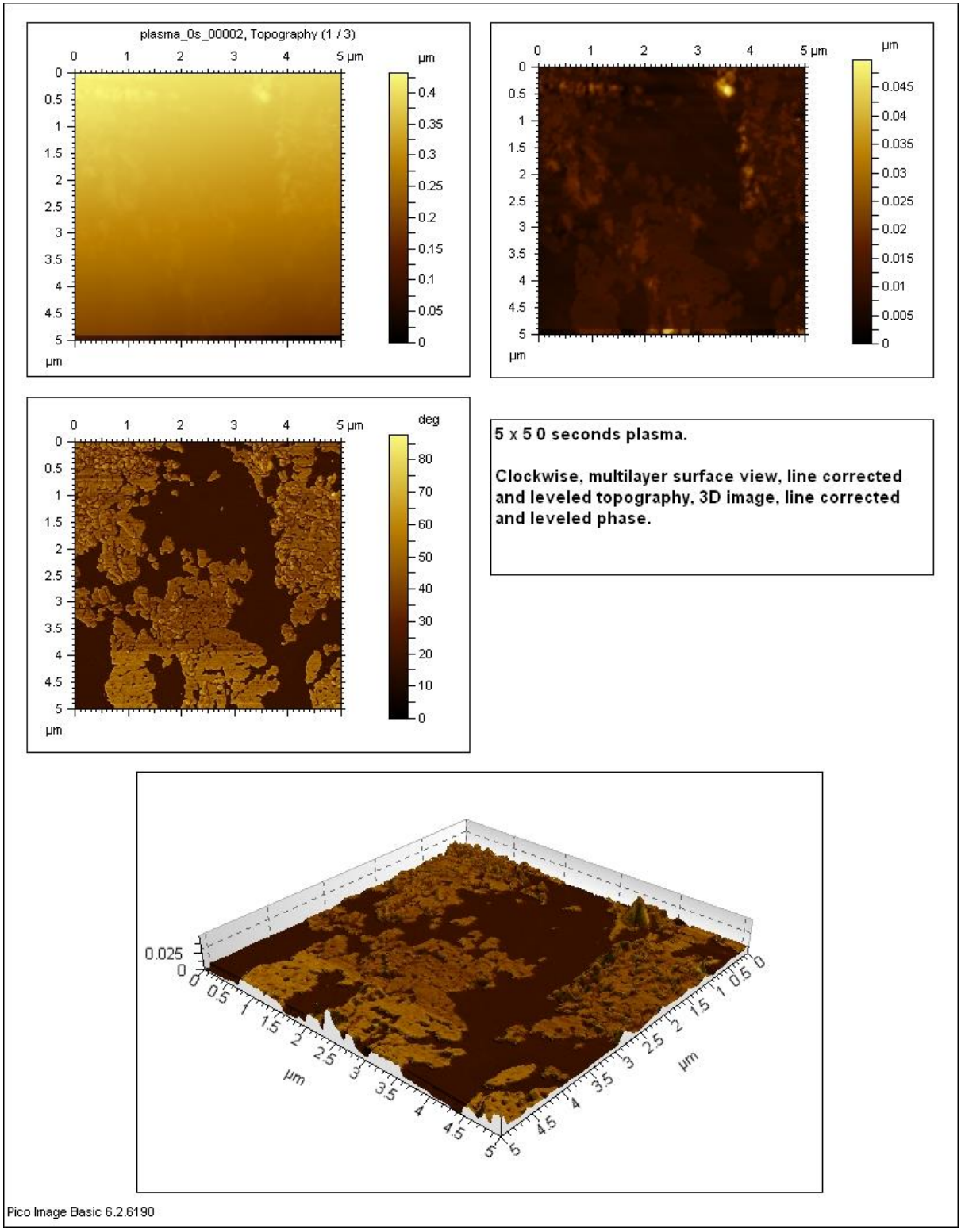

Figure C1. AFM image of a silicon wafer prior to plasma treatment. Ethanol residues present.

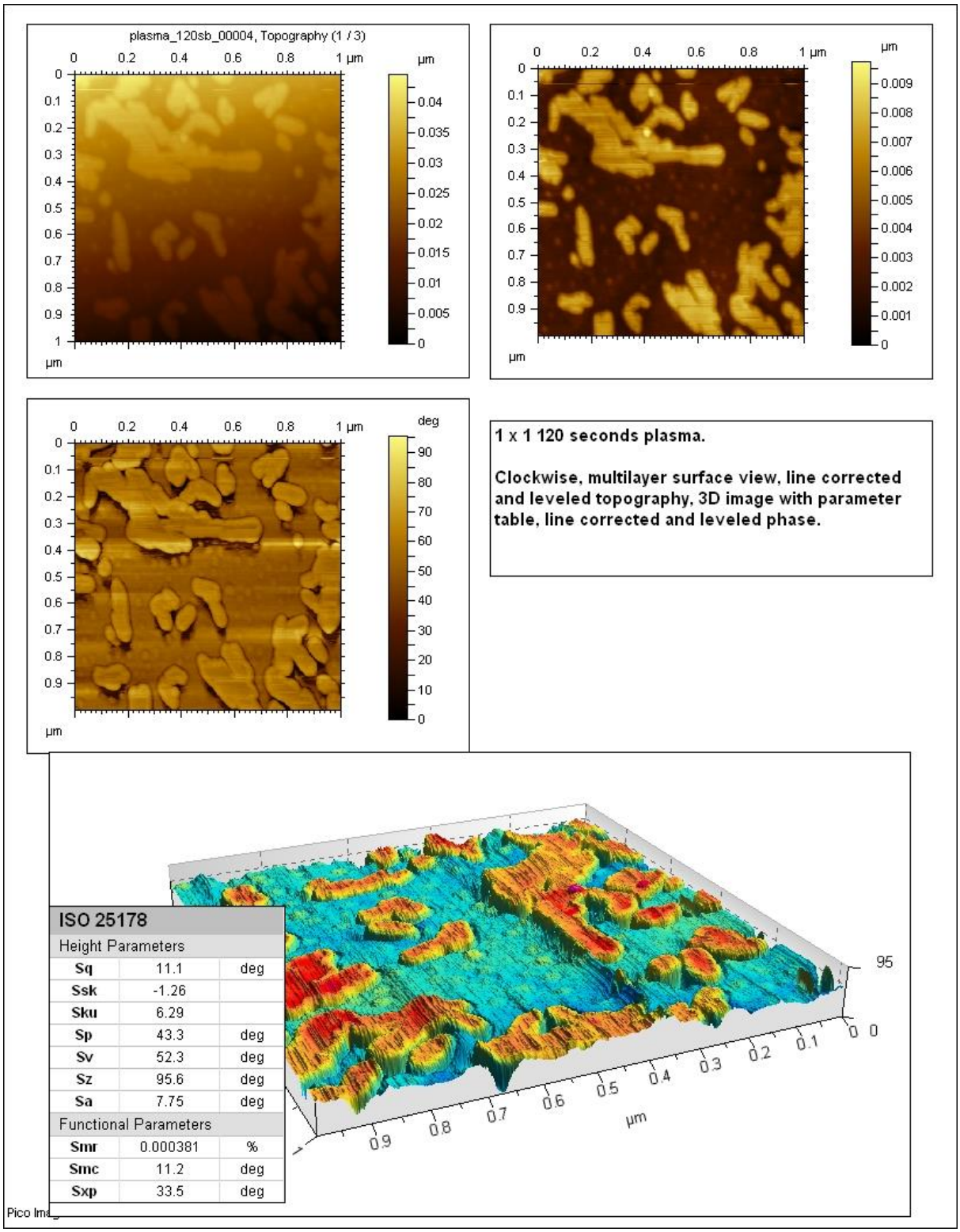

Figure C2. AFM image of a silicon wafer after plasma treatment. Ethanol residues present result in shadowing effect.

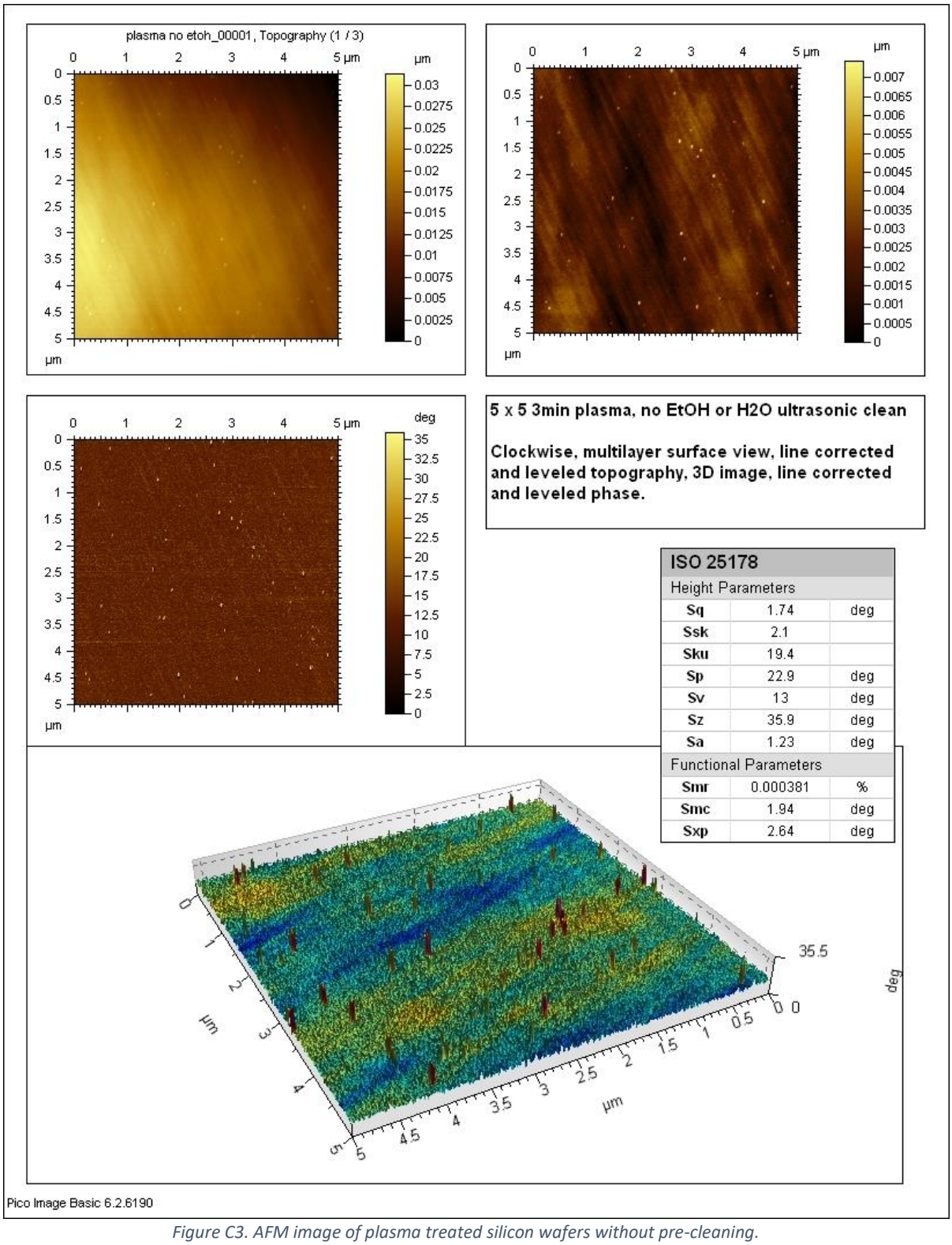

Figure C3. AFM image of plasma treated silicon wafers without pre-cleaning.

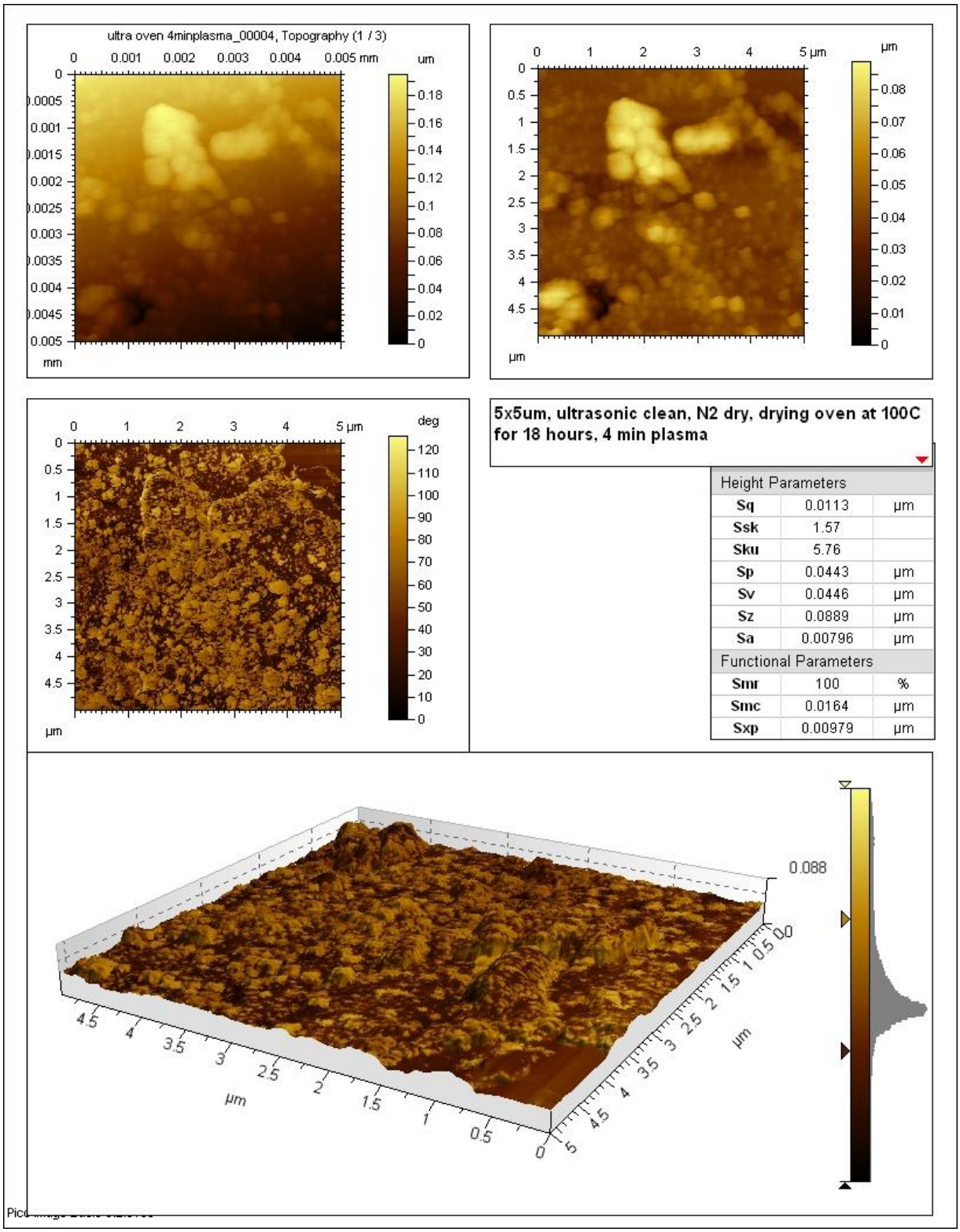

Figure C4. AFM image showing the results of oven drying.

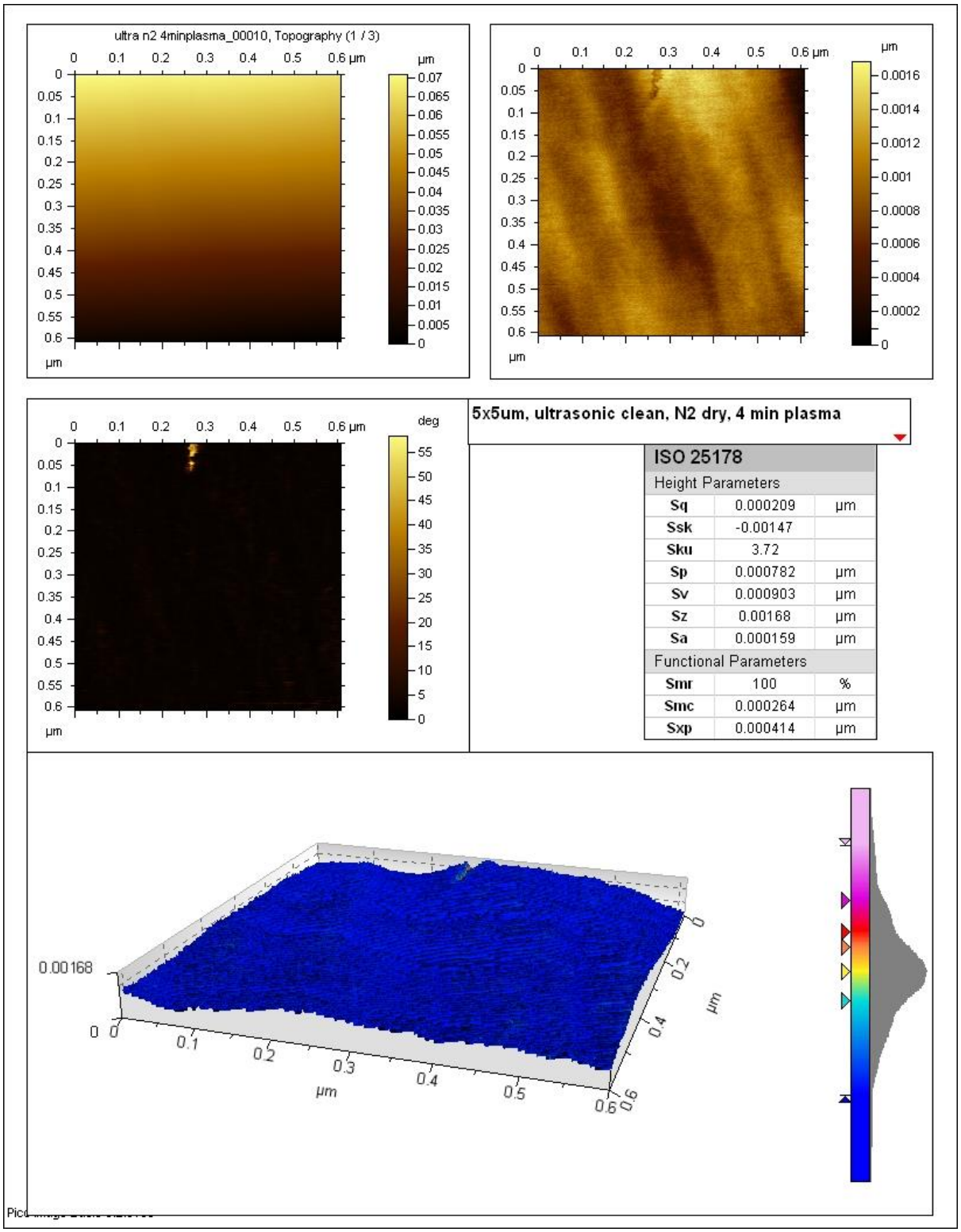

Figure C5. AFM image showing the results of extended nitrogen drying.

6.4 Appendix D. High quality OTS SAM

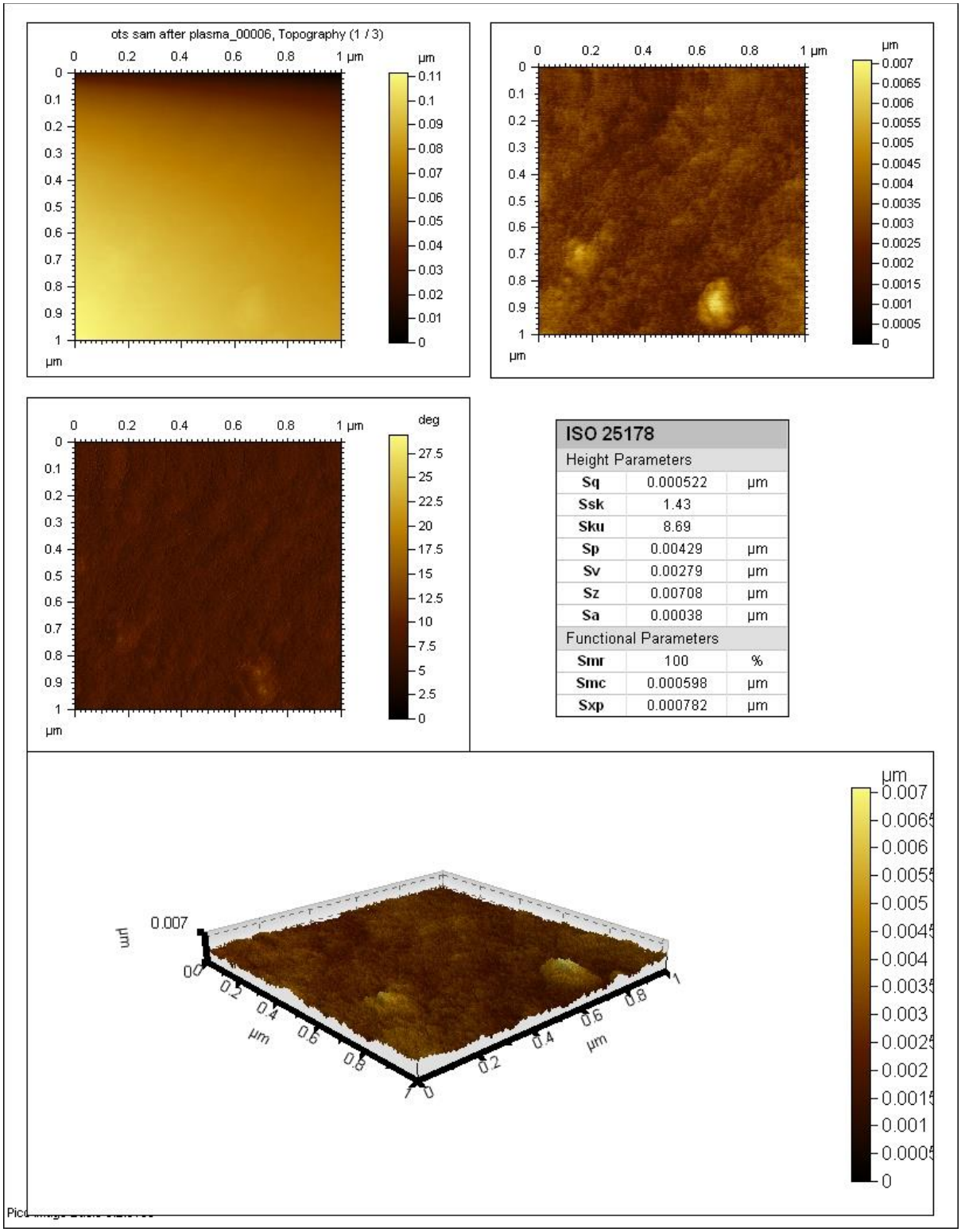

Figure D1. AFM images of OTS SAM after plasma treatment.

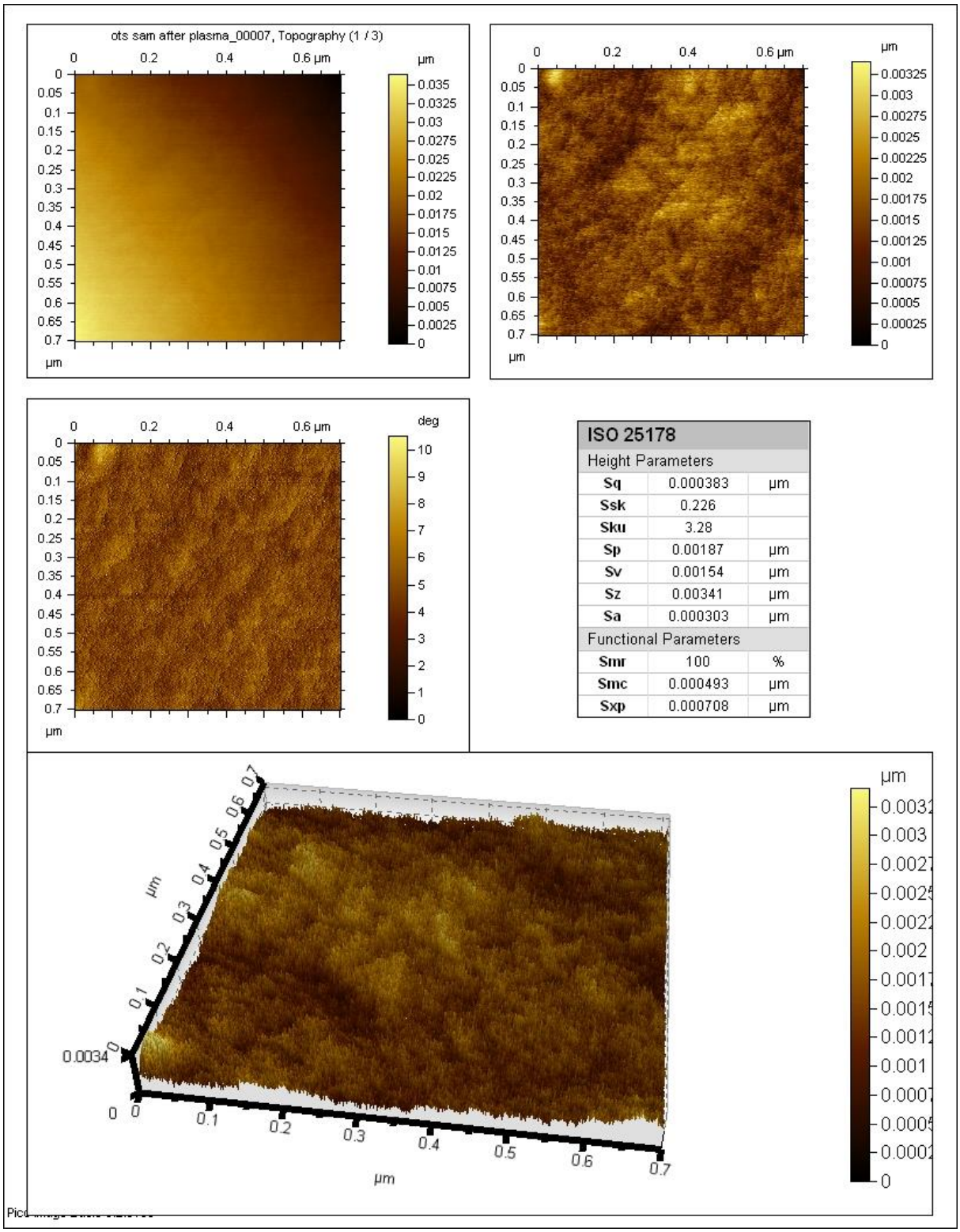

Figure D2. AFM images of OTS SAM after plasma treatment.

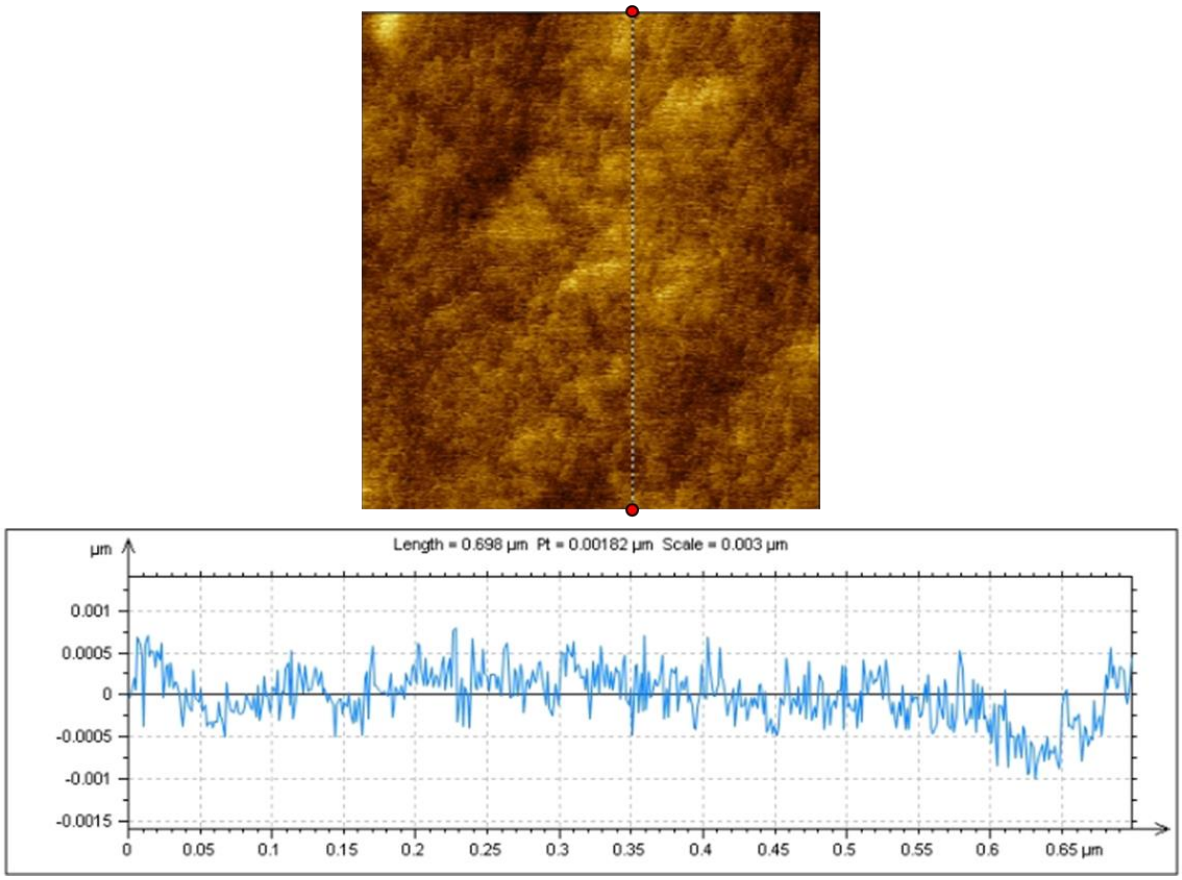

Figure D3. Line profile and resultant roughness.

6.5 Appendix E, NMR Predictions

6.5.1 Ester Prediction

ChemNMR ^{13}C Estimation

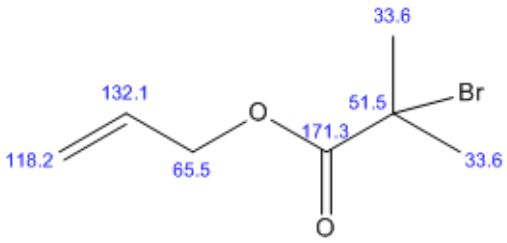

Estimation quality is indicated by color: good, medium, rough

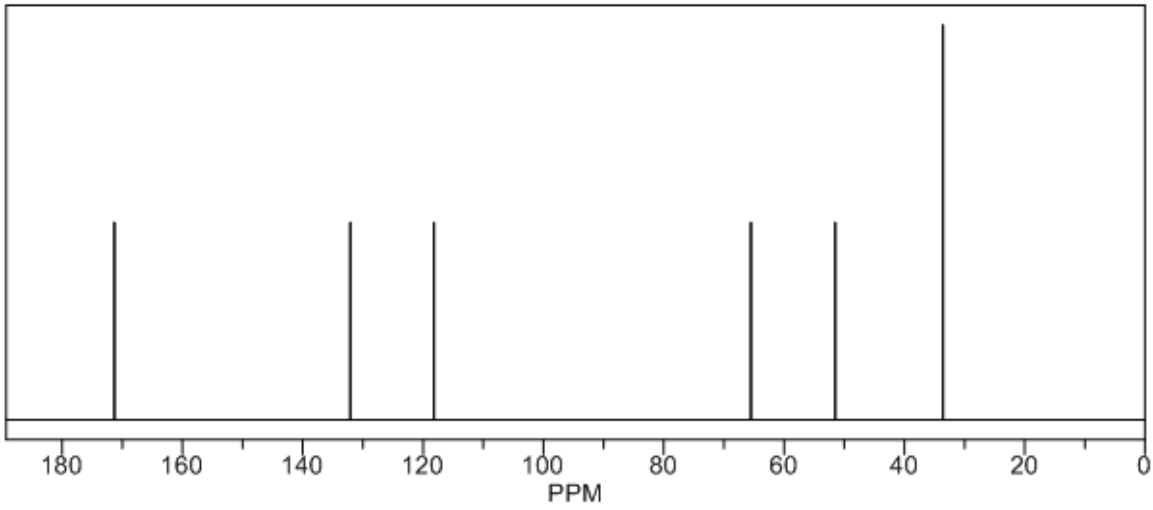

Figure 6.1. Carbon[13] NMR estimation of the ester.

```
Protocol of the C-13 NMR Prediction: (Lib=S)

Node     Shift    Base + Inc.   Comment (ppm rel. to TMS)

C   51.5              -2.3      aliphatic
                      21.8         1 alpha -C(=O)-O
                      18.2         2 alpha -C
                      18.9         1 alpha -Br
                      -2.5         1 gamma -C
                       0.4         1 delta -C=C
                      -3.0         general corrections
C   171.3            166.0      1-carboxyl
                      13.5         1 -C(C)C
                      -5.0         1 -C from O-carboxyl
                      -3.2         general corrections
CH2 65.5              -2.3      aliphatic
                      19.5         1 alpha -C=C
                      54.9         1 alpha -O-C=O
                      -2.5         1 gamma -C
                       0.6         2 delta -C
                      -0.7         1 delta -Br
                      -4.0         general corrections
CH  132.1            123.3      1-ethylene
                      14.2         1 -C-O
                      -5.4         general corrections
CH2 118.2            123.3      1-ethylene
                      -8.2         1 -C-O
                       3.1         general corrections
CH3 33.6              -2.3      aliphatic
                       9.1         1 alpha -C
                       2.0         1 beta -C(=O)-O
                       9.4         1 beta -C
                      11.0         1 beta -Br
                       0.3         1 delta -C
                       4.1         general corrections
CH3 33.6              -2.3      aliphatic
                       9.1         1 alpha -C
                       2.0         1 beta -C(=O)-O
                       9.4         1 beta -C
                      11.0         1 beta -Br
                       0.3         1 delta -C
                       4.1         general corrections
```

Figure 6.2. Carbon[13] NMR estimation of the ester, detailed chemical shifts.

ChemNMR ^{1}H Estimation

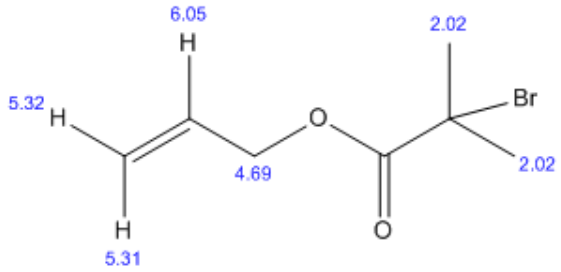

Estimation quality is indicated by color: good, medium, rough

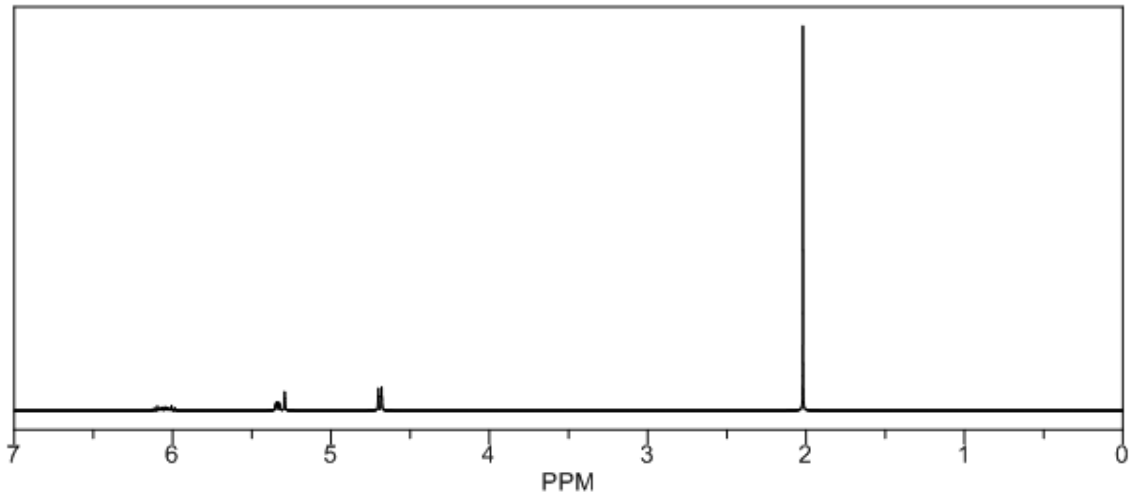

Figure 6.3. Hydrogen[1] NMR estimation of the ester.

```
Protocol of the H-1 NMR Prediction (Lib=SU Solvent=DMSO 300 MHz):

Node     Shift    Base + Inc.   Comment (ppm rel. to TMS)

CH2 4.69              1.37      methylene
                         0.63      1 alpha -C=C
                         2.75      1 alpha -OC(=O)-C
                        -0.06      general corrections
CH3 2.02              0.86      methyl
                         0.83      1 beta -Br
                         0.28      1 beta -C(=O)OC
                         0.05      1 beta -C
CH3 2.02              0.86      methyl
                         0.83      1 beta -Br
                         0.28      1 beta -C(=O)OC
                         0.05      1 beta -C
H   6.05              5.25      1-ethylene
                         0.64      1 -C-O gem
                         0.16      general corrections
H   5.32              5.25      1-ethylene
                        -0.01      1 -C-O cis
                         0.08      general corrections
H   5.31              5.25      1-ethylene
                        -0.02      1 -C-O trans
                         0.08      general corrections

1H NMR Coupling Constant Prediction

shift   atom index  coupling partner, constant and vector

4.69        3
                   11   6.2  H-CH-C(sp2)-H
                   12  -1.0  H-CH>CH=CH<H
                   13  -1.0  H-CH>CH=CH>H
2.02        8
2.02       10
6.05       11
                    3   6.2  H-C(sp2)-CH-H
                   12  16.8  H>C=CH>H
                   13  10.0  H>C=CH<H
5.32       12
                   13   2.1  H-C(sp2)-H
                   11  16.8  H>CH=C>H
                    3  -1.0  H>CH=CH<CH-H
5.31       13
                   12   2.1  H-C(sp2)-H
                   11  10.0  H>CH=C<H
                    3  -1.0  H>CH=CH>CH-H
```

Figure 6.4. Hydrogen[1] NMR estimation of the ester, detailed chemical shifts.

6.5.2 Ester Results

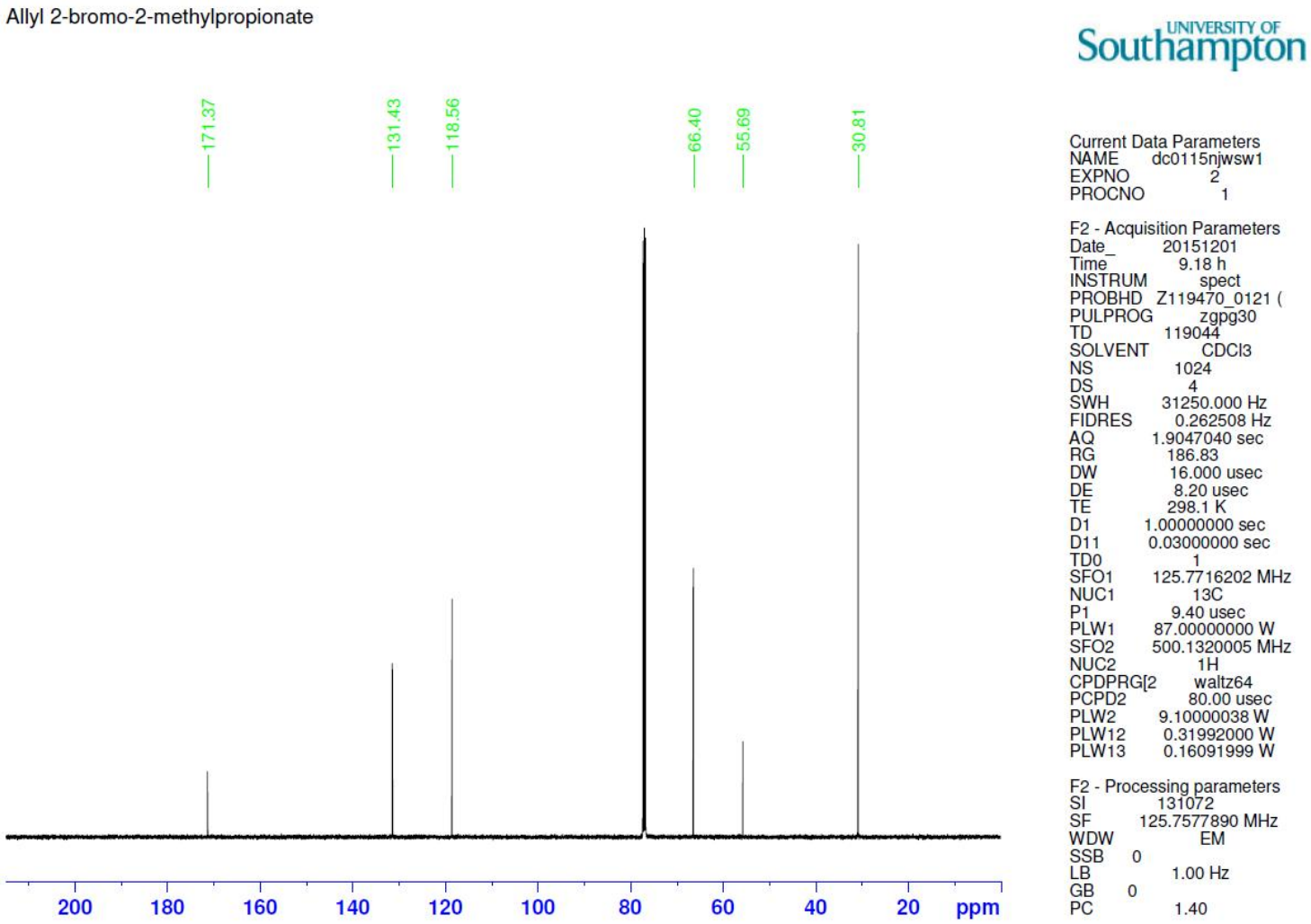

Figure 6.5. Carbon NMR of ester.

Allyl 2-bromo-2-methylpropionate

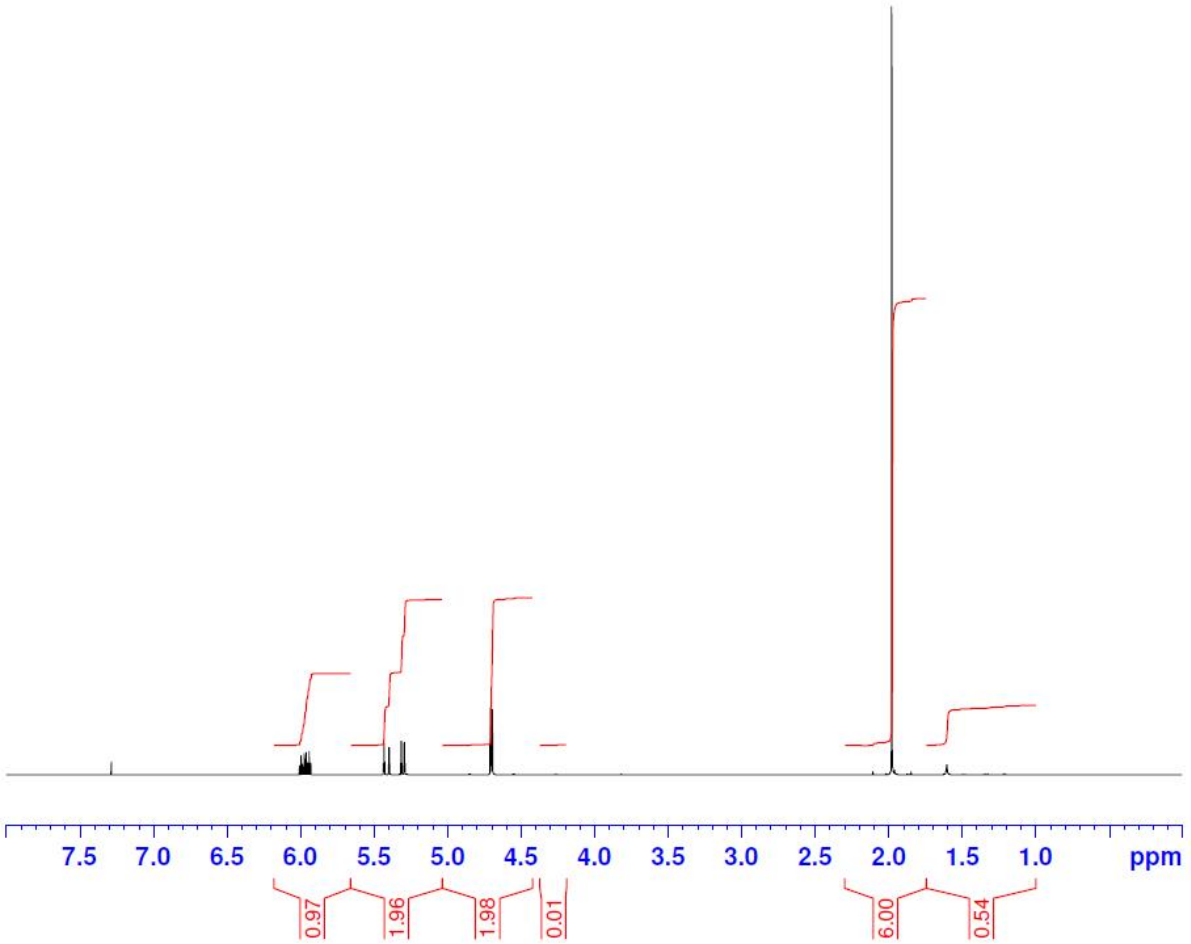

Current Data Parameters
NAME dc0115njwsw1
EXPNO 1
PROCNO 1

F2 - Acquisition Parameters
Date_ 20151201
Time 9.15 h
INSTRUM spect
PROBHD Z119470_0121 (
PULPROG zg30
TD 131072
SOLVENT CDCl3
NS 16
DS 0
SWH 7002.801 Hz
FIDRES 0.053427 Hz
AQ 9.3585405 sec
RG 107.91
DW 71.400 usec
DE 11.62 usec
TE 298.0 K
D1 0.10000000 sec
TD0 1
SFO1 500.1325006 MHz
NUC1 1H
P1 15.00 usec
PLW1 9.10000038 W

F2 - Processing parameters
SI 131072
SF 500.1300000 MHz
WDW no
SSB 0
LB 0 Hz
GB 0
PC 4.00

Figure 6.6. Hydrogen NMR with integration.

Allyl 2-bromo-2-methylpropionate

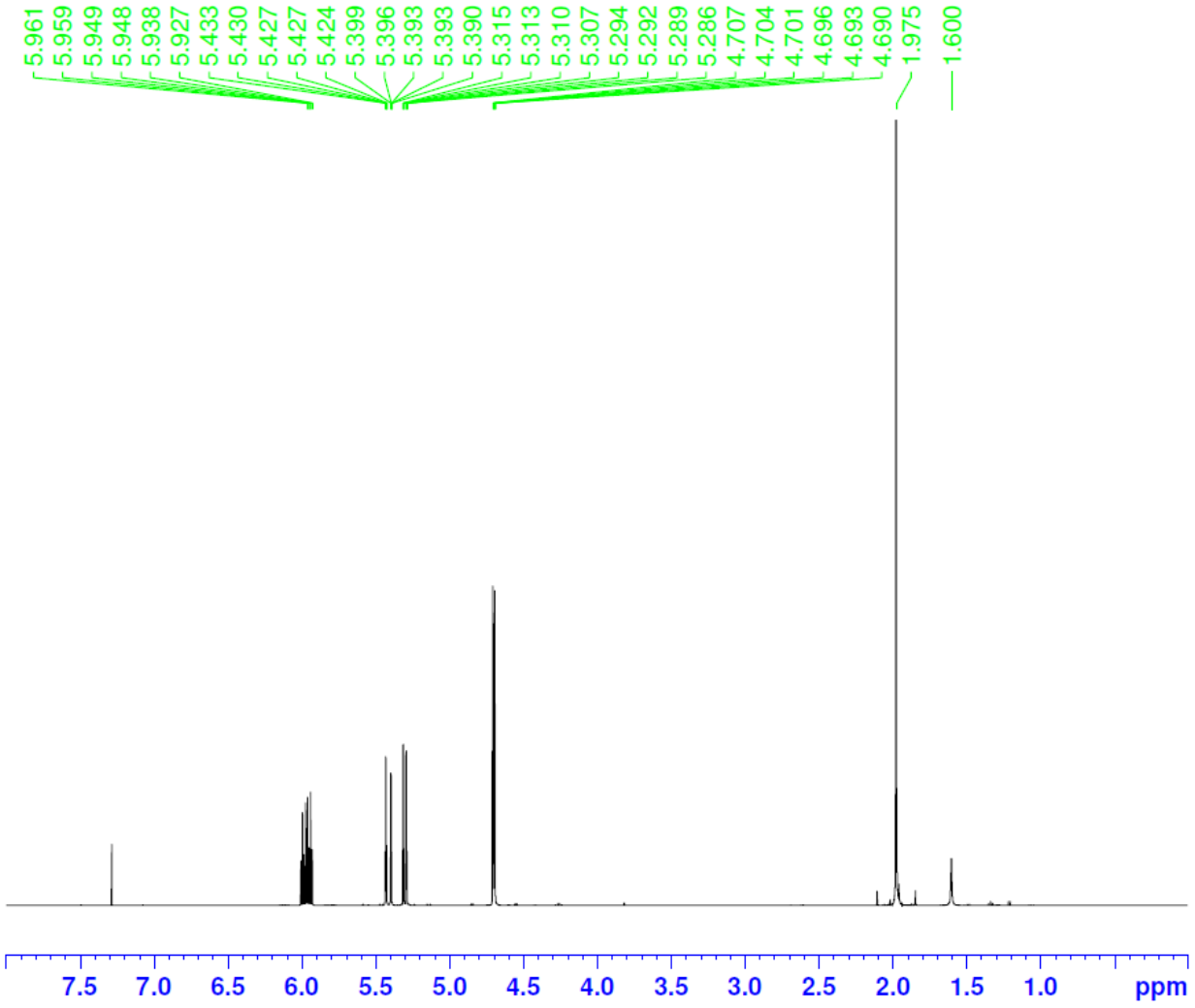

Current Data Parameters
NAME dc0115njwsw1
EXPNO 1
PROCNO 1

F2 - Acquisition Parameters
Date_ 20151201
Time 9.15 h
INSTRUM spect
PROBHD Z119470_0121 (
PULPROG zg30
TD 131072
SOLVENT CDCl3
NS 16
DS 0
SWH 7002.801 Hz
FIDRES 0.053427 Hz
AQ 9.3585405 sec
RG 107.91
DW 71.400 usec
DE 11.62 usec
TE 298.0 K
D1 0.10000000 sec
TD0 1
SFO1 500.1325006 MHz
NUC1 1H
P1 15.00 usec
PLW1 9.10000038 W

F2 - Processing parameters
SI 131072
SF 500.1300000 MHz
WDW no
SSB 0
LB 0 Hz
GB 0
PC 4.00

Figure 6.7. Hydrogen NMR with picked peaks.

6.5.3 ATRP Initiator Prediction

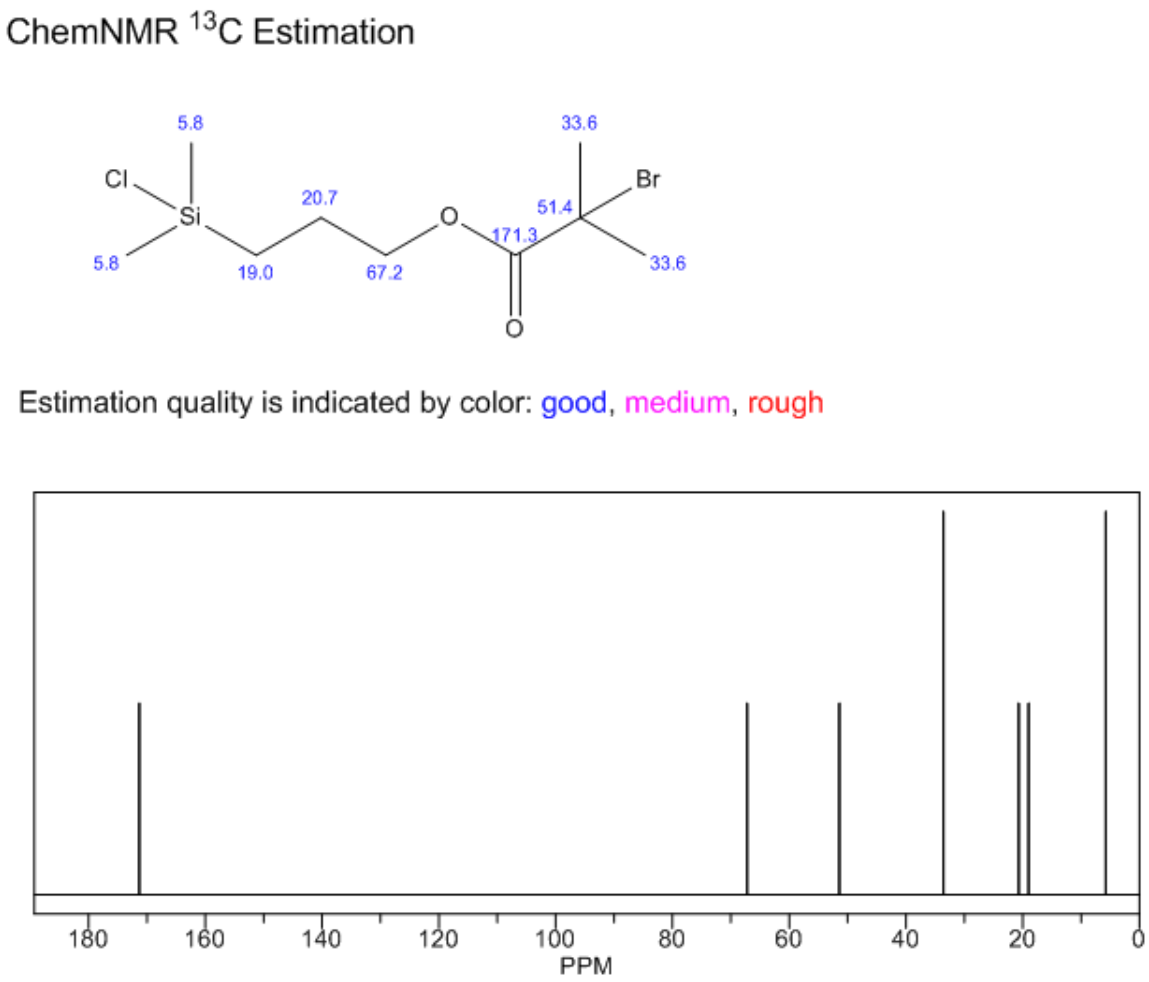

Figure 6.8. Carbon[13] NMR estimation of the ATRP initiator.

```
Protocol of the C-13 NMR Prediction: (Lib=S)


Node     Shift    Base + Inc.   Comment (ppm rel. to TMS)

C   51.4              -2.3      aliphatic
                      21.8         1 alpha -C(=O)-O
                      18.2         2 alpha -C
                      18.9         1 alpha -Br
                      -2.5         1 gamma -C
                       0.3         1 delta -C
                      -3.0         general corrections
CH2 19.0              -2.3      aliphatic
                       9.1         1 alpha -C
                     -20.0         1 alpha -Si
                      28.2         3 beta -C
                      10.0         1 beta -Cl
                      -6.0         1 gamma -O-C=O
CH3 5.8               -2.3      aliphatic
                     -20.0         1 alpha -Si
                      18.8         2 beta -C
                      10.0         1 beta -Cl
                      -2.5         1 gamma -C
                       0.3         1 delta -C
                       1.5         general corrections
CH3 5.8               -2.3      aliphatic
                     -20.0         1 alpha -Si
                      18.8         2 beta -C
                      10.0         1 beta -Cl
                      -2.5         1 gamma -C
                       0.3         1 delta -C
                       1.5         general corrections
C   171.3            166.0      1-carboxyl
                      13.5         1 -C(C)C
                      -5.0         1 -C from O-carboxyl
                      -3.2         general corrections
CH2 67.2              -2.3      aliphatic
                       9.1         1 alpha -C
                      54.9         1 alpha -O-C=O
                       9.4         1 beta -C
                      -2.5         1 gamma -C
                       0.1         1 gamma -Si
                       1.2         4 delta -C
                      -0.5         1 delta -Cl
                      -0.7         1 delta -Br
                      -1.5         general corrections
CH2 20.7              -2.3      aliphatic
                      18.2         2 alpha -C
                       6.5         1 beta -O-C=O
                       9.4         1 beta -Si
                      -5.0         2 gamma -C
                      -5.1         1 gamma -Cl
                       0.3         1 delta -C
                      -1.3         general corrections
CH3 33.6              -2.3      aliphatic
                       9.1         1 alpha -C
                       2.0         1 beta -C(=O)-O
                       9.4         1 beta -C
```

Figure 6.9. Carbon13 NMR estimation of the ATRP initiator, detailed chemical shifts.

ChemNMR ^{1}H Estimation

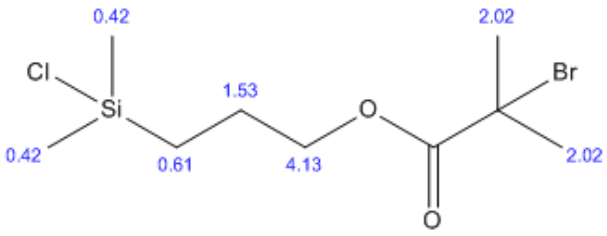

Estimation quality is indicated by color: good, medium, rough

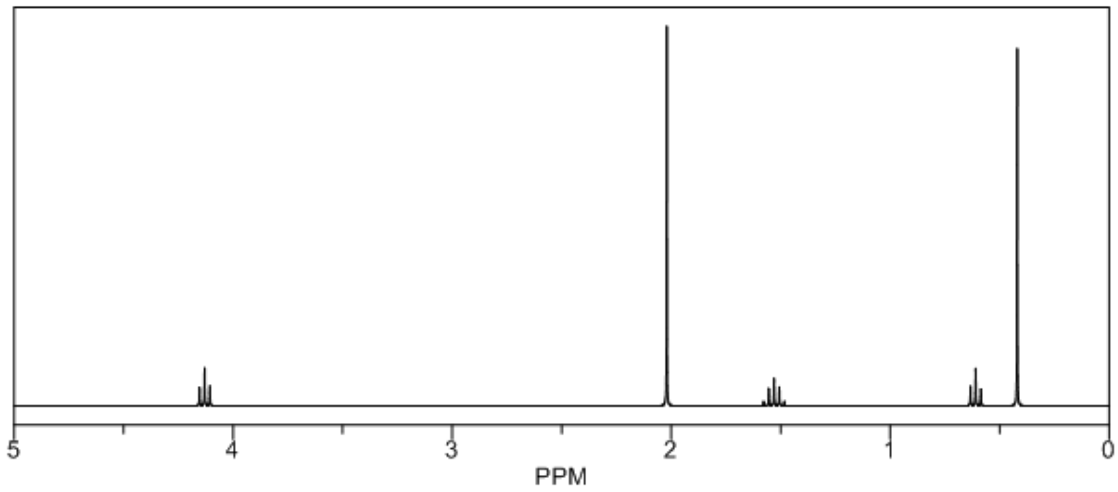

Figure 6.10. Hydrogen[1] NMR estimation of the ATRP initiator.

```
Protocol of the H-1 NMR Prediction (Lib=SU Solvent=DMSO 300 MHz):


Node     Shift    Base + Inc.   Comment (ppm rel. to TMS)

CH2 0.61              1.37      methylene
                        -0.70      1 alpha -Si
                        -0.06      1 beta -C
CH3 0.42              0.86      methyl
                        -0.44      1 alpha -Si(C)(C)Cl
CH3 0.42              0.86      methyl
                        -0.44      1 alpha -Si(C)(C)Cl
CH2 4.13              1.37      methylene
                         2.75      1 alpha -OC(=O)-C
                        -0.06      1 beta -C
                         0.07      general corrections
CH2 1.53              1.37      methylene
                        -0.08      1 beta -Si
                         0.24      1 beta -OC(=O)-C
CH3 2.02              0.86      methyl
                         0.83      1 beta -Br
                         0.28      1 beta -C(=O)OC
                         0.05      1 beta -C
CH3 2.02              0.86      methyl
                         0.83      1 beta -Br
                         0.28      1 beta -C(=O)OC
                         0.05      1 beta -C

1H NMR Coupling Constant Prediction

shift   atom index  coupling partner, constant and vector

0.61         10
                           9   7.1         H-CH-CH-H
0.42         12
0.42         13
4.13          8
```

Figure 6.11. Hydrogen[1] NMR estimation of the ATRP initiator, detailed chemical shifts.

6.5.4 ATRP Initiator Results

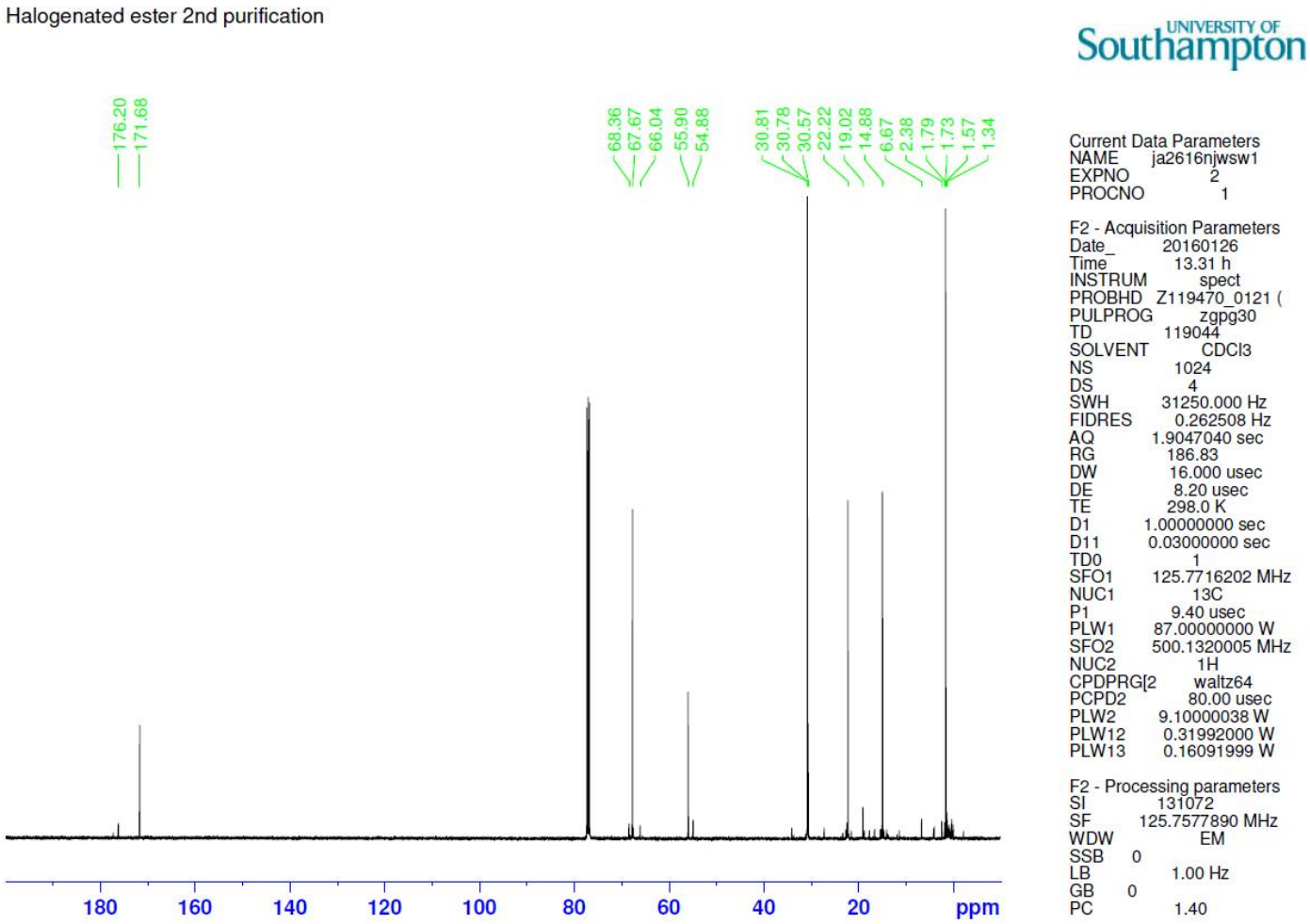

Figure 6.12. Carbon NMR of Initiator.

Halogenated ester 2nd purification

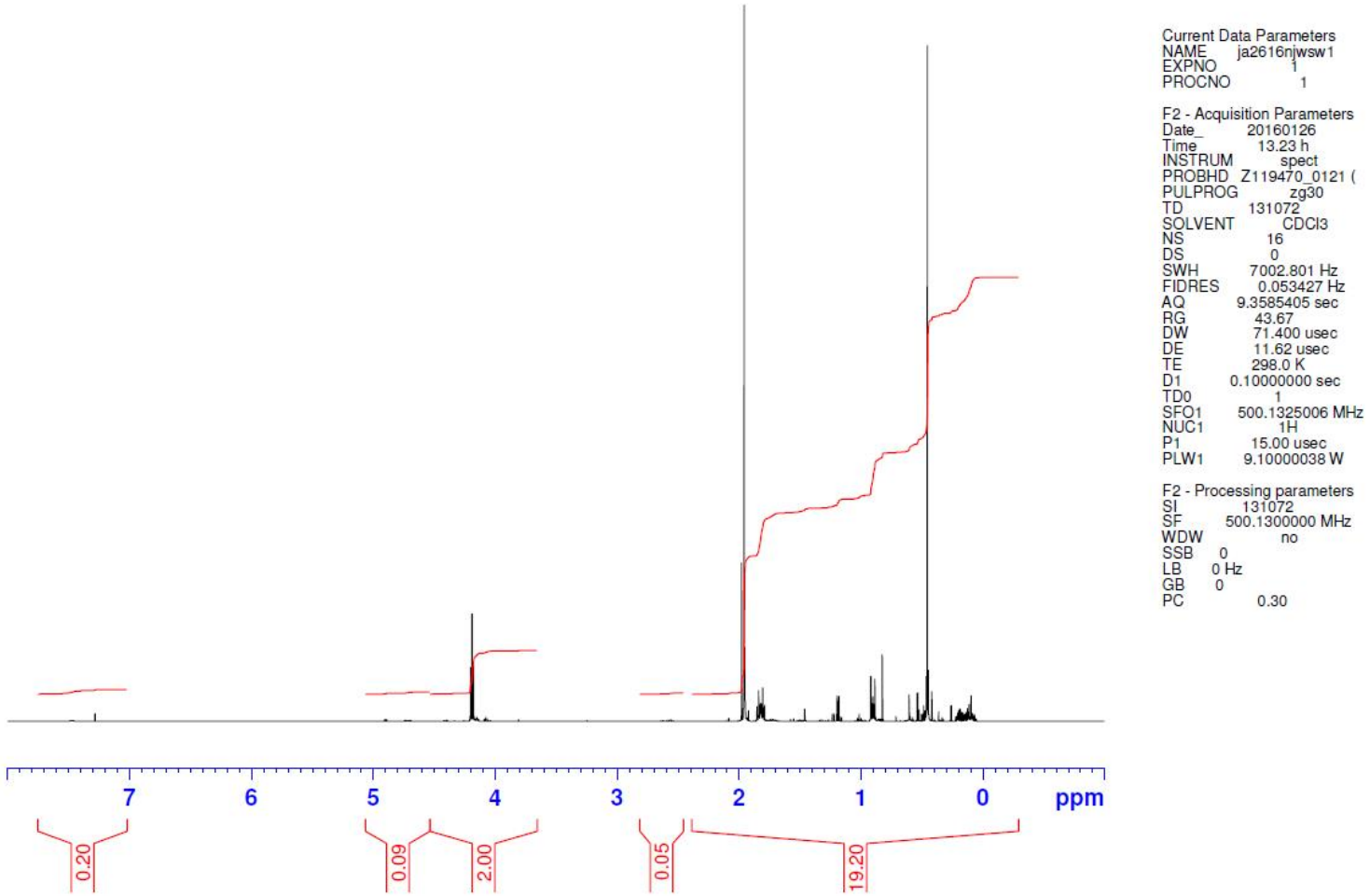

Current Data Parameters
NAME ja2616njwsw1
EXPNO 1
PROCNO 1

F2 - Acquisition Parameters
Date_ 20160126
Time 13.23 h
INSTRUM spect
PROBHD Z119470_0121 (
PULPROG zg30
TD 131072
SOLVENT CDCl3
NS 16
DS 0
SWH 7002.801 Hz
FIDRES 0.053427 Hz
AQ 9.3585405 sec
RG 43.67
DW 71.400 usec
DE 11.62 usec
TE 298.0 K
D1 0.10000000 sec
TD0 1
SFO1 500.1325006 MHz
NUC1 1H
P1 15.00 usec
PLW1 9.10000038 W

F2 - Processing parameters
SI 131072
SF 500.1300000 MHz
WDW no
SSB 0
LB 0 Hz
GB 0
PC 0.30

Figure 6.13. Carbon NMR of ATRP Initiator with integration peaks

7 References

[1] K. Holmberg, P. Andersson, and A. Erdemir, "Global energy consumption due to friction in passenger cars," *Tribology International,* vol. 47, pp. 221-234, 3// 2012.

[2] K. Holmberg, P. Andersson, N.-O. Nylund, K. Mäkelä, and A. Erdemir, "Global energy consumption due to friction in trucks and buses," *Tribology International,* vol. 78, pp. 94-114, 10// 2014.

[3] Z. Tang and S. Li, "A review of recent developments of friction modifiers for liquid lubricants (2007–present)," *Current Opinion in Solid State and Materials Science,* vol. 18, pp. 119-139, 6// 2014.

[4] M. Ratoi, V. B. Niste, H. Alghawel, Y. F. Suen, and K. Nelson, "The impact of organic friction modifiers on engine oil tribofilms," *RSC Advances,* vol. 4, pp. 4278-4285, 2014.

[5] M. Ratoi, V. Anghel, C. Bovington, and H. A. Spikes, "Mechanisms of oiliness additives," *Tribology International,* vol. 33, pp. 241-247, 4// 2000.

[6] S. Loehlé, C. Matta, C. Minfray, T. L. Mogne, R. Iovine, Y. Obara*, et al.*, "Mixed lubrication of steel by C18 fatty acids revisited. Part I: Toward the formation of carboxylate," *Tribology International,* vol. 82, Part A, pp. 218-227, 2// 2015.

[7] V. Anghel, C. Bovington, and H. A. Spikes, "Thick-boundary-film formation by friction modifier additives," *Lubrication Science,* vol. 11, pp. 313-335, 1999.

[8] C. J. Reeves, P. L. Menezes, T.-C. Jen, and M. R. Lovell, "The influence of fatty acids on tribological and thermal properties of natural oils as sustainable biolubricants," *Tribology International,* vol. 90, pp. 123-134, 10// 2015.

[9] H. Zhao, A. Neville, A. Morina, R. Vickerman, and J. Durham, "Improved anti-shudder performance of ATFs—Influence of a new friction modifier and surface chemistry," *Tribology International,* vol. 46, pp. 62-72, 2// 2012.

[10] T. Reddyhoff, I. S. Y. Ku, A. S. Holmes, and H. A. Spikes, "Friction Modifier Behaviour in Lubricated MEMS Devices," *Tribology Letters,* vol. 41, pp. 239-246, 2011/01/01 2011.

[11] K. Topolovec Miklozic, J. Graham, and H. Spikes, "Chemical and Physical Analysis of Reaction Films Formed by Molybdenum Dialkyl-Dithiocarbamate Friction Modifier Additive Using Raman and Atomic Force Microscopy," *Tribology Letters,* vol. 11, pp. 71-81, 2001/08/01 2001.

[12] A. Morina, A. Neville, M. Priest, and J. H. Green, "ZDDP and MoDTC interactions in boundary lubrication—The effect of temperature and ZDDP/MoDTC ratio," *Tribology International,* vol. 39, pp. 1545-1557, 12// 2006.

[13] S. Jiang, R. Frazier, E. S. Yamaguchi, M. Blanco, S. Dasgupta, Y. Zhou*, et al.*, "The SAM Model for Wear Inhibitor Performance of Dithiophosphates on Iron Oxide," *The Journal of Physical Chemistry B,* vol. 101, pp. 7702-7709, 1997/09/01 1997.

[14] W. Yue, C. Liu, Z. Fu, C. Wang, H. Huang, and J. Liu, "Effects of molybdenum dithiocarbamate and zinc dialkyl dithiophosphate additives on tribological behaviors of hydrogenated diamond-like carbon coatings," *Materials & Design,* vol. 64, pp. 601-607, 12// 2014.

[15] M. Skjoedt, R. Butts, D. N. Assanis, and S. V. Bohac, "Effects of oil properties on spark-ignition gasoline engine friction," *Tribology International,* vol. 41, pp. 556-563, 6// 2008.

[16] J. A. Williams, "The Behaviour of Sliding Contacts Between Non-Conformal Rough Surfaces Protected by 'Smart' Films," *Tribology Letters,* vol. 17, pp. 765-778, 2004/11/01 2004.

[17] L. Wang, M. Nie, and J. Rumbol, "Self-assembled monolayer (SAM) protective films for hybrid contacts," *Tribology - Materials, Surfaces & Interfaces,* vol. 6, pp. 75-83, 2012.

[18] S. Korcek, J. Sorab, M. D. Johnson, and R. K. Jensen, "Automotive lubricants for the next millennium," *Industrial Lubrication and Tribology,* vol. 52, pp. 209-220, 2000.

[19] H. Spikes, "Low- and zero-sulphated ash, phosphorus and sulphur anti-wear additives for engine oils," *Lubrication Science,* vol. 20, pp. 103-136, 2008.

[20] C. Haensch, S. Hoeppener, and U. S. Schubert, "Chemical modification of self-assembled silane based monolayers by surface reactions," *Chemical Society Reviews,* vol. 39, pp. 2323-2334, 2010.
[21] C. Vericat, M. E. Vela, G. Benitez, P. Carro, and R. C. Salvarezza, "Self-assembled monolayers of thiols and dithiols on gold: new challenges for a well-known system," *Chemical Society Reviews,* vol. 39, pp. 1805-1834, 2010.
[22] J. A. Williams and H. R. Le, "Tribology and MEMS," *Journal of Physics D: Applied Physics,* vol. 39, p. R201, 2006.
[23] B. W. Ewers and J. D. Batteas, "The role of substrate interactions in the modification of surface forces by self-assembled monolayers," *RSC Advances,* vol. 4, pp. 16803-16812, 2014.
[24] R. L. Jones, B. L. Harrod, and J. D. Batteas, "Intercalation of 3-Phenyl-1-proponal into OTS SAMs on Silica Nanoasperities to Create Self-Repairing Interfaces for MEMS Lubrication†," *Langmuir,* vol. 26, pp. 16355-16361, 2010/11/02 2010.
[25] J. E. Raynor, J. R. Capadona, D. M. Collard, T. A. Petrie, and A. J. García, "Polymer brushes and self-assembled monolayers: Versatile platforms to control cell adhesion to biomaterials (Review)," *Biointerphases,* vol. 4, pp. FA3-FA16, 2009.
[26] I. Luzinov, D. Julthongpiput, V. Gorbunov, and V. V. Tsukruk, "Nanotribological behavior of tethered reinforced polymer nanolayer coatings," *Tribology International,* vol. 34, pp. 327-333, 5// 2001.
[27] R. Bielecki, M. Crobu, and N. Spencer, "Polymer-Brush Lubrication in Oil: Sliding Beyond the Stribeck Curve," *Tribology Letters,* vol. 49, pp. 263-272, 2013/01/01 2013.
[28] K. Matyjaszewski and J. Xia, "Atom Transfer Radical Polymerization," *Chemical Reviews,* vol. 101, pp. 2921-2990, 2001/09/01 2001.
[29] L. Wang, R. J. K. Wood, T. J. Harvey, S. Morris, H. E. G. Powrie, and I. Care, "Wear performance of oil lubricated silicon nitride sliding against various bearing steels," *Wear,* vol. 255, pp. 657-668, 8// 2003.
[30] A. Ulman, "Formation and structure of self-assembled monolayers," *Chemical reviews,* vol. 96, pp. 1533-1554, 1996.
[31] R. G. Nuzzo and D. L. Allara, "Adsorption of bifunctional organic disulfides on gold surfaces," *Journal of the American Chemical Society,* vol. 105, pp. 4481-4483, 1983/06/01 1983.
[32] S. A. Kulkarni, S. A. Mirji, A. B. Mandale, R. P. Gupta, and K. P. Vijayamohanan, "Growth kinetics and thermodynamic stability of octadecyltrichlorosilane self-assembled monolayer on Si (100) substrate," *Materials Letters,* vol. 59, pp. 3890-3895, 12// 2005.
[33] T. Manifar, A. Rezaee, M. Sheikhzadeh, and S. Mittler, "Formation of uniform self-assembly monolayers by choosing the right solvent: OTS on silicon wafer, a case study," *Applied Surface Science,* vol. 254, pp. 4611-4619, 5/30/ 2008.
[34] F. Schreiber, "Structure and growth of self-assembling monolayers," *Progress in Surface Science,* vol. 65, pp. 151-257, 11// 2000.
[35] S. Frank, "Self-assembled monolayers: from 'simple' model systems to biofunctionalized interfaces," *Journal of Physics: Condensed Matter,* vol. 16, p. R881, 2004.
[36] W. Yang and F. Zhou, "Polymer brushes for antibiofouling and lubrication," *Biosurface and Biotribology,* vol. 3, pp. 97-114, 2017/09/01/ 2017.
[37] K. Bierbaum, M. Grunze, A. A. Baski, L. F. Chi, W. Schrepp, and H. Fuchs, "Growth of Self-Assembled n-Alkyltrichlorosilane Films on Si(100) Investigated by Atomic Force Microscopy," *Langmuir,* vol. 11, pp. 2143-2150, 1995/06/01 1995.
[38] D. K. Aswal, S. Lenfant, D. Guerin, J. V. Yakhmi, and D. Vuillaume, "Self assembled monolayers on silicon for molecular electronics," *Analytica Chimica Acta,* vol. 568, pp. 84-108, 5/24/ 2006.
[39] T. Balgar, R. Bautista, N. Hartmann, and E. Hasselbrink, "An AFM study of the growth kinetics of the self-assembled octadecylsiloxane monolayer on oxidized silicon," *Surface Science,* vol. 532–535, pp. 963-969, 6/10/ 2003.

[40] R. Walsh, "Bond dissociation energy values in silicon-containing compounds and some of their implications," *Accounts of Chemical Research,* vol. 14, pp. 246-252, 1981/08/01 1981.
[41] J. Dong, A. Wang, K. Y. S. Ng, and G. Mao, "Self-assembly of octadecyltrichlorosilane monolayers on silicon-based substrates by chemical vapor deposition," *Thin Solid Films,* vol. 515, pp. 2116-2122, 12/5/ 2006.
[42] K. Bierbaum, M. Kinzler, C. Woell, M. Grunze, G. Haehner, S. Heid*, et al.*, "A Near Edge X-ray Absorption Fine Structure Spectroscopy and X-ray Photoelectron Spectroscopy Study of the Film Properties of Self-Assembled Monolayers of Organosilanes on Oxidized Si(100)," *Langmuir,* vol. 11, pp. 512-518, 1995/02/01 1995.
[43] T. A. Witten and L. M. Sander, "Diffusion-Limited Aggregation, a Kinetic Critical Phenomenon," *Physical Review Letters,* vol. 47, pp. 1400-1403, 11/09/ 1981.
[44] M. M. Sung, C. Carraro, O. W. Yauw, Y. Kim, and R. Maboudian, "Reversible Liquid−Liquid Transitions in the Early Stages of Monolayer Self-Assembly," *The Journal of Physical Chemistry B,* vol. 104, pp. 1556-1559, 2000/02/01 2000.
[45] I. Doudevski, W. A. Hayes, J. T. Woodward, and D. K. Schwartz, "Atomic force microscope imaging of molecular aggregation during self-assembled monolayer growth," *Colloids and Surfaces A: Physicochemical and Engineering Aspects,* vol. 174, pp. 233-243, 11/15/ 2000.
[46] D. Appelhans, D. Ferse, H. J. P. Adler, W. Plieth, A. Fikus, K. Grundke*, et al.*, "Self-assembled monolayers prepared from ω-thiophene-functionalized n-alkyltrichlorosilane on silicon substrates," *Colloids and Surfaces A: Physicochemical and Engineering Aspects,* vol. 161, pp. 203-212, 1/15/ 2000.
[47] D. K. Schwartz, S. Steinberg, J. Israelachvili, and J. A. N. Zasadzinski, "Growth of a self-assembled monolayer by fractal aggregation," *Physical Review Letters,* vol. 69, pp. 3354-3357, 12/07/ 1992.
[48] Y. Wang and M. Lieberman, "Growth of Ultrasmooth Octadecyltrichlorosilane Self-Assembled Monolayers on SiO2," *Langmuir,* vol. 19, pp. 1159-1167, 2003/02/01 2003.
[49] M. Salmeron, "Generation of defects in model lubricant monolayers and their contribution to energy dissipation in friction," *Tribology Letters,* vol. 10, pp. 69-79, 2001/01/01 2001.
[50] I. Choi, Y. Kim, S. K. Kang, J. Lee, and J. Yi, "Phase Separation of a Mixed Self-Assembled Monolayer Prepared via a Stepwise Method," *Langmuir,* vol. 22, pp. 4885-4889, 2006/05/01 2006.
[51] I. Doudevski and D. K. Schwartz, "Concentration Dependence of Self-Assembled Monolayer Island Nucleation and Growth," *Journal of the American Chemical Society,* vol. 123, pp. 6867-6872, 2001/07/01 2001.
[52] V. V. Tsukruk, I. Luzinov, and D. Julthongpiput, "Sticky Molecular Surfaces: Epoxysilane Self-Assembled Monolayers," *Langmuir,* vol. 15, pp. 3029-3032, 1999/04/01 1999.
[53] J. J. Benítez, S. Kopta, D. F. Ogletree, and M. Salmeron, "Preparation and Characterization of Self-Assembled Monolayers of Octadecylamine on Mica Using Hydrophobic Solvents," *Langmuir,* vol. 18, pp. 6096-6100, 2002/08/01 2002.
[54] Z. Kang, Q. Liu, and Y. Liu, "Preparation and micro-tribological property of hydrophilic self-assembled monolayer on single crystal silicon surface," *Wear,* vol. 303, pp. 297-301, 6/15/ 2013.
[55] N. Rozlosnik, M. C. Gerstenberg, and N. B. Larsen, "Effect of Solvents and Concentration on the Formation of a Self-Assembled Monolayer of Octadecylsiloxane on Silicon (001)," *Langmuir,* vol. 19, pp. 1182-1188, 2003/02/01 2003.
[56] D. K. Schwartz, "MECHANISMS AND KINETICS OF SELF-ASSEMBLED MONOLAYER FORMATION," *Annual Review of Physical Chemistry,* vol. 52, pp. 107-137, 2001.
[57] B. Cui, J. Zhang, and J. Chen, "Tribological properties of poly(amide amine) and small molecule composite self-assembled monolayers: Influence of functional group of small molecule," *Tribology International,* vol. 62, pp. 149-154, 6// 2013.

[58] M. Masuko, H. Miyamoto, and A. Suzuki, "Tribological characteristics of self-assembled monolayer with siloxane bonding to Si surface," *Tribology International,* vol. 40, pp. 1587-1596, 10// 2007.
[59] N. Satyanarayana and K. S. Sujeet, "Tribology of PFPE overcoated self-assembled monolayers deposited on Si surface," *Journal of Physics D: Applied Physics,* vol. 38, p. 3512, 2005.
[60] S. Song, L. Liu, and J. Zhang, "Annealing improves tribological property of poly(octadecene-alt-maleic anhydride) self-assembled film," *Applied Surface Science,* vol. 257, pp. 10254-10260, 9/15/ 2011.
[61] K. Wang, D. Xiong, and Y. Niu, "Novel lubricated surface of titanium alloy based on porous structure and hydrophilic polymer brushes," *Applied Surface Science,* vol. 317, pp. 875-883, 10/30/ 2014.
[62] D. Xiong, Y. Deng, N. Wang, and Y. Yang, "Influence of surface PMPC brushes on tribological and biocompatibility properties of UHMWPE," *Applied Surface Science,* vol. 298, pp. 56-61, 4/15/ 2014.
[63] L. G. Yu, E. S. Yamaguchi, M. Kasrai, and G. M. Bancroft, "Study of silane-based antiwear additives: Wear and chemistry," *Tribology International,* vol. 44, pp. 692-701, 6// 2011.
[64] J. Zhao, M. Chen, Y. An, J. Liu, and F. Yan, "Preparation of polystyrene brush film by radical chain-transfer polymerization and micromechanical properties," *Applied Surface Science,* vol. 255, pp. 2295-2302, 12/30/ 2008.
[65] B. D. Booth, N. J. Martin, E. A. Buehler, C. McCabe, and G. K. Jennings, "Tribological characterization of gradient monolayer films from trichlorosilanes on silicon," *Colloids and Surfaces A: Physicochemical and Engineering Aspects,* vol. 412, pp. 57-63, 10/20/ 2012.
[66] K. Busuttil, N. Nikogeorgos, Z. Zhang, M. Geoghegan, C. A. Hunter, and G. J. Leggett, "The mechanics of nanometre-scale molecular contacts," *Faraday Discussions,* vol. 156, pp. 325-341, 2012.
[67] J. Feng, G. H. Xu, Y. An, and X. Zeng, "Construction of the homogeneously mixed SAM composed of octyltriethoxysilane and octadecyltrichlorosilane by taking advantage of the molecular steric restriction," *Colloids and Surfaces A: Physicochemical and Engineering Aspects,* vol. 316, pp. 194-201, 3/5/ 2008.
[68] N. R. Glass, R. Tjeung, P. Chan, L. Y. Yeo, and J. R. Friend, "Organosilane deposition for microfluidic applications," *Biomicrofluidics,* vol. 5, pp. -, 2011.
[69] D. S. Grierson and R. W. Carpick, "Nanotribology of carbon-based materials," *Nano Today,* vol. 2, pp. 12-21, 10// 2007.
[70] J. Li and X. Z. Li, "The preparation and tribological characteristics of phosphorylated 3-aminopropyltriethoxysilane self-assembled film," *Applied Surface Science,* vol. 255, pp. 6159-6163, 4/1/ 2009.
[71] S. Liu, J. Ou, Z. Li, S. Yang, and J. Wang, "Layer-by-layer assembly and tribological property of multilayer ultrathin films constructed by modified graphene sheets and polyethyleneimine," *Applied Surface Science,* vol. 258, pp. 2231-2236, 1/15/ 2012.
[72] J. Q. Ma, C. J. Pang, Y. F. Mo, and M. W. Bai, "Preparation and tribological properties of multiply-alkylated cyclopentane (MAC)–octadecyltrichlorosilane (OTS) double-layer film on silicon," *Wear,* vol. 263, pp. 1000-1007, 9/10/ 2007.
[73] M.-K. Park, G. Sakellariou, S. Pispas, N. Hadjichristidis, and R. Advincula, "On the quantitative adsorption behavior of multi-zwitterionic end-functionalized polymers onto gold surfaces," *Colloids and Surfaces A: Physicochemical and Engineering Aspects,* vol. 326, pp. 115-121, 9/1/ 2008.
[74] S.-L. Ren, S.-R. Yang, J.-Q. Wang, W.-M. Liu, and Y.-P. Zhao, "Preparation and Tribological Studies of Stearic Acid Self-Assembled Monolayers on Polymer-Coated Silicon Surface," *Chemistry of Materials,* vol. 16, pp. 428-434, 2004/02/01 2004.
[75] C. Zhang, S. Zhang, P. Gao, H. Ma, and Q. Wei, "Superhydrophobic hybrid films prepared from silica nanoparticles and ionic liquids via layer-by-layer self-assembly," *Thin Solid Films,* vol. 570, Part A, pp. 27-32, 11/3/ 2014.

[76] G. Yang, C. Zhang, S. Zhang, L. Yu, and P. Zhang, "Preparation of sandwich-like self-assembled n-octanethiol film containing doped silver nanoparticles on silicon wafer and evaluation of its tribological properties," *Materials Research Bulletin,* vol. 55, pp. 88-94, 7// 2014.

[77] N. Satyanarayana, S. K. Sinha, and M. P. Srinivasan, "Friction and wear life evaluation of silane based self assembled monolayers on silicon surface," in *Tribology and Interface Engineering Series*. vol. Volume 48, M. P. G. D. D. Dowson and A. A. Lubrecht, Eds., ed: Elsevier, 2005, pp. 821-826.

[78] S. Han, K. Suga, M. Fujihira, and B.-E. Park, "Novel tip modification method for measurement of the adhesive force between a silanized surface and a locally modified tip using atomic force microscopy," *Journal of the Korean Physical Society,* vol. 64, pp. 63-68, 2014/01/01 2014.

[79] K. Raiber, A. Terfort, C. Benndorf, N. Krings, and H.-H. Strehblow, "Removal of self-assembled monolayers of alkanethiolates on gold by plasma cleaning," *Surface Science,* vol. 595, pp. 56-63, 12/5/ 2005.

[80] D. Skácelová, V. Danilov, J. Schäfer, A. Quade, P. Sťahel, M. Černák*, et al.*, "Room temperature plasma oxidation in DCSBD: A new method for preparation of silicon dioxide films at atmospheric pressure," *Materials Science and Engineering: B,* vol. 178, pp. 651-655, 5/15/ 2013.

[81] D. Skácelová, M. Stupavská, P. Sťahel, and M. Černák, "Modification of (1 1 1) and (1 0 0) silicon in atmospheric pressure plasma," *Applied Surface Science,* vol. 312, pp. 203-207, 9/1/ 2014.

[82] L. Wu, L. Cai, A. Liu, W. Wang, Y. Yuan, and Z. Li, "Self-assembled monolayers of perfluoroalkylsilane on plasma-hydroxylated silicon substrates," *Applied Surface Science,* vol. 349, pp. 683-694, 9/15/ 2015.

[83] M. Wiegand, M. Reiche, and U. Gösele, "Time‐Dependent Surface Properties and Wafer Bonding of O 2 ‐ Plasma ‐ Treated Silicon (100) Surfaces," *Journal of The Electrochemical Society,* vol. 147, pp. 2734-2740, July 1, 2000 2000.

[84] V. Bhatt and S. Chandra, "Silicon Nitride Films Deposited by RF Sputtering for Microstructure Fabrication in MEMS," *Journal of Electronic Materials,* vol. 38, pp. 1979-1989, 2009/09/01 2009.

[85] R. Maboudian and C. Carraro, "SURFACE CHEMISTRY AND TRIBOLOGY OF MEMS," *Annual Review of Physical Chemistry,* vol. 55, pp. 35-54, 2004/06/01 2004.

[86] D. Xu, W. H. Yu, E. T. Kang, and K. G. Neoh, "Functionalization of hydrogen-terminated silicon via surface-initiated atom-transfer radical polymerization and derivatization of the polymer brushes," *Journal of Colloid and Interface Science,* vol. 279, pp. 78-87, 11/1/ 2004.

[87] H. Sano, M. Zhao, D. Kasahara, K. Murase, T. Ichii, and H. Sugimura, "Formation of uniform ferrocenyl-terminated monolayer covalently bonded to Si using reaction of hydrogen-terminated Si(1 1 1) surface with vinylferrocene/n-decane solution by visible-light excitation," *Journal of Colloid and Interface Science,* vol. 361, pp. 259-269, 9/1/ 2011.

[88] R. Boukherroub, "Chemical reactivity of hydrogen-terminated crystalline silicon surfaces," *Current Opinion in Solid State and Materials Science,* vol. 9, pp. 66-72, 2// 2005.

[89] S. Y. Lee, Y. Choi, E. Ito, M. Hara, H. Lee, and J. Noh, "Growth, solvent effects, and thermal desorption behavior of octylthiocyanate self-assembled monolayers on Au(111)," *Physical Chemistry Chemical Physics,* vol. 15, pp. 3609-3617, 2013.

[90] S. Hsieh, W.-J. Chao, P.-Y. Lin, and C.-W. Hsieh, "Influence of molecular packing on the corrosion inhibition properties of self-assembled octadecyltrichlorosilane monolayers on silicon," *Corrosion Science,* vol. 80, pp. 427-433, 3// 2014.

[91] M. E. McGovern, K. M. R. Kallury, and M. Thompson, "Role of Solvent on the Silanization of Glass with Octadecyltrichlorosilane," *Langmuir,* vol. 10, pp. 3607-3614, 1994/10/01 1994.

[92] L. T. Zhuravlev, "Concentration of hydroxyl groups on the surface of amorphous silicas," *Langmuir,* vol. 3, pp. 316-318, 1987/05/01 1987.

[93] J. C. Love, L. A. Estroff, J. K. Kriebel, R. G. Nuzzo, and G. M. Whitesides, "Self-Assembled Monolayers of Thiolates on Metals as a Form of Nanotechnology," *Chemical Reviews,* vol. 105, pp. 1103-1170, 2005/04/01 2005.
[94] A. Borruto, G. Crivellone, and F. Marani, "Influence of surface wettability on friction and wear tests," *Wear,* vol. 222, pp. 57-65, 11// 1998.
[95] B. D. Beake, J. S. G. Ling, and G. J. Leggett, "Correlation of friction, adhesion, wettability and surface chemistry after argon plasma treatment of poly(ethylene terephthalate)," *Journal of Materials Chemistry,* vol. 8, pp. 2845-2854, 1998.
[96] D. Devaprakasam, O. P. Khatri, N. Shankar, and S. K. Biswas, "Boundary lubrication additives for aluminium: A journey from nano to macrotribology," *Tribology International,* vol. 38, pp. 1022-1034, 11// 2005.
[97] Z. Pawlak, W. Urbaniak, and A. Oloyede, "The relationship between friction and wettability in aqueous environment," *Wear,* vol. 271, pp. 1745-1749, 7/29/ 2011.
[98] R. Prioli, L. G. Jacobsohn, M. E. H. Maia da Costa, and F. L. Freire, Jr., "Nanotribological Properties of Amorphous Carbon-Fluorine Films," *Tribology Letters,* vol. 15, pp. 177-180, 2003/10/01 2003.
[99] Y. C. Jung and B. Bhushan, "Wetting Behavior of Water and Oil Droplets in Three-Phase Interfaces for Hydrophobicity/philicity and Oleophobicity/philicity," *Langmuir,* vol. 25, pp. 14165-14173, 2009/12/15 2009.
[100] E. Bormashenko, Y. Bormashenko, G. Whyman, R. Pogreb, A. Musin, R. Jager*, et al.*, "Contact Angle Hysteresis on Polymer Substrates Established with Various Experimental Techniques, Its Interpretation, and Quantitative Characterization," *Langmuir,* vol. 24, pp. 4020-4025, 2008/04/01 2008.
[101] K.-Y. Yeh, L.-J. Chen, and J.-Y. Chang, "Contact Angle Hysteresis on Regular Pillar-like Hydrophobic Surfaces," *Langmuir,* vol. 24, pp. 245-251, 2008/01/01 2008.
[102] M. Callewaert, C. Grandfils, L. Boulangé-Petermann, and P. G. Rouxhet, "Adsorption of poly(N-isopropylacrylamide) on glass substrata," *Journal of Colloid and Interface Science,* vol. 276, pp. 299-305, 8/15/ 2004.
[103] D. Song, B. Song, H. Hu, X. Du, and Z. Ma, "Contact angle and impinging process of droplets on partially grooved hydrophobic surfaces," *Applied Thermal Engineering,* vol. 85, pp. 356-364, 6/25/ 2015.
[104] S. Shibuichi, T. Yamamoto, T. Onda, and K. Tsujii, "Super Water- and Oil-Repellent Surfaces Resulting from Fractal Structure," *Journal of Colloid and Interface Science,* vol. 208, pp. 287-294, 12/1/ 1998.
[105] D. Janssen, R. De Palma, S. Verlaak, P. Heremans, and W. Dehaen, "Static solvent contact angle measurements, surface free energy and wettability determination of various self-assembled monolayers on silicon dioxide," *Thin Solid Films,* vol. 515, pp. 1433-1438, 12/5/ 2006.
[106] A. Cricenti, G. Longo, M. Luce, R. Generosi, P. Perfetti, D. Vobornik*, et al.*, "AFM and SNOM characterization of carboxylic acid terminated silicon and silicon nitride surfaces," *Surface Science,* vol. 544, pp. 51-57, 10/10/ 2003.
[107] H. Cheng and Y. Hu, "Influence of chain ordering on frictional properties of self-assembled monolayers (SAMs) in nano-lubrication," *Advances in Colloid and Interface Science,* vol. 171–172, pp. 53-65, 3// 2012.
[108] H. Fischer, "The Persistent Radical Effect In “Living” Radical Polymerization," *Macromolecules,* vol. 30, pp. 5666-5672, 1997/09/01 1997.
[109] A. Checco, H. Schollmeyer, J. Daillant, P. Guenoun, and R. Boukherroub, "Nanoscale Wettability of Self-Assembled Monolayers Investigated by Noncontact Atomic Force Microscopy," *Langmuir,* vol. 22, pp. 116-126, 2006/01/01 2006.
[110] J. Ma, J. Liu, Y. Mo, and M. Bai, "Effect of multiply-alkylated cyclopentane (MAC) on durability and load-carrying capacity of self-assembled monolayers on silicon wafer," *Colloids and Surfaces A: Physicochemical and Engineering Aspects,* vol. 301, pp. 481-489, 7/5/ 2007.

[111] B. Lego, M. François, W. G. Skene, and S. Giasson, "Polymer Brush Covalently Attached to OH-Functionalized Mica Surface via Surface-Initiated ATRP: Control of Grafting Density and Polymer Chain Length," *Langmuir,* vol. 25, pp. 5313-5321, 2009/05/05 2009.
[112] C. F. Sun, M. Zhang, F. Zhou, P. Gao, Y. Q. Xia, and W. M. Liu, "Tribological Behavior of Multiply-Alkylated Cyclopentanes (MACs)-Cu Nanoparticles Composite Thin Film," *Journal of Macromolecular Science Part B-Physics,* vol. 50, pp. 1006-1017, 2011/05/03 2011.
[113] L. B. Picraux, C. D. Zangmeister, and J. D. Batteas, "Preparation and Structure of a Low-Density, Flat-Lying Decanethiol Monolayer from the Densely Packed, Upright Monolayer on Gold," *Langmuir,* vol. 22, pp. 174-180, 2006/01/01 2006.
[114] J. Tersoff and D. R. Hamann, "Theory and Application for the Scanning Tunneling Microscope," *Physical Review Letters,* vol. 50, pp. 1998-2001, 06/20/ 1983.
[115] G. Binnig, H. Rohrer, C. Gerber, and E. Weibel, "Surface Studies by Scanning Tunneling Microscopy," *Physical Review Letters,* vol. 49, pp. 57-61, 07/05/ 1982.
[116] G. Binnig and H. Rohrer, "Scanning tunneling microscopy\char22{}from birth to adolescence," *Reviews of Modern Physics,* vol. 59, pp. 615-625, 07/01/ 1987.
[117] M. Sprik, E. Delamarche, B. Michel, U. Roethlisberger, M. L. Klein, H. Wolf*, et al.*, "Structure of Hydrophilic Self-Assembled Monolayers: A Combined Scanning Tunneling Microscopy and Computer Simulation Study," *Langmuir,* vol. 10, pp. 4116-4130, 1994/11/01 1994.
[118] K. Edinger, A. Goelzhaeuser, K. Demota, C. Woell, and M. Grunze, "Formation of self-assembled monolayers of n-alkanethiols on gold: a scanning tunneling microscopy study on the modification of substrate morphology," *Langmuir,* vol. 9, pp. 4-8, 1993/01/01 1993.
[119] L. Qin, W. Zhao, H. Hou, Y. Jin, Z. Zeng, X. Wu*, et al.*, "Achieving excellent anti-corrosion and tribological performance by tailoring the surface morphology and chemical composition of aluminum alloys," *RSC Advances,* vol. 4, pp. 60307-60315, 2014.
[120] S. V. Merzlikin, N. N. Tolkachev, T. Strunskus, G. Witte, T. Glogowski, C. Wöll*, et al.*, "Resolving the depth coordinate in photoelectron spectroscopy – Comparison of excitation energy variation vs. angular-resolved XPS for the analysis of a self-assembled monolayer model system," *Surface Science,* vol. 602, pp. 755-767, 2/1/ 2008.
[121] W. A. M. Aarnink, A. Weishaupt, and A. van Silfhout, "Angle-resolved X-ray photoelectron spectroscopy (ARXPS) and a modified Levenberg-Marquardt fit procedure: a new combination for modeling thin layers," *Applied Surface Science,* vol. 45, pp. 37-48, 8// 1990.
[122] A.-S. Duwez, "Exploiting electron spectroscopies to probe the structure and organization of self-assembled monolayers: a review," *Journal of Electron Spectroscopy and Related Phenomena,* vol. 134, pp. 97-138, 2// 2004.
[123] R. Bielecki, E. Benetti, D. Kumar, and N. Spencer, "Lubrication with Oil-Compatible Polymer Brushes," *Tribology Letters,* vol. 45, pp. 477-487, 2012/03/01 2012.
[124] M. Biesalski and J. Rühe, "Synthesis of a Poly(p-styrenesulfonate) Brush via Surface-Initiated Polymerization," *Macromolecules,* vol. 36, pp. 1222-1227, 2003/02/01 2003.
[125] B. Lin, A. K. Tieu, H. Zhu, B. Kosasih, O. Novareza, and G. Triani, "Tribological performance of aqueous copolymer lubricant in loaded contact with Si and coated Ti film," *Wear,* vol. 302, pp. 1010-1016, 4// 2013.
[126] E. Turan and T. Caykara, "Construction of hydroxyl-terminated poly(N-isopropylacrylamide) brushes on silicon wafer via surface-initiated atom transfer radical polymerization," *Journal of Polymer Science Part A: Polymer Chemistry,* vol. 48, pp. 3880-3887, 2010.
[127] J. J. Gooding, F. Mearns, W. Yang, and J. Liu, "Self-assembled monolayers into the 21st century: recent advances and applications," *Electroanalysis,* vol. 15, // 2003.
[128] D. Samanta and A. Sarkar, "Immobilization of bio-macromolecules on self-assembled monolayers: methods and sensor applications," *Chemical Society Reviews,* vol. 40, pp. 2567-2592, 2011.

[129] A. Kumar, H. A. Biebuyck, and G. M. Whitesides, "Patterning Self-Assembled Monolayers: Applications in Materials Science," *Langmuir,* vol. 10, pp. 1498-1511, 1994/05/01 1994.
[130] R. K. Smith, P. A. Lewis, and P. S. Weiss, "Patterning self-assembled monolayers," *Progress in Surface Science,* vol. 75, pp. 1-68, 6// 2004.
[131] M. Mrksich and G. M. Whitesides, "Patterning self-assembled monolayers using microcontact printing: A new technology for biosensors?," *Trends in Biotechnology,* vol. 13, pp. 228-235, 6// 1995.
[132] A. Y. Fadeev and T. J. McCarthy, "Self-Assembly Is Not the Only Reaction Possible between Alkyltrichlorosilanes and Surfaces: Monomolecular and Oligomeric Covalently Attached Layers of Dichloro- and Trichloroalkylsilanes on Silicon," *Langmuir,* vol. 16, pp. 7268-7274, 2000/09/01 2000.
[133] S.-J. Chun, S.-Y. Lee, G.-Y. Jeong, and J. H. Kim, "Fabrication of hydrophobic self-assembled monolayers (SAM) on the surface of ultra-strength nanocellulose films," *Journal of Industrial and Engineering Chemistry,* vol. 18, pp. 1122-1127, 5/25/ 2012.
[134] B. D. Booth, S. G. Vilt, J. B. Lewis, J. L. Rivera, E. A. Buehler, C. McCabe*, et al.*, "Tribological Durability of Silane Monolayers on Silicon," *Langmuir,* vol. 27, pp. 5909-5917, 2011/05/17 2011.
[135] Y. Song, R. Premachandran Nair, M. Zou, and Y. A. Wang, "Adhesion and friction properties of micro/nano-engineered superhydrophobic/hydrophobic surfaces," *Thin Solid Films,* vol. 518, pp. 3801-3807, 5/3/ 2010.
[136] J. Cancino and S. A. S. Machado, "Microelectrode array in mixed alkanethiol self-assembled monolayers: Electrochemical studies," *Electrochimica Acta,* vol. 72, pp. 108-113, 6/30/ 2012.
[137] M. J. Wirth, R. W. P. Fairbank, and H. O. Fatunmbi, "Mixed Self-Assembled Monolayers in Chemical Separations," *Science,* vol. 275, pp. 44-47, January 3, 1997 1997.
[138] J. Cancino, C. A. Razzino, V. Zucolotto, and S. A. S. Machado, "The use of mixed self-assembled monolayers as a strategy to improve the efficiency of carbamate detection in environmental monitoring," *Electrochimica Acta,* vol. 87, pp. 717-723, 1/1/ 2013.
[139] T. Deng, J.-S. Li, S.-Y. Huan, H.-F. Yang, H. Wang, G.-L. Shen*, et al.*, "Quartz crystal microbalance bioaffinity sensor for biotin based on mixed self-assembled monolayers and metastable molecular complex receptor," *Biosensors and Bioelectronics,* vol. 21, pp. 1545-1552, 2/15/ 2006.
[140] A. Brechling, M. Sundermann, U. Kleineberg, and U. Heinzmann, "Characterization of DMPC bilayers and multilamellar islands on hydrophobic self-assembled monolayers of ODS/Si(100) and mixed ODS-DDS/Si(100)," *Thin Solid Films,* vol. 433, pp. 281-286, 6/2/ 2003.
[141] M. V. Bracamonte, O. E. L. Pérez, M. L. Teijelo, G. A. Rivas, and N. F. Ferreyra, "Quaternized chitosan mediated assembly of gold nanoparticles multilayers," *Electrochimica Acta,* vol. 146, pp. 178-185, 11/10/ 2014.
[142] F. Bordi, C. Cametti, and A. Gliozzi, "Impedance measurements of self-assembled lipid bilayer membranes on the tip of an electrode," *Bioelectrochemistry,* vol. 57, pp. 39-46, 7// 2002.
[143] H. T. Tien and A. L. Ottova, "From self-assembled bilayer lipid membranes (BLMs) to supported BLMs on metal and gel substrates to practical applications," *Colloids and Surfaces A: Physicochemical and Engineering Aspects,* vol. 149, pp. 217-233, 4/15/ 1999.
[144] R. P. Richter, R. Bérat, and A. R. Brisson, "Formation of Solid-Supported Lipid Bilayers: An Integrated View," *Langmuir,* vol. 22, pp. 3497-3505, 2006/04/01 2006.
[145] S. Terrettaz, M. Mayer, and H. Vogel, "Highly Electrically Insulating Tethered Lipid Bilayers for Probing the Function of Ion Channel Proteins," *Langmuir,* vol. 19, pp. 5567-5569, 2003/07/01 2003.
[146] F. Berger, J. Delhalle, and Z. Mekhalif, "Self-assembled bilayers based on organothiol and organotrimethoxysilane on zinc platform," *Applied Surface Science,* vol. 256, pp. 7131-7137, 9/15/ 2010.

[147] Z. Zhu, G. Xu, Y. An, and C. He, "Construction of octadecyltrichlorosilane self-assembled monolayer on stainless steel 316L surface," *Colloids and Surfaces A: Physicochemical and Engineering Aspects,* vol. 457, pp. 408-413, 9/5/ 2014.
[148] K. Deng, R. J. Collins, M. Mehregany, and C. N. Sukenik, "Performance Impact of Monolayer Coating of Polysilicon Micromotors," *Journal of The Electrochemical Society,* vol. 142, pp. 1278-1285, April 1, 1995 1995.
[149] Y. Liu, P. Liu, Y. Xiao, and J. Luo, "Investigation on growth process and tribological behavior of mixed alkylsilane self-assembled molecular films in aqueous solution," *Applied Surface Science,* vol. 258, pp. 8533-8537, 9/1/ 2012.
[150] M. Cichomski, K. Kośla, J. Grobelny, W. Kozłowski, and W. Szmaja, "Tribological and stability investigations of alkylphosphonic acids on alumina surface," *Applied Surface Science,* vol. 273, pp. 570-577, 5/15/ 2013.
[151] F. E. Kennedy, Y. Lu, and I. Baker, "Contact temperatures and their influence on wear during pin-on-disk tribotesting," *Tribology International,* vol. 82, Part B, pp. 534-542, 2// 2015.
[152] R. Novak and T. Polcar, "Tribological analysis of thin films by pin-on-disc: Evaluation of friction and wear measurement uncertainty," *Tribology International,* vol. 74, pp. 154-163, 6// 2014.
[153] D. L. Burris and W. G. Sawyer, "Addressing Practical Challenges of Low Friction Coefficient Measurements," *Tribology Letters,* vol. 35, pp. 17-23, 2009/07/01 2009.
[154] T. L. Schmitz, J. E. Action, J. C. Ziegert, and W. G. Sawyer, "The Difficulty of Measuring Low Friction: Uncertainty Analysis for Friction Coefficient Measurements," *Journal of Tribology,* vol. 127, pp. 673-678, 2005.
[155] T. J. Kamps, J. C. Walker, R. J. Wood, P. M. Lee, and A. G. Plint, "Reproducing automotive engine scuffing using a lubricated reciprocating contact," *Wear,* vol. 332–333, pp. 1193-1199, 5// 2015.
[156] C. B. Mohan, C. Divakar, K. Venkatesh, K. Gopalakrishna, K. S. Mahesh Lohith, and T. N. Naveen, "Design and development of an advanced linear reciprocating tribometer," *Wear,* vol. 267, pp. 1111-1116, 6/15/ 2009.
[157] D. H. Hwang and K. H. Zum Gahr, "Transition from static to kinetic friction of unlubricated or oil lubricated steel/steel, steel/ceramic and ceramic/ceramic pairs," *Wear,* vol. 255, pp. 365-375, 8// 2003.
[158] M. Kosinskiy, S. I.-U. Ahmed, Y. Liu, and J. A. Schaefer, "A compact reciprocating vacuum microtribometer," *Tribology International,* vol. 56, pp. 81-88, 12// 2012.
[159] E.-S. Yoon, R. A. Singh, H.-J. Oh, and H. Kong, "The effect of contact area on nano/micro-scale friction," *Wear,* vol. 259, pp. 1424-1431, 7// 2005.
[160] B. Bhushan and S. Sundararajan, "Micro/nanoscale friction and wear mechanisms of thin films using atomic force and friction force microscopy," *Acta Materialia,* vol. 46, pp. 3793-3804, 7/1/ 1998.
[161] S. P. Ho, R. W. Carpick, T. Boland, and M. LaBerge, "Nanotribology of CoCr–UHMWPE TJR prosthesis using atomic force microscopy," *Wear,* vol. 253, pp. 1145-1155, 12// 2002.
[162] B. Bhushan, "Micro/nanotribology and its applications to magnetic storage devices and MEMS," *Tribology International,* vol. 28, pp. 85-96, 3// 1995.
[163] K.-H. Cha and D.-E. Kim, "Investigation of the tribological behavior of octadecyltrichlorosilane deposited on silicon," *Wear,* vol. 251, pp. 1169-1176, 10// 2001.
[164] V. DePalma and N. Tillman, "Friction and wear of self-assembled trichlorosilane monolayer films on silicon," *Langmuir,* vol. 5, pp. 868-872, 1989/05/01 1989.
[165] E. E. Flater, W. R. Ashurst, and R. W. Carpick, "Nanotribology of Octadecyltrichlorosilane Monolayers and Silicon: Self-Mated versus Unmated Interfaces and Local Packing Density Effects," *Langmuir,* vol. 23, pp. 9242-9252, 2007/08/01 2007.
[166] M. Garcia-Parajo, C. Longo, J. Servat, P. Gorostiza, and F. Sanz, "Nanotribological Properties of Octadecyltrichlorosilane Self-Assembled Ultrathin Films Studied by Atomic Force Microscopy: Contact and Tapping Modes," *Langmuir,* vol. 13, pp. 2333-2339, 1997/04/01 1997.

[167] R. A. Singh, J. Kim, S. W. Yang, J.-E. Oh, and E.-S. Yoon, "Tribological properties of trichlorosilane-based one- and two-component self-assembled monolayers," *Wear,* vol. 265, pp. 42-48, 6/25/ 2008.
[168] L. Wang and R. J. K. Wood, "Acoustic emissions from lubricated hybrid contacts," *Tribology International,* vol. 42, pp. 1629-1637, 12// 2009.
[169] A. Wang, S. Yan, B. Lin, X. Zhang, and X. Zhou, "Aqueous lubrication and surface microstructures of engineering polymer materials (PEEK and PI) when sliding against Si3N4," *Friction,* vol. 5, pp. 414-428, December 01 2017.
[170] S. Strobl, T. Lube, P. Supancic, M. Stoiser, O. Schöppl, and R. Danzer, "Mechanical properties of silicon nitride rolling elements in dependence of size and shape," *Journal of the European Ceramic Society,* vol. 34, pp. 4167-4176, 12// 2014.
[171] L. Wang, R. W. Snidle, and L. Gu, "Rolling contact silicon nitride bearing technology: a review of recent research," *Wear,* vol. 246, pp. 159-173, 11// 2000.
[172] K. Thoma, L. Rohr, H. Rehmann, S. Roos, and J. Michler, "Materials failure mechanisms of hybrid ball bearings with silicon nitride balls," *Tribology International,* vol. 37, pp. 463-471, 6// 2004.
[173] S. A. Baker, M. J. Dellavecchia, B. W. Smith, and J. D. Winefordner, "Analysis of silicon nitride bearings with laser ablation inductively coupled plasma mass spectrometry," *Analytica Chimica Acta,* vol. 355, pp. 113-119, 11/28/ 1997.
[174] R. C. Dante and C. K. Kajdas, "A review and a fundamental theory of silicon nitride tribochemistry," *Wear,* vol. 288, pp. 27-38, 5/30/ 2012.
[175] B. S. Bal and M. N. Rahaman, "Orthopedic applications of silicon nitride ceramics," *Acta Biomaterialia,* vol. 8, pp. 2889-2898, 8// 2012.
[176] V. Ferreira, H. N. Yoshimura, and A. Sinatora, "Ultra-low friction coefficient in alumina–silicon nitride pair lubricated with water," *Wear,* vol. 296, pp. 656-659, 8/30/ 2012.
[177] Y. Hibi and Y. Enomoto, "Tribochemical wear of silicon nitride in water, n-alcohols and their mixtures," *Wear,* vol. 133, pp. 133-145, 9// 1989.
[178] J. Xu and K. Kato, "Formation of tribochemical layer of ceramics sliding in water and its role for low friction," *Wear,* vol. 245, pp. 61-75, 10// 2000.
[179] S. Hampshire, "Silicon nitride ceramics - review of structure, processing and properties," *Journal of Achievements in Materials and Manufacturing Engineering,* 2007.
[180] F. L. Riley, "Silicon Nitride and Related Materials," *Journal of the American Ceramic Society,* vol. 83, pp. 245-265, 2000.
[181] H. Bhaskaran, B. Gotsmann, A. Sebastian, U. Drechsler, M. A. Lantz, M. Despont*, et al.*, "Ultralow nanoscale wear through atom-by-atom attrition in silicon-containing diamond-like carbon," *Nat Nano,* vol. 5, pp. 181-185, 03//print 2010.
[182] R. S. Gates and S. M. Hsu, "Silicon Nitride Boundary Lubrication: Effect of Sulfonate, Phenate and Salicylate Compounds," *Tribology Transactions,* vol. 43, pp. 269-274, 2000/01/01 2000.
[183] W. Hartung, A. Rossi, S. Lee, and N. Spencer, "Aqueous Lubrication of SiC and Si3N4 Ceramics Aided by a Brush-like Copolymer Additive, Poly(l-lysine)-graft-poly(ethylene glycol)," *Tribology Letters,* vol. 34, pp. 201-210, 2009/06/01 2009.
[184] H. K. Hunt and A. M. Armani, "Bioconjugation Strategies for Label-Free Optical Microcavity Sensors," *Selected Topics in Quantum Electronics, IEEE Journal of,* vol. 20, pp. 121-133, 2014.
[185] M. M. Sung, G. J. Kluth, and R. Maboudian, "Formation of alkylsiloxane self-assembled monolayers on Si3N4," *Journal of Vacuum Science & Technology A,* vol. 17, pp. 540-544, 1999.
[186] G. J. Kluth, M. M. Sung, and R. Maboudian, "Thermal Behavior of Alkylsiloxane Self-Assembled Monolayers on the Oxidized Si(100) Surface," *Langmuir,* vol. 13, pp. 3775-3780, 1997/07/01 1997.
[187] M. Kölbel, R. W. Tjerkstra, G. Kim, J. Brugger, C. J. M. van Rijn, W. Nijdam*, et al.*, "Self-Assembled Monolayer Coatings on Nanostencils for the Reduction of Materials Adhesion," *Advanced Functional Materials,* vol. 13, pp. 219-224, 2003.

[188] J. Diao, D. Ren, J. R. Engstrom, and K. H. Lee, "A surface modification strategy on silicon nitride for developing biosensors," *Analytical Biochemistry,* vol. 343, pp. 322-328, 8/15/ 2005.
[189] R. Barattin and N. Voyer, "Chemical modifications of AFM tips for the study of molecular recognition events," *Chemical Communications,* pp. 1513-1532, 2008.
[190] V. V. Tsukruk and V. N. Bliznyuk, "Adhesive and Friction Forces between Chemically Modified Silicon and Silicon Nitride Surfaces," *Langmuir,* vol. 14, pp. 446-455, 1998/01/01 1998.
[191] B. Daniel and H. Christofer, "Determination of pull-off forces of textured silicon surfaces by AFM force curve analysis," *Journal of Micromechanics and Microengineering,* vol. 17, p. 1326, 2007.
[192] U. Zaghloul, G. Papaioannou, B. Bhushan, F. Coccetti, P. Pons, and R. Plana, "On the reliability of electrostatic NEMS/MEMS devices: Review of present knowledge on the dielectric charging and stiction failure mechanisms and novel characterization methodologies," *Microelectronics Reliability,* vol. 51, pp. 1810-1818, 9// 2011.
[193] Z. Yapu, "Stiction and anti-stiction in MEMS and NEMS," *Acta Mechanica Sinica,* vol. 19, pp. 1-10, 2003/02/01 2003.
[194] E. Kutnyanszky and G. J. Vancso, "Nanomechanical properties of polymer brushes by colloidal AFM probes," *European Polymer Journal,* vol. 48, pp. 8-15, 1// 2012.
[195] T. Ito, M. Namba, P. Bühlmann, and Y. Umezawa, "Modification of Silicon Nitride Tips with Trichlorosilane Self-Assembled Monolayers (SAMs) for Chemical Force Microscopy," *Langmuir,* vol. 13, pp. 4323-4332, 1997/08/01 1997.
[196] J. E. Headrick and C. L. Berrie, "Alternative Method for Fabricating Chemically Functionalized AFM Tips: Silane Modification of HF-Treated Si3N4 Probes," *Langmuir,* vol. 20, pp. 4124-4131, 2004/05/01 2004.
[197] C. D. Frisbie, L. F. Rozsnyai, A. Noy, M. S. Wrighton, and C. M. Lieber, "Functional Group Imaging by Chemical Force Microscopy," *Science,* vol. 265, pp. 2071-2074, September 30, 1994 1994.
[198] S. S. Kelkar, D. Chiavetta, and C. A. Wolden, "Formation of octadecyltrichlorosilane (OTS) self-assembled monolayers on amorphous alumina," *Applied Surface Science,* vol. 282, pp. 291-296, 10/1/ 2013.
[199] D. Wang, Y. Ni, Q. Huo, and D. E. Tallman, "Self-assembled monolayer and multilayer thin films on aluminum 2024-T3 substrates and their corrosion resistance study," *Thin Solid Films,* vol. 471, pp. 177-185, 1/3/ 2005.
[200] B. Panjwani and S. K. Sinha, "Tribology and hydrophobicity of a biocompatible GPTMS/PFPE coating on Ti6Al4V surfaces," *Journal of the Mechanical Behavior of Biomedical Materials,* vol. 15, pp. 103-111, 11// 2012.
[201] P. F. Li, Y. Xu, and X.-H. Cheng, "Chemisorption of thermal reduced graphene oxide nano-layer film on TNTZ surface and its tribological behavior," *Surface and Coatings Technology,* vol. 232, pp. 331-339, 10/15/ 2013.
[202] P. F. Li, H. Zhou, and X.-H. Cheng, "Nano/micro tribological behaviors of a self-assembled graphene oxide nanolayer on Ti/titanium alloy substrates," *Applied Surface Science,* vol. 285, Part B, pp. 937-944, 11/15/ 2013.
[203] S. Jadhav, "Self-assembled monolayers (SAMs) of carboxylic acids: an overview," *Central European Journal of Chemistry,* vol. 9, pp. 369-378, 2011/06/01 2011.
[204] M. Ratoi, C. Bovington, and H. Spikes, "Mechanism of metal carboxylate friction modifier additive behaviour," 2001.
[205] Y. Wan, Y. Wang, Q. Zhang, Z. Wang, Z. Xu, C. Liu*, et al.*, "Enhanced tribology durability of a self-assembled monolayer of alkylphosphonic acid on a textured copper substrate," *Applied Surface Science,* vol. 259, pp. 147-152, 10/15/ 2012.
[206] Q. Zhang, Y. Wan, Y. Li, S. Yang, and W. Yao, "Friction reducing behavior of stearic acid film on a textured aluminum substrate," *Applied Surface Science,* vol. 280, pp. 545-549, 9/1/ 2013.

[207] R. Simič and M. Kalin, "Adsorption mechanisms for fatty acids on DLC and steel studied by AFM and tribological experiments," *Applied Surface Science,* vol. 283, pp. 460-470, 10/15/ 2013.
[208] S. Watson, L. Wang, M. Nie, S. Hinder, and K. Stokes, "Polymer Brushes for Silicon Nitride-Steel Contacts: a Colloidal Force Microscopy Study," presented at the 72nd STLE Annual Meeting and Exhibition, 2017.
[209] S. Watson, S. Dennington, L. Wang, M. Nie, S. Hinder, and K. Stokes, "Polymer brush lubrication of the silicon nitride-steel contact: a colloidal force microscopy study," *RSC Advances,* vol. 7, pp. 42667-42676, 2017.
[210] O. Azzaroni, "Polymer brushes here, there, and everywhere: Recent advances in their practical applications and emerging opportunities in multiple research fields," *Journal of Polymer Science Part A: Polymer Chemistry,* vol. 50, pp. 3225-3258, 2012.
[211] Q. Wei, M. Cai, F. Zhou, and W. Liu, "Dramatically Tuning Friction Using Responsive Polyelectrolyte Brushes," *Macromolecules,* vol. 46, pp. 9368-9379, 2013/12/10 2013.
[212] J. Yan, B. Li, F. Zhou, and W. Liu, "Ultraviolet Light-Induced Surface-Initiated Atom-Transfer Radical Polymerization," *ACS Macro Letters,* vol. 2, pp. 592-596, 2013/07/16 2013.
[213] R. Bielecki, P. Doll, and N. Spencer, "Ultrathin, Oil-Compatible, Lubricious Polymer Coatings: A Comparison of Grafting-To and Grafting-From Strategies," *Tribology Letters,* vol. 49, pp. 273-280, 2013/01/01 2013.
[214] T. Goren, N. D. Spencer, and R. Crockett, "Impact of chain morphology on the lubricity of surface-grafted polysaccharides," *RSC Advances,* vol. 4, pp. 21497-21503, 2014.
[215] S. Edmondson, V. L. Osborne, and W. T. S. Huck, "Polymer brushes via surface-initiated polymerizations," *Chemical Society Reviews,* vol. 33, pp. 14-22, 2004.
[216] T. Kreer, "Polymer-brush lubrication: a review of recent theoretical advances," *Soft Matter,* vol. 12, pp. 3479-3501, 2016.
[217] B. Li, B. Yu, Q. Ye, and F. Zhou, "Tapping the Potential of Polymer Brushes through Synthesis," *Accounts of Chemical Research,* vol. 48, pp. 229-237, 2015/02/17 2015.
[218] S. Edmondson and S. P. Armes, "Synthesis of surface-initiated polymer brushes using macro-initiators," *Polymer International,* vol. 58, pp. 307-316, 2009.
[219] S. Edmondson, C.-D. Vo, S. P. Armes, and G.-F. Unali, "Surface Polymerization from Planar Surfaces by Atom Transfer Radical Polymerization Using Polyelectrolytic Macroinitiators," *Macromolecules,* vol. 40, pp. 5271-5278, 2007/07/01 2007.
[220] S. Peng and B. Bhushan, "Smart polymer brushes and their emerging applications," *RSC Advances,* vol. 2, pp. 8557-8578, 2012.
[221] F. Zhou and W. T. S. Huck, "Surface grafted polymer brushes as ideal building blocks for "smart" surfaces," *Physical Chemistry Chemical Physics,* vol. 8, pp. 3815-3823, 2006.
[222] C. Xu, T. Wu, J. D. Batteas, C. M. Drain, K. L. Beers, and M. J. Fasolka, "Surface-grafted block copolymer gradients: Effect of block length on solvent response," *Applied Surface Science,* vol. 252, pp. 2529-2534, 1/31/ 2006.
[223] P. Mocny and H.-A. Klok, "Tribology of surface-grafted polymer brushes," *Molecular Systems Design & Engineering,* 2016.
[224] C. Yoshikawa, J. Qiu, C.-F. Huang, Y. Shimizu, J. Suzuki, and E. van den Bosch, "Non-biofouling property of well-defined concentrated polymer brushes," *Colloids and Surfaces B: Biointerfaces,* vol. 127, pp. 213-220, 3/1/ 2015.
[225] Y. Inoue and K. Ishihara, "Reduction of protein adsorption on well-characterized polymer brush layers with varying chemical structures," *Colloids and Surfaces B: Biointerfaces,* vol. 81, pp. 350-357, 11/1/ 2010.
[226] B. F. L. Lai, A. L. Creagh, J. Janzen, C. A. Haynes, D. E. Brooks, and J. N. Kizhakkedathu, "The induction of thrombus generation on nanostructured neutral polymer brush surfaces," *Biomaterials,* vol. 31, pp. 6710-6718, 9// 2010.
[227] S. Yamamoto, M. Ejaz, Y. Tsujii, and T. Fukuda, "Surface Interaction Forces of Well-Defined, High-Density Polymer Brushes Studied by Atomic Force Microscopy. 2. Effect of Graft Density," *Macromolecules,* vol. 33, pp. 5608-5612, 2000/07/01 2000.

[228] A. Olivier, F. Meyer, J.-M. Raquez, P. Damman, and P. Dubois, "Surface-initiated controlled polymerization as a convenient method for designing functional polymer brushes: From self-assembled monolayers to patterned surfaces," *Progress in Polymer Science,* vol. 37, pp. 157-181, 1// 2012.
[229] R. Barbey, L. Lavanant, D. Paripovic, N. Schüwer, C. Sugnaux, S. Tugulu*, et al.*, "Polymer Brushes via Surface-Initiated Controlled Radical Polymerization: Synthesis, Characterization, Properties, and Applications," *Chemical Reviews,* vol. 109, pp. 5437-5527, 2009/11/11 2009.
[230] W. Hadasha and B. Klumperman, "Atom transfer radical polymerization as a powerful tool in the synthesis of molecular brushes," *Polymer International,* vol. 63, pp. 824-834, 2014.
[231] J. Pyun, T. Kowalewski, and K. Matyjaszewski, "Synthesis of Polymer Brushes Using Atom Transfer Radical Polymerization," *Macromolecular Rapid Communications,* vol. 24, pp. 1043-1059, 2003.
[232] R. Toomey and M. Tirrell, "Functional Polymer Brushes in Aqueous Media from Self-Assembled and Surface-Initiated Polymers," *Annual Review of Physical Chemistry,* vol. 59, pp. 493-517, 2008.
[233] A. T. Nguyen, J. Baggerman, J. M. J. Paulusse, C. J. M. van Rijn, and H. Zuilhof, "Stable Protein-Repellent Zwitterionic Polymer Brushes Grafted from Silicon Nitride," *Langmuir,* vol. 27, pp. 2587-2594, 2011/03/15 2011.
[234] C. Kang, R. M. Crockett, and N. D. Spencer, "Molecular-Weight Determination of Polymer Brushes Generated by SI-ATRP on Flat Surfaces," *Macromolecules,* vol. 47, pp. 269-275, 2014/01/14 2014.
[235] O. Nuyken and S. Pask, "Ring-Opening Polymerization—An Introductory Review," *Polymers,* vol. 5, p. 361, 2013.
[236] S. Penczek and G. Moad, "Glossary of terms related to kinetics, thermodynamics, and mechanisms of polymerization (IUPAC Recommendations 2008)," in *Pure and Applied Chemistry* vol. 80, ed, 2008, p. 2163.
[237] K. Udipi, R. S. Davé, R. L. Kruse, and L. R. Stebbins, "Polyamides from lactams via anionic ring-opening polymerization: 1. Chemistry and some recent findings," *Polymer,* vol. 38, pp. 927-938, 2// 1997.
[238] C. W. Bielawski and R. H. Grubbs, "Living ring-opening metathesis polymerization," *Progress in Polymer Science,* vol. 32, pp. 1-29, 1// 2007.
[239] C. J. Hawker, "Molecular Weight Control by a "Living" Free-Radical Polymerization Process," *Journal of the American Chemical Society,* vol. 116, pp. 11185-11186, 1994/11/01 1994.
[240] D. Benoit, V. Chaplinski, R. Braslau, and C. J. Hawker, "Development of a Universal Alkoxyamine for “Living” Free Radical Polymerizations," *Journal of the American Chemical Society,* vol. 121, pp. 3904-3920, 1999/04/01 1999.
[241] M. Semsarilar and S. Perrier, "'Green' reversible addition-fragmentation chain-transfer (RAFT) polymerization," *Nat Chem,* vol. 2, pp. 811-820, 10//print 2010.
[242] J. Chiefari, Y. K. Chong, F. Ercole, J. Krstina, J. Jeffery, T. P. T. Le*, et al.*, "Living Free-Radical Polymerization by Reversible Addition−Fragmentation Chain Transfer: The RAFT Process," *Macromolecules,* vol. 31, pp. 5559-5562, 1998/08/01 1998.
[243] G. Moad, E. Rizzardo, and S. H. Thang, "Living Radical Polymerization by the RAFT Process," *Australian Journal of Chemistry,* vol. 58, pp. 379-410, 2005.
[244] B. Giechaskiel, M. Maricq, L. Ntziachristos, C. Dardiotis, X. Wang, H. Axmann*, et al.*, "Review of motor vehicle particulate emissions sampling and measurement: From smoke and filter mass to particle number," *Journal of Aerosol Science,* vol. 67, pp. 48-86, 1// 2014.
[245] J. Yan, B. Li, B. Yu, W. T. S. Huck, W. Liu, and F. Zhou, "Controlled Polymer-Brush Growth from Microliter Volumes using Sacrificial-Anode Atom-Transfer Radical Polymerization," *Angewandte Chemie International Edition,* vol. 52, pp. 9125-9129, 2013.
[246] D. Neugebauer, "Two decades of molecular brushes by ATRP," *Polymer,* vol. 72, pp. 413-421, Aug 18 2015.

[247] M. Kato, M. Kamigaito, M. Sawamoto, and T. Higashimura, "Polymerization of Methyl Methacrylate with the Carbon Tetrachloride/Dichlorotris-(triphenylphosphine)ruthenium(II)/Methylaluminum Bis(2,6-di-tert-butylphenoxide) Initiating System: Possibility of Living Radical Polymerization," *Macromolecules,* vol. 28, pp. 1721-1723, 1995/02/01 1995.

[248] J.-S. Wang and K. Matyjaszewski, "Controlled/"living" radical polymerization. atom transfer radical polymerization in the presence of transition-metal complexes," *Journal of the American Chemical Society,* vol. 117, pp. 5614-5615, 1995/05/01 1995.

[249] P. Król and P. Chmielarz, "Recent advances in ATRP methods in relation to the synthesis of copolymer coating materials," *Progress in Organic Coatings,* vol. 77, pp. 913-948, 5// 2014.

[250] H. Liu, C. T. O'Mahony, F. Audouin, C. Ventura, M. Morris, and A. Heise, "Random Poly(methyl methacrylate-co-styrene) Brushes by ATRP to Create Neutral Surfaces for Block Copolymer Self-Assembly," *Macromolecular Chemistry and Physics,* vol. 213, pp. 108-115, 2012.

[251] W. Song, C. Xiao, L. Cui, Z. Tang, X. Zhuang, and X. Chen, "Facile construction of functional biosurface via SI-ATRP and “click glycosylation”," *Colloids and Surfaces B: Biointerfaces,* vol. 93, pp. 188-194, 5/1/ 2012.

[252] X. Huang and M. J. Wirth, "Surface-Initiated Radical Polymerization on Porous Silica," *Analytical Chemistry,* vol. 69, pp. 4577-4580, 1997/11/01 1997.

[253] M. Ejaz, S. Yamamoto, K. Ohno, Y. Tsujii, and T. Fukuda, "Controlled Graft Polymerization of Methyl Methacrylate on Silicon Substrate by the Combined Use of the Langmuir−Blodgett and Atom Transfer Radical Polymerization Techniques," *Macromolecules,* vol. 31, pp. 5934-5936, 1998/08/01 1998.

[254] E. Turan, S. Demirci, and T. Caykara, "Synthesis of thermoresponsive poly(N-isopropylacrylamide) brush on silicon wafer surface via atom transfer radical polymerization," *Thin Solid Films,* vol. 518, pp. 5950-5954, 8/31/ 2010.

[255] H. Fischer, "The Persistent Radical Effect: A Principle for Selective Radical Reactions and Living Radical Polymerizations," *Chemical Reviews,* vol. 101, pp. 3581-3610, 2001/12/01 2001.

[256] Y. Higaki, M. Kobayashi, T. Hirai, and A. Takahara, "Direct polymer brush grafting to polymer fibers and films by surface-initiated polymerization," *Polymer Journal,* vol. 50, p. 101, 10/11/online 2017.

[257] H. Gao and K. Matyjaszewski, "Synthesis of functional polymers with controlled architecture by CRP of monomers in the presence of cross-linkers: From stars to gels," *Progress in Polymer Science,* vol. 34, pp. 317-350, 4// 2009.

[258] K. Matyjaszewski, "Atom Transfer Radical Polymerization (ATRP): Current Status and Future Perspectives," *Macromolecules,* vol. 45, pp. 4015-4039, 2012/05/22 2012.

[259] L. J. T. Landherr, C. Cohen, P. Agarwal, and L. A. Archer, "Interfacial Friction and Adhesion of Polymer Brushes," *Langmuir,* vol. 27, pp. 9387-9395, 2011.

[260] K. Ohno, T. Morinaga, K. Koh, Y. Tsujii, and T. Fukuda, "Synthesis of Monodisperse Silica Particles Coated with Well-Defined, High-Density Polymer Brushes by Surface-Initiated Atom Transfer Radical Polymerization," *Macromolecules,* vol. 38, pp. 2137-2142, 2005/03/01 2005.

[261] K. Matyjaszewski, P. J. Miller, N. Shukla, B. Immaraporn, A. Gelman, B. B. Luokala*, et al.*, "Polymers at Interfaces: Using Atom Transfer Radical Polymerization in the Controlled Growth of Homopolymers and Block Copolymers from Silicon Surfaces in the Absence of Untethered Sacrificial Initiator," *Macromolecules,* vol. 32, pp. 8716-8724, 1999/12/01 1999.

[262] M. Husseman, E. E. Malmström, M. McNamara, M. Mate, D. Mecerreyes, D. G. Benoit*, et al.*, "Controlled Synthesis of Polymer Brushes by “Living” Free Radical Polymerization Techniques," *Macromolecules,* vol. 32, pp. 1424-1431, 1999/03/01 1999.

[263] D. B. Karstedt, US Patent US3775452, 1971.

[264] W. Zhou, H. Liu, H. Ye, H. Cui, R. Wang, J. Li*, et al.*, "Synthesis and adsorption behaviors of poly(2-(dimethylamino)ethyl methacrylate) brushes on silica particles by surface-initiated atom transfer radical polymerization," *Powder Technology,* vol. 249, pp. 1-6, 11// 2013.
[265] W. Feng, J. L. Brash, and S. Zhu, "Non-biofouling materials prepared by atom transfer radical polymerization grafting of 2-methacryloloxyethyl phosphorylcholine: Separate effects of graft density and chain length on protein repulsion," *Biomaterials,* vol. 27, pp. 847-855, 2// 2006.
[266] D. J. Siegwart, J. K. Oh, and K. Matyjaszewski, "ATRP in the design of functional materials for biomedical applications," *Prog Polym Sci,* vol. 37, pp. 18-37, Jan 1 2012.
[267] K. Matyjaszewski, H. Dong, W. Jakubowski, J. Pietrasik, and A. Kusumo, "Grafting from Surfaces for "Everyone": ARGET ATRP in the Presence of Air," *Langmuir,* vol. 23, pp. 4528-4531, 2007/04/01 2007.
[268] S. Munirasu, R. G. Karunakaran, J. Rühe, and R. Dhamodharan, "Synthesis and Morphological Study of Thick Benzyl Methacrylate–Styrene Diblock Copolymer Brushes," *Langmuir,* vol. 27, pp. 13284-13292, 2011/11/01 2011.
[269] E. Turan and T. Caykara, "A facile route to end-functionalized poly(N-isopropylacrylamide) brushes synthesized by surface-initiated SET-LRP," *Reactive and Functional Polymers,* vol. 71, pp. 1089-1095, 11// 2011.
[270] E. Öztürk, E. Turan, and T. Caykara, "Fabrication of ultrahydrophobic poly(lauryl acrylate) brushes on silicon wafer via surface-initiated atom transfer radical polymerization," *Applied Surface Science,* vol. 257, pp. 1015-1020, 11/15/ 2010.
[271] A. Nomura, K. Okayasu, K. Ohno, T. Fukuda, and Y. Tsujii, "Lubrication Mechanism of Concentrated Polymer Brushes in Solvents: Effect of Solvent Quality and Thereby Swelling State," *Macromolecules,* vol. 44, pp. 5013-5019, 2011/06/28 2011.
[272] S. Yamamoto, M. Ejaz, Y. Tsujii, M. Matsumoto, and T. Fukuda, "Surface Interaction Forces of Well-Defined, High-Density Polymer Brushes Studied by Atomic Force Microscopy. 1. Effect of Chain Length," *Macromolecules,* vol. 33, pp. 5602-5607, 2000/07/01 2000.
[273] D. A. Shipp and K. Matyjaszewski, "Kinetic Analysis of Controlled/"Living" Radical Polymerizations by Simulations. 2. Apparent External Orders of Reactants in Atom Transfer Radical Polymerization," *Macromolecules,* vol. 33, pp. 1553-1559, 2000/03/01 2000.
[274] K. L. Beers, S. G. Gaynor, K. Matyjaszewski, S. S. Sheiko, and M. Möller, "The Synthesis of Densely Grafted Copolymers by Atom Transfer Radical Polymerization," *Macromolecules,* vol. 31, pp. 9413-9415, 1998/12/01 1998.
[275] T. Pintauer and K. Matyjaszewski, "Structural aspects of copper catalyzed atom transfer radical polymerization," *Coordination Chemistry Reviews,* vol. 249, pp. 1155-1184, 6// 2005.
[276] B. Zhu and S. Edmondson, "Polydopamine-melanin initiators for Surface-initiated ATRP," *Polymer,* vol. 52, pp. 2141-2149, 5/4/ 2011.
[277] F. Jiang, W. H. Meyer, and J. Zhang, "Dense poly(4-vinyl pyridine) brushes grafting from silica nanoparticles via atom transfer radical polymerization," *Colloids and Surfaces A: Physicochemical and Engineering Aspects,* vol. 436, pp. 302-308, 9/5/ 2013.
[278] Y. Liu, Y. Xiao, and J. Luo, "Preparation of poly (N-isopropylacrylamide) brush bonded on silicon substrate and its water-based lubricating property," *Science China Technological Sciences,* vol. 55, pp. 3352-3358, 2012/12/01 2012.
[279] A. M. Elsen, J. Burdyńska, S. Park, and K. Matyjaszewski, "Activators Regenerated by Electron Transfer Atom Transfer Radical Polymerization in Miniemulsion with 50 ppm of Copper Catalyst," *ACS Macro Letters,* vol. 2, pp. 822-825, 2013/09/17 2013.
[280] J. Ran, L. Wu, Z. Zhang, and T. Xu, "Atom transfer radical polymerization (ATRP): A versatile and forceful tool for functional membranes," *Progress in Polymer Science,* vol. 39, pp. 124-144, 1// 2014.
[281] N. V. Tsarevsky and K. Matyjaszewski, ""Green" Atom Transfer Radical Polymerization: From Process Design to Preparation of Well-Defined Environmentally Friendly Polymeric Materials," *Chemical Reviews,* vol. 107, pp. 2270-2299, 2007/06/01 2007.

[282] K. Min, H. Gao, and K. Matyjaszewski, "Use of Ascorbic Acid as Reducing Agent for Synthesis of Well-Defined Polymers by ARGET ATRP," *Macromolecules,* vol. 40, pp. 1789-1791, 2007/03/01 2007.
[283] W. Jakubowski and K. Matyjaszewski, "Activator Generated by Electron Transfer for Atom Transfer Radical Polymerization," *Macromolecules,* vol. 38, pp. 4139-4146, 2005/05/01 2005.
[284] T. Pintauer and K. Matyjaszewski, "Atom transfer radical addition and polymerization reactions catalyzed by ppm amounts of copper complexes," *Chemical Society Reviews,* vol. 37, pp. 1087-1097, 2008.
[285] C. Sun, F. Zhou, L. Shi, B. Yu, P. Gao, J. Zhang*, et al.*, "Tribological properties of chemically bonded polyimide films on silicon with polyglycidyl methacrylate brush as adhesive layer," *Applied Surface Science,* vol. 253, pp. 1729-1735, 12/15/ 2006.
[286] R. A. E. Wright, K. Wang, J. Qu, and B. Zhao, "Oil-Soluble Polymer Brush-Grafted Nanoparticles as Effective Lubricant Additives for Friction and Wear Reduction," *Angewandte Chemie International Edition,* pp. n/a-n/a, 2016.
[287] F. Seeliger and K. Matyjaszewski, "Temperature Effect on Activation Rate Constants in ATRP: New Mechanistic Insights into the Activation Process," *Macromolecules,* vol. 42, pp. 6050-6055, 2009/08/25 2009.
[288] J. Klein, E. Kumacheva, D. Mahalu, D. Perahia, and L. J. Fetters, "Reduction of frictional forces between solid surfaces bearing polymer brushes," *Nature,* vol. 370, pp. 634-636, 08/25/print 1994.
[289] G. Fontani, R. Gaspari, N. D. Spencer, D. Passerone, and R. Crockett, "Adsorption and Friction Behavior of Amphiphilic Polymers on Hydrophobic Surfaces," *Langmuir,* vol. 29, pp. 4760-4771, 2013/04/16 2013.
[290] R. Heeb, R. M. Bielecki, S. Lee, and N. D. Spencer, "Room-Temperature, Aqueous-Phase Fabrication of Poly(methacrylic acid) Brushes by UV-LED-Induced, Controlled Radical Polymerization with High Selectivity for Surface-Bound Species," *Macromolecules,* vol. 42, pp. 9124-9132, 2009/11/24 2009.
[291] H. Sakata, M. Kobayashi, H. Otsuka, and A. Takahara, "Tribological Properties of Poly(methyl methacrylate) Brushes Prepared by Surface-Initiated Atom Transfer Radical Polymerization," *Polym J,* vol. 37, pp. 767-775, 10//print 2005.
[292] M. Kobayashi, M. Kaido, A. Suzuki, and A. Takahara, "Tribological properties of cross-linked oleophilic polymer brushes on diamond-like carbon films," *Polymer,* vol. 89, pp. 128-134, 4/20/ 2016.
[293] S. Jahn and J. Klein, "Hydration Lubrication: The Macromolecular Domain," *Macromolecules,* vol. 48, pp. 5059-5075, 2015/08/11 2015.
[294] S. Desseaux, J. P. Hinestrosa, N. Schüwer, B. S. Lokitz, J. F. Ankner, S. M. Kilbey*, et al.*, "Swelling Behavior and Nanomechanical Properties of (Peptide-Modified) Poly(2-hydroxyethyl methacrylate) and Poly(poly(ethylene glycol) methacrylate) Brushes," *Macromolecules,* 2016/06/17 2016.
[295] J. Klein, Y. Kamiyama, H. Yoshizawa, J. N. Israelachvili, G. H. Fredrickson, P. Pincus*, et al.*, "Lubrication forces between surfaces bearing polymer brushes," *Macromolecules,* vol. 26, pp. 5552-5560, 1993/10/01 1993.
[296] A. Laschewsky, "Structures and Synthesis of Zwitterionic Polymers," *Polymers,* vol. 6, p. 1544, 2014.
[297] J. B. Schlenoff, "Zwitteration: Coating Surfaces with Zwitterionic Functionality to Reduce Nonspecific Adsorption," *Langmuir,* vol. 30, pp. 9625-9636, 2014/08/19 2014.
[298] D. Irfachsyad, D. Tildesley, and P. Malfreyt, "Dissipative particle dynamics simulation of grafted polymer brushes under shear," *Physical Chemistry Chemical Physics,* vol. 4, pp. 3008-3015, 2002.
[299] O. Tairy, N. Kampf, M. J. Driver, S. P. Armes, and J. Klein, "Dense, Highly Hydrated Polymer Brushes via Modified Atom-Transfer-Radical-Polymerization: Structure, Surface Interactions, and Frictional Dissipation," *Macromolecules,* vol. 48, pp. 140-151, 2015/01/13 2015.

[300] N. S. Bhairamadgi, S. P. Pujari, F. A. M. Leermakers, C. J. M. van Rijn, and H. Zuilhof, "Adhesion and Friction Properties of Polymer Brushes: Fluoro versus Nonfluoro Polymer Brushes at Varying Thickness," *Langmuir,* vol. 30, pp. 2068-2076, 2014/03/04 2014.
[301] M. Kobayashi, Y. Terayama, N. Hosaka, M. Kaido, A. Suzuki, N. Yamada*, et al.*, "Friction behavior of high-density poly(2-methacryloyloxyethyl phosphorylcholine) brush in aqueous media," *Soft Matter,* vol. 3, pp. 740-746, 2007.
[302] L. C. H. Moh, M. D. Losego, and P. V. Braun, "Solvent Quality Effects on Scaling Behavior of Poly(methyl methacrylate) Brushes in the Moderate- and High-Density Regimes," *Langmuir,* vol. 27, pp. 3698-3702, 2011/04/05 2011.
[303] E. S. Dehghani, S. N. Ramakrishna, N. D. Spencer, and E. M. Benetti, "Controlled Crosslinking Is a Tool To Precisely Modulate the Nanomechanical and Nanotribological Properties of Polymer Brushes," *Macromolecules,* vol. 50, pp. 2932-2941, 2017/04/11 2017.
[304] S. N. Ramakrishna, M. Cirelli, M. Divandari, and E. M. Benetti, "Effects of Lateral Deformation by Thermoresponsive Polymer Brushes on the Measured Friction Forces," *Langmuir,* vol. 33, pp. 4164-4171, 2017/05/02 2017.
[305] F. T. Limpoco, R. C. Advincula, and S. S. Perry, "Solvent Dependent Friction Force Response of Polystyrene Brushes Prepared by Surface Initiated Polymerization," *Langmuir,* vol. 23, pp. 12196-12201, 2007/11/01 2007.
[306] G. W. de Groot, M. G. Santonicola, K. Sugihara, T. Zambelli, E. Reimhult, J. Vörös*, et al.*, "Switching Transport through Nanopores with pH-Responsive Polymer Brushes for Controlled Ion Permeability," *ACS Applied Materials & Interfaces,* vol. 5, pp. 1400-1407, 2013/02/27 2013.
[307] A. T. Nguyen, J. Baggerman, J. M. J. Paulusse, H. Zuilhof, and C. J. M. van Rijn, "Bioconjugation of Protein-Repellent Zwitterionic Polymer Brushes Grafted from Silicon Nitride," *Langmuir,* vol. 28, pp. 604-610, Jan 2012.
[308] S. Gabriel, C. Jérôme, R. Jérôme, C.-A. Fustin, A. Pallandre, J. Plain*, et al.*, "One-Step Polymer Grafting from Silicon Nitride SPM Probes: From Isolated Chains to Brush Regime," *Journal of the American Chemical Society,* vol. 129, pp. 8410-8411, 2007/07/01 2007.
[309] P. Stoyanov and R. Chromik, "Scaling Effects on Materials Tribology: From Macro to Micro Scale," *Materials,* vol. 10, p. 550, 2017.
[310] R. Gong, S. Maclaughlin, and S. Zhu, "Surface modification of active metals through atom transfer radical polymerization grafting of acrylics," *Applied Surface Science,* vol. 254, pp. 6802-6809, 8/30/ 2008.
[311] H. J. Butt and M. Jaschke, "Calculation of thermal noise in atomic force microscopy," *Nanotechnology,* vol. 6, p. 1, 1995.
[312] S. M. Cook, T. E. Schäffer, K. M. Chynoweth, M. Wigton, R. W. Simmonds, and K. M. Lang, "Practical implementation of dynamic methods for measuring atomic force microscope cantilever spring constants," *Nanotechnology,* vol. 17, p. 2135, 2006.
[313] G. Haugstad, *Atomic Force Microscopy: Understanding Basic Modes and Advanced Applications*. Hoboken, New Jersey: John Wiley & Sons, 2012.
[314] A. Ramakrishnan, R. Dhamodharan, and J. Rühe, "Controlled Growth of PMMA Brushes on Silicon Surfaces at Room Temperature," *Macromolecular Rapid Communications,* vol. 23, pp. 612-616, 2002.
[315] K. Kitano, Y. Inoue, R. Matsuno, M. Takai, and K. Ishihara, "Nanoscale evaluation of lubricity on well-defined polymer brush surfaces using QCM-D and AFM," *Colloids and Surfaces B: Biointerfaces,* vol. 74, pp. 350-357, 11/1/ 2009.
[316] G. K. Raghuraman, R. Dhamodharan, O. Prucker, and J. Rühe, "A Robust Method for the Immobilization of Polymer Molecules on SiO2 Surfaces," *Macromolecules,* vol. 41, pp. 873-878, 2008/02/01 2008.
[317] M. G. Santonicola, G. W. de Groot, M. Memesa, A. Meszyńska, and G. J. Vancso, "Reversible pH-Controlled Switching of Poly(methacrylic acid) Grafts for Functional Biointerfaces," *Langmuir,* vol. 26, pp. 17513-17519, 2010/11/16 2010.

[318] M. o. Defence, "Fuels, Lubricants and Associated Products," in *DEF STAN 01-5 Issue 17*, ed. GLASGOW: DSTAN, 2011.
[319] BritishArmy. (2015, 25/2/16). *Bulldog & FV430 series*. Available: http://www.army.mod.uk/equipment/23239.aspx
[320] BritishArmy. (2015, 25/2/16). *Challenger 2 main battle tank*. Available: http://www.army.mod.uk/equipment/23236.aspx
[321] BBCNews. (2008, 25/2/16). *Q&A: Jackal armoured vehicles*. Available: http://news.bbc.co.uk/1/hi/uk/7781394.stm
[322] GeneralDynamicsLandSystems. (2010, 25/2/16). *OCELOT*. Available: http://www.gdls.com/products/specialty-vehicles/ocelot.php
[323] Navistardefense. (2011, 25/2/16). *International® MXT-MVA*. Available: http://www.navistardefense.com/navistardefense/vehicles/mxt_mv/mxt_mva_armored
[324] GeneralDynamicsLandSystems. (2016, 25/2/16). *COUGAR 6X6*. Available: http://www.gdls.com/products/mrap-family/cougar-6x6.php
[325] Iveco. (2010, 25/2/2016). *The Iveco range*. Available: http://www.iveco.com/en-us/press-room/kit/Pages/IAA2010LagammaIveco.aspx
[326] BritishArmy. (2015, 25/2/16). *Scimitar armoured reconnaissance vehicle*. Available: http://www.army.mod.uk/equipment/23241.aspx
[327] MODSales. (2016, 25/2/16). *Land Rover: Snatch 3.5 V8 Armoured*. Available: http://www.mod-sales.com/direct/vehicle/,37,/44385/Land_Rover.htm
[328] BritishArmy. (2015, 25/2/16). *Spartan & CVR(T) vehicles*. Available: http://www.army.mod.uk/equipment/23242.aspx
[329] MODSales. (2016, 25/2/16). *Alvis Stormer: Tracked Armoured Recon Vehicle*. Available: http://www.mod-sales.com/direct/vehicle/,37,/46202/Alvis_Stormer.htm
[330] BritishArmy. (2015, 25/2/16). *Vector*. Available: http://www.army.mod.uk/equipment/23246.aspx
[331] BritishArmy. (2015, 25/2/16). *Viking BVS10*. Available: http://www.army.mod.uk/equipment/23247.aspx
[332] DailyMail. (2012, 25/2/16). *The fatal flaws in Warrior's armour: Four years ago a coroner demanded better protection for our troops... did six soldiers pay with their lives yesterday because not enough has been done?* Available: http://www.dailymail.co.uk/news/article-2111812/Afghanistan-soldier-deaths-Did-6-pay-lives-flaws-Warriors-armour.html
[333] Thales. (2009, 25/2/16). *THALES ANNOUNCES WARTHOG CONTRACT WITH ST KINETICS*. Available: https://www.thalesgroup.com/en/content/thales-announces-warthog-contract-st-kinetics
[334] GeneralDynamicsLandSystems. (2016, 25/2/16). *COUGAR 4X4*. Available: http://apps.webofknowledge.com/UA_GeneralSearch_input.do?product=UA&search_mode=GeneralSearch&SID=Z1NgFfDN2V4WGiUSw2D&preferencesSaved=
[335] S. Watson, L. Wang, M. Nie, and K. Stokes, "Development of polymer brushes for the lubrication of silicon nitride-steel contacts," presented at the 71st STLE Annual Meeting and Exhibition, 2016.
[336] A. Halperin and E. B. Zhulina, "Atomic Force Microscopy of Polymer Brushes: Colloidal versus Sharp Tips," *Langmuir,* vol. 26, pp. 8933-8940, 2010/06/01 2010.
[337] M. Kumar Vyas, K. Schneider, B. Nandan, and M. Stamm, "Switching of friction by binary polymer brushes," *Soft Matter,* vol. 4, pp. 1024-1032, 2008.
[338] W. A. Ducker, T. J. Senden, and R. M. Pashley, "Direct measurement of colloidal forces using an atomic force microscope," *Nature,* vol. 353, pp. 239-241, 09/19/print 1991.
[339] S. N. Ramakrishna, R. M. Espinosa-Marzal, V. V. Naik, P. C. Nalam, and N. D. Spencer, "Adhesion and Friction Properties of Polymer Brushes on Rough Surfaces: A Gradient Approach," *Langmuir,* vol. 29, pp. 15251-15259, 2013/12/10 2013.
[340] J. Lee, "Intrinsic adhesion force of lubricants to steel surface," *Journal of Pharmaceutical Sciences,* vol. 93, pp. 2310-2318, 9// 2004.

[341] J. Zekonyte, A. Cavaleiro, and T. Polcar, "Frictional properties of self-adaptive chromium doped tungsten–sulfur–carbon coatings at nanoscale," *Applied Surface Science,* vol. 303, pp. 381-387, 6/1/ 2014.
[342] B. Craig, "SAM Coatings for Silicon Nitride ", University of Southampton, 2012.
[343] E. Pretsch, P. Bühlmann, and M. Badertscher, *Structure Determination of Organic Compounds*. Springer-Verlag Berlin Heidelberg, 2009.
[344] H. E. Gottlieb, V. Kotlyar, and A. Nudelman, "NMR Chemical Shifts of Common Laboratory Solvents as Trace Impurities," *The Journal of Organic Chemistry,* vol. 62, pp. 7512-7515, 1997/10/01 1997.
[345] C. M. Herzinger, B. Johs, W. A. McGahan, J. A. Woollam, and W. Paulson, "Ellipsometric determination of optical constants for silicon and thermally grown silicon dioxide via a multi-sample, multi-wavelength, multi-angle investigation," *Journal of Applied Physics,* vol. 83, pp. 3323-3336, 1998.
[346] A. H. Al-Bayati, K. G. Orrman-Rossiter, J. A. van den Berg, and D. G. Armour, "Composition and structure of the native Si oxide by high depth resolution medium energy ion scatering," *Surface Science,* vol. 241, pp. 91-102, 1/1/ 1991.
[347] C. E. Taylor, S. D. Garvey, and J. E. Pemberton, "Carbon Contamination at Silver Surfaces: Surface Preparation Procedures Evaluated by Raman Spectroscopy and X-ray Photoelectron Spectroscopy," *Analytical Chemistry,* vol. 68, pp. 2401-2408, 1996/01/01 1996.
[348] T. L. Barr and S. Seal, "Nature of the use of adventitious carbon as a binding energy standard," *Journal of Vacuum Science & Technology A,* vol. 13, pp. 1239-1246, 1995.
[349] P. Singh, S. M. Shivaprasad, M. Lal, and M. Husain, "Angle-dependent XPS analysis of silicon nitride film deposited on screen-printed crystalline silicon solar cell," *Solar Energy Materials and Solar Cells,* vol. 93, pp. 19-24, 1// 2009.
[350] ExxonMobil, "SpectraSyn 4 PAO," ed, 2016.
[351] O. Kahle, U. Wielsch, H. Metzner, J. Bauer, C. Uhlig, and C. Zawatzki, "Glass transition temperature and thermal expansion behaviour of polymer films investigated by variable temperature spectroscopic ellipsometry," *Thin Solid Films,* vol. 313–314, pp. 803-807, 2/13/ 1998.
[352] N. Vourdas, A. G. Boudouvis, and E. Gogolides, "Plasma etch rate measurements of thin PMMA films and correlation with the glass transition temperature," *Journal of Physics: Conference Series,* vol. 10, p. 405, 2005.
[353] J. Zekonyte and T. Polcar, "Friction Force Microscopy Analysis of Self-Adaptive W–S–C Coatings: Nanoscale Friction and Wear," *ACS Applied Materials & Interfaces,* vol. 7, pp. 21056-21064, 2015/09/30 2015.
[354] S. Watson, M. Nie, L. Wang, and K. Stokes, "Challenges and developments of self-assembled monolayers and polymer brushes as a green lubrication solution for tribological applications," *RSC Advances,* vol. 5, pp. 89698-89730, 2015.
[355] H. Ma, J. a. He, X. Liu, J. Gan, G. Jin, and J. Zhou, "Surface Initiated Polymerization from Substrates of Low Initiator Density and Its Applications in Biosensors," *ACS Applied Materials & Interfaces,* vol. 2, pp. 3223-3230, 2010/11/24 2010.
[356] A. Casoli, M. Brendlé, J. Schultz, P. Auroy, and G. Reiter, "Friction Induced by Grafted Polymeric Chains," *Langmuir,* vol. 17, pp. 388-398, 2001/01/01 2001.
[357] H. Hyuga, Y.-i. Yoshizawa, K. Hirao, D. Amutha Rani, and M. I. Jones, "Tribological Behavior of Si3N4 and Si3N4/Carbon Fiber Composites Against Stainless Steel Under Water Lubrication for a Thrust-Bearing Application," *International Journal of Applied Ceramic Technology,* vol. 5, pp. 111-118, 2008.
[358] A. International, "ASTM A295 / A295M-14, Standard Specification for High-Carbon Anti-Friction Bearing Steel," ed. West Conshohocken, PA,, 2014.
[359] A. International, "ASTM F2730 / F2730M-14, Standard Specification for Silicon Nitride Cylindrical Bearing Rollers," ed. West Conshohocken, PA, 2014.

[360] J. Zhang, S. Xiao, M. Shen, L. Sun, F. Chen, P. Fan*, et al.*, "Aqueous lubrication of poly(N-hydroxyethyl acrylamide) brushes: a strategy for their enhanced load bearing capacity and wear resistance," *RSC Advances,* vol. 6, pp. 21961-21968, 2016.
[361] H. Dong, M. Zhu, J. A. Yoon, H. Gao, R. Jin, and K. Matyjaszewski, "One-Pot Synthesis of Robust Core/Shell Gold Nanoparticles," *Journal of the American Chemical Society,* vol. 130, pp. 12852-12853, 2008/10/01 2008.